UNIVERSITY OF SOUTHAMPTON

FACULTY OF MEDICINE

Clinical and Experimental Sciences

Volume 1 of 1

Epithelial-biofilm interaction in primary ciliary dyskinesia

by

Samuel Anthony Collins

Thesis for degree of Doctor of Philosophy

March 2017

UNIVERSITY OF SOUTHAMPTON

ABSTRACT

FACULTY OF MEDICINE

Thesis for degree of Doctor of Philosophy

EPITHELIAL-BIOFILM INTERACTION IN PRIMARY CILIARY DYSKINESIA

Samuel Anthony Collins

Primary ciliary dyskinesia (PCD) is an inherited disorder of motile cilia that affects around 1 in 15,000 live births and its defining feature is a lack of mucociliary clearance. This results in progressive lung disease, upper airway symptoms and, potentially, situs inversus and infertility. PCD is characterised by early colonisation of the lower airways with bacteria, resulting in progressive lung function decline. Non-typeable *Haemophilus influenzae* (NTHi) is the commonest of these colonising bacteria in children and is also cultured in many other lung conditions such as cystic fibrosis, chronic obstructive pulmonary disease and bronchiectasis. NTHi forms biofilms on airway epithelium; a phenotype associated with increased tolerance to antibiotic treatment and resistance to host immunity.

This work hypothesised that, in addition to lack of mucociliary clearance, the PCD airway has intrinsically dysregulated responses to colonising bacteria. This may be, in part, due to extremely low airway nitric oxide (NO). Thus, exogenous NO may represent a potential therapeutic adjunct in the treatment of lower airway infection. Systematic review and meta-analysis were used to define NO levels in PCD airway and healthy/disease controls. Then an established model of a 72h NTHi biofilm in vitro and on cultured primary respiratory epithelium was employed. NO treatment of these biofilms was investigated using a targeted NO compound (PYRRO-C3D) with the NO-treated NTHi in vitro biofilms subjected to label-free proteomic analyses to identify mechanisms underlying these treatment effects. Label-free proteomic analysis was also employed to identify differences in healthy and PCD epithelial proteome following exposure to 72h NTHi biofilm, as well as identifying NTHi proteins present.

Systematic review and meta-analysis showed that PCD patients had extremely low nasal NO (mean 19.4nl/min) compared to healthy (265nl/min) and CF patients (123.2nl/min). This was independent of genotype or ultrastructural defect, thus there was a common epithelial defect across almost all PCD patients. PYRRO-C3D was effective in enhancing antibiotic treatment of

NTHi biofilms in vitro and on cultured respiratory epithelium ($p<0.05$). This effect was more pronounced on PCD epithelium (2 log fold CFU drop) than healthy (1 log fold). Inhibition of NO release and scavenging of NO showed the effect to be NO mediated. Proteomic analysis revealed NO-induced upregulation of metabolic pathways and translational machinery, as well as a D-methionine uptake lipoprotein and iron metabolism. However, methionine isomers reversed the antibiotic enhancing effect of PYRRO-C3D. Pathway analysis of proteomic data from the co-culture model demonstrated that healthy epithelium responds to NTHi colonisation by cytoskeletal remodelling, metabolic upregulation and initial hyper-proliferation as well as suppression of acute inflammation via downregulation of S100 proteins. PCD epithelium appears to show a lesser degree of hyper-proliferation and fails to downregulate pro-inflammatory S100 proteins to the same extent. NTHi proteins were also identified in the analysis, with 14 present in both the co-culture samples and in vitro work, suggesting they warrant further investigation. OMPp5 (a HSP70 protein) is of particular interest as a potential biomarker or vaccine target.

In conclusion, almost all PCD patients have extremely low airway NO regardless of underlying genotype, suggesting a common epithelial dysfunction. PCD epithelium may not respond adequately to NTHi colonisation as there is a failure of both normal proliferation and inflammatory suppression through downregulation of S100 proteins. Changes in intracellular calcium flux is a potential common mechanism behind failure of ciliary beat, low nitric oxide and S100/innate immune dysfunction. NO can also be successfully used as a targeted therapeutic adjunct in NTHi biofilms and may be particularly effective in PCD due to the constitutively low NO during colonisation. NO induces metabolic and translational changes in NTHi that make it more sensitive to treatment with macrolides and, potentially, other translation-targeting antibiotics. Proteins such as OMPp5 are common to in vitro and ex vivo biofilm models, suggesting the validity of in vitro models and showing promise as potential biomarkers of significant NTHi colonisation or targets of vaccines.

Table of Contents

List of tables

List of figures

List of accompanying materials

Collins SA, Gove K, Walker W, Lucas JSA. Nasal nitric oxide screening for primary ciliary dyskinesia: systematic review and meta-analysis. Eur Respir J. 2014 Dec 16;44(6):1589–99.

Collins SA, Kelso MJ, Rineh A, Yepuri NR, Coles J, Jackson CL, Halladay GD, Walker WT, Webb JS, Hall-Stoodley L, Connett GJ, Feelisch M, Faust SN, Lucas JSA, Allan RN. Cephalosporin-3'-diazeniumdiolate NO-donor prodrug PYRRO-C3D enhances azithromycin susceptibility of Non-typeable *Haemophilus influenzae* biofilms. Antimicrob Agents Chemother. 2016 Dec 5;AAC.02086-16.

DECLARATION OF AUTHORSHIP

I, Samuel Anthony Collins, declare that this thesis and the work presented in it are my own and has been generated by me as the result of my own original research.

Epithelial-biofilm interaction in primary ciliary dyskinesia

I confirm that:

1. This work was done wholly or mainly while in candidature for a research degree at this University;
2. Where any part of this thesis has previously been submitted for a degree or any other qualification at this University or any other institution, this has been clearly stated;
3. Where I have consulted the published work of others, this is always clearly attributed;
4. Where I have quoted from the work of others, the source is always given. With the exception of such quotations, this thesis is entirely my own work;
5. I have acknowledged all main sources of help;
6. Where the thesis is based on work done by myself jointly with others, I have made clear exactly what was done by others and what I have contributed myself;
7. Parts of this work have been published as:

Collins SA, Gove K, Walker W, Lucas JSA. Nasal nitric oxide screening for primary ciliary dyskinesia: systematic review and meta-analysis. Eur Respir J. 2014 Dec 16;44(6):1589–99.
Collins SA, Kelso MJ, Rineh A, *et al.* Cephalosporin-3'-diazeniumdiolate NO-donor prodrug PYRRO-C3D enhances azithromycin susceptibility of Non-typeable *Haemophilus influenzae* biofilms. Antimicrob Agents Chemother. 2016 Dec 5;AAC.02086-16.

Signed:

Date:.....

Acknowledgements

I would like to thank the many people who have helped me complete this PhD. My supervisor, Prof. Jane Lucas has been an invaluable source of advice, guidance and training from our early work together right through to completion of my PhD. Thank you for providing the perfect balance of insight, direction and "leaving me to get on with it"!

I am eternally grateful to Dr. Raymond Allan for introducing me to the world of microbiology and expertly guiding me through the minutiae of laboratory bacterial work, protein handling and the dark arts of proteomics. This PhD would have been impossible without his dedication, patience and wealth of knowledge. Thanks to Dr. Gary Connett for his input and level-headed career advice throughout.

The Southampton PCD team have welcomed me into their fold, in particular Claire Jackson, Janice Coles and James Thompson who taught me cell culture techniques and helped me nurse, feed and cajole my nasal brushings to fruition. I would also like to acknowledge Dr Paul Skipp (Centre for Proteomic Research, University of Southampton) for assistance with protein preparation, performing mass spectrometry runs and helping me work through the challenges of label-free proteomics. Dr Michael Kelso (University of Wollongong, Australia) kindly provided the PYRRO-C3D compound for the NO work. Dr Dave Johnson was invaluable, and always patient, in helping with the confocal imaging of biofilms. Dr Stuart Clarke kindly provided haemophilus strains and Dr Stephen Thirdborough assisted with limma analysis and use of R software. I would also like to thank Dr Woolf Walker who began the co-culture work that led to this thesis, including his preliminary work in characterising the Haemophilus influenzae strains and establishing the co-culture model.

I am also extremely grateful to all the patients and volunteers who made this work possible by providing nasal brushing samples.

Finally, thank you to my wonderful wife Amanda for always reminding me that there's a way to get through any road block and that there are always options at every turn. I dedicate this thesis to Amanda, and my children Jake and Alba.

Definitions and Abbreviations

ADMA	Asymmetric dimethyl arginine
ALI	Air-liquid interface
ASL	Airway surface liquid
BAL	Bronchoalveolar lavage
BHI	Brain-heart infusion
c-di-GMP	Cyclic-di-guanosine-5’-monophosphate
CF	Cystic fibrosis
CFTR	Cystic fibrosis related transmembrane conductance regulator
CFU	Colony forming unit
COPD	Chronic obstructive pulmonary disease
CRS	Chronic rhinosinusitis
CSF	Cerebrospinal fluid
CT	Computed tomography
CV	Crystal violet
DEA/NO	Diethylamine NONOate
DGC	Diguanylate cyclases
DMSO	Dimethyl sulfoxide
DRC	Dynein regulatory complex
DTT	Dithiothreitol
eDNA	Extracellular DNA
FDR	False discovery rate
FEV_1	Forced expiratory volume in one second
FISH	Fluorescent in-situ hybridisation

FVC	Forced vital capacity
GO	Gene ontology
HBSS	Hanks Balanced Salt Solution
HRCT	High resolution computed tomography
HSP	Heat shock protein
IDA	Inner dynein arm
KEGG	Kyoto Encyclopaedia of Genes and Genomes
LCI	Lung clearance index
LC/MS	Liquid chromatography tandem mass spectrometry
LDS-PAGE	Lithium dodecyl sulphate polyacrylamide gel electrophoresis
LOS	Lipooligosaccharide
LPS	Lipopolysaccharide
MBW	Multiple breath washout
MCC	Mucociliary clearance
MOI	Multiplicity of infection
MS	Mass spectrometry
MSSA	Methicillin sensitive *Staphylococcus aureus*
MRSA	Methicillin resistant Staphylococcus aureus
NAD	Nicotinamide-adenine dinucleotide
NBS	Newborn screening
NET	Neutrophil extracellular trap
NF-κB	Nuclear factor kappa B
NGS	Next generation sequencing
NLR	Nucleotide-binding and oligomerisation domain-like receptor
NO	Nitric oxide

nNO	Nasal nitric oxide
NOS	Nitric oxide synthase
NTHi	non-typeable Haemophilus influenzae
ODA	Outer dynein arm
OM	Otitis media
OMP	Outer membrane protein
PAMP	Pathogen associated molecular pattern
PANTHER	Protein Analysis Through Evolutionary Relationships
PBB	Persistent bacterial bronchitis
PBP	Penicillin-binding protein
PCD	Primary ciliary dyskinesia
PCL	Periciliary fluid layer
PCR	Polymerase chain reaction
PDE	Phosphodiesterase
PMN	Polymorphonuclear lymphocytes
PRR	Pattern recognition receptor
PYRRO-C3D	Cephalosporin-3’-diazeniumdiolate NO-donor prodrug
QS	Quorum sensing
RGMC	Reduced generation of motile cilia
RNI	Reactive nitrogen intermediates
ROC	Receive operating characteristics
ROS	Reactive oxygen species
SEM	Scanning electron microscope
SDS	Sodium dodecyl sulphate
SILAC	Stable isotope labelling by amino acids in cell culture

SNP	Sodium nitroprusside
TEAB	Triethylammonium bicarbonate
TEER	Trans-epithelial electrical resistance
TEM	Transmission electron microscopy
TFA	Trifluoracetic acid
TLR	Toll-like receptor

Chapter 1: Introduction

1.1 Primary ciliary dyskinesia

Primary ciliary dyskinesia (PCD) is an inherited disorder of ciliary function affecting motile cilia and sperm flagella. It has an incidence of around 1 in 15,000 live births [1,2] but the diagnosis may frequently be missed and the incidence is as high as 1 in 2,200 in a defined British Asian population [3]. The first description of PCD was by Siewert in 1904 who recognised the association of *situs inversus* (where visceral organs are on the wrong side), bronchiectasis and sinusitis [4]. This triad became known as Kartagener's syndrome following his 1935 description of the disease [5]. In 1976 Afzelius linked the disease to cilial dysfunction and termed it "immotile cilia syndrome" [6]. It was subsequently noted that *situs inversus* was not a universal feature and that some patients had ciliary motion. The term primary ciliary dyskinesia was suggested in a letter to the Lancet by Dr Sleigh of the University of Southampton on behalf of a number of international researchers [7] and this term was subsequently adopted. The use of "primary" differentiates PCD from secondary ciliary dyskinesia as a result of external insults such as infection, pollutants or epithelial damage.

1.1.1 Cilial structure and function

Motile cilia are found in the respiratory epithelium, brain ependymal cells, spinal cord and fallopian tubes. The axonemal structure is also shared with spermatozoa flagella. The normal structure of a motile cilial axoneme (the body of the cilia) is shown in Figure 1-1. The "9+2" arrangement of 9 microtubule doublets and a single central pair runs the length of the axoneme with nexin protein links connecting the doublets to each other. Radial spokes project inwards towards the central pair and are important for maintaining orientation of the microtubules. At one end of the spoke, the head interacts with the central pair, whilst at the other end it attaches to the doublets at the dynein regulatory complex (DRC). The base of the cilia terminates where the axoneme connects to the basal body.

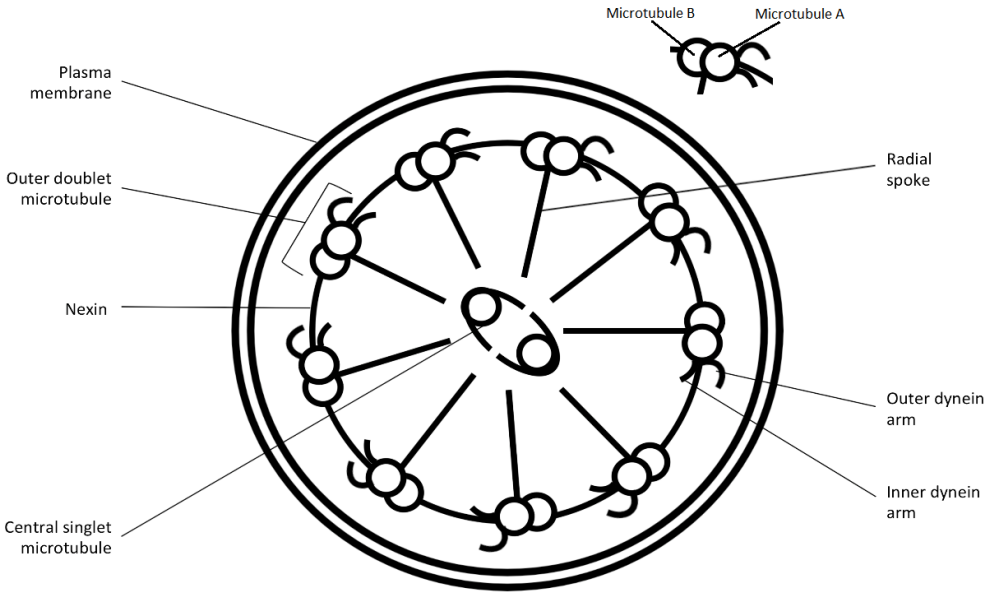

Figure 1-1. **Diagram of normal structure of a motile human cilium in cross-section.** Each outer doublet consists of an A and B microtubule. The A tubule from one doublet is connected to the B tubule of the adjacent doublet via the dynein arms. The dynein arms bind and release to cause ciliary motion.

The mechanical action of the cilia is driven by the dynein arms attached to the outer doublets. There is an outer arm (ODA) and an inner arm (IDA) attached to the A tubule of the doublet. Within the arm is a heavy chain ATPase, several light chains and an intermediate chain that together mediate attachment. ATP binding and hydrolysis results in attachment then detachment of the dynein arm from the adjacent microtubule (Figure 1-2). The sequential action results in the sliding of one doublet against the other [8]. It is likely that outer dynein arms drive linear sliding forces whilst inner dynein arms contribute to bending forces [9]

The “9+2” arrangement of the cilial axoneme is shared by spermatozoa, therefore male PCD patients may have immotile sperm and be infertile, but may have offspring through assisted reproduction techniques such as intra-cytoplasmic sperm injection [10]. Male infertility is not a universal feature of PCD as not all motile cilia proteins that may be mutated in PCD are present in sperm flagella. Dysfunctional cilia in the fallopian tubes mean female patients may have fertility problems and may be at increased risk of ectopic pregnancy [11], though this association remains unproven.

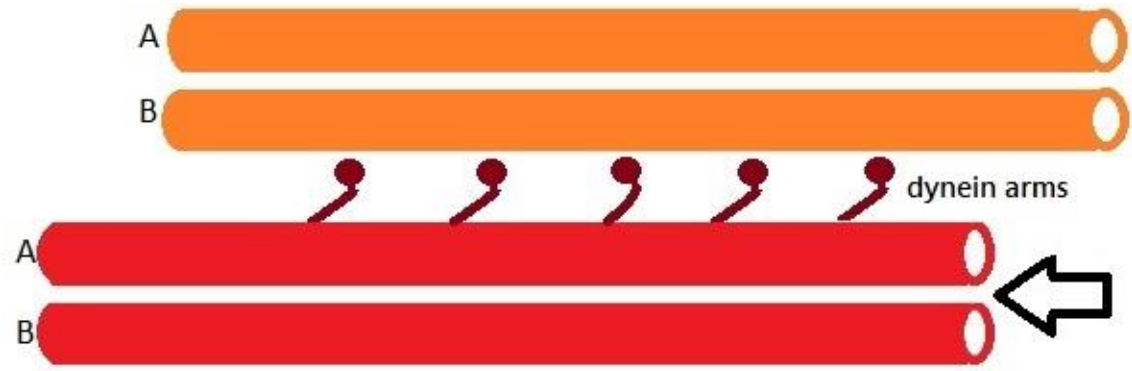

Figure 1-2. **Mechanical action of dynein arms in ciliary motion**. Microtubule doublets each have an A and B microtubule. The heavy chain portion of the dynein arm on the A tubule binds and releases the B tubule on the adjacent doublet via the binding/hydrolysis of ATP. This sequential action results in sliding of the tubules against each other.

In humans, nodal cilia are motile "9+0" cilia that lack the central pair and are only found during embryogenesis. They are termed nodal as they arise in the embryonic node and their rotating motion helps to determine left-right asymmetry. Fifty percent of PCD patients have *situs inversus* as failure of these nodal cilia results in a random left-right assignment of major organs [12]. There are also non-motile "9+0" sensory cilia that are found on a variety of tissues such as renal tubules, bile ducts and retinas. The overlap in structure and proteome between these motile and non-motile cilia accounts for the association between PCD and rare syndromes such as autosomal recessive polycystic kidney disease, oro-facial digital syndrome and retinitis pigmentosa [13]. Sensory cilia are also called primary cilia, which may cause confusion with primary ciliary dyskinesia.

The respiratory tract is lined by pseudostratified columnar epithelium; which are either ciliated or unciliated. Ciliated cells have around 200 cilia per cell. Cilia are present in the nasal cavity and continuously from the trachea to the terminal bronchioles (16^{th} to 19^{th} generation of airway branching), cilia are completely absent from respiratory bronchioles [14]. Ciliated cells appear to become sparser further down the bronchial tree, with one study showing 56% ciliated cells in the trachea but only 15% by the 5^{th} generation of bronchi [15]. Cilia sit within the periciliary fluid layer of the epithelial surface and move the mucus layer towards the oropharynx where it can be swallowed or expectorated (Figure 1-3). Normal ciliary beat frequency is approximately 11-20Hz (at 37°C) with PCD cilia usually showing either reduced or hyper-frequent beating, often with poor co-ordination and lack of full sweeping motion [8]. It is now accepted that it is failure of co-ordination, or appropriate ciliary beat pattern, that

results in impaired mucociliary clearance rather than merely a slowing in the rate of ciliary beating [16,17]. Indeed some PCD patients may have normal ciliary beat frequency [16] but a lack of mucociliary clearance.

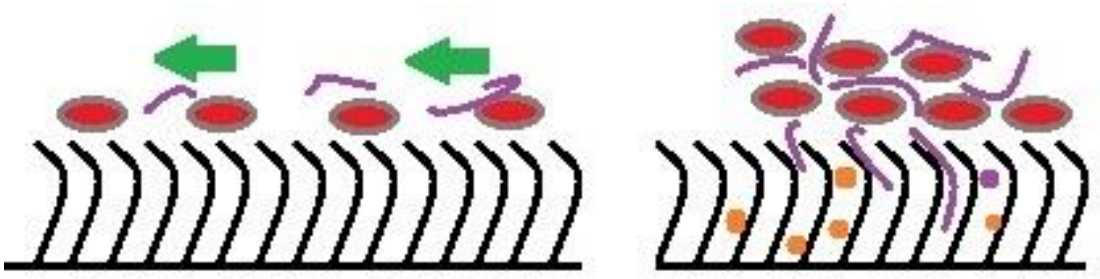

Figure 1-3. **Schematic diagram of mucociliary clearance in human lung**. Normal clearance (left) shows bacteria (red), particulates and mucus (purple) moved towards the mouth, aided by cough clearance. On the right, impaired ciliary action results in aggregation of bacteria and mucus, allowing adherence of bacteria and the potential establishment of biofilm. Bacterial colonisation also causes local inflammatory cells (orange) to be recruited and contributes to airway damage.

Failure of mucociliary clearance allows bacteria to remain in the airways leading to long-term colonisation and the potential for local airway inflammation/damage. The presence of bacteria triggers migration of immune cells, including macrophages and neutrophils. However, these may fail to eradicate the infection and, instead, contribute to ongoing local inflammation at the site of infection, with eventual airway damage. If this process is left unchecked, it can result in bronchiectasis; the irreversible dilatation of scarred, damaged airways. Bronchiectatic airways lack elasticity, have ongoing damage and further impaired mucociliary clearance [18]. Cole originally proposed the "vicious cycle hypothesis" of bronchiectasis where any number of different "insults" (mucociliary clearance defects, immune dysfunction, severe acute infection) result in persistence of microbes within the airway causing chronic inflammation and further impairment of mucociliary clearance [19]. This process is common to both PCD and cystic fibrosis (CF), however it is unclear whether the predisposition in PCD is purely lack of mucociliary clearance or other factors increase bacterial persistence and local inflammation.

1.1.2 Pathophysiology of ciliary dysfunction in PCD

PCD is characterised by a failure of mucociliary clearance, however this may result from a number of different abnormalities in ciliary beat frequency and pattern. PCD results from a

range of genetic mutations that may give rise to a variety of defects in ciliary structure and/or axonemal proteins that lead to ciliary dysfunction. According to the ciliome.com collaboration (www.ciliome.com, searched 12th December 2016) [20], there are around 2000 genes encoding structural, signalling and transport proteins involved in ciliogenesis and cilial function. Therefore, there are a huge number of potential protein abnormalities that could lead to ciliary dysfunction.

1.1.2.1 Genetics of PCD

In 1999, DNAI1 was the first gene for PCD identified [21] and, to date, the number of genes known to be associated with PCD has increased to 35 [22]. Despite this rapid expansion in knowledge, only approximately 70% of PCD patients have an identifiable genetic mutation. DNAH5 mutations account for around 60% of these. These genetic mutations fall into a number of categories that result in either absent or dysfunctional ciliary beating (Table 1-1).

Gene	Structural defect
Abnormalities in dynein proteins	
DNAI1	ODA defect
DNAH5	ODA defect
DNAH11	Hyper-frequent beat abnormalities (normal structure)
DNAI2	ODA defect
DNALI1	ODA defect
NME8	ODA defect
ARMC4	ODA defect
DNAH6	IDA defect, microtubular disorganisation
Genes for assembly or transport of axonemal proteins	
DNAAF1	ODA and IDA defects
DNAAF2	ODA and IDA defects
DNAAF3	ODA and IDA defects
CCDC39	IDA defect, microtubular disorganisation
CCDC40	IDA defect, microtubular disorganisation

CCDC103	ODA and IDA defects
CCDC114	ODA defect
CCDC151	ODA defect
DNAAF5	ODA defect
CCDC65	Normal/occasional microtubular disorganisation
ZMYND10	ODA and IDA defects
SPAG1	ODA and IDA defects
C21orf59	ODA and IDA defects
Central pair abnormalities	
RSPH9	Variable central pair/transposition defects
RSPH4A	Variable central pair/transposition defects
RSPH1	Variable central pair/transposition defects
RSPH3	Variable central pair/radial spoke absence
HYDIN	Normal
DNAJB13	Central pair defects
Nexin-dynein complex defects (normal ultrastructure)	
DRC1	Normal/occasional microtubular disorganisation
GAS8	Normal
CCDC65	Normal
Genes causing PCD with associated syndromes	
OFD1	Unknown
BBS genes	Variable
RPGR	Variable
Genes causing reduced number of motile cilia	
CCNO	Reduced number of cilia but normal beating
MCIDAS	Reduced number and impaired beat pattern

Table 1-1. **Summary of the known PCD causative genes**. Published genes known to be affected in PCD [23]

Since PCD was originally diagnosed solely by detection of ultrastructural defects using transmission electron microscopy (TEM), it is unsurprising that the earliest genetic mutations

identified are those associated with specific ultrastructural defects. The commonest defects identified by TEM in PCD patients are absence of ODA (c.43%), followed by combined ODA and IDA defect (c.24%), IDA defect with microtubular disorganisation (12%), transposition (12%) and radial spoke defects (9%) [24]. Microtubular disorganisation and transposition refer to abnormally placed outer pairs and absence of central pair respectively. Loss of the dynein arms or radial spoke defects result in static or twitching cilia that lack mucociliary clearance [25]. Transposition can lead to circular motion that, despite having a relatively normal beat frequency, does not produce co-ordinated ciliary beating capable of effective mucociliary clearance [25]. In these cases, the genetic mutation results in absence or mislocalisation of the ciliary protein (e.g. DNAH5 and ODA absence). It is also possible for factors involved in transport and construction of cilia to be defective and this results in absence of specific elements from the axoneme (e.g. CCDC39 and ODA/IDA defects). Finally, around 16% of PCD patients have no ultrastructural defect on TEM [23]. Many of the causative genes in these patients affect proteins that are not visible at the resolution of TEM but still affect ciliary beat. The best example of this is the DNAH11 mutation that affects dynein heavy chains and results in normal ultrastructure on TEM but hyper-frequent or twitching ciliary beating [26].

Some recent data has supported some genotype-phenotype (or ultrastructure-phenotype) correlation in PCD. In a UK cohort of 151 adult patients, there was an accelerated decline in those with absence of IDA and microtubular disorganisation [27]. This was supported by data from a US cohort of 118 paediatric patients [28]. Data on RSPH1 mutations suggests mutations in this gene may be associated with a milder phenotype [29,30].

1.1.3 Clinical features of PCD

1.1.3.1 Neonatal period

Patients with PCD commonly have symptoms from birth, with over 75% of neonates with PCD requiring supplemental oxygen for several days or weeks [28,31,32]. As mentioned above, around 50% of PCD patients will have *situs inversus* and approximately 6% show heterotaxy (*situs ambiguus*) where there are abnormalities of left-right patterning in the heart [33]. A small number may present with hydrocephalus (accumulation of excess cerebrospinal fluid (CSF) in the cerebral ventricles) [34] due to the presence of cilia in the cerebral ventricles that contribute to CSF dynamics. Persistent nasal discharge is usually present from birth, as is persistent wet cough [35].

1.1.3.2 Childhood

Lack of mucociliary clearance predisposes to recurrent pulmonary exacerbations with chronic sinopulmonary infection, the microbiology of which is discussed below. Chronic wet cough is a typical feature and the majority of children with PCD develop chronic middle ear infection with effusion [32]. Bronchiectasis may develop as early as infancy [36] but this is rare and is more common in later childhood; indeed the overall incidence during childhood may be as high as 61% [32] with one study showing 22% of children had bronchiectasis at diagnosis [31].

Lung function may be impaired early in childhood with a study of the Danish PCD cohort showing impaired forced expiratory volume in 1 second (FEV_1) (defined as FEV_1 of 59-79% predicted) in 36% of pre-school children (age<6 years) [37]. Although some studies show that this impairment can be stabilised [38], the Danish cohort data does not support this and suggests that lung function may deteriorate, stabilise or improve through childhood for, as yet, unknown reasons [37]. Some of this may be due to the fact that spirometry, using measurement of FEV_1 and forced vital capacity (FVC), is not a sensitive measure of airways disease [39,40]. Green *et al* used multiple breath washout (MBW) to measure lung clearance index (LCI) in the same Danish cohort and found this was abnormal in 81% of children [41].

1.1.3.3 Adulthood

It is common for the diagnosis of PCD to be missed until adulthood. Despite increasing awareness of the disease, in a 2010 survey of European PCD centres, 10% of patients were diagnosed at 15 years of age or older [2]. A greater proportion of those diagnosed in adulthood have bronchiectasis, indeed this is a common reason for referral and can affect up to 98% of adult PCD patients [32]. Adult patients also present with diminished lung function as measured by FEV_1 and FVC [38]. Data on life expectancy and accurate fertility data are not known.

Although PCD usually has a less severe disease course than CF, lung disease can be severe and progressive with up to 25% of adult PCD patients in the USA in respiratory failure [32] and some patients progressing to lung transplantation [42].

1.1.4 Diagnosis of PCD

1.1.4.1 Ultrastructural defects

Early diagnosis of PCD was initially by transmission electron microscopy alone, relying on the identification of specific, visible, defects in the cilial structure when viewed in section. However, it is now known that only around 70% of PCD patients have an identifiable ultrastructural abnormality [24] as described in 1.1.2.1. Some mutations such as RSPH1 cause variable TEM findings [30,43]

Since 30% of patients are known to have no identifiable structural abnormality, their diagnosis relies on other tests.

1.1.4.2 Ciliary beat abnormalities on video microscopy

TEM analysis is now, usually, paired with high speed video analysis of ciliary beat frequency and pattern [23]. Nasal brushing samples are viewed under a microscope at 100x magnification, with video recording undertaken at around 500 frames per second (fps), before being viewed at 30fps. Beat frequency can then be measured alongside ciliary beat pattern and co-ordination assessment. Normal frequency is 11-20Hz [17] at 37^{o}C with PCD cilia either static, slow or hyper-frequent. Beat frequency can be normal with abnormal beat pattern [17].

A recently described variant of PCD is reduced generation of motile cilia (RGMC) [44,45]. CCNO mutations affect the basal bodies and lead to a reduced number of normally beating cilia on the cell surface leading to a disease phenotype that is, typically, more severe than classical PCD [45]. Mutations in MCIDAS result in impaired control of CCNO leading to cilia that are both reduced in number and dyskinetic; this also results in severe lung disease [44]. RGMC can result in diagnostic difficulties as both video and electron microscopy rely on the identification of a sufficient number of cilia for analysis.

1.1.4.3 Nasal nitric oxide

In 1994, Lundberg *et al* discovered that patients with PCD had significantly lower nasal nitric oxide (nNO) levels than healthy controls [46]. This was confirmed by a number of subsequent studies [47]. Nasal NO screening is a highly sensitive and specific tool in those aged over 6 years of age using velum closure techniques [48,49]. The recent advent of portable nitric oxide analysers has meant wider adoption of nNO screening is possible, however there have yet to

be sufficient studies with these analysers to set disease specific cut-offs and there is a lack of standardised operating protocols [47,50]. Likewise, nNO is lower in young children making it less discriminatory in this age group alongside the difficulties in getting young children to co-operate with the testing [47].

1.1.4.4 Other diagnostic tests

In addition to those described above, a number of other tests are available but not in routine practice in the UK. These include genetic testing (which is standard in many European countries and the US/Canada (1.1.2.1), mucociliary clearance tests [51] and immunofluorescent staining of specific ciliary proteins [52].

1.1.5 Bacterial colonisation in PCD

A lack of normal mucociliary clearance makes PCD patients susceptible to chronic infections of the lung. Although data on colonisation rates are not as readily available as in CF, it seems these two diseases share many of the same culturable organisms [32,53,54]. It is also important to distinguish the organisms that are cultured by conventional means following expectorated or induced sputum samples from the total range of organisms in the lung, termed the microbiome [55,56].

1.1.5.1 Colonisation rates in PCD

In 2004, Noone *et al* published on the phenotypic features of PCD patients in the US and found that of 15 paediatric patients studied, 80% grew NTHi at some time and 46% grew *Staphylococcus aureus* [32]. *Pseudomonas aeruginosa* is known to be associated with accelerated lung function decline in CF patients [57] and possibly PCD patients [53] and, in the Noone *et al* study, was seen in 20% of patients at some time. However only 1 child grew the chronic form that is termed “mucoid” and is virtually impossible to eradicate [58]. By adulthood, *H.influenzae* rates had dropped to 22% and *S.aureus* to 14%, whilst mucoid *P.aeruginosa* had increased to 27%. A small Italian study by Santamaria *et al* included 13 children and 6 adults with PCD, of which 12 children were positive for *H.influenzae* (92%) and 2 for *S.aureus* (15%) [59]. Adults rates were 67% and 0% respectively [59].

More recent European data from 105 patients in France showed *H.influenzae* rates peaking in early childhood (around 30%) then falling into adulthood (to around 10%). *S.aureus* increased throughout childhood to around 15% by 22-24 years of age, with a similar pattern seen in

P.aeruginosa. This study also noted a high prevalence of *Streptococcus pneumoniae* in children that decreased by adulthood [53].

Data from an Israeli study in 34 PCD patients aged 2 to 32 years showed *H.influenzae* colonisation rates of 65% with *S.aureus* (MSSA and MRSA) at 24% [60], whilst the Danish PCD cohort studied 107 patients aged 0-74 years with 5450 cultures over 11 years and found *H.influenzae* to be the most frequent pathogen isolated. The next most common were *P.aeruginosa, S.pneumoniae, Moraxella catarrhalis* and *S.aureus* [61].

Davis *et al* studied 118 paediatric PCD patients over 6 years and 22% were colonised with *H.influenzae* (the commonest pathogen) [28]. There was no correlation between colonising pathogen and ultrastructural defect [28].

Shah *et al* described a UK adult cohort of 151 patients and cumulative colonisation rates over the follow-up period of 7 years. 42% of patients were colonised with *H.influenzae* at some point and 44% were culture positive for *P.aeruginosa.* Interestingly, there was no correlation between *P.aeruginosa* colonisation and accelerated lung function decline but FEV_1 was lower at diagnosis if the patient was already colonised with *P.aeruginosa*.

These studies are summarised in Table 1-2 but are consistent in identifying *H.influenzae* as the commonest pathogen isolated in adults and children with PCD.

Study	Patients	H.influenzae	S.aureus	S.pneumoniae	P.aeruginosa
Noone *et al* 2004	31 children	80%	46%	NR	20%
	47 adults	22%	14%	NR	27%
Santamaria *et al* 2008	13 children	92%	15%	15%	0%
	6 adults	67%	0%	0%	33%
Lefeuvre *et al* 2014	105 (3-29y)	65%	17%	48%	NR
Cohen-Cymberknoh *et al* 2013	34 (2-32y)	65%	24%	NR	41%
Alanin *et al* 2015	107 (0-74y)	NR	NR	NR	39%
Davis *et al* 2015	118 children	22%	19%	14%	9%
Shah *et al* 2016	151 adults	42%	20%	26%	44%

Table 1-2. **Summary of colonisation rates in PCD**. Reported rates of culture-positive sputum in adult and paediatric PCD patients. NR-not reported. [27,28,32,53,59–61]

1.1.5.2 Microbiome

Advances in DNA sequencing have allowed the study of the full range of bacteria in the lower airways of patients and not just those that are culturable by conventional means. This usually involves sequencing of 16S ribosomal DNA that is not present in humans and is unique to each bacterial species. Whilst the lower airways were traditionally thought to be sterile, these studies have shown there to be numerous species of bacteria present in both healthy and diseased lung. Also, rather than individual bacterial species resulting in clinical features, characteristics of the bacterial community such as variety and relative abundance are related to disease outcomes [55,62].

The only study, to date, of the PCD airway microbiome was undertaken by Rogers *et al* in Southampton and involved 24 PCD patients aged 4 to 73 years [56]. Over a 7 month period, 26 expectorated sputum samples and 7 bronchoalveolar lavage (BAL) samples were collected and analysed by conventional culture and using 16S ribosomal qPCR. The commonest genera detected in lower airway samples from patients were *Streptococcus* (n=21), *Neisseria* (n=20), *Haemophilus* (n=20), *Prevotella* (n=20) and *Veillonella* (n=20). Staphylococcal species were detected in 11 patients. However this does not reflect the relative abundance of these genera in each patient and the predominant genera (bacterial species present in the highest quantity in each patient) identified were *Pseudomonas* (n=5), *Neisseria* (n=5), *Ralstonia* (n=4), *Haemophilus* (n=4), *Streptococcus* (n=2) and *Prevotella* (n=2). Of course, this reflects a small sample of PCD patients across a wide age range, which may not be representative of children or adults with PCD. It does, however, confirm the presence of *Haemophilus* genera in the majority of PCD patients' microbiomes. Interestingly, the microbiome was shown to be relatively stable over time.

1.2 Cystic Fibrosis: potential insights into PCD epithelium

If lung disease in PCD is caused purely by deficiencies in mucociliary clearance, then the innate immune response to bacterial colonisation should be preserved. However, the disease process may also cause other, unanticipated, defects in epithelial responses. For example, extremely

low airway nitric oxide is an almost universal feature in PCD regardless of the causative mutation. Similarly, cystic fibrosis is a chronic suppurative lung disease with many similarities to PCD that has a range of dysfunctional epithelial responses as a consequence of the underlying mutation. These dysfunctional responses give insights into potential sources of epithelial dysfunction that may exist in PCD airway.

Cystic fibrosis (CF) is an inherited disorder of chloride transport that affects over 10,000 people in the UK, giving it an incidence of around 1 in 2500 [63] that has been extensively studied in comparison to PCD. Disordered response to infection in CF would not be predicted from the initial functional disease-causing airway change (abnormal solute channel function), therefore close examination of the pathogenesis of CF lung disease may provide possible insights into the PCD lung.

As they are both characterised by chronic suppurative lung disease with persistent wet cough and bronchiectasis, PCD is often been treated in much the same way as CF. However, there is a paucity of evidence that this should be the case [64] and evidence is now building that lung disease in PCD is different in nature to that seen in CF [60]. Research into PCD has lagged behind CF, largely due to PCD being a rarer and underdiagnosed disease with no diagnostic gold standard test. This meant that many patients were not identified and it was difficult to gain sufficient numbers to conduct detailed studies into PCD. This has changed in recent years with Figure 1-4 showing the increase in the number of PubMed citations that have “primary ciliary dyskinesia” in the title over the last 27 years.

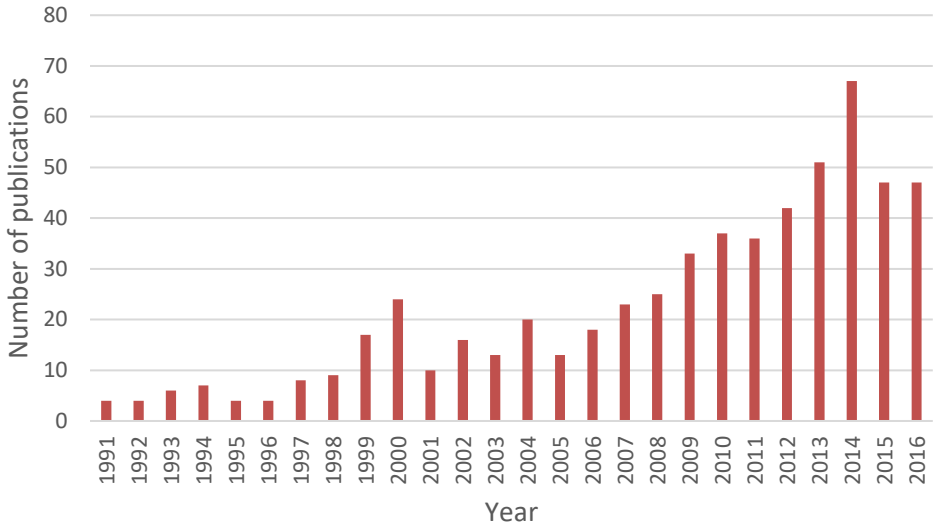

Figure 1-4. **Number of indexed publications per year in PubMed with "primary ciliary dyskinesia" in the title**. 2016 data up to 30/9/16

However, this is still small when compared to the number of papers with cystic fibrosis in the title (Figure 1-5). Even taking into account the fact that the incidence of PCD is about ¼ that of CF [1,2] there is a disproportionate focus on CF and, therefore, there is a much larger body of evidence to examine in CF.

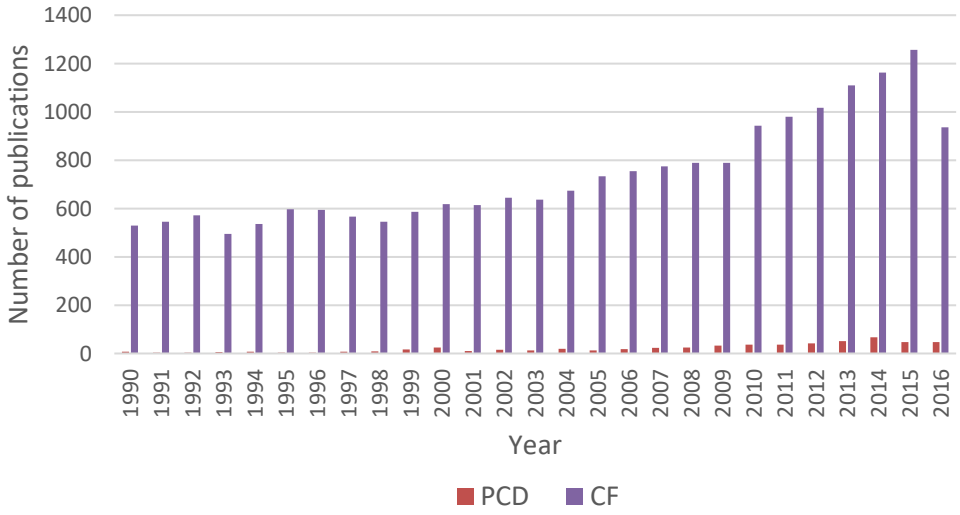

Figure 1-5. **Number of indexed publications per year in PubMed with "primary ciliary dyskinesia" or "cystic fibrosis" in the title**. 2016 data up to 30/9/16.

1.2.1 Cystic fibrosis versus PCD

1.2.1.1 PCD insights from physiological airway changes in CF

CF is caused by mutations in the gene coding for the cystic fibrosis transmembrane conductance regulator (CFTR). CFTR is primarily responsible for cyclic adenosine monophosphate (cAMP) dependent chloride transport across epithelial cell membranes. The commonest mutation causing CF is a deletion of the codon for phenylalanine (F) at position 508 of the CFTR gene, previously termed ΔF508 and now renamed to p.Phe508del [65]. Patients who are homozygous for p.Phe508del account for around 52% of UK patients and over 90% of patients have at least one p.Phe508del mutation [63]. In total there have been over 1900 other mutations identified in the CFTR gene [66], many of which have a variable phenotype that is dependent on the "class" of mutation. In PCD, however, these classes of mutation may each occur in any of the known or, as yet, unknown PCD-associated genes (currently 35 different genes accounting for around 2/3 PCD patients [23]). Using the underlying genetic mutation to study PCD pathogenesis is, therefore, much more difficult.

The net result of dysfunctional CFTR is impaired chloride (Cl^-) efflux [67] leading to increased sodium (Na^+) influx, via CFTR control of epithelial Na^+ channels (ENaC) [68], and defects in bicarbonate ion transport (HCO_3^-) [69]. However, current evidence points to at least 2 separate downstream effects of mutations in CFTR; impaired mucociliary transport and defects in antimicrobial activity that together result in progressive CF lung disease [70]. PCD certainly has the former but it is not known if PCD patients have constitutional defects in antimicrobial activity.

One of the main sequelae of failure of CFTR ion transport is a reduction in the airway surface liquid (ASL) layer on the airway epithelial cells. The ASL depletion leads to concentration of mucus and colonisation with typical CF organisms, including *H.influenzae* [71]. A reduction in ASL, as well as dysfunction of this layer, may set up an environment that is ripe for bacterial colonisation and potentially initiates early inflammation in the CF lung independent of bacteria. PCD does not seem to have intrinsic defects in the periciliary fluid, however lack of ciliary motion, bacterial colonisation and inflammation may affect the airway surface layer.

Failure of mucus clearance is common to both PCD and CF. In CF, thickened, difficult-to-clear mucus forms plugs within the airway, encouraging bacterial colonisation in a number of ways. The thickened meshwork within the plugs favours biofilm rather than mobile planktonic

growth [72] along with increased binding of bacteria to mucins [73]. The thickened mucus layer also inhibits defence mechanisms by limiting movement/diffusion of neutrophils and antimicrobial substances [74] (1.4.1).

Evidence from piglet models of CF may go some way to explaining why CF lung disease is more severe than PCD despite CF mucociliary clearance being normal early in life. Although particle clearance seems to be identical in CF and wild-type airways, following cholinergic mucus secretion CF submucosal glands produce strands of mucus that remain anchored to the glands [75,76]. This interferes with the usual cleavage of mucins by host/bacterial proteases prior to removal by the mucociliary escalator. Although PCD airways lack mucociliary clearance, cough remains effective as the mucus is less adherent to the epithelial surface. CF airways may also be more acidic than in PCD, which promotes sustained inflammation and inhibits bacterial clearance[77,78].

It is not known whether PCD airways are inherently pro-inflammatory or if inflammation is all secondary to infection. CFTR dysfunction alone seems to play a role in the pro-inflammatory state of CF airways, with CF infants showing increased induction of IL-8 and tumour necrosis factor (TNF) compared to healthy infants even in the absence of infection [79]. Of particular significance to this work is the role of CFTR related changes in toll-like receptors (TLRs), nuclear factor kappa B (NF-κB) signalling and type 1 interferon responses [80]. TLRs are particularly important pattern recognition receptors that sense the presence of bacteria and mediate the host response to colonisers such as *S.aureus, H.influenzae and P.aeruginosa* [81].

Finally, recent work has involved genome-wide association studies (GWAS) in CF patients. Meta-analysis of 2 of these studies by Corvol *et al* found 5 loci that modify disease severity in CF patients. The 5 loci were associated with genes coding for mucins, ion transporters, *P.aeruginosa* susceptibility and an HLA region associated with lung function variation in CF and other diseases [82]. There may be similar disease modifiers in PCD that are related to the severity of lung function decline without being related to the disease-causing mutation.

1.2.1.2 Differences in clinical course

The introduction of newborn screening (NBS) in London reduced the average age at diagnosis for CF (excluding those with meconium ileus) from 2.4 years to 3 weeks [83]. By contrast, the average age for diagnosis of PCD in Europe is 5.8 years for those without *situs inversus* and 3.5 years for those with [2].

Despite both being classified as chronic suppurative lung diseases, CF and PCD differ in their presentation and disease progression. CF patients are often diagnosed through newborn screening, a prospect which is still some way off for PCD [22]. Those not picked up by screening often present with failure to thrive in infancy due to pancreatic insufficiency or may present with persistent wet cough. PCD patients usually have a productive cough from birth along with neonatal rhinitis (nasal discharge) and often have neonatal respiratory distress [84].

PCD tends to follow a less severe course, demonstrated by the fact that many patients are not diagnosed until well into adulthood [2]. PCD is not, however, a uniform disease and there is a burden of morbidity and mortality that includes respiratory failure, need for lung transplantation and premature death [42]. This, partially, reflects the multitude of different genes and mutations causing PCD, however the reasons for the different disease progression in CF and PCD remain unclear.

1.2.1.3 Early bacterial colonisation

Despite differences in pathophysiology, early bacterial colonisation in PCD and CF is by a similar, restricted range of pathogens. *H.influenzae* and *S.aureus* are amongst the commonest early colonisers in both diseases, along with *P.aeruginosa* (Figure 1-6).

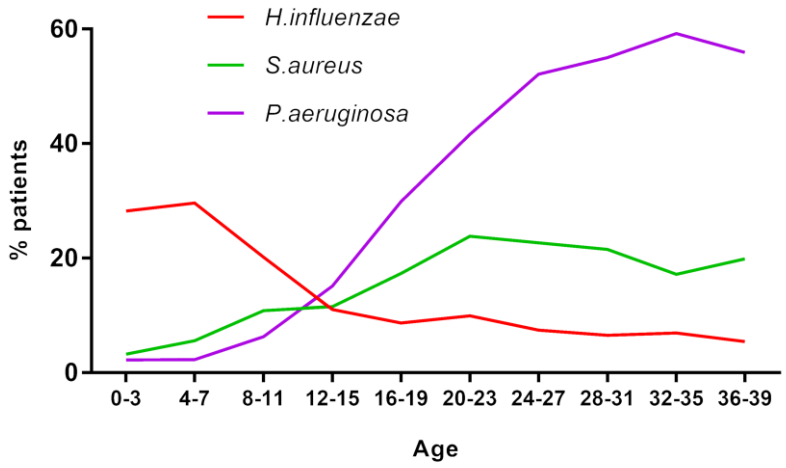

Figure 1-6. **Bacterial colonisation rates in cystic fibrosis**. Rates are cross-sectional by age group and are patients with 3 repeated cultures that are positive for the same organism (chronic colonisation). Adapted from Cystic Fibrosis Trust Report 2015 [63].

As described in 1.1.5.1, there is a paucity of data on PCD patients, but broad patterns of colonisation are similar to that seen in CF with early *H.influenzae* infection that wanes once *P.aeruginosa* rates increase. *S.aureus* increases throughout childhood [32]. A number of studies have also noted a high prevalence of positive cultures for *S.pneumoniae* in PCD patients compared to CF [32,56,59], though the significance of this has not been confirmed.

Application of next generation sequencing (NGS) techniques to the microbiome of CF and PCD lower airway samples has provided insights into the wide range of organisms that co-exist in the lungs of these patients. The only study, to date, in PCD by Rogers *et al* is described in 1.1.5.2 and confirms the presence of *Haemophilus* genera as well as a range of other dominant genera including Neisseria and Streptococcus [56]. This was, however, a small study across a wide age range. More studies using NGS have been done in CF and have revealed similar pathogens to Rogers *et al* study in PCD, with exception of Ralstonia which was seen in greater abundance in the PCD microbiome [56]. Interestingly, a study by van der Gast *et al* also showed remarkable similarities in early microbiome of children with CF, non-CF bronchiectasis and persistent bacterial bronchitis [85] suggesting common airway changes that allow these bacteria to colonise. The microbiome in PCD and CF also seems to be stable over time and is modified only briefly by acute exacerbations or treatment with intravenous antibiotics [56,62,86]. This raises the possibility that similar species colonise all chronic suppurative airways and that it is minor changes in microbiome composition, along with changes in host response, that determine disease course.

There are currently clear guidelines produced by the Cystic Fibrosis Trust on the treatment of positive bacterial cultures from CF patients [87] that include recommendations for aggressive treatment of *H.influenzae, S.aureus and P.aeruginosa*. Guidelines do not exist for PCD, largely due to a paucity of evidence of the long-term clinical implications of colonisation by these bacteria; although evidence is emerging that *P.aeruginosa* colonisation has similar damaging effects on lung function in PCD as it does in CF [53]. As a result, PCD patients' treatment is often based on a combination of CF guidelines and clinician preference and there is, therefore, a need to define the role of these bacteria in PCD lung disease.

1.2.1.4 Differences in mucociliary clearance

As described in 1.1, failure of effective ciliary function characterises PCD. However, patients with CF appear to have preserved ciliary function in the early stages of the disease with impairments related to infection and inflammation [88]. Locke *et al* used inhaled radionucleotide tracers to study mucociliary clearance in 24 adult CF, 9 paediatric CF and 9 healthy patients [89]. There was no significant difference between CF and healthy patients where there was no history of *P.aeruginosa* colonisation. In CF patients with any positive *P.aeruginosa* culture from sputum or throat in the previous 2 years, mucociliary clearance was significantly reduced compared to both healthy and *P.aeruginosa* negative patients [89] . This is backed up by previous studies on CFTR -/- mice that showed *P.aeruginosa* infection significantly impaired particle transport rates in the lung [90]. Human studies of mucociliary clearance in CF, however, have provided equivocal results with some showing increased transport rates in CF, some no change and some showing a decreased transport [88].

1.2.1.5 Studies directly comparing CF and PCD

There has been little direct work comparing these two diseases, despite the reliance on CF research in the treatment of PCD. Cohen-Cymberknoh *et al* compared 34 patients with PCD to 88 with pancreatic-insufficient CF (CF-PI) and 42 pancreatic-sufficient CF (CF-PS) patients, including both paediatric and adult patients in all groups [60]. CF-PS patients have, generally, milder lung disease and sufficient CFTR activity to preserve pancreatic exocrine function. Both groups of CF patients showed the previously described correlation between increasing age, decreasing FEV_1 and more severe lung disease (as assessed by chest CT scan). However, PCD patients did not show the same association between FEV_1 and CT findings; FEV_1 was often normal even in those with severe lung disease on CT. Distribution of lung disease on CT also differed with PCD favouring the lower lobes and CF the upper lobes. CF patients showed a correlation between *P.aeruginosa* infection and FEV_1 decline but PCD patients did not. Overall, not only did PCD patients tend to have less severe lung disease, the authors concluded that the underlying mechanisms were likely to be different [60].

Santamaria *et al* compared high resolution CT (HRCT) scans of 20 PCD patients and 20 age-matched CF controls. They found more severe lung disease in CF patients and, unlike Cohen-Cymberknoh, some correlation between FEV_1 and CT in PCD patients [59].

Constituents of CF and PCD mucus have been compared by a small number of studies. Bush *et al* compared mucus properties and IL-8 concentrations in 19 PCD and 30 CF patients. They found that IL-8 concentrations were significantly higher in PCD sputum than CF but there were no differences in the physical or transport properties of the mucus [91]. This goes against the theory that CF lung disease is more severe due to thicker, more viscous mucus and the inherent pro-inflammatory nature of CFTR deficient cells. Recent data has backed up these findings as Grasemann *et al* studied 13 CF and 11 PCD patients aged 5.8 to 17.9 years undergoing exacerbations with culturable *H.influenzae* or *S.aureus*. They found more neutrophils and higher neutrophil elastase activity in PCD sputum than in CF [92]. However, following oral antibiotics these markers were significantly reduced in PCD sputum but not in CF. Interestingly, those with *H.influenzae* had significantly greater IL-8 and neutrophil elastase levels than those with only *S.aureus* or normal flora, despite similar quantities of neutrophils in sputum [92].

Nitric oxide is low in PCD airways, particularly nasal NO, and CF patients appear to have levels that are lower than healthy patients but not as low as PCD [32,49,93]. This represents another potential difference in the microenvironment of the PCD and CF airways.

Therefore, the question remains as to whether CF and PCD epithelium are colonised by similar bacteria because they share dysfunctional immune responses to these organisms. Alternatively, these organisms, particularly NTHi, may colonise all compromised airway epithelium and differences in epithelial immune response is responsible for the long term differences in clinical outcomes between PCD and CF.

1.3 Epithelial responses to bacterial infection

The epithelial lining of the airway was originally thought to act simply as a physical barrier to the entry of microbes and other toxic agents, however, it has become clear that the epithelium plays a more active role in protecting the lung. The primary defence mechanisms are mucus production, mucociliary clearance (including cough), recruitment of immune cells (e.g. macrophages, neutrophils), and secretion of antimicrobial peptides. Innate immune dysfunction may be impaired in CF and could account for the more severe lung disease seen when compared to PCD [80]. Although the lower airways were originally thought to be sterile, modern DNA sequencing techniques have shown that numerous bacterial species co-exist in the airway and the epithelium is integral to the complex task of differentiating harmless

commensals from pathogens [94]; this also causes difficulties in characterising appropriate epithelial responses to pathogens and commensals.

Mucociliary clearance is discussed above and the immune cell recruitment will not be discussed in detail as the air-liquid interface model employed in this work lacks these adaptive responses.

Airway epithelium plays an active role in innate defences beyond its barrier function. The epithelium consists of a pseudostratified layer of ciliated and unciliated cells that arise from the basal cells beneath. These basal cells are also the progenitors of secretory cells within the epithelium. The epithelium also has secretory, serous, Club, neuroendocrine and goblet cells that secrete a range of mucins and anti-microbial peptides including lysozyme, lactoferrin [95], β-defensins [96], leukoprotease inhibitors, peroxidase [97], LL-37 [98] and nitric oxide (see 1.6.1.1). The submucosal glands secrete defense proteins and are regulated in response to injury or infection.

Mucus production within airways is also an important innate defense mechanism. Mucins are glycoproteins produced by goblet cells, club cells and within submucosal glands. These linked mucins form a barrier to colonisation as well as carrying bacteria on the mucociliary escalator [99]. Many mucins are tethered to the epithelium and cleaved by host/pathogen proteases to trap bacteria before removal; this process may fail in CF airways and result in permanently tethered mucus [75,76].

Epithelial barrier function is also important in innate airway immunity. Rather than forming a static barrier to ingress, the permeability of the epithelium is highly regulated by control of tight junctions between epithelial cells [100]. Gap junctions between cells allow propagation of paracrine signals, ions and intracellular signals. Within gap junctions, there are connexins that have a role in co-ordinating ciliary motion by propagating calcium and inositol triphosphate signals [101,102], as well as playing a role in regulating mucus production [103] and innate immunity. Cx43 is a connexin essential for activation of NF-κB via toll-like receptor 2 (TLR2) causing IL-8 release and recruitment of neutrophils [104,105]. The role connexins play in calcium waves may link TLR2 activation to ciliary co-ordination. Gap junctions appear to be important in TLR2 responses and, interestingly, CFTR deficient cells seem to lack effective control of this activation pathway and this may contribute to the pro-inflammatory nature of CF epithelium [106,107]. The calcium/gap junction/TLR axis, therefore, provides a potential

mechanism for impaired epithelial response to infection in cells with dysfunctional cilia. It has also been shown that response to NTHi is mediated by TLR2/NF-κB [108,109] and TLR2 deficient mice more susceptible to both *S.aureus* [110] and *S.pneumoniae* infection [111]. This raises the possibility that TLR dysfunction partially explains the dominance of these organisms and NTHi in the early bacterial colonisation of PCD patients.

As well as the barrier, mucus and mucociliary clearance functions, the epithelium also recognises and responds to specific pathogens by initiating host responses. Epithelial cells are able to bind pathogen-associated molecular patterns (PAMPs) via pathogen recognition receptors (PRRs). PAMPs are usually highly conserved microbial elements such as lipopolysaccharide (LPS) that are essential for pathogen survival and, therefore, cannot be downregulated by pathogens in an attempt to avoid detection by host immunity. The commonest PRRs found on epithelial cells are toll-like receptors (TLRs) and nucleotide-binding and oligomerization domain (NOD)-like receptors (NLRs) [112]. TLRs exist in the membranes of both the cell surface and intracellular compartments and vary in the PAMPs they bind; for example TLR2 mentioned above can bind bacterial cell wall components whilst TLR7 is endosomal and recognises foreign nucleic acid [112]. TLRs trigger signalling pathways such as NF-κB that initiate the pro-inflammatory response [113]. As mentioned above, TLRs have an important role in response to NTHi [108,109], *S.aureus* [110]*, S.pneumoniae* [111] *and P.aeruginosa* [104], and are implicated in dysfunctional response to infection in CFTR-deficient cells [106,107]. NF-κB is also implicated in increased expression of the mucin MUC5B, which could account for mucus dysfunction in CF [114].

Airway epithelium also generates nitric oxide via the enzyme inducible nitric oxide synthase (iNOS) in response to infection. This is discussed further in 1.6.1.1.

1.3.1 Epithelial response to NTHi infection in PCD

Little is known about specific epithelial responses in PCD lung, however work by Walker undertaken in Southampton compared cytokine responses in PCD, healthy and 16HBE immortalised epithelial cells co-cultured with a 72 hour NTHi biofilm. No significant differences were seen when comparing PCD and healthy epithelium secretion of FGF, G-CSF, GM-CSF, IL-1ra, IL-8, VEGF, TNFα and MIP1a at 24, 48 or 72 hours [115]. The use of a virally transformed, immortalised respiratory epithelial cell line (16HBE cells) on which to grow the NTHi biofilm, showed significantly reduced cytokine responses, particularly for IL-8 [115], an important cytokine present in PCD and CF inflammatory processes [92], reinforcing that

immortalised cell lines do not, necessarily, accurately reflect *in vivo* responses. Walker also measured levels of the cationic antimicrobial peptide LL-37 with a slightly higher level produced by PCD on day 1 but no statistically significant differences at any time points [115].

As described in 1.1.4.3, airway nitric oxide is low in PCD. Walker *et al* measured the NO production of PCD and non-PCD cultured respiratory epithelium after 72 hour culture with NTHi. NO levels (measured indirectly via nitrite concentration) were lower in PCD epithelium prior to co-culture, though this was not statistically significant. Both PCD and non-PCD cultures demonstrated an increase in NO production following co-culture with the PCD levels remaining lower than non-PCD but again this was not statistically significant [116]. This contrasts with work by Smith *et al* who used a 2 hour exposure to *S.pneumoniae* and showed no increase in NO production (detected using an NO probe) in PCD epithelium whilst healthy epithelium increased significantly. They also measured NOS2 expression and found this to be increased in healthy but not PCD epithelium which could partly explain the failure of PCD epithelium to increase NO production [117]. Of course, the different bacteria and exposure times may account for these differences, as well as the use of nitrite detection rather than direct NO detection.

1.4 Bacterial biofilms

The human race was long plagued by acute bacterial disease characterised by highly pathogenic planktonic bacteria such as *Yersinia pestis, Vibrio cholerae*, M*ycobacterium tuberculosis, Salmonella typhi* and *Streptococcus pyogenes* (causing rheumatic fever) [118]. The advent of antibiotics meant that these diseases became relatively easily treated in developed countries and, as a result, biofilms now represent a large proportion of the burden of bacterial disease [119]. The ability to form biofilms is common to a large number of bacterial species [120].

Since their first description nearly 40 years ago by Costerton *et al* [121], the definition of biofilm has evolved and remains hotly debated. In 2002, Costerton and Donlan updated the definition to

> *"..a microbially derived sessile community characterized by cells that are irreversibly attached to a substratum or interface or to each other, are embedded in a matrix of*

extracellular polymeric substances that they have produced, and exhibit an altered phenotype with respect to growth rate and gene transcription."[122]

Bacterial biofilms consist of bacteria embedded within a self-secreted matrix of polysaccharides, proteins and DNA that, along with a slow growing phenotype, make bacteria more resistant to innate and acquired immunity, as well as antibiotics [123]. Biofilms are formed in response to external stressors such as hypoxia, nutrient deprivation or competing pathogens [124,125].

Biofilms are characterised by a relatively sessile state in the bacteria that adhere to either inert surfaces (e.g. indwelling catheters, tracheostomy tubes), within aggregates or adherent to live tissue. By adopting a more slow-growing and metabolically inactive state, the bacteria are more resistant to immune cells, antibiotics and attack from other bacterial species [126]. The bacteria produce an extra-cellular matrix (ECM) that helps to form the structure of the biofilm and acts as a barrier to ingress of immune cells. The ECM also inhibits the action of antibiotics by impeding antibiotic diffusion, targeting β-lactamase production, repelling anionic antibiotics (e.g. tobramycin) via anionic moieties with the ECM and modifying the local environment to impair mechanism of action (e.g. acidification) [127]. These biofilms also show cross-talk and co-ordination through differential gene expression and signalling to allow nutrient trafficking and triggering of dispersal of bacteria back to the planktonic state [128].

Biofilm disease is found in heart, teeth, middle ear infections, prosthetic joints, bone, chronic wounds and all types of indwelling catheters/stents [129]. Biofilms are a barrier to *Pseudomonas aeruginosa* eradication in CF and increasing evidence suggests that biofilms are also important in persistence of NTHi [130,131] (1.5.1).

1.4.1 Biofilms in respiratory disease

Biofilm formation has been shown to play an important role in the upper and lower airway diseases such as otitis media, chronic rhinosinusitis and CF [129]. The most extensively studied species in CF is *P.aeruginosa* which chronically infects the lungs of CF (and PCD) patients and results in decreased lung function [132]. Initial culture-positive infections can be cleared with aggressive antibiotic treatment, however once it has adopted a "mucoid" form it is virtually impossible to eradicate. The term mucoid refers to the appearance of cultured colonies on agar and represents the switch to a highly resistant biofilm mode of infection [130]. The mucoid appearance is largely due to upregulation of alginate production [133].

1.4.1.1 *Pseudomonas aeruginosa* as the respiratory biofilm exemplar

P.aeruginosa colonisation of CF airways is, perhaps, the most widely studied respiratory biofilm and is often used as an exemplar of biofilm formation mechanics. *P.aeruginosa* biofilms in CF lungs were first identified over 35 years ago as mucoid colonies within sputum samples [134]. These were subsequently found to be biofilms surrounded by polymorphonuclear leukocytes (PMNs) that have been recruited in response to infection [135,136]. Failure of the PMNs to clear the bacterial biofilm contributes to ongoing inflammation and tissue damage. Additionally, *P.aeruginosa* is seen to induce necrosis of PMNs *in vitro* via secretion of rhamnolipid [137] resulting in *P.aeruginosa* biofilm aggregates surrounded by necrotic PMNs [133]. A study of post mortem lung from CF patients infected with *P.aeruginosa* showed abundant biofilm in the conducting airways along with a large number of PMNs. Interestingly, the biofilms were present as small aggregates with very few bacteria (under a thousand) and were not attached to the respiratory epithelial surface [133].

In vitro studies of *P.aeruginosa* biofilm show that bacteria attach to a surface and develop into microcolonies by secreting extracellular matrix consisting of polysaccharides, proteins and DNA [138]. Three main polysaccharides are involved; Psl, Pel and alginate, with the latter being detected in high quantities in CF lung [139]. This high level of alginate leads to the presence of a particular colony appearance of *P.aeruginosa* on culture plates that is termed “mucoid” [140]. Psl appears critical to attachment both *in vitro* and *in vivo* [141] with Pel playing a secondary role but remains important for colony formation at an air-liquid interface [142]. Extracellular DNA (eDNA) also forms part of the matrix and is derived from lysed bacterial cells [143] and dead neutrophils/secreted neutrophil extracellular traps (NETs) [144].

Cyclic diguanosine-5’-monophosphate (c-di-GMP) is believed to be central to the control of *P.aeruginosa* biofilm formation. High levels of c-di-GMP lead to increased production of adhesins and extracellular matrix, whilst low levels promote biofilm dispersal [145]. c-di-GMP is synthesised by diguanylate cyclases (DGCs) and broken down by phosphodiesterases (PDEs) (Figure 1-7), both of which have sensory domains that can respond to external stimuli [146]. C-di-GMP acts via four effector proteins (Alg44, FimX, PeID and FleQ) and has been shown to directly promote the extracellular matrix proteins Pel, Psl and alginate described above [145,147]. Specific PDEs have also been linked to biofilm formation in response to nutrient deprivation [148], hypoxia [149] and nitric oxide [150,151].

Figure 1-7. **Cyclic-di-GMP metabolism in *P.aeruginosa***. c-di-GMP is generated from 2 GTP molecules by diguanylate cyclases with GGDEF domains; degradation involves phosphodiesterases containing HD-GYP and EAL domains. Increase in c-di-GMP levels promotes biofilm formation whilst a drop favours motility, virulence and biofilm dispersal. [242]

Another characteristic feature of biofilms is quorum sensing (QS); signalling between different bacteria within a biofilm microcolony alongside more localised production of substances that are trafficked to the biofilm as a whole [152]. For example, when *P.aeruginosa* form "mushroom shaped" colonies *in vitro*, the cap grows using substances provided by the stalk, including the Pel exoprotein [153]. Additionally, the size and structure of biofilms means there is a gradient of nutrients, oxygen and pH across the colony resulting in differential metabolic activity [154]. This is an important consideration when studying an *in vitro* or *in vivo* biofilm *en masse* such as when extracting DNA or proteins from an entire biofilm.

QS in *P.aeruginosa* is mediated by 3 systems, two of which use N-acyl-homoserine lactones (HSL) with the other using quinolones [155]. The first of the HSL systems is termed the Las system and is usually the first to be activated, whilst the other HSL system is Rhl as it is responsible for expression of rhamnolipid [156]. The quinolone system is mediated via the Pseudomonas quinolone signal (PQS) with the three systems interacting such that Las stimulates Rhl and PQS, PQS activates Rhl and Rhl inhibits PQS [157]. In addition, environmental stimuli, nutrient availability and the presence of other bacteria alter the expression profile of these signals [158]. This complex sensing of environment and resulting changes in physiology across the bacterial colony allows *P.aeruginosa* to evade immune attack and to tolerate antibiotics [159]. Presence of QS in human *P.aeruginosa* infections has been shown by screening 200 isolates from urine, lung and wound; only 5 strains lacked Las activity and these were found to be poor biofilm formers *in vitro* [160].

As mentioned above, much that has been learnt about *P.aeruginosa* biofilms through *in vitro* growth on abiotic surfaces. However, there is evidence to suggest that airway *P.aeruginosa* biofilms are not attached to a surface, but rather exist embedded in mucus [73].

P.aeruginosa biofilms seem extremely adept at avoiding PMN killing, as well as inducing PMN necrosis [133] through rhamnolipid [137] and using PMN derived NETs to enhance biofilm structure [161]. The structure of the biofilm also resists ingress of neutrophils and macrophages [161]. *P.aeruginosa* sheds flagella once in a biofilm, which prevents binding of PMNs and macrophages whilst the alginate also interferes with this process [162]. *P.aeruginosa* also actively secretes substances such as pyocanin that interfere with immune function [163].

Biofilms are also tolerant to antibiotics. This differs from antibiotic resistance which is specific, genetically determined mechanisms that disrupt the mechanism of action of antibiotics. Biofilm tolerance exists through physical and physiological changes associated with biofilm formation. Certain antibiotics such as aminoglycosides (gentamicin, azithromycin, tobramycin) and floroquinolones (ciprofloxacin) target metabolic processes in the bacteria and are, therefore, less effective against the metabolically downregulated bacterial population in a biofilm [154]. Although these bacteria remain susceptible to antibiotics that disrupt the cell membrane (e.g. colistin), even if the vast majority of bacteria within the biofilm are killed there seem to be small populations of persister cells that retain the ability to repopulate [164]. Additionally, the extracellular matrix itself can resist antibiotic attack; by being negatively charged the matrix repels positively charged antibiotics such as tobramycin [165]. Alginate within the matrix also prevents ingress of antibiotics [166].

1.4.1.2 Dispersal and the biofilm lifecycle

As mentioned above, biofilm is highly regulated by quorum signalling in response to stimuli such as hypoxia, nutrient stress and reactive oxygen/nitrite species. However, this process is part of the continuous life cycle of biofilm forming bacteria involving seeding, biofilm attachment/formation, growth, maturation and dispersal as depicted in Figure 1-8.

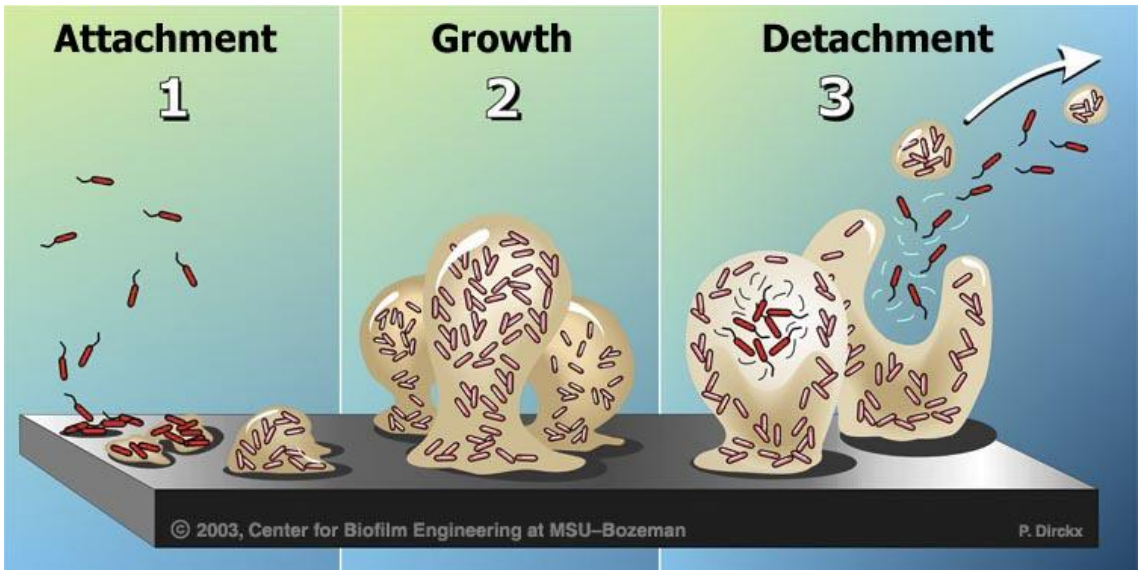

Figure 1-8. **Life cycle of biofilm forming bacteria**. 1) Planktonic bacteria attach to a surface or aggregate and begin to secrete extracellular matrix/eDNA and assume a more slow-growing phenotype. 2) Growth of the biofilm continues with sessile bacteria replicating slowly within the organised matrix. 3) Within the mature biofilm, populations of bacteria from the centre of the microcolony revert to a more planktonic phenotype. Signals from outside and within the microcolony are detected and cause breakdown of the matrix with release of the planktonic bacteria as well as shearing of colonies of biofilm encased sessile bacteria. *Reproduced with permission from Montana State University Center for Biofilm Engineering.*

Dispersal from within mature biofilm microcolonies has been described as a size-related phenomenon. Microcolonies of *P.aeruginosa* that reached around 80µm in a flow-cell model initiated seeding dispersal [140] (as opposed to passive shearing of biofilm from the external surface). Dispersal also occurs in response to external triggers such as external nutrient availability [167], scarcity of nutrients within the microcolony [168] or hypoxia [149].

Nitric oxide has been implicated in the control of this dispersal mechanism in a number of bacterial species. Initially dispersal in *P.aeruginosa* was noted to occur alongside generation of reactive oxygen intermediates and reactive nitrogen intermediates (RNI); NO is one type of RNI [169]. By exposing *P.aeruginosa* biofilms to non-toxic levels of NO (500nM sodium nitroprusside), Barraud *et al* noted biofilm dispersal and increased susceptibility to tobramycin [150]. As switching from sessility to motility had previously been linked to guanyl cyclase domains (GGDEF) and EAL phosphodiesterases (PDEs) via their role in regulating cyclic-di-GMP levels, the Barraud group then noted increases in PDE activity and a fall in c-di-GMP associated with NO-induced dispersal of *P.aeruginosa* biofilm [170]. NO-induced dispersal was also seen in *E.coli, Serratia marcescens* [171], *S.aureus* [172] and multi-species biofilms [171]. Later work by Heine *et al* found a specific locus termed NO-induced biofilm dispersal locus A (NbdA),

consisting of an MHYT domain, that can detect NO and is bound to GGDEF and EAL domains [151]. This constitutes a potential NO sensing domain in *P.aeruginosa,* as this species lacks the more common H-NOX (Heme-Nitric Oxide/Oxygen) domains that detect NO and are found in a wide range of prokaryotes and eukaryotes [173]. NO may also target redox metal sites such as heme or sulphur containing complexes [174] with iron levels having a potential role in biofilm dispersal [175], including direct modulation by NO [176]. Another region that is critical for biofilm dispersal in *P.aeruginosa* is the biofilm dispersion locus A (*bdlA*), with *bdlA* mutants unable to disperse and displaying elevated c-di-GMP levels [177]. The LapG protease may also be involved in NO dispersal since *P.aeruginosa* deficient in LapG does not disperse in response to exogenous NO [170]. The possible dispersal mechanisms in *P.aeruginosa* are summarised in (Figure 1-9).

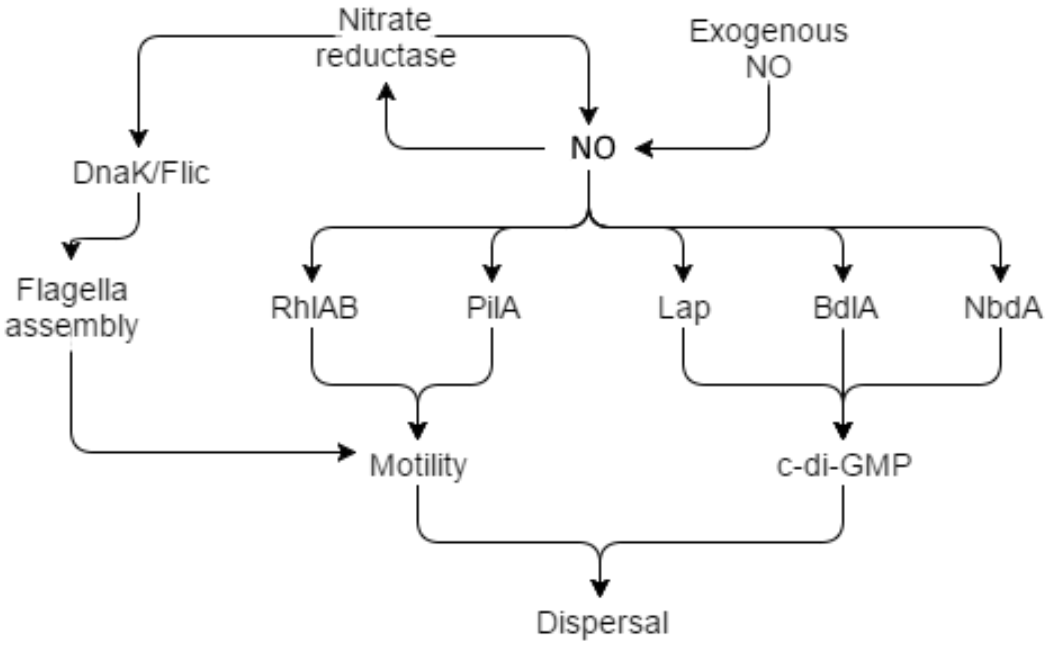

Figure 1-9. **Summary of potential control of dispersal in *P.aeruginosa*.** Nitric oxide (NO) may be generated by nitrite reductase (NIR) or be external. NO results in decreased c-di-GMP levels through the NbdA and BdlA activation of phosphodiesterases (and potentially the Lap system). NO also upregulates pili (PilA) and rhamnolipid (RhlAB) to increase motility. NIR may also have an NO independent role in motility via Dnak/Flic associated stimulation of flagella assembly. [487]

1.4.2 Models used to study biofilm formation

Much of the knowledge of bacterial biofilms has arisen through the study of biofilm growth on inert surfaces such as glass or polystyrene. These models use a non-biological surface submerged in fluid that is either static or under continuous flow. This approach has allowed

high-throughput approaches to assessing biofilm mass/attachment in response to a range of stimuli. Use of knockout strains of bacteria has also provided insight into the roles that motility, quorum sensing and virulence factors play in biofilm attachment, structure and antibiotic tolerance [138,159,178]

Although the growth of biofilm on abiotic surfaces may be relevant to certain clinical situations, such as catheter-associated infections, these *in vitro* models do not correlate with the *in vivo* biofilm formation seen in the lung. For example, *P.aeruginosa* biofilms *in vitro* grow as adherent, thick biofilms that include water channels between "mushroom" structures [179]. However, *P.aeruginosa* biofilms from CF airways are not attached to the epithelial surface but instead found within mucus and surrounded by neutrophils. These aggregates are also much smaller than *in vitro* biofilms [133]. These differences have important consequences for conclusions drawn from *in vitro* studies, particularly those that conclude specific factors are essential for biofilm formation when these are associated with attachment of *in vitro* biofilm which is not a feature of *in vivo* biofilm. Despite these differences, Alhede *et al* compared biofilms formed within aggregates in culture media (unattached to a surface) with those from a flow-chamber, surface attached model and found similar growth rates, matrix components and tolerance to antibiotics [180]

In vitro models have also shown the importance of nutrient and oxygen gradients across biofilms that lead to regional variation in growth rate and virulence [181], however studies using FISH to monitor *P.aeruginosa* growth rates showed growth was related to concentration of neutrophils rather than aggregate size in both human CF lung and mouse models of *P.aeruginosa* infection [136]. It is, therefore, important to consider the lack of these components in *in vitro* (and some *ex vivo)* biofilm models when extrapolating to *in vivo* biofilm behaviour.

A number of animal models have been developed to study *in vivo* biofilm associated respiratory tract infections. The chinchilla model is used in acute otitis media [182], rat/mouse models for lung infection [136,183] and porcine models in CF [184]. Of course, it is desirable to limit the use of animals in research and use of these models comes with their own set of practical issues and inter-species differences in immune response. *Ex vivo* airway models are, therefore, an attractive prospect for studying epithelial-biofilm interaction.

1.5 Haemophilus influenzae

H.influenzae is a gram negative coccobacillus belonging to the *Pasteurellaceae* family that is a non-motile, facultative anaerobe. *H.influenzae* is categorised according to its capsular polysaccharides (a-f) or termed non-typeable if it lacks the capsule (NTHi). It gained the label *influenzae* as it was wrongly attributed as the cause of influenza prior to the identification of the influenza virus in 1933 [185]. It is also notable in being the first free-living organism to have its entire genome sequenced (1,830,140 base pairs) [186]. *H.influenzae* are pleomorphic, showing spherical, oval, coccobacilli or rod-shaped morphologies and can occasionally form filaments or threads. They vary in size at around 0.4-1.0µm in diameter by 2µm in length [187]. *H.influenzae* require X-factor (protoporphyrin IX/hemin) and V factor (nicotinamide adenine dinucleotide, NAD) for growth, both of which are found in lysed red blood cells. The requirement for V factor, which is released by *S.aureus* means that *H.influenzae* will show satellitism; growth within the haemolytic zone of *S.aureus* colonies. The requirement for X and V factors necessitates growth on chocolate agar, producing flat/slightly convex and non-pigmented smooth colonies This requirement for factors X and V is not found in all *Haemophilus* species and is not unique to this genus, therefore other biochemical reactions can be used to classify the bacteria; *H.influenzae* are Kovac's oxidase test (for presence of cytochrome oxidase) positive and have variable catalase, urease, ornithine decarboxylase and indole-test positivity; nitrates are reduced beyond nitrites. Unlike some other *Haemophilus species, H.influenzae* does not cause β-haemolysis on a blood agar plate. *H.influenzae* are capable of fermentation of glucose, galactose and xylose but not fructose, lactose, mannose or sucrose [187]. Differentiation between capsular and non-typeable strains can be achieved using the agglutination test with polyvalent antisera (antibodies to the capsule antigens a-f) [187]. Growth can occur at temperatures as low as 25°C but is optimal at 35-37 °C in a CO_2-enriched environment. These conditions are reflective of the fact that *H.influenzae* are obligate parasites of the mucous membranes of the respiratory tract, mouth, and vagina. Although the optimum pH for growth is said to be around 7.6 [187], this can vary with strain and site of isolation of the bacteria [188]. For example, isolates from middle ear infection (otitis media) seem to favour an alkaline environment [188]. Studies of the typical antibiotic sensitivity of *H.influenzae* show that this species is typically sensitive to penicillins (MIC_{50} 0.25-0.5µg/ml), cephalosporins (0.0004-4µg/ml), macrolides (1-8µg/ml) and quinolones (0.004-0.03µg/ml) [189]. However, many strains possess/acquire antibiotic resistance mechanisms

such as β-lactamase, β-lactamase negative penicillin resistance (usually penicillin-binding-protein alterations), efflux pumps (macrolides, penicillins) and ribosomal alterations (macrolides, tetracyclines) [189],

Although the lack of a capsule leads to strains of NTHi being grouped together, these strains are genetically heterogeneous with a large redundant genome. For example, some NTHi strains have the genes necessary for capsule synthesis whilst others do not [190]. Although not used widely in clinical practice, it is possible to classify NTHi strains using a technique known as multilocus sequence typing (MLST) that defines strains by single nucleotide polymorphisms within housekeeping and 16S rRNA genes [191]. This approach has been useful in analysing clinical outbreaks [192] and identifying mechanisms behind antimicrobial resistance [193]. The heterogeneity in NTHi strains also highlights the difficulties in developing vaccines against these pathogens since this genetic diversity even extends to outer membrane proteins [194].

When entering the respiratory tract NTHi initially come into contact with mucus, and those bacteria that are not cleared by the mucociliary escalator bind to this mucus layer. Indeed, NTHi may directly inhibit ciliary function through secretion of bacterial lipooligosaccharide (LOS) [195] and protein D [196] in order to reduce this clearance. Exposure to NTHi culture supernatant induces upregulation of protein kinase C in epithelial cell cultures, resulting in decreased ciliary beat frequency and a reduction in the number of ciliated cells [197]. Immunogobulin A (IgA) plays an important part in the defence of the respiratory epithelium by inhibiting adherence and interacting with humoral defences. Many strains of NTHi posesses IgA1 proteases that cleave IgA and negate its effect on the bacterium, however these proteases are not essential for pathogenicity [198,199].

If mucociliary clearance of the NTHi fails then a number of surface structures and receptors mediate attachment to the epithelium. Although non-motile, NTHi possess hemagglutinating pili that are hair-like projections from the cell surface [200] and may assist in binding to damaged areas of epithelium [201]. This may partially explain the ability of NTHi to colonise patients with a wide range of lung diseases that have degrees of epithelial damage. However, non-piliated strains of NTHi are still able to bind to the epithelium, therefore there must be other cell-surface adhesins that are important [202]. Two such proteins are the high-molecular weight (HMW) proteins 1 and 2 that are found in NTHi but not in capsulated *H.influenzae* [203,204]. Returning to the wide genetic diversity in NTHi strains mentioned above, 25% of NTHi strains lack HMW expression [205] but these strains are still able to adhere to the epithelium. This preserved binding is potentially due to the presence of *H. influenzae* adhesin

(Hia) that is present in around 80% of HMW1/2 deficient strains. These HMW1/2 deficient strains usually possess pilus expression so there is a need for some, but not all, of these surface proteins to bind the epithelium [205]. Even strains of NTHi without pili, HMW1/2 or Hia still retain some epithelial binding capacity which may be due to the product of the *hap* gene (Hap protein) which shows many similarities to the IgA1 proteases mentioned above but without the same capacity to cleave IgA [206]. In addition it seems that heat shock protein 70 (HSP70) expressed at the bacterial surface is able to bind to the epithelial surface [207]. So, in summary, NTHi possess a range of surface receptors that mediate binding to the epithelial surface, however not all strains express all of these adhesins. There is also evidence that, since these adhesins are highly immunogenic [208] they are essential to establish colonisation but trigger a florid immune response. Data from CF supports this as expression of adhesins was highly correlated with chronic colonisation, in particular there was association between Hia and biofilm formation [209]. Chronic colonisation subsequently results in bacterial changes that attempt to evade host immunity. For example, *H.influenzae* exhibit phase variation that results in loss of pili expression [200] and downregulate HMW1/2 in response to the immune response [210].

NTHi can invade the epithelium, a process that is partially mediated by the Hap protein described above [199,211]. Once within the epithelial cell, the NTHi can both evade extracellular immune responses and access intracellular nutrients such as sequestered iron.

NTHi also possess a range of outer membrane proteins (OMPs) that may have a role in binding to epithelium as well as a range of other cellular functions. Although there have been over 30 identified OMPs, the majority of those present at the cell surface are P1, P2, P4, P5 and P6 [212]. The numbering system reflects the decreasing molecular weight of the predominant proteins identified on gel electrophoresis. Whilst these proteins perform a range of functions including epithelial adherence [213], evasion of host immunity [214] and porin activity [215], they also induce strong antibody responses in the host [216–218]. NTHi thus alters the structure of these proteins during the course of colonisation in order to evade the host response [219]

Lipopolysaccharide is a feature of Gram-negative bacteria and is composed of a lipid anchored in the cell wall and a polysaccharide extracellular chain. In the case of NTHi these chains are slightly shorter and termed oligosaccharides, thus NTHi possess lipooligosaccharides (LOS). LOS seems to play a role in adhesion to the epithelium with higher molecular weight forms

better at adhering to the epithelium but also being more immunogenic [220]. Switching to lower molecular weight LOS, as well as other structural variation contributes to evasion of host immunity following colonisation [220].

NTHi triggers the immune response of the respiratory epithelium via a number of receptors. The importance of TLR2 is discussed in 1.3, however the other interactions are shown in Figure 1-10, highlighting the importance of NF-κB. It is unclear how the balance between NTHi and lung is altered during colonisation or acute infection, however NTHi seems particularly adept at proliferating in diseased lung. For example, COPD is the fourth commonest cause of death worldwide [221] and NTHi has been identified as a major cause of lung inflammation and exacerbations [222,223]. An IgE-mediated reaction to NTHi may also contribute to the bronchial hyper-responsiveness seen in COPD [224]. Interestingly, COPD patients have impaired macrophage function, therefore clearance of NTHi may be impaired [225]. Aside from the role it plays in COPD, CF and PCD lungs (1.2.1.3), NTHi is also the commonest pathogen isolated in persistent bacterial bronchitis in children [226] and in bronchiectasis patients of all ages [227].

The intracellular response to NTHi is primarily via NF-κB activation (Figure 1-10), which increases airway inflammation and may be exacerbated by other cytokines that NTHi induces the epithelium to secrete [228]. TLR2 (1.3) is also important in stimulating the production of TGF-β and EGFR growth factors [229]. Under normal circumstances, this inflammatory response is carefully controlled to prevent host damage, particularly via deubiquitinases downregulating NF-κB [230,231]. An alteration in the balance of this inflammatory process during disease may be responsible for the colonisation and inflammation in the lower airways of chronic suppurative lung disease patients.

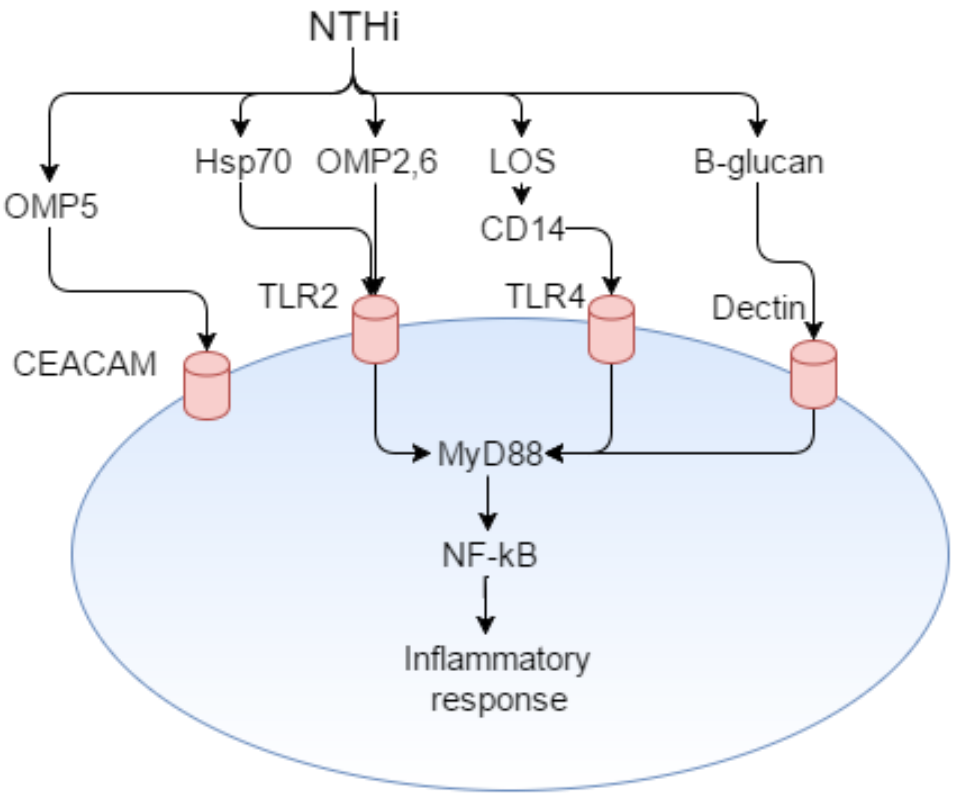

Figure 1-10. **Non-typeable *Haemophilus influenzae* major receptor interactions with respiratory epithelium**. NTHi causes activation of TLR2, TLR4 and dectin receptors that upregulated MyD88 activity and result in an increase in transcription of NF-κB, which then switches on transcription of pro-inflammatory mediators. CEACAM binding increases CD105 levels and inhibits shedding of epithelial cells by the host. CEACAM- carcinoembryonic antigen-related cell-adhesion molecules; TLR, toll-like receptors; HSP70, heat shock protein 70; LOS, lipooligosaccharide; MyD88, myeloid differentiation antigen 88; NF-κB, nuclear factor κB; OMP, outer membrane protein. [233]

H.influenzae is a common commensal in the upper respiratory tract with NTHi being found in the upper airway of up to 80% of healthy children [232]. Although this carriage is usually completely asymptomatic [232], defects in host response can result in otitis media, chronic rhinosinusitis and migration to lower airways to cause chronic lung infection [233]. The burden of NTHi disease is relatively high in children; it is identified in 55-95% of cases of acute otitis media, 44-68% of bacterial conjunctivitis, 41% of bacterial sinusitis and 81% of persistent bacterial bronchitis [234]. In adults, NTHi is in 20-94% of bronchial lavages from community-acquired pneumonia patients, in the blood of 2-10% of patients with bacteraemic pneumonia and present in sputum in over 90% of acute exacerbations in chronic obstructive pulmonary disease (COPD) [234].

When looking at *Haemophilus* colonisation and inflammatory markers in sputum, PCD patients colonised with *H.influenzae* had significantly greater IL-8 and neutrophil elastase levels in

sputum than those with either oral flora or *S.aureus* [92]. This reinforces the idea that once NTHi colonises the lower airways it is part of a pro-inflammatory micro-environment.

The response of host tissues to NTHi is discussed further below under an analysis of proteomic studies in NTHi (1.8.2), however Baddal *et al* used RNA sequencing of primary cultured respiratory epithelium and NTHi. The host underwent cytoskeletal remodelling and innate immune upregulation, whilst NTHi modified virulence and adapted to the host response [235] (Figure 1-11). This model does, however, appear to mimic a florid acute infective process with 100% epithelial cell death at 72 hours.

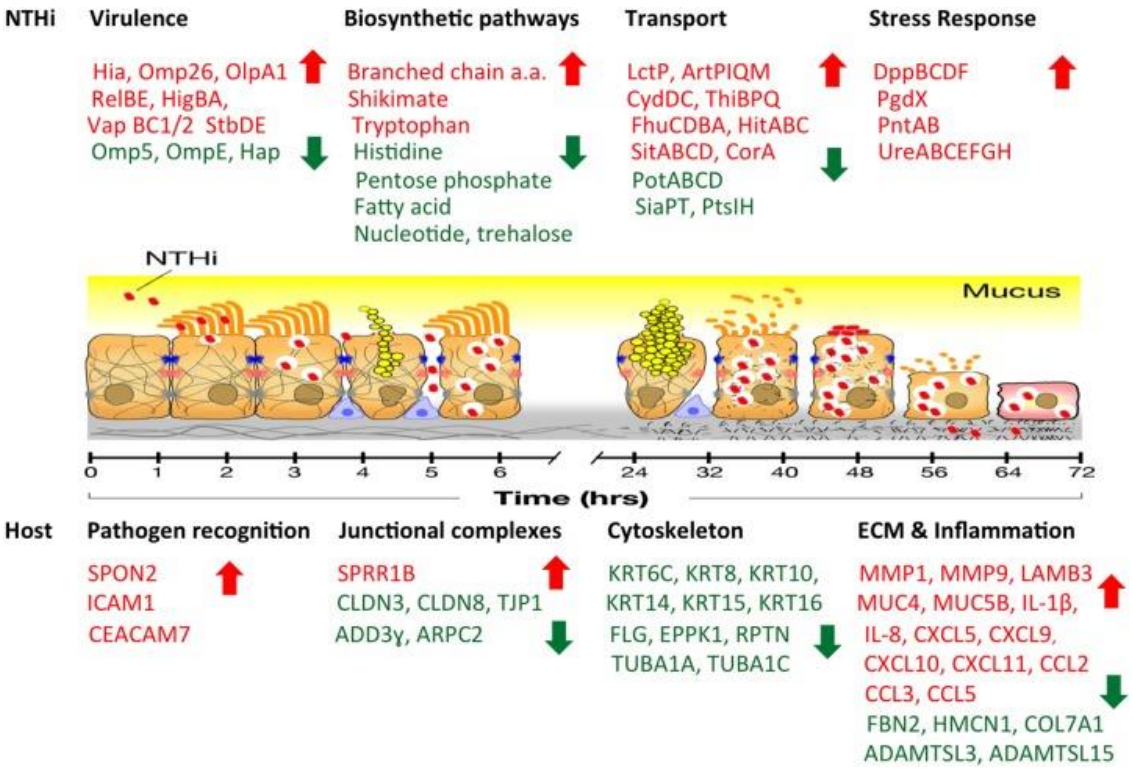

Figure 1-11. **Summary of NTHi and host changes during NTHi infection of bronchial epithelial cells.** NTHi virulence factors are upregulated during early infection but are modulated by 72 hours to promote persistence. Host responses by changes in cytoskeletal rearrangement, changes in junctional complexes and an innate immune response. Model used an acute otitis media strain of NTHi that induced cell death by 72 hours. *Reproduced with permission from American Society for Microbiology* [383].

NTHi seems to have the ability to either asymptomatically colonise or trigger extensive inflammation depending on the prevailing host environment. This is exemplified in a study by Hasegawa *et al* of 1005 infants under 1 year who were hospitalised for bronchiolitis (a viral infection causing inflammation of the lower airway). The authors analysed the nasopharyngeal

microbiota of these infants using 16S ribosomal sequencing and found that dominance of *Haemophilus* was associated with a higher risk of admission to intensive care than *Moraxella*, *Streptococcus* or mixed profiles [236]. Since these were all infants who were healthy prior to their admission, nasopharyngeal colonisation with *Haemophilus* would have been asymptomatic, however a change in the airway dynamics in the form of viral-induced inflammation may have allowed *Haemophilus* to induce the type of inflammation described above. Allied to the linking of NTHi to COPD, bronchiectasis, persistent bacterial bronchitis and severe asthma as well as the isolation of NTHi from a large proportion of upper and lower airway infections, this suggests that NTHi is an expertly opportunistic pathogen when airway defences are compromised.

1.5.1 Evidence for *H.influenzae* biofilms in disease

Identification of biofilms or biofilm-associated proteins/genes in a number of diseases supports the importance of biofilm formation in NTHi airway disease. NTHi biofilms have been identified on tympanostomy tubes from humans with chronic otitis media, human adenoids from chronic rhinosinusitis patients and in chinchilla models of chronic rhinosinusitis [237]. Hall-Stoodley *et al* examined 50 middle ear mucosa biopsies from 26 children undergoing tympanostomy tube placement [238]. 46 of 50 biopsies had evidence of biofilm formation on confocal microscopy [238]. Those patients who also had middle ear effusions were assessed for *H.influenzae, Moraxella catarrhalis* and *S.pneumoniae* by conventional culture and PCR. Although only 19% were culture positive for bacteria, all were PCR positive with 24/27 PCR positive for *H.influenzae*. This demonstrates that biofilms are present in almost all chronic otitis media infections, that these biofilm infections are often not detected by conventional culture techniques and that *H.influenzae* is the commonest pathogen responsible for these biofilm-associated infections [238].

Additionally, biofilm associated NTHi gene expression is seen in sputum from COPD patients positive for NTHi [239] and NTHi is able to form biofilms on a cultured respiratory epithelium [131]. Another study took 50 different NTHi isolates from otitis media, conjunctivitis, CF and non-CF lower respiratory tract, and found that all isolates had the ability to form *in vitro* biofilms [240]. In a cohort study of 300 Italian CF patients followed over 5 years, 21% grew NTHi at some point, yielding 79 isolates. All 79 were able to form biofilms on plastic [209].

NTHi also exhibit quorum signalling that is a key feature of other biofilm-forming bacteria (1.4.1.1). Auto-inducer 2 (AI-2) is a quorum signal common to a number of different bacterial species and is under the control of the *luxS* gene; NTHi mutants of *luxS* show impaired biofilm formation [178]. NTHi also possess AI-2 independent quorum signalling mechanisms such as QseB/C that contribute to biofilm formation [241].

Starner *et al* examined NTHi bronchoalveolar lavage samples from 10 CF patients and found electron microscopic evidence of biofilm formation by NTHi [131]. These isolates were able to grow biofilms on plastic and were successfully co-cultured with Calu-3 immortalised cells at air-liquid interface, forming biofilms with decreased susceptibility to antibiotics and initiating chemokine and cytokine responses from the epithelial cells [131]. Growth of NTHi biofilm has also been confirmed on primary epithelial cells at air-liquid interface from PCD patients [116].

Despite the strong evidence that NTHi disease involves biofilm formation, the mechanism behind NTHi biofilm regulation is poorly understood in comparison to *P.aeruginosa* and a number of differences exist in the type of biofilm formed both *in vitro* and *in vivo*. Whilst *P.aeruginosa* and *S.aureus* form adherent biofilms *in vitro*, they seem to form respiratory biofilms that are embedded in mucus and not attached to the epithelial surface [73]; contrastingly *in vivo* NTHi biofilm attaches directly to epithelium [237].

The extensive study of c-di-GMP in *P.aeruginosa* suggests a pivotal role for this molecule in biofilm formation [145] as well as in other bacterial species such as *E.coli*, *Shewanella oneidensis* and *Pseudomonas fluorescens* [242]. However, complete genome sequencing of NTHi (Rd KW20 strain) as well as *H.ducreyi, H.parainfluenzae and H.parasuis,* characterising between 1,711 and 2,021 proteins per strain, found no GGDEF, EAL or HD-GYP domains that perform the cyclase and phosphodiesterase functions central to c-di-GMP metabolism (Figure 1-7) [243]. It is likely that other, as yet unknown, intracellular messengers are involved in NTHi biofilm formation and control. Although a number of bacterial proteins have been implicated in biofilm formation, including nucleases [244], proteases [216], surfaces proteins [213,245], protein D [196], heavy metals [246,247] and DNA binding proteins [248], there has been no identified system linking extracellular signals, intracellular mediators and downstream modulation of dispersal/biofilm formation mechanisms.

1.6 Nitric oxide

1.6.1 Nitric oxide in the human

Nitric oxide (NO) has a wide range of biological roles within prokaryotic and eukaryotic organisms. NO is a signalling molecule in vasculature, innate and adaptive immunity [249], ovulation, immune maturation and many other physiological processes . Its generation in the human host derives from metabolism of L-arginine by one of four enzymes (NO synthases, l-arginine decarboxylase (ADC), arginases and l-arginine:glycine aminotransferase (AGAT)) or by reduction of nitrite. There are three subtypes of NO synthases previously known as neuronal, inducible and endothelial but now termed NOS1, NOS2 and NOS3 respectively. NOS1 is found in nervous tissue and skeletal muscle, whilst NOS3 is found in the vascular endothelium and regulates the vasodilatory effects of NO. NOS2 (iNOS) is the isoform involved in immune responses and present in respiratory epithelium [250]. The generation of NO through NOS2 is shown in Figure 1-12.

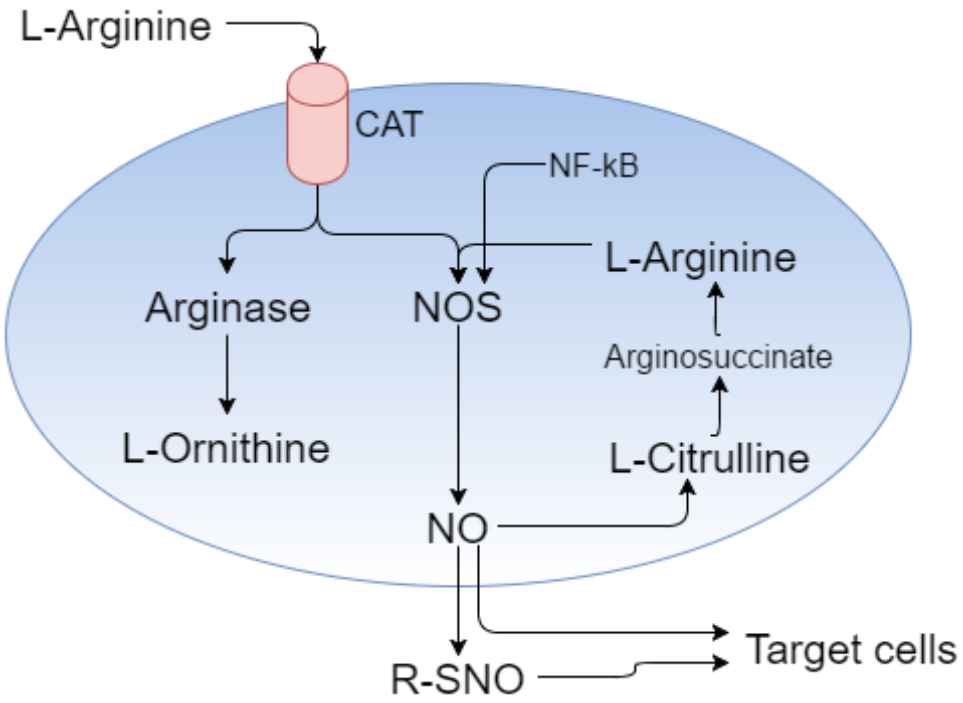

Figure 1-12. **Nitric oxide (NO) generation.** L-arginine is metabolised by arginase or nitric oxide synthase (NOS) after entering the cell via the cationic amino acid transport (CAT) system. NO acts either directly on the target cell or via binding to thiol groups to generate S-nitrosothiols (R-SNO). NOS2 (inducible NOS) is upregulated by external factors, including NF- κB. [260]

1.6.1.1 NO in response to infection

NO generated by NOS2 (iNOS) has a role in the differentiation and maturation of T cells, B cells and NK cells [251]. However, within the respiratory epithelium, NO is also employed as a direct antimicrobial response when generated by dendritic cells, neutrophils and eosinophils [252,253]. By interfering with a number of different biological systems within the bacteria, the metabolic activity can be sufficiently impaired to allow elimination by the host immune system. NO may also trigger dispersal of biofilms to enhance host killing of bacteria (1.4.1.1) [254]. NOS2 is induced by a variety of extracellular signals, such as LPS and cytokines, leading to tyrosine kinase activation and an increase in NF-κB.

1.6.1.1.1 Airway epithelium and NO

NO has been shown to regulate a variety of functions within the airway including smooth muscle tone, ciliary function, electrolyte transport, mucus secretion, barrier maintenance and innate defense mechanisms [255]. NO appears to have wide ranging signalling roles through transcription factor activation, gene expression and post-translational modification.

NO was first studied in vasodilatation following its identification as the endothelium-derived relaxing factor (EDRF) [256,257]; work that earned a 1998 Nobel prize. This vasodilatory role is present in the pulmonary vasculature and is utilised in treating pulmonary hypertension [258]. NO also mediates bronchodilation via nonadrenergic noncholinergic (NANC) nerves [259].

Despite the fact that NOS2 has been found in alveolar type II cells, fibroblasts, smooth muscle cells, mast cells, neutrophils and chondrocytes in the airway [260], NO in exhaled breath seems to be almost entirely derived from the epithelium [261] with exhaled NO levels closely correlated with NOS2 activity in patients [262]. Earlier studies in mice suggested an important role for macrophage-derived NO in airway immunity however, in contrast to mouse macrophages, human macrophages express little NOS2 and have a highly methylated NOS2 transcription site (preventing transcription) [263]. Also, TLR2 activation in macrophages appears to cause NO-dependent responses in mice but not in humans [264]. Unlike the conducting airways, macrophages are important for host defense in the alveolus, where their cytokine production is inhibited by NO [265]. It is likely that PCD alveoli do not have lower NO levels than healthy patients [266], therefore it is at the conducting airway level where differences in NO occur.

The role of epithelial NO in the innate response to bacterial infection has also been demonstrated. Darling *et al* took epithelial cell lines from a CF patient and transfected them with NOS2. *P.aeruginosa* adherence was significantly reduced on the cells expressing NOS2, as was uptake of *P.aeruginosa* into the cells [267].

As mentioned in 1.3.1, Walker *et al* demonstrated that cultured epithelial cells produce NO in response to NTHi infection and pro-inflammatory cytokines (IL-1β,interferon-γ and tumour-necrosis factor-α) [116]. The response was seen in both healthy and PCD epithelium. This contrasts with Smith *et al* 's work with *S.pneumoniae* on cultured epithelial cells; NO and NOS2 increased in healthy but not PCD cells [117]. It should be noted that Smith *et al* used only a 2 hour co-culture period with *S.pneumoniae*, in contrast to Walker's 72 hours with NTHi. Also, Smith *et al* used direct detection of NO whilst Walker *et al* measured nitrite as a surrogate of NO.

Epithelial response to NTHi is largely dependent on TLR2 and downstream increases in NF-κB (Figure 1-10). In turn, NF-κB is the main controller of increased NOS2 levels in response to

infection. Therefore, there is a potential role for differences in NO production in response to NTHi in PCD and healthy lung.

As discussed in 1.1.4.3, nasal NO is used as a diagnostic test in PCD, since PCD patients typically have extremely low nNO levels compared to healthy and disease control patients. This implies that lack of effective ciliary motion leads to low NO levels, however there is a reciprocal relationship in that NO appears to be important in the control of ciliary beating. Bovine airway epithelium treated with NOS inhibitors L-NMMA and L-NAME show a significant slowing in ciliary beat frequency [268]. These inhibitors also blocked bradykinin/substance P stimulation of ciliary beating; an effect that was reversed by L-arginine (NO precursor) and SNP (an NO donor) [268]. There is also no clear correlation with degree of ciliary beating in PCD and nNO level; for example RSPH1 mutations lead to higher nNO levels than usually seen in PCD but there are large areas of static/slow ciliary beating [43] whilst DNAH11 mutations often have a stiff but fast ciliary beating but patients have extremely low nNO [269].

Stimulation of submucosal glands by methacholine, bradykinin, histamine and TNF-α leads to increased mucus production; an effect which is blocked by NOS inhibitors in the guinea pig trachea [270]. This suggests an NO-dependent pathway for increased mucus secretion in response to infection.

There has been some work linking NO to ion channel function in airway epithelium [271] with NO activating apical anion channels and baso-lateral potassium channels. However, it is unclear how this leads to differences in electrolyte balance in the epithelium or ASL in PCD, CF and healthy airways.

CF airways have NO levels higher than PCD but lower than healthy patients (1.2.1.5) and there seems to be dysfunction of NO metabolism within CF airway. Asymmetric dimethyl arginine (ADMA) is a by-product of breakdown of methylated arginine residues within proteins. ADMA inhibits NOS and, therefore, pushes L-arginine towards breakdown by arginase. CF sputum contains increased levels of ADMA compared to healthy sputum, with a decrease in levels following treatment with antibiotics; and ADMA levels are inversely correlated with exhaled NO and lung function [272]. Additionally, NOS produced S-nitrosothiols promote CFTR maturation and function, therefore NOS inhibition by ADMA may further exacerbate CFTR dysfunction [273]. In mouse models, ADMA also contributes to increased reactive oxygen and nitrogen species that exacerbate airway inflammation [274]. It is not known whether ADMA levels are altered in PCD lung and may have a role in low airway NO.

1.6.2 NO in bacteria

A number of bacterial species can use nitrate and nitrite as a source of energy in low oxygen conditions, leading to the generation of NO. Bacteria also employ a number of different strategies to scavenge or reduce the impact of host derived NO [275] and some species possess arginases that can degrade host L-arginine to deplete the available substrate for NO synthesis [276]. There is evidence that this process occurs within the lungs of patients with CF and PCD, including reduced sputum and systemic arginine bioavailability that is worsened during pulmonary exacerbations [272,277,278].

1.6.2.1 NO and bacterial biofilms

NO is known to be involved in the life cycle of bacterial biofilms, triggering the dispersal of established biofilms in species such as *Pseudomonas aeruginosa* [150], *E.coli, Serratia marcescens* [171], *S.aureus* [172] and multi-species biofilms [171]. Upon dispersal, bacteria return to a planktonic state and become more susceptible to antibiotics thus NO is a potential therapeutic adjunct in biofilm treatment. This is discussed further in 1.4.1.1 as it relates to *P.aeruginosa* and the influence of NO on biofilm dispersal via control of c-di-GMP. However, there is also evidence from *S.pneumoniae* that NO may be effective in treating biofilms through changes in metabolic regulation without a dispersal response [279].

Jardeleza *et al* used a sheep model of *S.aureus* in chronic rhinosinusitis (CRS). CRS is a treatment resistant disease involving inflammation of the nasal cavity and sinuses with evidence of bacterial biofilm formation and low NO levels [280]. Jardeleza *et al* used isosorbide mononitrate (ISMN), a long acting NO donor previously used as an anti-anginal, in liposomal form. This was administered directly into the frontal sinuses alongside invasive monitoring of blood pressure and heart rate. The liposomal ISMN significantly decreased biofilm burden assessed using fluorescence in situ hybridisation (FISH) analysis of *S.aureus* [281]. However, 10 minutes after the instillation of liposomal ISMN there was a significant drop in mean arterial pressure and increase in heart rate [281]. Cathie *et al* presented the proof of concept part of a randomised controlled trial of inhaled NO in the adjunctive treatment of *P.aeruginosa* in CF patients undergoing an acute exacerbation. Analysis of biofilm using FISH, CFU counts and qPCR suggested low dose NO was a potentially useful adjunctive therapy in this clinical situation [282], however publication of full trial results are awaited and data on side-effects was not available in the published conference proceedings.

1.6.3 NO and primary ciliary dyskinesia

In 1994 Lundberg *et al* described very low levels of NO in PCD that were most marked in the nasal cavity (nNO) [46]. nNO has subsequently become part of the diagnostic work-up of patients suspected of having PCD [283]. It is unclear why NO is low in PCD, however there is some evidence from CF of increased breakdown by bacteria [284], decreased L-arginine availability [285] and loss of NOS activity due to mechanochemical uncoupling [286]. NOS2 localisation and expression levels appear to be the same in PCD and healthy ciliated epithelium obtained from nasal polyp tissues [287], therefore low NO in PCD does not seem to be due to constitutive low NOS2 expression.

Work has also been done to assess whether lower NO levels in PCD are restricted to the nasal cavity or are present throughout the respiratory tract [266,288–290]. The studies all found that bronchial nNO was reduced in PCD compared with healthy controls. Two studies found alveolar NO was reduced [266,290] whilst two did not [288,289]; this is notable as there are no cilia in the acinar zone so NO levels may also be affected by other mechanisms outside of the cilia. Consistency of findings in the bronchi mean that PCD bacterial colonisation occurs in an airway with reduced NO.

One study has assessed the effects of indirect NO supplementation in PCD. Grasemann *et al* infused PCD patients with L-arginine and saw increases in exhaled and nasal NO but not to the levels seen in healthy controls [285]. It remains unclear what role enhanced NO release could play in treatment of bacterial infections as PCD epithelium cultured at ALI has been shown to be capable of producing NO in the face of *H.influenzae* infection [116].

As described in 1.6.1.1, NO also seems to be important in the control of ciliary beating, mucus production and as a local mediator of innate immunity. This raises the possibility that a number of different airway responses may be aberrant in the low NO environment of the PCD airway.

1.7 Cultured epithelial cells as an airway model

The study of responses to infection *in vivo* present a number of difficulties including sampling of tissues, access to epithelial cells, control of exposure and site of infection. Epithelial-derived cell lines were therefore created to allow easier study of cellular responses, however, Calu-3 and 16-HBE cell lines have been shown to lack some of the immune responses of primary epithelial cells [115,291].

Dvorak *et al* used whole genome transcriptomics to compare airway epithelial cells cultured at ALI with those freshly brushed from the airway and showed a large degree of overlap, with much of the difference accounted for by different proportions of cell type [292]. This was also shown by Pezzulo *et al* who comprehensively studied transcription profiles in primary airway cells at ALI (sourced from both trachea and bronchi), airway epithelium from healthy donor lungs, Calu-3 cell lines at ALI and submerged culture of healthy primary epithelial cells. Not only did cells grown at ALI closely resemble the *in vivo* airway epithelium, but there was remarkable similarity between different healthy donors when looking at samples from the same anatomical site. Primary cells grown at ALI were superior to Calu-3 cell lines and submerged culture in replicating *in vivo* expression. Tracheal and bronchial cells also greatly overlapped [291]. Again, differences were mostly accounted for by slightly different proportions of cell type.

In studies that compared response to immune stimulation and viral infection in brushed cells from the nose versus those from the airway, there was good correlation between the brushing sites [293,294]. However, these are often conducted in the study of asthma/atopic disease rather chronic suppurative lung diseases.

1.3.1 describes work from Walker that demonstrated impaired cytokine responses from immortalised 16HBE cells compared to cultured primary respiratory epithelium. This supports the use of primary cells when studying response to infection.

These findings are important as they suggest nasal cells are a useful surrogate for bronchial epithelium, cells grown at ALI can usefully replicate *in vivo* responses and that, as profiles are consistent between subjects, fewer biological replicates may be needed.

1.8 Proteomic analysis

Proteomics has been part of the rapid expansion in systems biology approaches to biological research (proteomics, genomics, transcriptomics etc.), however the ability to analyse many proteins concurrently was first published as far back as 1975 [295] using 2-D electrophoresis gels to differentiate cultures of *E.coli*. This was later combined with mass spectrometry (MS) and eventually employed a number of MS techniques that are “gel-free”. The fact that the genome of an organism is not translated in a “one gene, one functional protein” manner

means analysis of the cell's proteome can provide insight into functional and structural protein changes that are the ultimate effectors of cellular responses [296].

The ability of MS-based proteomic approaches to analyse huge numbers of proteins simultaneously allows interrogation of systems in a "hypothesis-free" manner [297]. For example p.Phe508del mutations in CF result in mis-folding of the CFTR channel in the endoplasmic reticulum and degradation of this protein [298]. By applying proteomic techniques to cells expressing wild-type and p.Phe508del CFTR, over 200 CFTR associated proteins were identified [299] and termed the "CFTR-interactome". These proteins were responsible for a number of roles including chaperoning the CFTR to the cell membrane and became potential targets to increase functional CFTR levels in the cells of those with p.Phe508del mutations.

Originally, quantification of proteins using MS required some form of metabolic or *in vivo* labelling such as stable isotope labelling by amino acids in cell culture (SILAC) or ^{15}N labelling and stable isotope probing (SIP) [297]. Techniques have also been developed to label without the need to metabolically incorporate the tag into the cell such as isobaric mass tags [300]. These remain the gold standard in quantitation but label free quantification has become increasingly accurate and reduces the complexity of sample preparation [301]. Quantification is achieved by spectral counting and area under the curve (AUC) analysis of the MS output.

1.8.1 Proteomic studies in CF and PCD

To date there is no published work that has used proteomic analysis in the study of PCD. Again, CF provides a useful benchmark as it is rather further ahead of PCD. Proteomics has provided insights into the role and trafficking of CFTR in cells [302], responses to CF-related pathogens such as *P.aeruginosa* [303] and biomarkers of CF-related organ damage [304]. Proteomic analysis of cell lines has revealed a huge number of proteins that are associated with CFTR trafficking and could be potential therapeutic targets [299]. For example, Ciarvardelli *et al* used combined proteomic/ionic analysis to show that CFTR mutations also affect calcium homeostasis and related Zinc cellular influx, adding to the complex nature of CF airway disease pathogenesis [305].

Pankow *et al* also used proteomics to study the CFTR interactome. Using wild-type and p.Phe508del bronchial epithelial cell lines and a co-purifying approach that identified proteins interacting with CFTR, 638 proteins were identified in the core CFTR interactome alongside 915 other potential interactors [306]. Of these, 209 were significantly different in the wild type

and p.Phe508del CFTR, resulting mainly from novel interactions. These proteins were primarily involved in the endoplasmic reticulum mediated degradation of p.Phe508del CFTR. Interestingly, CFTR function could be partially restored using RNA interference to block some of these proteins [306].

Proteomic analysis has also been applied to CF cell lines at ALI. Peters-Hall *et al* showed that, even in the absence of infection/inflammatory stimuli, the apical secretome of CF cells was substantially different in 70 of 666 identified proteins when compared to wild type HBE cells [307].

The studies published have used immortalised cell lines with induced p.Phe508del mutations [308]. There are no studies, to date, that have used proteomics in cultured cells at air-liquid interface in PCD or CF.

1.8.2 Proteomic studies of *non-typeable Haemophilus influenzae*

Post *et al* compared the proteome of planktonic versus *in vitro* biofilm NTHi using a SILAC metabolic labelling approach [309]. They showed a downregulation in proteins associated with metabolism and protein synthesis but a preserved ability to deal with oxidative stress and acquire essential growth factors such as heme and nicotinamide-adenine dinucleotide (NAD). These findings are consistent with those of Qu *et al* who analysed the proteomic expression of NTHi grown from pooled human sputum from patients with COPD [310]. When compared to planktonic NTHi cultures, the sputum strains showed increased expression of antioxidant, stress-response and nutrient uptake proteins.

Preciado *et al* identified 793 proteins in the lysates of planktonic NTHi clinical strain 12 using performed LC/MS proteomics [311]. There was a high degree of variability between batches of NTHi, with only 113 proteins present in all 3 batches. Of these 113, the majority contributed to biofilm formation (high molecular weight proteins), innate immunity evasion (IgA protease) or epithelial PAPs that bind TLR2 (OMP6). All 3 lysates promoted strong NF-κB stimulation in an epithelial cell line [311].

By using sonication, Wu *et al* were able to separate bacteria from biofilm extracellular matrix (ECM) at 24 and 96 hours, followed by protein extraction and LC/MS proteomic analysis [312]. Proteomic analysis was also performed on planktonic bacteria. 18 proteins were found only in the biofilm, of which 7 were membrane associated (OMP1, OMP2, OMP5) and 11 were

metabolic or transcription proteins [312]. They were unable to fully separate ECM from adherent bacteria but did find OMP2 and OMP5 in the soluble fraction of the ECM.

There have been few *in vivo* studies and none in CF or PCD. Das *et al* used a proteomic approach to study the secretome of an NTHi biofilm from the sinuses of a chinchilla model [313] with P2 and P5 outer membranes showing potential as biomarkers of NTHi biofilm formation.

The first application of proteomics looking at host and bacterial responses in infection was performed by Harrison *et al* using the chinchilla model of NTHi in acute otitis media [314]. Chinchillas were experimentally infected with a strain of NTHi isolated from a child with chronic otitis media before removal and lysis of middle ear epithelium. LC/MS analysis of these lysates showed significant changes in actin-associated proteins that may relate to intracellular invasion of NTHi and regulation of pro-inflammatory signalling. Metabolite profiles also suggested a degree of immune suppression by day 2 of infection [314]. The methods used also managed to identify 27 proteins from NTHi that indicated a major role for aerobic respiration during the infective process [314] with only some evidence of proteins identified in NTHi biofilm proteomic studies such as OMP2 and ClpB [311,312]. Although otitis media, particularly chronic OM, is known to be a biofilm disease there is the potential that bacterial responses in these early stages of infection are very different from lung infection, particularly as colonisation of the lung does not appear to be associated with an acute infective stage accompanied by purulent infection and strong host response.

Val *et al* used SILAC proteomics to study the response of epithelial cells to NTHi. Again, an immortalised cell line was used (murine middle ear epithelium) and cells were exposed to a lysate of cultured planktonic NTHi [315]. A proportion of the control epithelial cells were cultured with heavy arginine and lysine to facilitate MS analysis and the treatment samples were then exposed to the lysate for 2 hours and analysed at either 2 days (1 exposure), 4 days (2 exposures) or 7 days (3 exposures) before lysis and proteomic analysis. 2565 proteins were identified in total (with 1596 across all 6 samples). By analysing the 35 most abundant, differentially regulated proteins it was noted that there was an early upregulation in growth of epithelial tissue, proliferation of connective tissue and inflammation pathways (Ingenuity Pathway Analysis) with late (1 week) downregulation of these 3 pathways. Several cytoskeletal keratins were particularly abundant and were upregulated at 48 hours but not 96 hours or 7 days along with an Na+/H+ exchange regulatory co-factor. This study supports the idea that NTHi induces proliferation and cytoskeletal changes in epithelial cells and, as these

were lysates rather than bacteria, this is independent of intracellular invasion [315]. They also identified downregulation of histone and histone-associated proteins, suggesting a process of downregulation of transcription. The same group also published the proteomic analysis of these NTHi lysates, identifying 113 proteins common to all lysates [311]

Both the Val *et al* and Harrison *et al* studies use a model of acute infection of the middle ear, which involves virulent bacteria and severe acute inflammation. Use of bacterial lysates may be particularly immunogenic and induce far greater inflammation than lung colonisation. The publication of the proteome of the lysates should, however, allow comparison of these lysate experiments with other proteomic experiments on NTHi. Also, colonisation of lung epithelium does not involve the florid acute phase of acute otitis media and is likely to have a more tightly controlled inflammatory response. Indeed, epithelial hyperplasia appears to be a feature of chronic otitis media but not, to any significant degree, airway colonisation [316]. Whilst Harrison *et al* used an animal model, the Val *et al* study used an immortalised cell line, and therefore results may not extrapolate well to primary epithelial cells (1.7).

1.9 Rationale for this project

It is unclear whether the progressive lung disease in PCD is purely due to deficiencies in mucociliary clearance or if the epithelium is also dysfunctional, as is the case in cystic fibrosis. Although the cycle of airway damage, bacterial colonisation, inflammation and further damage is common to many airway diseases that lead to bronchiectasis, PCD shows a number of differences in sputum, distribution of lung disease and underlying pathogenesis that make it likely that different processes are governing the rate of lung disease progression. If PCD is simply a disease of mucociliary clearance, then the initial response of the epithelium to colonising bacteria should be the same as in healthy epithelium. If differences in the response exist, then this may be due to intrinsic differences in epithelial innate immunity.

A previously identified difference in PCD airways versus the airways of healthy individuals and those with other respiratory diseases is the airway nitric oxide level. Systematic review and meta-analysis of NO levels in PCD, CF, disease controls and healthy subjects can quantify the degree of this difference in airway NO.

Since *H.influenzae* is the commonest colonising bacteria in PCD, CF, and persistent bacterial bronchitis, and is identified in numerous chronic lung diseases, it is an ideal choice to examine differential responses in different diseased epithelia.

The colonisation of airway by *H.influenzae* involves biofilm formation. Biofilm lifecycle in many bacterial species is controlled by NO and there is, therefore, a link between bacterial colonisation and the PCD airway (which has low NO). There also exists the possibility to manipulate the biofilm using NO for therapeutic benefit.

1.9.1 Hypotheses

1. PCD lung disease progression is influenced both by the lack of mucociliary clearance and a disordered epithelial response to early bacterial colonisation of the lung.
2. Differences in airway nitric oxide exist between PCD and healthy subjects, which may account for differences in airway response to bacterial colonisation.
3. Nitric oxide control of biofilm formation is both a potential source of differential PCD and healthy airway response, and a means to therapeutically manipulate the biofilm.

1.9.2 Aims

1. Systematic review and meta-analysis of published data on airway nitric oxide levels as a potential causative agent in the differential response to infection in PCD and healthy airways.
2. Investigate targeted nitric oxide donors in the treatment of *H.influenzae* biofilm in PCD and healthy epithelium.
3. Identify mechanism underlying any NO-induced changes in *H.influenzae* biofilm.
4. Identify differences in the response of healthy and PCD epithelium to *H.influenzae* biofilm using label-free proteomic analysis.
5. Identify *H.influenzae* proteins associated with biofilm formation *in vitro* and on healthy and PCD epithelium.

Chapter 2: General Materials and Methods

2.1 Participants

Nasal brushing samples were obtained from healthy volunteers, PCD patients and CF patients under ethical approval by Southampton and South West Hampshire Research Ethics Committee (A) (REC numbers: 06/Q1702/109 and 08/H0502/126). PCD patients were diagnosed according to European guidelines [23,283] whilst CF patients had previously been diagnosed by sweat testing and were known to have p.Phe508del homozygous mutations.

2.2 Microbiology

Unless stipulated below, culture medium refers to brain-heart infusion (BHI) (Sigma-Aldrich, Dorset, UK) supplemented with 10µg/ml of hemin (Sigma-Aldrich) and 10µg/ml of β-nicotinamide-adenine dinucleotide (β-NAD) (Sigma-Aldrich). Chocolate horse blood agar plates (Oxoid, Basingstoke, UK) were used for *H.influenzae* culture and incubated at 37^{o}C in 5% CO_2.

2.2.1 Obtaining clinical isolates of *Haemophilus influenzae*

Previous work on a number of patient isolates had identified a strain of non-typeable *Haemophilus influenzae* (NTHi) with good biofilm forming potential; this was termed HI4 (Walker – unpublished). HI4 was used for all experiments using *H.influenzae* unless otherwise specified. Additional strains, termed HI3, HI5 and HI6 were used for validation of some of the nitric oxide work. HI3 and HI4 were gifted by W.Walker, University of Southampton and were from children with PCD who had been consistently colonised with NTHi for at least 4 years. HI5 and HI6 were obtained as part of a nasal carriage study of NTHi in healthy children and gifted by S.Clarke, University of Southampton. All isolates were stored in 22% glycerol at -80^{o}C which has been shown to preserve biofilm forming ability in NTHi [317].

2.2.2 Planktonic growth regression analysis

Five individual colonies were used to inoculate 10ml of medium and incubated at 37^{O}C in 5% CO_2 under static conditions. Measurements of optical density at a 600nm wavelength (OD_{600})

were recorded during the exponential growth phase using a Jenway 6300 spectrophotometer (Keison Products, Chelmsford, UK). 200µl of broth was removed at each measurement point and serially diluted to a 10^{-8} concentration in BHI. Each dilution was spot-plated onto agar in five 20µl drops. Following incubation overnight at $37^{O}C$ in 5% CO_2, colony forming units (CFUs) were counted and regression analysis performed to allow correlation of OD_{600} with CFUs/ml. The process was repeated with three biological and two technical replicates (total n=6). Results are shown in Appendix C.

2.2.3 Growth of *in vitro* biofilms

The static culture system used was in line with previous work using this NTHi model [115]. Isolates were grown in culture medium to the mid-exponential phase at an OD_{600} corresponding to $6x10^8$ CFUs/ml. 2ml of this broth was inoculated to each well of a polystyrene, non-treated 6 well plate (Corning Life Sciences, Amsterdam, Netherlands) with an additional 2ml of fresh, pre-incubated medium. Every 24 hours, the biofilms were fed by removing 1.8ml spent medium and supplementing with 2ml fresh pre-incubated medium. This provided fresh nutrients for growth but attempted to better replicate *in vivo* conditions by not removing all apical solution. For confocal microscopy, preparation was as above but volumes were halved and biofilms grown on CELLview plates (Grenier Bio One, UK).

2.2.4 Assessment of biofilm formation *in vitro*

Biofilms were prepared as per 2.2.3 and incubated for 72 hours. Biofilms were then washed twice with 2ml Hanks Balanced Salt Solution (HBSS, Gibco, Paisley, UK) to remove planktonic/non-adherent bacteria prior to assessment of biofilm and remove any residual media. Biofilm was assessed by 4 methods.

2.2.4.1 Crystal violet assay

Crystal violet (CV) was used to stain and provide a crude estimate of the total biological matter within the biofilm. 2ml of 0.1% crystal violet solution was added following washing. After 10 minutes this was removed and the well washed twice with 2ml of HBSS to remove residual stain then 2ml of 100% ethanol to solubilise the CV stained biofilm. OD_{600} was measured using 100% ethanol as the reference with appropriate dilution in ethanol as required to bring readings into the range of the spectrophtometer.

2.2.4.2 Colony forming unit assessment

1ml of BHI was added to each well and the biofilm mobilised using a sterile cell scraper. Samples were vortexed briefly 3 times to homogenise the broth and then put through log fold dilutions in BHI up to 1 in 10^7. These solutions were spot-plated (5 x 20µL) onto agar. Overnight incubation under static conditions at 37^OC in 5% CO_2 allowed calculation of CFUs present in the biofilm.

2.2.4.3 Scanning electron microscopy

Glass cover slips were sterilised with 100% ethanol for 24 hours before being air-dried and placed in the bottom of sterile polystyrene 6-well plates. Biofilms were then grown as per 2.2.3. A primary fixative solution of 3% gluteraldeyde, 0.1M sodium cacodylate and 0.15% Alcian blue (in order to better visualise the fine structures of biofilm matrix by aiding osmium tetroxide binding) was added to the wells and left for a maximum of 7 days at 5^OC ensuring there was no precipitation of the fixative. This fixative was replaced by secondary fixative of 0.1M sodium cacodylate for 1 hour then 0.1M Osmium Tetroxide/0.1M sodium cacodylate for 1 hour, followed by 0.1M sodium cacodylate for 1 hour. The biofilms then underwent an ethanol series with 10 minutes each of 30, 50, 70, 95 and 100% ethanol, followed by critical point drying using Balzers CPD 030 critical point dryer (BAL-TEC, Liechtenstein) before sputter coating with a gold/palladium mix using an E5100 sputter coater (Polaron, UK). Imaging was performed with an FEI Quanta 250 scanning electron microscope (FEI, Eindhoven, Netherlands) in SEM mode.

2.2.4.4 Confocal microscopy of *in vitro* biofilm

Confocal microscopy was used to assess *in vitro* biofilm viability and structure.

In vitro biofilms were grown on CELLview (Grenier Bio One) plates following the procedure described in 2.2.3. BacLight Live/Dead kit (Life Technologies, Paisley, UK) was prepared in HBSS as per manufacturer's instructions. Biofilms were then washed twice with HBSS and 500µL of the BacLight solution was applied to each well, followed by incubation in the dark for 15 minutes at room temperature. This was followed by an HBSS wash to remove residual stain and then the addition of 1ml 80:20 glycerol/distilled water solution in order that an x63 glycerol immersion lens could be used. 1µm sections were imaged on a Leica SP8 confocal microscope with inverted stand using a 63x glycerol immersion lens and a 1.3 numerical

aperture. Objective settings were HC PL APO CS2. The live stain used was SYTO9 with an excitation wavelength of 488nm and a detection window of 495-550nm. The dead stain used was propidium iodide at an excitation wavelength of 561nm and detection window of 580-700nm. 5 random fields of view were imaged per plate and analysed using COMSTAT 2.1 software [318,319] (using automatic thresholding and connected volume filtering).

2.3 Cell culture

2.3.1 Primary epithelial cell culture

All plasticware was collagen coated by making a 1:10 dilution of 3.1mg/ml Type 1 bovine collagen (Advanced Biomatrix, San Diego, CA) with ultra-high quality water and applying to the surface for 1 hour, followed by removal and drying for at least 1 hour.

PCD, CF and healthy epithelial cell samples were obtained by brushing the nasal turbinates of patients using a cytology brush (Olympus Keymed Ltd, 2mm diameter, Southend, UK) and immediately placing into the culture medium BEGM+; this contains SingleQuot (Clonetics™, Lonza, Castleford, UK) in 500ml BEGM (Clonetics) with 1% streptomycin/penicillin (Gibco) and 0.2% nystatin (Sigma-Aldrich). The cells were washed from the brushes using vigorous pipetting and the resulting solution placed onto a single well of a 12-well plate (Corning Life Sciences). BEGM+ was changed every other day. SingleQuot contains bovine pituitary extract (2ml), hydrocortisone (0.5ml), human epidermal growth factor (hEGF) (0.5ml), epinephrine (0.5ml), transferrin (0.5ml), insulin (0.5ml), retinoic acid (0.5ml), triiodothyronine (0.5ml), GA-1000 (0.5ml).

At 90% confluence, culture medium was removed and 0.5ml 0.25% trypsin-EDTA (Gibco) added for 5 minutes at 37^{o}C. The trypsin solution was then agitated by pipetting to ensure all cells were removed from the well surface. This solution was then added to 7ml BEGM+ and centrifuged at 1400xg for 7 minutes, followed by re-suspension into BEGM+ and seeding into 1 to 3 T25 flasks (dependent on original yield of brushing). Cells were grown to 90% confluence again, culture medium removed and 3ml 0.25% trypsin-EDTA (Gibco) added for 5 minutes at 37^{o}C. Cells were again agitated by pipetting and the solution added to 7ml BEGM+. This solution was centrifuged as above and re-suspended in 1ml ALI medium (50:50 mix of BEGM and Dulbecco's modified eagle medium (Gibco) supplemented with SingleQuot containing only 0.1ml/500ml hEGF plus penicillin, streptomycin, nystatin as per BEGM+) then centrifuged again as above. Cells were resuspended in ALI medium and 0.25ml added to the apical surface of

12mm transwells within a 12-well plate (0.4µm pore size) (Corning). Number of transwells seeded from each sample was dependent on number of original brushings in that samples, yield of brushing and rate of growth at earlier stages of culture. 1ml ALI medium was added to the underside. Apical and baso-lateral media were changed on Monday, Wednesday and Friday. Once confluent (taking between 3 and 5 days), both apical and baso-lateral media were removed and 0.65ml ALI+ was added to baso-lateral surface (ALI medium with 10nM retinoic acid). This established an air-liquid interface (ALI) and allowed development of a ciliated epithelial surface. Media change continued on Monday, Wednesday and Fridays.

2.3.2 Measurement of trans-epithelial electrical resistance in cultured cells

Formation of tight junctions between cultured cells was used as a surrogate of cell health [320] and to ensure a complete monolayer that was impervious to free movement of bacteria.

Using an EVOM^2 trans-epithelial electrical resistance (TEER) meter (World Precision Instruments, Sarasota, FL), TEER measurements were taken as the mean of 3 points around the well. The probe was rinsed in pre-warmed media prior to measurement and the measurements were all taken 1 hour after media change. For co-culture experiments, TEER measurements were taken when switching to antibiotic-free media; this allowed application of fresh, pre-warmed media to both baso-lateral and apical surfaces. Apical media was then removed until co-culture commenced. An empty well containing only culture media with no cells was used as the baseline and was subtracted from the cell layer measurement. TEER was normalised to the surface area of the insert (1.12cm^2) to give ohms*cm^2. A minimum of 800 ohms*cm^2 was required for co-culture to proceed and samples were discarded if there was a greater than 20% drop in TEER across the culture period.

2.3.3 ALI cells and co-culture

Methods were in keeping with previous work on the NTHi co-culture model [115,321,322]. Cultures were used between 3 and 4 weeks after confirmation of ciliation on light microscopy, but no later than 10 weeks after obtaining the nasal brushing.

ALI cells were switched to antibiotic-free ALI media the day before co-culture by placing 0.65ml baso-laterally and performing a single wash with 0.5ml antibiotic-free media apically. Prior to co-culture, the media was replaced again with 1ml baso-laterally and 0.65ml apically which

facilitated TEER measurements. The apical media was then removed and replaced with either fresh media (control) or NTHi (co-culture).

For NTHi co-culture work, a multiplicity of infection (MOI) of 100 was used with the bacteria appropriately diluted so that a 500µl suspension in ALI media provided the correct MOI. MOI of 100 was chosen as this had been used in all previous NTHi biofilm/co-culture work using this model [115,116]. Prior to commencing co-culture work, 3 ALI cultures from healthy subjects were removed from transwell membrane using 0.5ml 0.25% trypsin-EDTA (Gibco) and cell counted using trypan blue stain and a haemocytometer. This established a mean cell epithelial cell count in the ALI cultures of $5.4x10^5$, which was used to calculate the MOI for subsequent co-culture experiments. Bacteria were grown to mid-exponential phase in supplemented BHI (approximately 2 hours) and OD_{600} measured as per 2.2.2 to establish concentration of NTHi in the solution. This solution was then centrifuged for 5 minutes at 3500xg before re-suspension in an appropriate volume of ALI medium to give a final concentration of $1x10^8$ CFUs/ml ($5x10^7$ CFUs in 500µL). 500µL of this solution was then added to the apical surface of the epithelial cells and cultured for 72 hours at 37°C in 5% CO_2, with daily replacement of apical and baso-lateral ALI media.

Following completion of assays, wells were washed twice with HBSS (apically and baso-laterally) then excised with a sterile scalpel. Dependent on the assays performed, the wells were processed for CFU counts (see 2.2.4.2), SEM (2.2.4.3) or proteomic analysis (2.4.1.2).

2.4 Proteomic analysis

2.4.1 Protein extraction for bacterial cultures

Biofilms were washed twice with 2ml HBSS then suspended into 1ml HBSS using a cell scraper and vigorous pipetting. This solution of cells was then washed twice with 10ml HBSS by centrifugation at 10,000xg for 5 minutes at 4°C. Pellets were re-suspended in 1ml of 1M triethylammonium bicarbonate (TEAB) in HBSS with 4M guanidine hydrochloride to denature and solubilise proteins, and lysozyme (10mg/ml) to digest the cell wall. Samples were incubated for 30 minutes at 37°C before being bead beaten with 0.1mm zirconium oxide beads at 50Hz for 5 minutes to mechanically lyse the cells. Following centrifugation at 3,000xg for 2 minutes at room temperature, the supernatant (soluble fraction) was passed through a 0.22µm low-protein binding polyethersulfone (PES) filter to remove any remaining whole cells. The remaining fluid was added to 6 times its own volume of ice cold ethanol and the proteins

precipitated overnight at -20°C. The precipitated protein was harvested by centrifugation at 12,000g for 5 minutes at 4°C and re-suspended in 500µl-1ml of 100mM TEAB with 0.1% rapigest (Waters, Elstree, UK). Rapigest was chosen as a protein denaturant, rather than other options such as sodium dodecyl sulphate (SDS), as it is heat stable, does not interfere with trypsin and can be easily removed later in processing thus it is ideal for LC/MS proteomics.

2.4.1.1 Bradford's assay

Protein concentration was quantified using the Bradford's assay. 20µl of protein solution was added to 180µl of Coomassie blue (Sigma Aldrich) and OD_{600} was measured using Spectra Max 340 PC plate-reading spectrophotometer (Molecular Devices, Sunnyvale, US) controlled via ADAP software (Biochrom, Cambridge, UK). Known concentrations of serum bovine albumin (Sigma Aldrich) were used to construct a standard curve and calculate the protein concentration in the samples. A blank well of 100mM TEAB with 0.1% rapigest (Waters) and Coomassie blue was used as the negative control.

2.4.1.2 Processing of bacterial samples for mass spectrometry

Protein concentrations of individual protein samples were normalised to the same concentration with a total volume of 300-700µl, by adding 100mM TEAB solution. Solutions were heat treated at 80°C for 10 minutes then briefly vortexed. 100nM DTT solution in 100mM TEAB was added to give a final DTT concentration of 2.5nM followed by a further heat treatment of 60°C for 10 minutes. After cooling, the solution was spun at 10,000xg to collect the sample and Iodoacetamide added to give a final concentration of 7.5mM. This was incubated at room temperature for 30 minutes in the dark.

20µg trypsin (sequencing grade modified porcine trypsin, Promega, Southampton, UK) was added to 200µl of 100mM TEAB. 4µl of this trypsin solution was added per 300µl of each protein sample and incubated overnight at 37°C. The sample was briefly pulse-centrifuged to collect the samples and volume then measured. Trifluoroacetic acid (TFA) was added to give a concentration of 0.5% and the solution incubated for 30 minutes at 37°C before spinning at 13,000xg for 10 minutes. Supernatant was lyophilised and resuspended in 200mM ammonium formate with 100-200fmol of internal standard (*Saccharomyces cerevisiae* enolase).

2.4.2 Protein extraction for primary epithelial cells/bacterial co-culture

Trans-wells were washed twice with 1ml HBSS then the membrane was removed using a sterile scalpel and placed into 500µl of cell lysis buffer (100mM TEAB and 0.1% SDS with Halt™ protease/phosphatase inhibitor at 3x concentration (Life Technologies)) for 10 minutes at room temperature. Lysates were then frozen at -20°C for further processing.

2.4.2.1 Gel electrophoresis

To assess the quality of protein extraction and provide comparative 1D profile patterns, 1DE LDS-PAGE was performed.

Sample solutions were prepared by adding 26µl of sample to 10µl of NuPAGE® LDS buffer (Life Technologies) and 4µl of 500mM dithiothreitol (DTT) NuPAGE® reducing agent (Life technologies) which was then heat treated at 70°C for 10 minutes.

700ml running buffer was prepared (35ml MOPS concentrate with 665ml distilled water). 200ml was removed and 500µl antioxidant (Life technologies) added. A 4-12% Bis-Tris gel (Life technologies) was run using a Surelock™ tank (Life technologies) with 200ml NuPAGE® MOPS SDS running buffer (Life technologies) plus NuPAGE® antioxidant (Life technologies) in the central well and 500ml MOPS buffer solution in the remainder of the tank.

Gel wells were filled with 20µl sample solution flanked by 10µl Novex sharp™ (Life technologies) reference protein solution. Gels were run for approximately 35 minutes at 200 volts, or until the marker stain reached the bottom of the gel, followed by removal and staining with Colloidal blue stain (Life technologies) as per manufacturer's instructions. Gel was then destained with distilled water for 7 hours.

2.4.2.2 Processing of co-culture samples for mass spectrometry

Following preparation of co-culture samples as per 2.4.1.2, initial MS runs were unable to produce protein "hits" on the MS outputs. Despite attempts at additional C18 clean-up steps, the MS output was still not interpretable by the analysis software, therefore an alternative preparation method was used. Proteins were prepared as per 2.4.1 then further cleaned of contaminants by LDS-PAGE electrophoresis (2.4.2.1). Protein was quantified using the fluorometric Qubit system (ThermoFisher, Waltham, MA) as per manufacturer's instructions prior to addition of 10µg of protein to each well of the gel (in a total of 20µl prepared protein solution). The sample was run approximately 1cm into the gel then cut out and placed into

distilled water for storage at 4°C. At the same time, another gel was run to completion and stained to confirm the presence of a protein banding pattern. Due to processing problems, the unstained gel samples also failed to yield protein in the final analysis, so the samples from the equivalent stained gels were used (2.4.2.1).

Gel lanes were excised and cut into approximately 20 pieces prior to in-gel digestion [323]. Each slice was destained using 100 mM ammonium bicarbonate/20% acetonitrile, followed by reduction (10 mM DTT, Sigma, Dorset, UK) and alkylation (50 mM iodoacetamide, Sigma). An automated digestion robot (MassPrep, Waters, Manchester, UK) performed enzymatic digestion with trypsin (sequencing grade modified porcine trypsin, Promega) in 50 mM ammonium bicarbonate (Sigma). The digestion was performed overnight then samples were acidified with 0.1% formic acid (v/v) in 2% acetonitrile (v/v) and pooled for each sample.

2.4.3 Mass spectrometry

Mass spectrometer operations were performed by P.Skipp (University of Southampton). Separations were performed using a nanoAcquity UPLC system (Waters). For the first dimension separation, 1.0 µl of the peptide digest was injected onto a Symmetry C18, 180µm x 20mm trapping cartridge (Waters) followed by 5 minutes of trap column washing. Peptides were then separated using a 75µm i.d. x 250mm, 1.7µm BEH130 C18, column (Waters) using a linear gradient of 5 to 40% (buffer A = 0.1% formic acid in water, buffer B = 0.1% formic acid in acetonitrile) over 90 min with a wash to 85% at a flow rate of 300 nl/min. All separations were automated, performed on-line and sprayed directly into the nanospray source of the mass spectrometer.

All mass spectrometry was performed using a Waters G2-S Synapt HDMS mass spectrometer operating in MS^e mode. Data was acquired from 50 to 2000 *m/z* with ion mobility enabled using alternate low and high collision energy (CE) scans. Low CE was 5V and elevated, ramped from 20-40V. The lock mass of 100 fmol/µl Glu-fibrinopeptide, ($(M+2H)^{+2}$, *m/z* = 785.8426) was infused at 300 nl/min with acquisition every 13 seconds.

The raw mass spectra were processed using ProteinLynx Global Server Version 3.0 enabled through Symphony pipeline software (Waters, Manchester, UK) and the data processed to generate reduced charge state and de-isotoped precursor and associated product ion mass lists. These mass lists were searched against the human and *non-typeable H.influenzae* 3655

UniProt protein sequences (downloaded June 2016) [324]. A maximum of one missed cleavages was allowed for tryptic digestion and the variable modification was set to contain oxidation of methionine. Carboxyamidomethylation of cysteine was set as a fixed modification.

2.5 Statistical analysis

Graphs and statistical analysis of laboratory data were undertaken with GraphPad Prism® Software (version 7.01, 2016, GraphPad Software Inc.). Parametric data was analysed using the student t-test.

Meta-analysis of nitric oxide data was performed in StataSE (version 11, 2009, StataCorp) using the *metan* command. Generalised inverse variance method was used to calculate weighted mean differences in NO between groups.

For the proteomic analysis, identified proteins and quantities were initially analysed in Microsoft Excel to normalise results to total protein and calculate ratios of treated versus untreated. Figures were then transferred to GraphPad Prism® (version 7.01, 2016, GraphPad Software Inc.) for assessment of statistical significance via multiple student's t tests. Adjustment was made for multiple comparisons by setting false discovery rate (FDR) at 1% or 5% [325].

2.5.1 Pathway and network analysis

Proteomic studies usually identify many hundreds or thousands of individual proteins, therefore looking at each of these in isolation is not the most informative way to analyse these results. As the proteins are involved in many biological processes and pathways, analysis tools that look at linked proteins within the dataset are very useful. Three main analysis tools were used for the proteomic analyses with each providing a different, but complementary, approach to classification of identified proteins.

2.5.1.1 String database

To establish the connectivity of the proteins identified and represent this as a network, the results were analysed using the String database (release 10.0, 16/4/2016), an open source database of protein interactions that scores the network according to known and potential interactions (e.g. known interactions in other species) [326]. The database is a collaborative

project that contains 9,643,763 proteins across 2,031 organisms and a total of over 932 million interactions. There are seven possible types of connection between two proteins termed evidence channels;

1. Conservation – prokaryotic genes occurring within 300 base pairs of each other
2. Co-occurrence – proteins that are linked across species
3. Fusion – proteins where the genes are fused together
4. Co-expression – proteins that have genes co-expressed in the same or other species
5. Experiments – experimental data showing protein interaction in databases of these types of interaction
6. Database – present as part of a significant interaction group in curated databases of protein interaction
7. Text mining – the proteins appear together in a title or abstract of a PubMed entry

A score is applied to each of these channels based on the strength of that evidence, with the "string" score calculated by totalling the channels and correcting for chance of random interaction [326]. The network is then constructed based on low, medium or high strength of connection; this work used a medium strength (string score of over 0.5). String also provides a measure of whether the group of proteins are more connected than a randomly selected set; the protein-protein interaction (PPI) enrichment compares expected number of connections (if proteins were random) to those observed and calculates a p value. PPI enrichment p value of less than 0.05 was considered statistically significant (proteins are more connected than a set of proteins chosen at random). As well as constructing a network of identified proteins, additional proteins with the strongest connections can be added to show the strongest interactors with a protein or subset of proteins.

2.5.1.2 GO-PANTHER analysis

The Gene Ontology (GO) PANTHER overrepresentation test (release 20160715) was used to identify biological processes that were statistically more highly represented in the proteins identified. The GO database is a freely available, collaborative database that contains descriptions of gene products according to three ontologies; biological processes, cellular components and molecular functions [327,328]. This restricted annotation provides consistency across all organisms as well as linking easily to external analysis tools and databases. Rather than simply connecting the proteins in a network as the string database

does, the GO database features a hierarchical classification system for proteins in each of the 3 domains (biological, cellular, molecular). This work focused on the classification of proteins according to biological function. Once the identified proteins have been classified according to their GO entry, additional tools are required to search for the presence of proteins within the dataset that belong to shared ontologies.

Protein ANalysis THrough Evolutionary Relationships (PANTHER) is one such tool. It is an online tool for functional annotation of genomes/proteomes and pathways across numerous species [329,330]. The PANTHER database is generated by computational algorithms that define protein families according to sequence homology and then subfamilies according to shared functions. This database is then manually curated by the consortium to ensure accuracy and validity of the groupings. The second part of the database is an entirely manually curated database of pathways. Release 11.1 used in this analysis contained 13,096 families, 78,442 subfamilies and 177 pathways (www.PANTHERdb.org/data/).

The GO-PANTHER overrepresentation test used the PANTHER analysis tools and GO Ontology database to identify protein ontologies and pathways that are present at a higher rate than expected in the experimental dataset. Overrepresentation is calculated by taking the number of proteins involved in a particular ontology or pathway in the dataset (sample frequency) and comparing that to the proportion of proteins involved in that process in the reference database (background frequency). The p value is then calculated as the probability of the sample frequency given the background frequency. As there is multiple testing involved, Bonferroni correction for multiple analysis was applied at a significance level of 0.05 [329,330]. This work used the GO Ontology database version 1.2 (released 27/10/2016) imported to PANTHER and analysed against the *Homo sapiens* reference database (20,972 genes) and/or *Haemophilus influenzae 2655* strain reference database (1723 genes).

2.5.1.3 KEGG pathway analysis

Kyoto Encyclopaedia of Genes and Genomes (KEGG) was also searched from within string (release 80.1, 1/11/2016, 498 pathways). The KEGG database consists of sixteen component databases that are divided into systems information, genomic information, chemical information and health information. These databases are manually curated with experimental data on gene, protein and chemical interactions. The databases are then used to build a computer generated representation of biological systems followed by manually drawn KEGG pathways based on this representation [331,332]. KEGG uses a similar overrepresentation test

as GO-PANTHER, but applies the false discovery rate (FDR) approach rather than Bonferroni. Using two alternative pathway/ontology tools, with alternative means of constructing the pathways and slightly different statistical analysis, serves as extra validation of proteomic results.

2.5.1.4 InterPro Protein families

The InterPro protein families database classifies proteins according to shared domains and groups them into families based on this rather than known pathways. Again, this is a collaborative project featuring data from a number of different contributing databases [333]. The proteomic data was also searched using the InterPro database (release 59.0, 15/9/2016) for overrepresented protein domains. Like KEGG, InterPro uses the FDR approach to controlling for multiple testing. Thus, rather than belonging to the same pathway, a number of proteins may be overrepresented because they bind a common ligand or interact with a common secondary messenger.

Multiple t tests can be excessively restrictive in samples with a large number of proteins and, therefore, a linear models for microarray approach was also applied to the co-culture proteomic samples. Analysis used the *limma* module for *R* statistical package (FDR 5%).

Chapter 3: Nasal nitric oxide in primary ciliary dyskinesia patients – systematic review and meta-analysis

3.1 Introduction

As described in 1.6.3, PCD is characterised by low nasal nitric oxide (nNO) [46]. Since this appears to be independent of the causative mutation and disease severity, it is the only consistent epithelial dysfunction so far identified in PCD and could result in altered response to infection.

Following the first study describing this finding in 1994, there have been numerous papers comparing nNO in PCD with healthy controls and other diseases, including CF [32,48,49,93,334]. However, the studies used a variety of different analysers, sampling techniques, patient ages and controls, and there has not been a systematic review and meta-analysis of the findings. Despite inclusion of nNO in diagnostic guidelines [283] and publication of guidelines on nNO sampling [335], there is a lack of consensus on thresholds, alternative sampling methods and use in young children.

The studies suggest that CF airways have NO that is lower than healthy patients but not as low as PCD, therefore differences in airway NO are a potential source of the different airway responses to infection in PCD and CF.

3.2 Aims

To systematically review the evidence for decreased NO in PCD when compared to healthy and disease controls including CF, and to assess the consistency of differences in nNO in the following situations –

- nNO in PCD patients compared to healthy and cystic fibrosis controls when measuring nNO according the ATS/ERS guidelines [335] using a velum closure technique.
- nNO in patients with normal electron microscopy
- Use of varying respiratory manoeuvres during nNO measurement

- Use of nNO in young children (<5 years)
- Portable NO analysers versus stationery measurement

3.3 Methods

A protocol for publication of the systematic review in with regard to diagnostic use of nNO was defined prior to commencing the systematic review which can be seen in Appendix A.

3.3.1 Search strategy

MEDLINE, EMBASE, PreMedline In-Process & Other Non-Indexed citation, Web of Knowledge Science Citation Index (SCI), Web of Knowledge ISI Proceedings and Cochrane Systematic Reviews Database were all searched from inception to 16th April 2014. Citation lists were used to identify additional studies.

3.3.2 Study selection

Any study measuring nNO in PCD patients and describing nNO sampling technique, analyser, sampling rate patient age and method of PCD diagnosis

3.3.3 Data analysis and synthesis

Reported concentrations (parts per billion) were converted to nanolitres/minute (nl/min) using the formula *ppb x sampling rate (l/min)* to allow comparison between studies using different sampling rates. Two studies have reported good agreement between different analysers when using this conversion estimate [48,50].

Studies that reported mean nNO values with either standard deviation (SD) or standard error (SE/SEM) were included in meta-analysis. STATA 11.0 was used to perform a generalised inverse variance analysis of mean difference between nNO in PCD patients and healthy or cystic fibrosis controls. We also assessed studies for heterogeneity.

3.4 Results

96 publications were identified with the selection steps shown in Figure 3-1. The 35 studies assessed for eligibility are shown in Appendix B. QUADAS principles were used to assess risk of bias [336] with this rated as low in all areas except for lack of blinding.

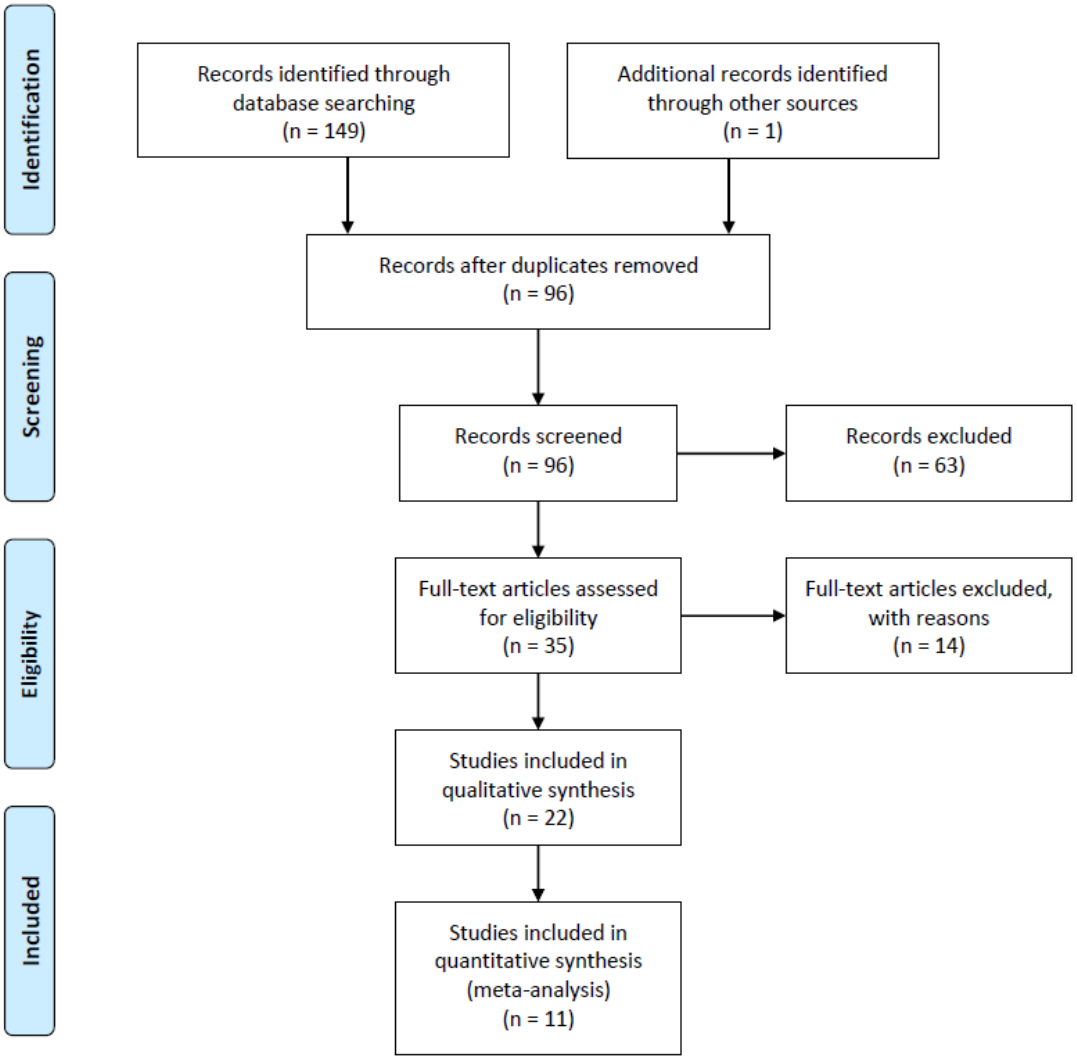

Figure 3-1. **PRISMA flow chart of study selection** [337]. Summary of studies identified through searching/additional sources and then excluded/included at each stage of the analysis.

3.4.1 nNO in PCD, healthy and disease control patients

19 manuscripts with 634 PCD patients reported nNO by velum closure methods on a stationery analyser. 18 of these compared PCD to healthy controls (n=582) and 11 compared PCD to CF (n=510). 1 paper used a portable analyser to compare PCD with bronchiectasis patients [338]. In all studies nNO was significantly lower in PCD than healthy controls or CF patients, as shown in Table 3-1 and Table 3-2.

	PCD			Healthy Controls			Cystic Fibrosis		
Study	**n**	**Mean**	**SD**	**n**	**Mean**	**SD**	**N**	**Mean**	**SD**
Wodehouse *et al* 2003 [93]	42	16.4	9.2	16	189.8	36.5	15	139.5	40.7
Csoma & Bush 2003 [334]	15	14.9	11.8	14	126.4	62.5			
Noone *et al* 2004 [32]	64	19	17	27	376	124	11	184	109
Corbelli *et al* 2004 [339]	17	16.4	4.35	24	268.4	138.5			
Piacentini *et al* 2008 [340]	10	8.9	5.7	26*	195	92.8			
Shoemark *et al* 2009 [289]	20	12.3	8.6	20	159.8	133.5			
Moreno Galdo *et al* 2010 [341]	9	22	29.9	37	224.5	37.1	210	109.5	27
Marthin & Nielsen 2011 [49]	45	19.0	13.6	57	272.4	76.0	49	124.8	103.7
Mateos-Coral *et al* 2011 [342]	20	17.9	13.7	19	366.5	131.7	32	138.8	84.1
Leigh *et al* 2013 [48]	149	20.7	24.1	78	304.6	118.8	77	134.0	73.5
Leigh *et al* 2013 [48] replication	71	23.3	18.0						
Marthin & Nielsen 2013 [50]	16	23.7	22.8	20	267	74.4	21	150.3	58.8
Combined	478	19.4	18.6	338	265.0	118.9	415	123.2	62.7
Ppb equivalents[#]									
NIOX (Flex/MINO)		64.7			883.3			410.7	
Eco Medics CLD 88		58.8			803.0			373.3	
Sievers		38.8			530.0			246.4	
LR2000		77.6			1060.0			492.8	

Table 3-1. **Summary of studies measuring nNO in primary ciliary dyskinesia (PCD), healthy control and cystic fibrosis groups using a stationary analyser with velum closure manoeuvre**. Equivalents for each type of analyser given by nl/min x sampling rate for each analyser. All other values in nanolitres/min (nl/min). ppb – parts per billion.

	PCD		Healthy Controls		Cystic Fibrosis	
Study	n	Outcome	n	Outcome	n	Outcome
Karadag *et al* 1999 [343]	21	Median 13.75 Range (0.83-239.8)	60	Median 138.3 Range (29-359.3)		
Narang *et al* 2002 [286]	31	Median 15.1 Range (0.8-230)	53	Median 179 Range (99.5-359.3)	17	Median 122.8 Range (7.8-285)
Horvath *et al* 2003 [344]	14	Median 13.6 Range(1.3-67.3)	37	Median 165.8 Range (80.5-335.8)	20	Median 85.8 Range (7.5-249.3)
Santamaria *et al* 2008 [345]	14	Median 3.3 IQR 3.3	14	Median 90.1 IQR 67.2		
Marthin & Nielsen 2011 [49] (consecutive referrals)	12	Median 15.9 95% CI (3-162)				
Walker *et al* 2013 [266]	14	Median 8.1 IQR (4.8-22.8)	18	Median 231.6 IQR (207-265.8)	12	Median 150.3 IQR (135-182.4)
Boon *et al* 2014 [346]	38	Median 16.8 IQR (8.1-35.7)	49	Median 236.4 IQR (198.3-295.8)	46	Median 109.5 IQR (75.6-169.5)
Harris *et al* 2014 [347]	11	Median 12.3 IQR (7.5-15.9)	15	208.2 IQR (181.2-240)	6	Median 139.5 IQR (99-227.7)

Table 3-2. **Studies reporting non-parametric summary statistics for nasal nitric oxide in primary ciliary dyskinesia (PCD), healthy control and cystic fibrosis groups measured via stationary analyser with velum closure manoeuvre**. All figures given in nl/min.

3.4.2 Meta-analysis

Meta-analysis was performed on the studies in Table 3-1 with a total of 478 PCD, 338 healthy and 415 PCD patients giving mean nNO (SD) of ; 19.4 nl/min (18.6) for PCD, 265.0 nl/min (118.9) for healthy and 123.2 nl/min (62.7) for CF. The weighted mean difference for PCD vs healthy was 231.1 nl/min (95% CI 193.3-268.9) and 114.1 nl/min (95%CI 101.5-126.8) for PCD vs CF (Figure 3-2).

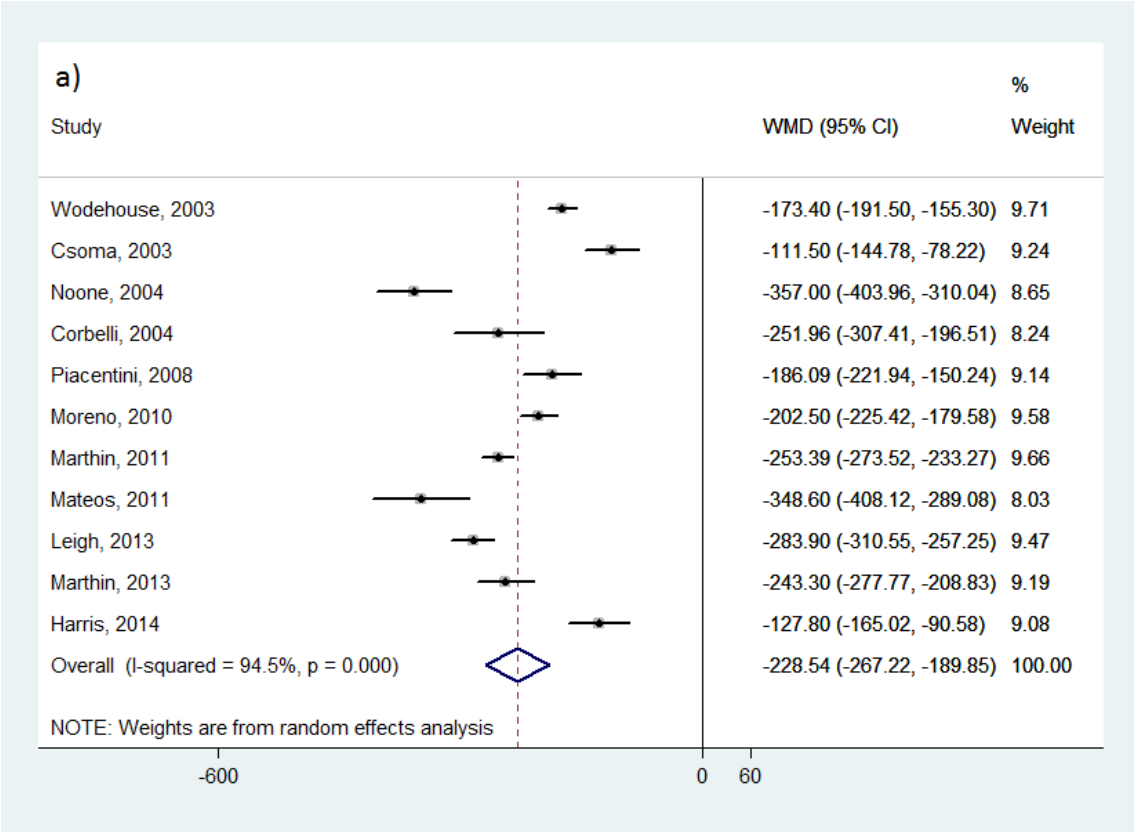

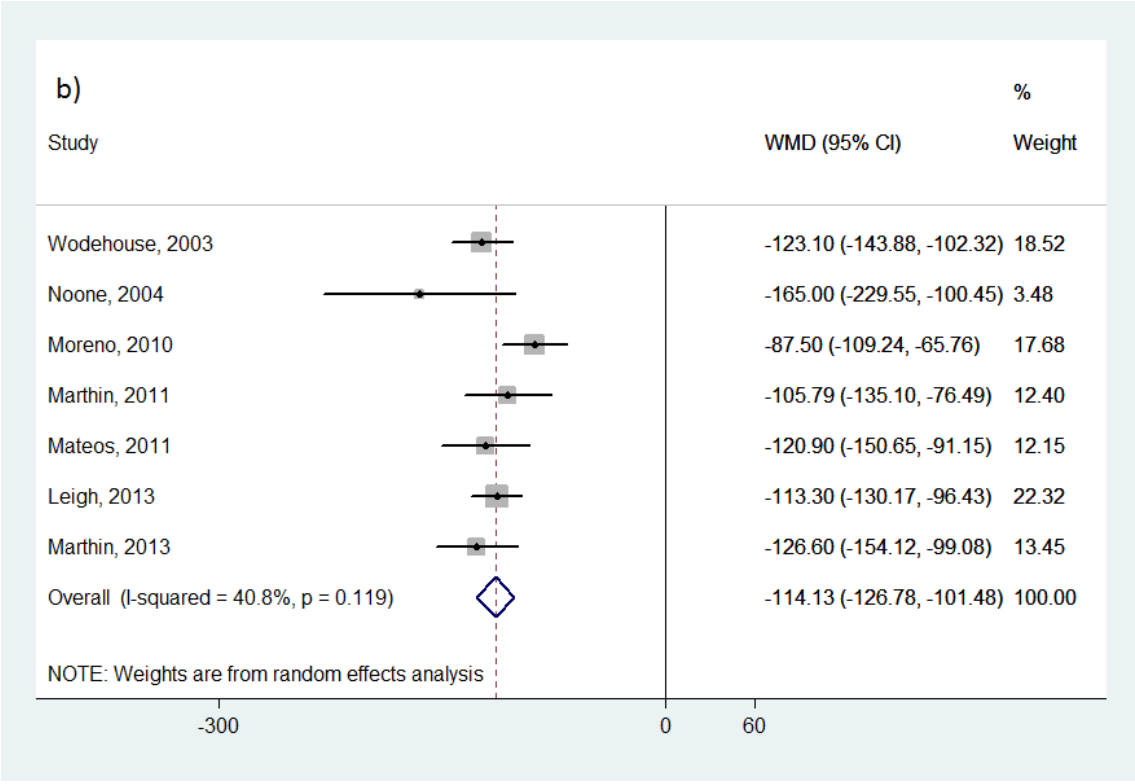

Figure 3-2. **Forest plots showing weighted mean difference (WMD) in mean nasal nitric oxide (nNO) between a) healthy controls and PCD and b) cystic fibrosis patients and PCD patients.** All data recorded using a stationary analyser and velum closure technique. Figures in nanolitres/min

Heterogeneity was expressed as I^2 (variation attributable to heterogeneity). There was a high degree of heterogeneity in the studies comparing PCD to healthy controls (I^2=93.9%) and a moderate level in the CF studies (I^2=40.8%).

3.4.3 Diagnostic thresholds

Nine studies calculated cut-offs for diagnostic accuracy (Table 3-3). Leigh *et al* used their cohort to calculate a threshold of 77nl/min, then rolled this out to 6 other diagnostics centres where 70 of 71 PCD patients were correctly identified [48]. Four other studies reported nNO levels in consecutive referrals but 2 were excluded due to lack of sampling/diagnostic detail [48,348]. Corbelli *et al* found mean nNO for positive referrals was 16.4nl/min versus 159.2nl/min for negative referrals ($p<0.05$) [339]. Marthin *et al* found median nNO was 15.9nl/min in 12 positive referrals versus 204.3nl/min in 46 negative referrals ($p<0.0001$) [49]. Their threshold of 52.5nl/min identified 55/59 PCD cases.

Study	n	Cut-off (nl/min)	Sensitivity	Specificity
Mateos-Corral *et al* 2011* [342]	44	60.8	100%	100%
Narang *et al* 2002 [286]	157	25	75%	96%
		62.5	97%	90%
Horvath *et al* 2003 [344]	102	46.8	93%	95%
Corbelli *et al* 2004 [339]	34	126	94%	88%
Marthin & Nielsen 2011 [49]	94	Breath hold 52.5	91.1%	100%
		Oral exhalation 72.6	94.3%	100%
		Tidal breathing 47.4	94.4%	100%
Leigh *et al* 2013 [48]	227	77	98%	>99.9%
Marthin & Nielsen 2013 [50]	57	78.6	100%	100%

Harris *et al* 2014 [347]	47	38	100%	95%
Boon *et al* [346]	226	90	89.5%	87.3%

Table 3-3. **Summary of studies presenting sensitivity and specificity of their cut-off values for nNO (nl/min) for PCD versus healthy patients.** *bronchiectasis patients included in healthy control group.

Seven studies compared PCD to non-CF bronchiectasis; 5 found levels in bronchiectasis similar to healthy controls [93,286,289,342,344], 1 used a portable analyser in only a small number of patients [338] and 1 found levels lower in bronchiectasis than healthy controls (90.3nl/min versus 224.5nl/min mean) [341]. PCD nNO was also significantly lower than patients with asthma [48,266,341,346], chronic obstructive pulmonary disease (COPD) [48,338] and humoral immunodeficiency [346].

3.4.4 Nasal nitric oxide in "atypical PCD"

PCD patients with normal ultrastructure on TEM have previously been described as "atypical". Two studies showed that patients with normal ultrastructure had low nNO levels; Leigh *et al* had 10 patients with DNAH11 mutation (known to have normal TEM) who all had nNO below 77nl/min [48], Pifferi *et al* had 4 patients with normal ultrastructure and nNO below 22nl/min [349].

RSPH1 mutations have recently been associated with PCD with a milder phenotype and higher nNO levels; in one study, mean nNO was 98.3nl/min with 12/18 above 77nl/min [30], however the mechanism for this is unclear.

3.4.5 Different manoeuvres for nNO sampling

3.4.5.1 Tidal breathing

Four studies compared tidal breathing to velum closure, with nNO lower in tidal breathing in both PCD and control patients but still significantly different from each other [49,50,340,342] (Table 3-4). Meta-analysis showed that nNO levels were significantly different between tidal breathing and velum closure for healthy controls (182.2 nl/min v 278.8nl/min, $p<0.0001$) and CF patients (91.5 nl/min v 132.7 nl/min, $p<0.0001$) but not in PCD patients (21.6nl/min v 19.8 nl/min). The standard deviations are also larger in tidal breathing (PCD 48.6 and healthy 127.4) than in velum closure (18.2 and 99.4), thus reducing discriminatory value.

	PCD			Healthy Controls			Cystic Fibrosis		
Study	n	Tidal	VC	n	Tidal	VC	n	Tidal	VC
Piacentini *et al* 2008 [340] Mean (SD)				15	100.8 (17.4)	206.3 (29.1)			
Piacentini *et al* 2010 [350] Mean (SD)				43	86.3 (39.1)				
Degano *et al* 2011 [287] Median (IQR)	5	6.5 (4.5-8)		10	105 (83.5-127)				
Marthin & Nielsen 2011 [49] Mean (SD)	54	25.8 (61.7)	19.0 (13.6)	52	160.2 (64.9)	272.4 (76.0)	17	72.9 (48.2)	124.8 (103.7)
Mateos-Corral *et al* 2011 [342] Mean (SD)	20	13.3 (9.5)* 10.0 (6.5)#	17.9 (13.7)	19	281.3 (231.9)* 234.7 (191.8)#	366.5 (131.7)	32	107.6 (58.6)* 85.7 (54.6)#	138.8 (84.1)
Marthin & Nielsen 2013 [50] Mean (SD)	16	17.7 (16.8)	23.7 (22.8)	21	145.8 (46.7)	267 (74.4)	21	81.9 (44.0)	150.3 (58.8)
Boon *et al* [346] Median (IQR)	38	8.4 (6-22.2)	16.8 (8.1-35.7)	49	150 (106.5-180)	236.4 (198.3-295.8)	46	54 (36-87)	109.5 (75.6-169.6)

Table 3-4 **Studies reporting measurements for tidal breathing technique of nasal nitric oxide sampling for PCD, healthy and cystic fibrosis patients via stationary analyser.** Velum closure (VC) measurement shown if performed in the same set of patients. nl/min. * mouth open measurement, # mouth closed

3.4.5.2 Humming

Since humming rapidly empties the paranasal sinuses, this produces a peak of nNO in healthy patients but not in those with PCD [351]. Amongst 3 studies that assessed humming, it was not possible to convert readings to nl/min but all 3 found a significant difference between PCD and healthy/CF controls [342,345,352]. Mateos-Corral *et al* found a 123ppb cut-off was 100%

sensitive, whilst Santamaria *et al* reported 100% specificity and sensitivity at a cut-off of 48.7ppb.

3.4.6 Young children

As nNO levels are lower in children [350,353] and they are often unable to co-operate with specific respiratory manoeuvres, using nNO in PCD diagnostics in children is more problematic.

Baraldi *et al* measured nNO in 2 PCD patients aged 4 and 6 months, then compared them with 5 healthy infants (range 1.3-7 months). Nasal NO levels in the two PCD patients were 9.4 and 12.7 nl/min whilst the mean for the healthy controls was 32.5 nl/min (range 24.8 to 41.7). The lower levels in healthy controls make false positive results more likely [354]. Stehling *et al* found a nNO of less than 5ppb on day 4 of life in a PCD patient; (sampling methods not stated) whilst six healthy neonates (2-24 days) had a mean nNO of 171.2ppb [355]. Marthin *et al* reported a 16 day old with nNO of 2.7nl/min and a 16 week old with nNO of 3.3nl/min both with PCD. Overall false positive rate was 39% in children under 6 years performing nNO during tidal breathing, nevertheless the negative predictive value was 99% [49].

Piacentini *et al* measured nNO in 2 uncooperative PCD patients and 50 healthy children under a year of age during tidal breathing. The 2 infants with PCD had nNO levels of 2.2 and 12.5 nl/min. They reported mean nNO levels of 38.4nl/min (+/- 4.9) in healthy children under 6 months (n=26) and 92.7nl/min (+/- 13.8) for those aged 6-12 months (n=24). Their analysis showed that a cut-off of 16.2nl/min for under 6 months of age had a sensitivity of 90% and specificity of 81% for diagnosis of PCD [340].

3.4.7 Portable analysers

Four studies used portable nNO analysers with 3 comparing this to a stationery analyser [50,338,347,352] as shown in Table 3-5. Velum closure proved difficult in these studies as it required a breath hold for 45 seconds; Harris *et al* , therefore, abandoned this and reported only tidal breathing measurements [347], whilst Marthin & Nielsen reported a 70% success rate for breath hold measurements [50]. 2ml/s sampling had no advantages over 5ml/s and could not be used with breath hold [50,347].

	PCD		Healthy Controls		Cystic Fibrosis	
Study	Stationary	Portable	Stationary	Portable	Stationary	Portable
Montella *et al* 2011 [352]	1.5	2.6	13.7	12.4	9.5	13.4
Nasal exhalation	(1.0-2.3)	(1.9-3.5)	(9.6-19.5)	(8.9-17.6)	(7.0-13.0)	(10.4-17.3)
Median (range)	n=14	n=14	n=13	n=13	n=11	n=11
Harrison *et al* 2012 [338]		7.2		125.7		12
Tidal breathing		(4.1)		(22.8)		(11.7)
Mean (SD)		n=4		n=5		n=6
Marthin & Nielsen 2013 [50]	23.7	19.2	267	180.9	150.3	97.2
Breath hold	(22.8)	(18.7)	(74.4)	(57.7)	(58.8)	(41.6)
Mean (SD)	n=16	n=12	n=20	n=21	n=21	n=8
Harris *et al* 2014 [347]	12.3	5.4	208.2	112.6		
Tidal breathing - MINO	(8.4)	(3.3)	(58.8)	(88.0)		
Breath hold - Flex	n=11	n=12	n=15	n=15		
Median (IQR)						

Table 3-5 **Summary of studies reporting nasal nitric oxide measurements with a portable nitric oxide analyser in PCD and healthy controls +/- cystic fibrosis patients**. Stationary analyser readings shown for comparison if measured. Nanolitres/min (nl/min)

Marthin & Nielsen confirmed significant differentiation between PCD, CF and healthy with a portable analyser ($p<0.0001$) [50]. Receiver operating characteristics (ROC) analysis gave a nasal exhalation cut-off of 6.9nl/min (sensitivity 100%, specificity 85%) [352], tidal breathing cut-off of 30nl/min (100%, 95%) [347], and 64nl/min breath hold (100%, 95.2%) or 43nl/min tidal (100%, 100%) [50].

3.5 Discussion

Nasal nitric oxide levels are significantly lower in PCD than in healthy controls and those with other respiratory diseases, including CF. This finding can be utilised in PCD diagnosis as velum closure measurements give excellent sensitivity and specificity. However, this finding is consistent across a number of different sampling methods and breathing manoeuvres.

Since healthy young children have lower levels of nNO than older children/adults [350,353], testing is less accurate in the pre-school age group. This is further exacerbated by the need to perform tidal breathing measurements in many of these children. However, nNO levels seem to be consistently lower in PCD than healthy patients.

The limited studies that have been performed on portable nNO analysers suggest they are reliable in measuring nNO, however they have a number of limitations. The currently available device (NIOX Flex, Aerocrine, Sweden) does not have a real-time display of the nNO reading so it is impossible to check the validity of the reading (reading should be taken at plateau).

Other manoeuvres, such as humming, appear to discriminate well between PCD and controls but there are limited studies, many of which use differing sampling methods and this this limits its clinical usefulness.

With the possible exception of RSPH1 mutation patients [30], those with normal ciliary ultrastructure appear to have the same nNO levels as those with identified ciliary abnormalities. This implies a consistent deficiency in NO across almost all types of ultrastructural abnormality and regardless of underlying mutation (notwithstanding the potential outlier of RSPH1 mutations).

When applying the evidence to diagnosis of PCD, it is important to select appropriate threshold values. The meta-analysis data here show that a cut-off of 75.2nl/min (mean + 3 standard deviations) would miss 0.15% of PCD cases, which agrees well with the 77nl/min suggested by the largest study in this review (n=227) [43] and 78.6nl/min suggested by Marthin *et al* [49]. Other studies' cut-offs range from 38 to 126nl/min (Table 3-3), therefore it is important to establish consistent approaches across centres. These thresholds have been calculated on velum closure in older children and adults, therefore further work will be needed to find thresholds for other groups/analysers as described in 3.4.5 and 3.4.6. It is also necessary to differentiate between the threshold needed for screening to select patients for further assessment (high sensitivity needed in order not to miss cases) as opposed to use of

nNO as part of a diagnostic pathway (balance of sensitivity and specificity to complement other testing).

The data used in this meta-analysis has a number of limitations. The high degree of heterogeneity means the results should be interpreted with more caution and may reflect that many comparison groups included a wide range of ages. Struben *et al* found that mean nNO in healthy 6-17 year olds was 135nl/min as opposed to the meta-analysis result of 271.6nl/min [353]. It is also impossible to confirm the appropriateness of reporting parametric summary statistics in these studies, this is particularly relevant as the means are often close to zero for PCD patients with large standard deviations. Lastly, readings have been converted to nl/min and, although there is evidence that this is valid [48,50], different sampling rates may affect readings differently according to nasal cavity size and osteomeatal patency.

Since nasal NO is used in the diagnosis of PCD, the majority of the evidence relates to differences in this measurement between healthy, CF and PCD patients. However, there is some evidence that lower airway NO is also lower in PCD. Walker *et al* showed that bronchial and alveolar NO were lower in PCD patients than healthy controls whilst alveolar NO was also lower in CF patients than healthy controls [266]. This is despite there being no ciliated epithelium in the alveoli, and suggests a more widespread dysfunction of NO metabolism in PCD. Other studies have supported this with a finding of lower exhaled NO levels in PCD than healthy patients [289,334,344,356]. Airway NO levels in CF do not seem to be consistently different from healthy controls [357,358].

It is not clear from this data whether a lower NO level is protective or harmful in the PCD airway. There is some evidence that reduced NO in CF is caused by inhibition of NOS2 (inducible NOS) in response to inflammation [359] or by bacterial scavenging of available L-arginine for NO synthesis by the epithelium [277]. These factors could both play a role in increased/decreased susceptibility to bacterial colonisation in PCD. It is not known whether similar processes, or others involved in NO metabolism, are operating in the PCD airway.

3.6 Conclusions

This systematic review and meta-analysis confirms that nNO levels are reduced in PCD compared to healthy controls, disease controls and patients with CF. The difference between CF and PCD airways is a potential source of differential responses to bacterial infection. It also

demonstrates that PCD can show consistent epithelial dysfunction across numerous different mutated genes, beat patterns and ultrastructural defects.

Velum closure measurement of nNO in patients over 6 years of age is highly accurate but should still be interpreted alongside clinical history [49]. Tidal breathing measurement, portable analysers and measurement in young children are still useful but are less accurate. Future work on PCD diagnostics should focus on standardising methods for measurement, particularly among younger children, and defining appropriate thresholds for different clinical settings (screening vs diagnosis) and analytical approaches.

It is unclear whether low NO is protective or harmful in PCD airways with bacterial colonisation. There is, therefore, a possible role for NO as a therapeutic adjunct in treatment of airway infection in PCD.

Chapter 4: Treatment of NTHi biofilm with a targeted nitric oxide donor

4.1 Introduction

Nitric oxide has been identified as a potential adjuvant treatment for bacterial infection through biofilm disruption and, as PCD airways have low NO, this treatment could be more effective in PCD patients. Bacterial biofilms present a huge disease burden, particularly in those with chronic suppurative lung diseases such as PCD and CF. These biofilms are significantly more tolerant to antibiotic treatment and novel treatments are needed to combat these infections (1.4). Nitric oxide (NO) has been shown to have a role in both the life-cycle of bacterial biofilms and the host response to bacterial infection. Biofilm formation is characterised by a progression of attachment, establishment, death and release that is shown in Figure 4-1. NO is believed to play a role in triggering the dispersal of established biofilms [150,171,172] via regulation of c-di-GMP levels (1.6.2.1).

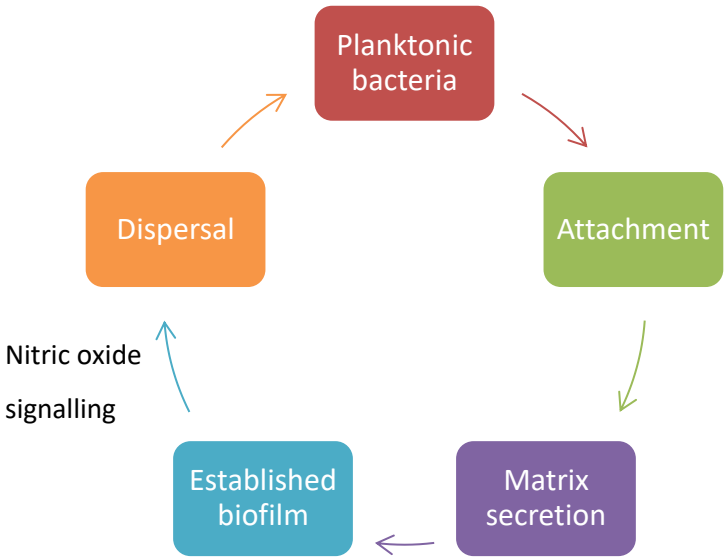

Figure 4-1. **Life cycle of bacterial biofilms.** Bacterial biofilms are not static populations of sessile bacteria; planktonic bacteria begin biofilm formation by attachment to substrate or each other, followed by matrix secretion and metabolic changes within the bacterial population that result in established biofilm. Exogenous factors such as hypoxia and nutrient availability determine the behaviour of the biofilm micro-colonies; various triggers cause dispersal of bacteria from these colonies and, potentially, formation of biofilm at distant sites. Nitric oxide appears to be important in signalling this dispersal in a number of bacterial species.

Exogenous NO triggers biofilm dispersal in a number of bacterial species including *P.aeruginosa* [150], *E.coli, Serratia marcescens* [171], *S.aureus* [172] and in multi-species biofilms [171]. Although the mechanisms, and underlying enzymatic control, involved in this process have been identified in these species (1.6.2.1), whole genome sequencing has failed to identify similar enzyme domains in NTHi or related *Haemophilus* species such as *Haemophilus ducreyii* and *Haemophilus parainfluenzae* [243]. Despite this, work by Walker, using sodium nitroprusside (SNP) as an NO donor, showed a drop in CFUs in NTHi biofilm which worked synergistically with cefotaxime to further reduce CFUs [115]. There was a small but significant increase in the supernatant CFU count, suggesting there may be some triggering of dispersal by nitric oxide.

Since bacterial biofilms are less susceptible to antibiotic treatment, triggering dispersal is a potential means of enhancing bacterial killing by concomitantly administered antibiotics. NO also forms part of the killing apparatus of epithelial cells and macrophages, therefore bacteria

have developed mechanisms to evade exogenous NO attack, including limiting the availability of substrate for NO synthesis [360]. NO is synthesised from L-arginine via nitric oxide synthase (NOS) and data from Grasemann *et al* showed a decreased availability of L-arginine in CF patients undergoing an exacerbation [272,277]. Likewise, PCD patients showed similar deficiencies during pulmonary exacerbations [278]. Given this data and the low NO levels in PCD airways demonstrated in Chapter 3:, NO is a potential treatment for bacterial colonisation of the lower airways and may be particularly effective in the low NO environment of the PCD lung.

Since NO has a wide range of physiological effects, if NO is to be used as a therapeutic agent then there is a need for targeting of the NO release. Administration of NO donors to humans causes changes in pulmonary and systemic vascular resistance that are potentially harmful. For example, SNP was used as an NO donor in Walker's work [115] and is also used intravenously to treat malignant hypertension, producing dramatic falls in systemic blood pressure [361]. Likewise, inhaled NO can cause significant systemic and pulmonary blood pressure drops [362]. Data in humans is limited, given the potentially harmful effects of NO, but a case series as early as 1967 noted 2 deaths from NO contamination of nitrous oxide cylinders used for anaesthesia. In both cases, there was a dramatic drop in systemic blood pressure resulting in cardiac arrest [363].

Jardeleza *et al* used liposomal isosorbide mononitrate as a topical NO donor in a sheep model of chronic rhinosinusitis; within 10 minutes of treatment there was a significant drop in mean systemic arterial blood pressure [281]. Therefore, there remain major concerns over the safety of non-targeted NO administration in humans. Despite this, preliminary results from the Reducing Antibiotic Tolerance Using Nitric Oxide (RATNO) trial of low dose NO adjunctive treatment for *P.aeruginosa* eradication in CF are promising [282] but full publication of safety data is still awaited. Another consideration is that nitric oxide has an extremely short half-life of a few seconds, therefore a compound with a sustained NO release may be needed to effectively disperse bacterial biofilms *in vivo*.

4.1.1 Cephalosporin-3'-diazeniumdiolate NO-donor prodrug (PYRRO-C3D)

PYRRO-C3D is a pro-drug consisting of a cephalosporin antibiotic (cephaloram) attached to a diazeniumdiolate (NONOate) group (Figure 4-2). PYRRO-C3D releases an NO donor (PYRRO-NO) upon cleavage of the β-lactam ring within cephaloram by β-lactamase [364]. The released

PYRRO-NO compound then rapidly releases NO. Since β-lactamase is only found in certain bacterial species, and is not produced by humans, the NO release is targeted to the site of bacterial colonisation. *H.influenzae* can produce β-lactamase and is therefore a potential target for PYRRO-C3D. The targeting of NO release to the site of bacterial colonisation can help reduce the unwanted side-effects of other exogenous NO donors such as sodium nitroprusside that may result in cardiovascular instability [362].

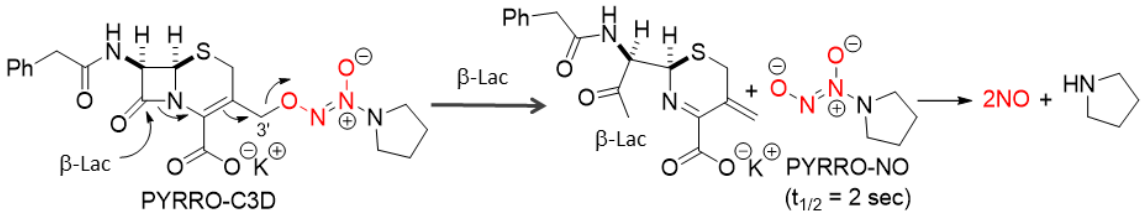

Figure 4-2. **Cephalosporin-3'-diazeniumdiolate pro-drug (PYRRO-C3D) structure** [364]. Cephaloram (cephalosporin) contains a β-lactam ring that is cleaved by bacterial β-lactamase, resulting in release of the NONOate group (PYRRO-NO).

There are, however, certain considerations regarding the use of PYRRO-C3D as a treatment. Firstly, the cephaloram portion of PYRRO-C3D will still retain antibiotic activity through its β-lactam ring. Although β-lactamase cleavage of cephaloram should prevent bacterial killing, it is possible that a proportion of this dose may have a direct cidal effect through this moiety. Secondly, adjunctive treatment with antibiotics that contain β-lactam rings (e.g. penicillins, cephalosporins) could potentially interfere with PYRRO-C3D cleavage by competing for β-lactamase active sites. Other classes of antibiotic should therefore be considered as an adjuvant therapy alongside PYRRO-C3D. Azithromycin is a macrolide antibiotic that works by reversibly binding to the P site of the bacterial 50S ribosomal unit and preventing the enzyme peptidyltransferase from adding additional amino acids to any growing peptide chain. As macrolides do not have a β-lactam ring, they will not compete with PYRRO-C3D for β-lactamase activity, therefore, they are a good choice for co-administration with PYRRO-C3D. Also, NTHi is usually sensitive to macrolides [365] and azithromycin itself may have anti-biofilm properties against NTHi [366].

4.2 Aim

To assess the ability of the targeted NO donor PYRRO-C3D to enhance antibiotic susceptibility of NTHi biofilms *in vitro* and on healthy/PCD cultured epithelium.

4.3 Methods

4.3.1 Biofilms

NTHi biofilms were grown *in vitro* as per 2.2.3. After 72 hours, biofilms were washed with HBSS to remove planktonic and non-adherent bacteria, as well as removing all culture media. Biofilms were then subjected to a 2 hour exposure with the relevant treatment. Scanning electron microscopy (SEM) (2.2.4.3) was used to confirm biofilm formation.

Co-culture of HI4 with primary epithelial cell cultures grown at air-liquid interface was undertaken as per 2.3.3. Wells were washed with HBSS then 1ml fresh media applied to the baso-lateral surface and 500µl of media containing the treatment applied to the apical surface. Treatment lasted 2 hours.

4.3.2 B-lactamase production

Nitrocef™ disks (Hardy Diagnostics, Santa Maria, USA) were used to test for the production of β-lactamase by bacteria as per manufacturer's instructions. Bacterial colonies from agar plates were smeared onto the disc surface with a colour change from yellow to red indicating β-lactamase production.

4.3.3 Treatments

4.3.3.1 PYRRO-C3D

PYRRO-C3D was gifted by Michael Kelso, University of Wollongong and made up as a 10mM stock solution in dimethyl sulfoxide (DMSO) before dilution to appropriate concentration in media. It has previously been confirmed that DMSO has no effect on NTHi biofilm viability at the maximum final concentration of 0.5% (R.Allan – unpublished). DEA/NO was prepared in DMSO immediately prior to use as per PYRRO-C3D preparation.

4.3.3.2 Antibiotics

Azithromycin dose of 4mg/ml was used in line with previous work (R.Allan – unpublished). Oral azithromycin powder (Sandoz, Boucherville, Canada) was made up as per manufacturer's instructions to 40mg/ml with sterile water then diluted in appropriate media. Amoxicillin was used as a β-lactam antibiotic to assess for interference with β-lactamase cleavage of PYRRO-C3D; intravenous preparation powder (Aprilia, Via Fossignano, Italy) was prepared with water then appropriate media to make the necessary concentrations.

4.3.4 Assays

4.3.4.1 Planktonic assays

Assay of the effect of PYRRO-C3D on planktonic growth was performed using a flat-bottomed polystyrene 96 well plate (Corning Life Sciences). Cultures were grown to mid-exponential phase then centrifuged at 3500xg for 5 minutes. 20µl supernatant was transferred to each well with 180µl of PYRRO-C3D solution at concentrations from 1µM to 200µM. After 24 hours, optical density (OD_{600}) was measured using Spectra Max 340 PC plate-reading spectrophotometer (Molecular Devices, Sunnyvale, US) controlled by ADAP software (Biochrom, Cambridge, UK).

4.3.4.2 Nitric oxide probe

An ISO-NO nitric oxide detector (World Precision Instruments, Springvale, Florida) was used to detect the release of NO from PYRRO-C3D under certain experimental conditions. For experiments in solution, 3ml of PBS was placed in a well of a 12 well plate (Corning Life Sciences) with the probe inserted into the solution so the tip was completely submerged. For measurement involving cultured primary epithelial cells, 750µl of PBS was placed on the apical surface of the cells and the probe submerged so the tip was just above the cell monolayer. Prior to use, the probe was submerged in deionised water for at least 24 hours then placed in PBS with current passing through for an hour to zero the readout. Readings were taken over time on at least 2 separate occasions and presented in graphical format.

4.3.5 Assessment of biofilm treatment

Following treatment, *in vitro* biofilms and those on primary epithelial cells were assessed for viability using CFU counts (2.2.4.2). *In vitro* biofilms were also fluorescently labelled with a

Live/Dead stain, then imaged with confocal microscopy (2.2.4.4). Crude assessment of *in vitro* biofilm biomass was also undertaken with the crystal violet assay (2.2.4.1).

4.4 Results

Formation of 72h biofilm by NTHi *in vitro* was confirmed using scanning electron microscopy (SEM) (Figure 4-3). Images showed evidence of organised individual bacteria encased within secreted extracellular matrix that are adherent to the underlying glass coverslip surface (they were not removed by the HBSS washes).

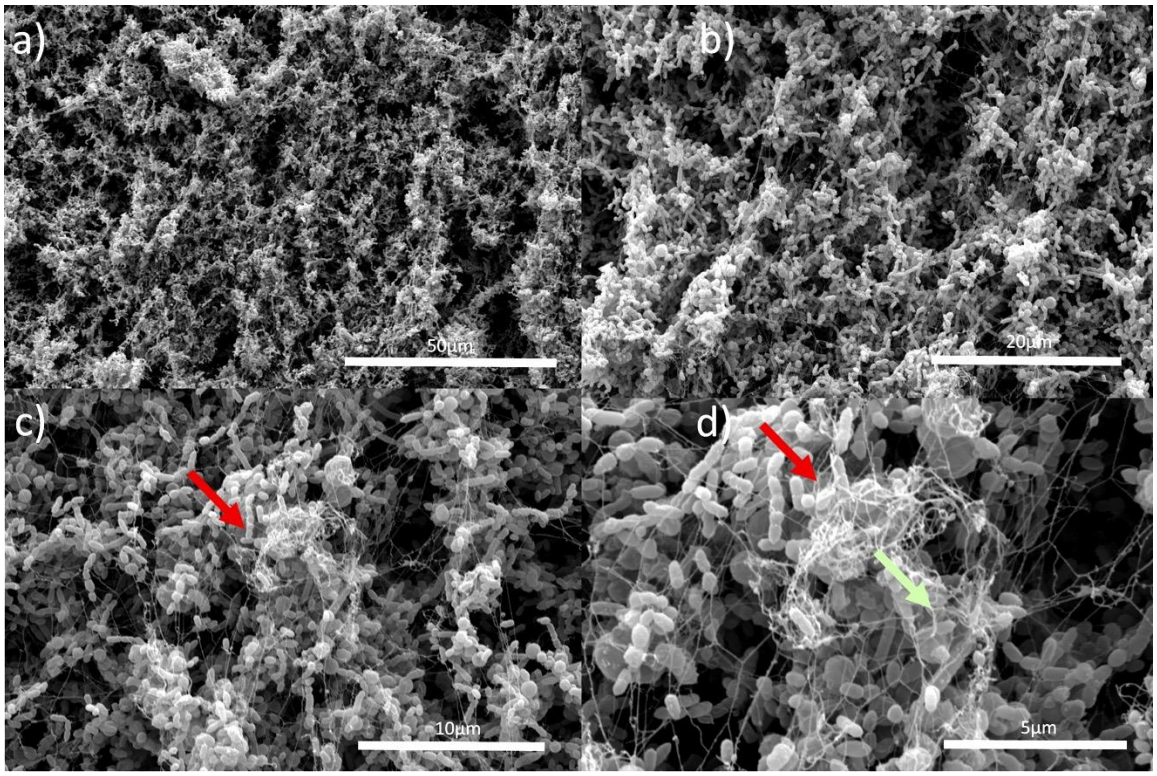

Figure 4-3.**Scanning electron microscope images of NTHi (HI4 isolate) biofilm *in vitro*.** NTHi was cultured for 72 hours on glass cover slips in wells of a 6 well polystyrene culture plate. Evidence of organisation of individual bacteria (red arrows) within secreted extracellular matrix (green arrow) at a) 150x b) 2700x c) 5000x d) 10,000x magnifications.

Confocal imaging of the biofilm using Live/Dead staining (2.2.4.4) confirmed biofilm architecture containing both live bacteria and dead/eDNA staining. The biofilm appears to have an organised structure containing mostly live bacteria on the apical surface with a band

of dead/eDNA stain below this. The base of the biofilm is more densely packed and contains a mixture of live and dead staining.

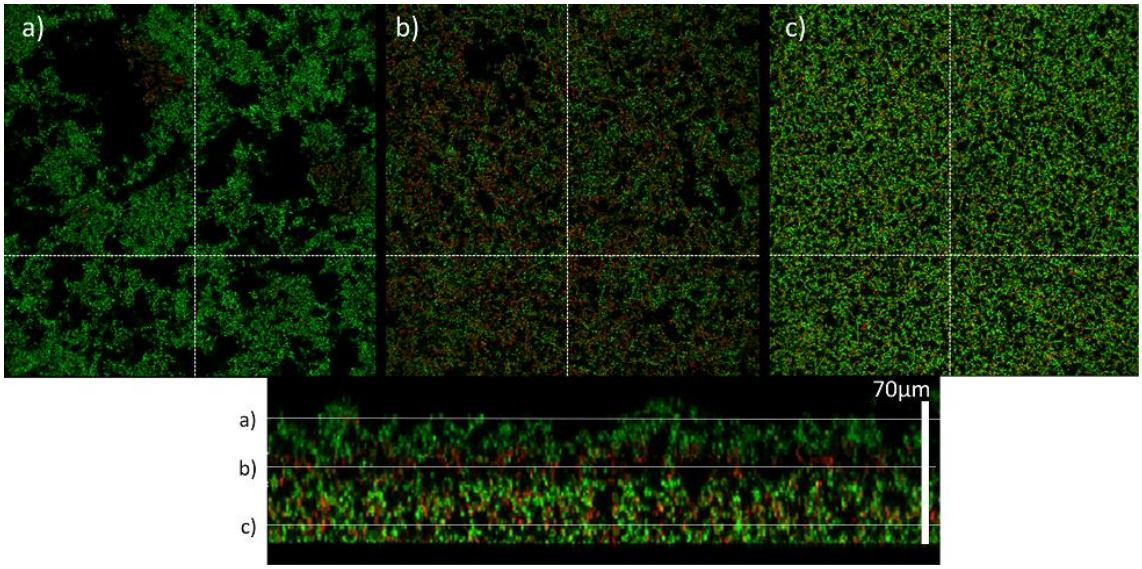

Figure 4-4. **Confocal imaging of *in vitro* 72h NTHi biofilm using live/dead staining**. NTHi (HI4 isolate) cultured for 72 hours in glass-bottomed CELLview plates then stained with BacLight live/dead stain. Green fluorescence shows live bacteria, red shows dead bacteria/extracellular DNA. Cross sections are shown at three different levels indicated by the cross sectional image below. There is evidence of biofilm architecture with distinct stratification at **a)** largely live bacteria at the apical surface, **b)** a mixture of some live staining but predominantly dead/eDNA staining **c)** a mixture of live and dead staining within a more densely packed basal layer.

4.4.1 β-lactamase producing NTHi and NO release from PYRRO-C3D

NTHi is not a universal producer of β-lactamase, with variability even within different isolates of the same species [367]. Therefore, β-lactamase production was confirmed in the NTHi strains to ensure they could potentially cleave PYRRO-C3D to release NO (4.3.2). HI3, HI4 and HI6 were β-lactamase producers, HI5 was not. The release of NO from PYRRO-C3D by β-lactamase cleavage was confirmed using the NO probe. NO concentration was zero in a solution of β-lactamase (Penicillinase from *Bacillus cereus*, Sigma-Aldrich) at 10u/ml, but rapidly increased to a maximum of 625nM following addition of PYRRO-C3D at 50µM before slowly declining over the next 135 minutes (Figure 4-5).

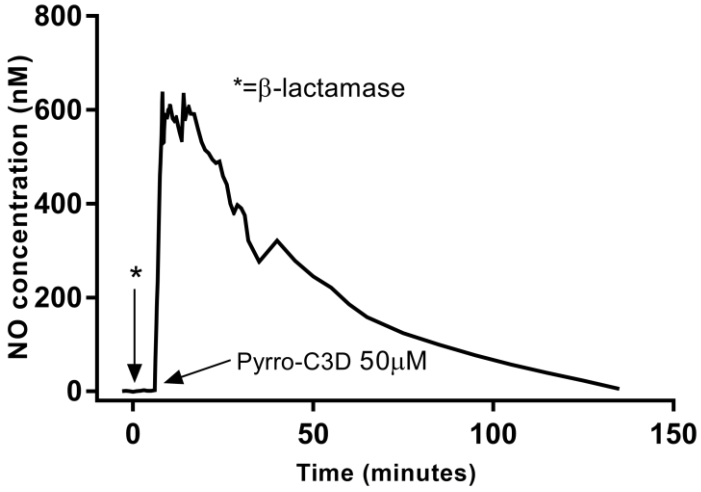

Figure 4-5. **β-lactamase is required for release of nitric oxide (NO) from PYRRO-C3D.** NO levels measured using an NO probe submerged in 3ml PBS solution following addition of 30u β-lactamase then PYRRO-C3D at a 50μM concentration. n=2.

A solution of planktonic NTHi (HI4) at mid-exponential growth phase was then used to confirm its ability to cleave PYRRO-C3D and release NO. A baseline NO of 120nM was produced by NTHi in solution, however addition of 50μM PYRRO-C3D immediately produced a spike in NO that rose to a maximum of 204nM after 2 minutes. Addition of the β-lactamase inhibitor clavulanate quenched the reaction and returned the NO level to baseline (Figure 4-6).

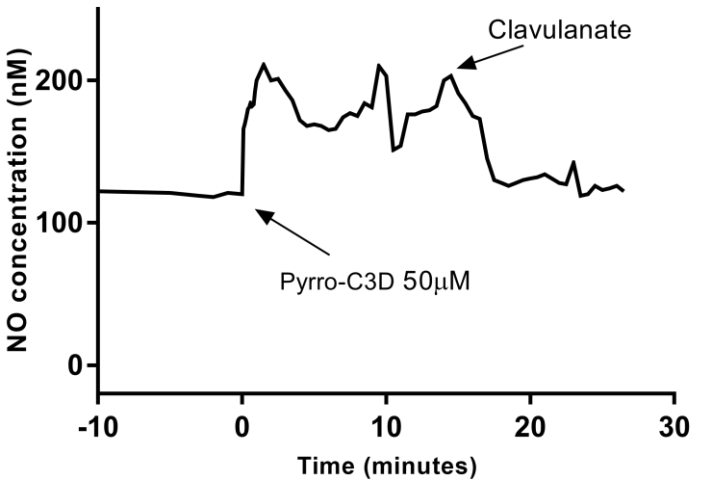

Figure 4-6. **β-lactamase producing NTHi cleaves PYRRO-C3D to release nitric oxide (NO)**. NO measured using NO-probe submerged in 3ml PBS solution. Baseline NO is established at

around 120nM with a rapid rise following addition of PYRRO-C3D 50µM. Addition of clavulanate (β-lactamase inhibitor) causes a return to baseline. n=2.

4.4.2 PYRRO-C3D and planktonic NTHi

The growth of NTHi was inhibited by increasing concentrations of PYRRO-C3D until complete inhibition of growth was seen at 100µM. This effect was attributed to the action of the cephaloram component of PYRRO-C3D, as this alone also caused growth inhibition at concentrations above 100µM. However, the NO donor portion of PYRRO-C3D (DEA/NO) did not cause cytotoxicity and seems to be responsible for the small increase in planktonic growth around 50µM (Figure 4-7).

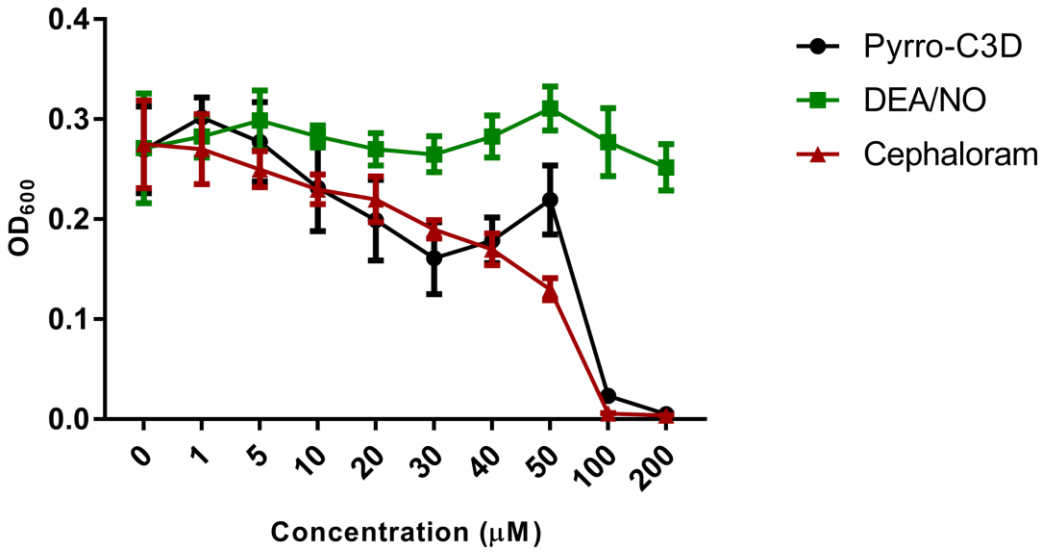

Figure 4-7. **Cephaloram within PYRRO-C3D inhibits planktonic NTHi growth with complete inhibition of growth above 100µM.** Effect of increasing concentrations of PYRRO-C3D, cephaloram and DEA/NO (NO donor) on planktonic growth of β-lactamase producing NTHi over 24 hours (HI4 isolate). OD_{600} – optical density at wavelength of 600nm. n=3.

4.4.3 PYRRO-C3D and NTHi biofilm

PYRRO-C3D was applied to *in vitro* 72h NTHi biofilms for 2 hours at concentrations from 10nM to 200µM with no significant reduction in CFU counts observed (Figure 4-8). 50µM PYRRO-C3D was therefore chosen as the concentration to be used in subsequent assays in order that PYRRO-C3D be adjunctive rather than cytotoxic to planktonic/biofilm bacteria. In contrast to planktonic NTHi, there was no significant reduction in viability at 100 and 200µM

concentrations, showing that the biofilm is inherently more tolerant to the effect of PYRRO-C3D and that an additional antibiotic is needed to treat the biofilm. 50µM PYRRO-C3D was then used alongside 4mg/ml azithromycin to assess its effect on NTHi biofilm and was found to enhance the efficacy of azithromycin treatment by causing a 4.6 fold reduction in CFUs ($1.8x10^8$ vs $3.9x10^7$ CFU/cm^2, $p<0.05$) (Figure 4-9).

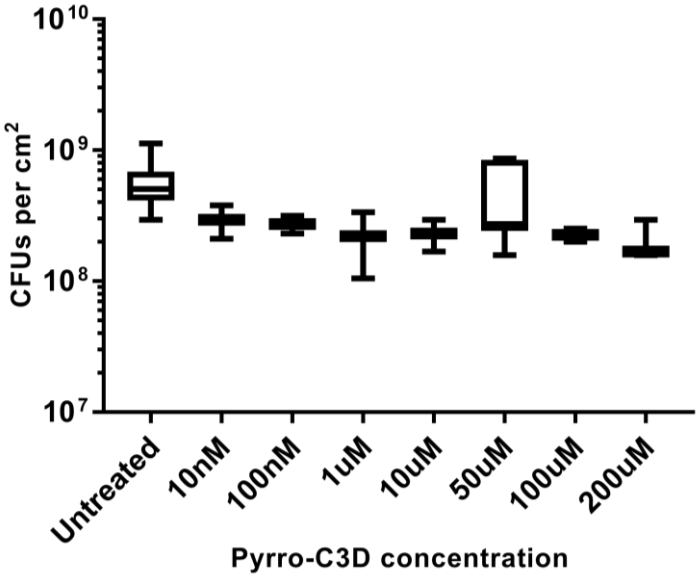

Figure 4-8. **Concentrations of PYRRO-C3D up to 200µM do not affect viability of NTHi biofilms.** Effect of increasing concentration of PYRRO-C3D on viability of 72h NTHi (HI4 isolate) biofilms after 2 hour treatment time. CFU – colony forming units. n=5

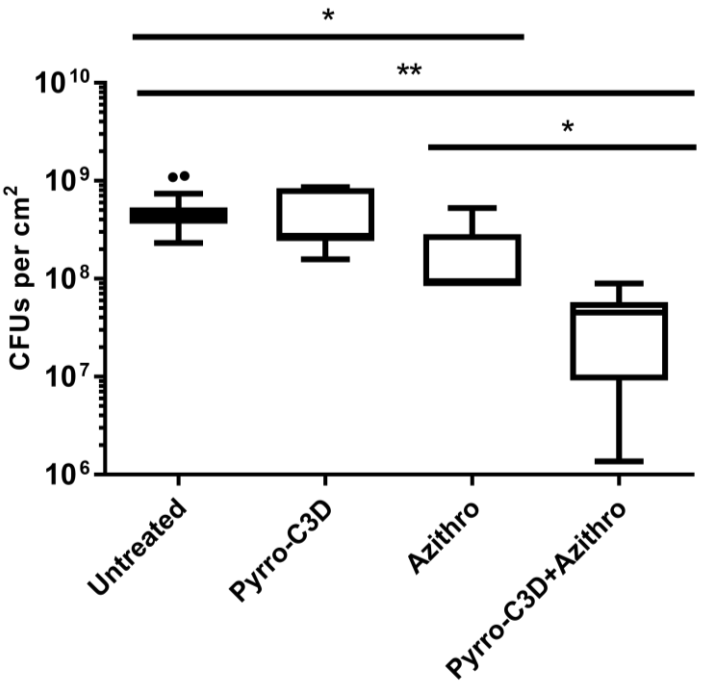

Figure 4-9. **PYRRO-C3D enhances azithromycin treatment of NTHi biofilms.** Effect of 2 hour treatment with PYRRO-C3D (50µM) and Azithromycin (4mg/ml) alone or in combination on viability of 72h NTHi (HI4 isolate) biofilms. CFU – colony forming units. *p<0.05, **p<0.001 (n=8)

4.4.4 Fluorescent labelling and confocal imaging

In vitro biofilms were also assessed using fluorescent labelling and confocal microscope imaging. Samples were prepared as per 2.2.4.4 using the BacLight live/dead fluorescent stain (ThermoFisher, Waltham, USA). PYRRO-C3D alone compared to untreated biofilm caused a significant increase in both live staining from 35.8 to 47.5µm^3/µm^2 ($p<0.05$) and dead/eDNA staining from 8.9 to 25.0µm^3/µm^2 ($p<0.05$). Azithromycin did not change live staining ($p=0.83$) but did cause a significant increase in dead staining from 8.9 to 21.2 µm^3/µm^2 ($p<0.05$). As the "dead" part of the stain is propidium iodide, this will stain both cells with permeable cell membranes and extracellular DNA (eDNA). Since eDNA forms part of biofilm matrix, red fluorescence will reflect both of these facets of the biofilm. Compared to azithromycin alone, PYRRO-C3D and azithromycin together resulted in a significant reduction in the biomass of live bacteria from 35.0 to 22.7µm^3/µm^2 ($p<0.05$) and dead bacteria/eDNA from 21.2 to 9.5µm^3/µm^2 ($p<0.05$) (Figure 4-10).

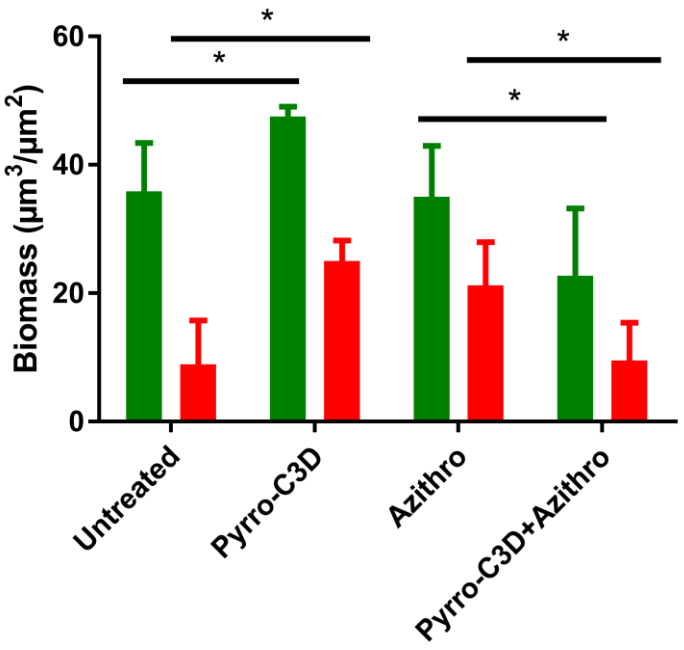

Figure 4-10. **PYRRO-C3D in combination with azithromycin reduces both live and "dead" staining within NTHi biofilm.** Biomass of live bacteria (green) and dead bacteria/extracellular DNA (red) in a 72h NTHi (HI4 isolate) *in vitro* biofilm following treatment with PYRRO-C3D (50uM), Azithromycin (4mg/ml) alone or in combination. Fluorescent labelling with BacLight live/dead stain and confocal imaging followed by COMSTAT2 image analysis. *p<0.05. (n=5, 4 fields of view in each)

4.4.5 Other strains and biofilm dispersal

In order to demonstrate that the effect of PYRRO-C3D was not specific to this strain of NTHi (HI4), the assay was repeated with another PCD patient strain (HI3) and two strains from nasal carriage in healthy children (HI5 and HI6). HI5 strain did not produce β-lactamase, whilst HI3 and HI6 did. Figure 4-11 shows that the HI3 strain biofilm is significantly more susceptible to azithromycin in the presence of 50µM PYRRO-C3D ($1.3x10^8$ vs $4.7x10^7$ CFU/cm^2, $p<0.05$). The effect was also seen in the HI6 strain ($1.8x10^8$ vs $2.5\ x10^7$ CFU/cm^2, $p<0.001$) but not in HI5 biofilm (the non β-lactamase producing strain, $p=0.24$).

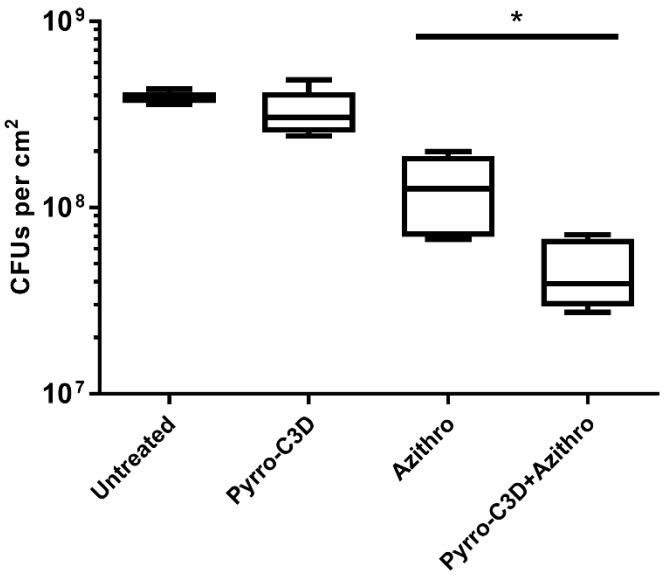

Figure 4-11. **PYRRO-C3D is effective in enhancing azithromycin sensitivity in the HI3 strain of NTHi.** Effect of 2 hour treatment with PYRRO-C3D (50µM) and azithromycin (4mg/ml), alone or in combination, on viability of 72h biofilm of NTHi strain HI3 biofilm. CFU - colony forming unit. n=5, *p<0.05

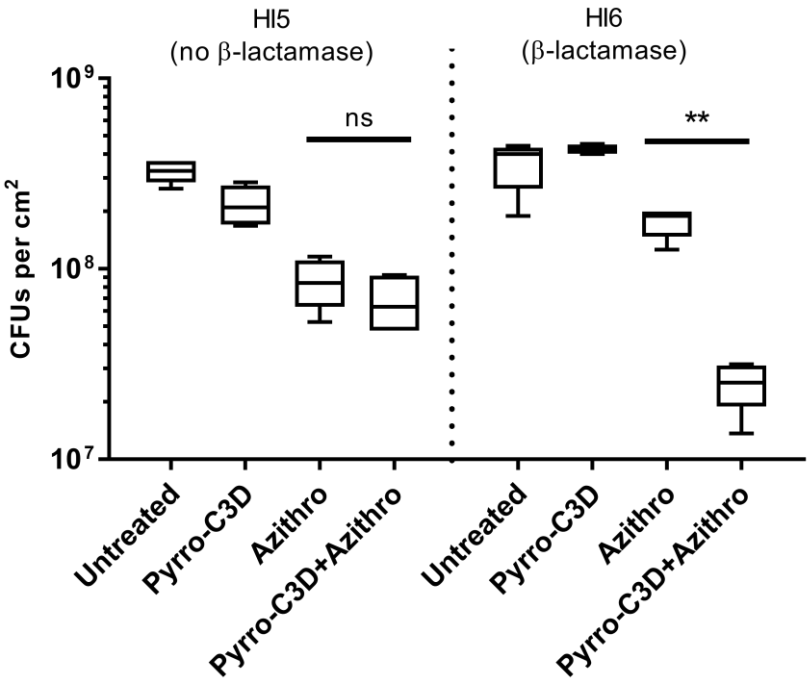

Figure 4-12. **PYRRO-C3D is effective in enhancing azithromycin sensitivity only in biofilms from β-lactamase producing strains of NTHi.** Effect of PYRRO-C3D (50µM) and azithromycin (4mg/ml) alone or in combination on NTHi strain HI5 and HI6 72h biofilm viability following 2 hour treatment time. CFU - colony forming unit. n=5, **p<0.001 ns-not significant

Previous work on NO and bacterial biofilms identified the triggering of dispersal. However, Figure 4-13 shows that, rather than causing dispersal, compared to untreated biofilm, PYRRO-C3D decreases the number of bacteria in the supernatant above the NTHi biofilm from $1.2x10^8$ to $6.9x10^7$ CFUs/ml, $p<0.05$). Azithromycin also significantly reduced the bacteria in the supernatant to $1.6x10^7$ CFUs/ml ($p<0.001$ vs untreated) but, in contrast to the biofilm, PYRRO-C3D did not enhance this effect ($p=0.10$). As biofilms were washed with HBSS prior to the assay, the collected supernatant represented only those bacteria released during the 2 hour assay time. The planktonic data in Figure 4-7 suggests this is due to antibiotic killing in the supernatant (cephaloram in PYRRO-C3D or azithromycin) as previous work by Walker using NO alone (in the form of SNP) showed no significant difference in supernatant CFUs at equivalent NO concentrations to those used in this work [115].

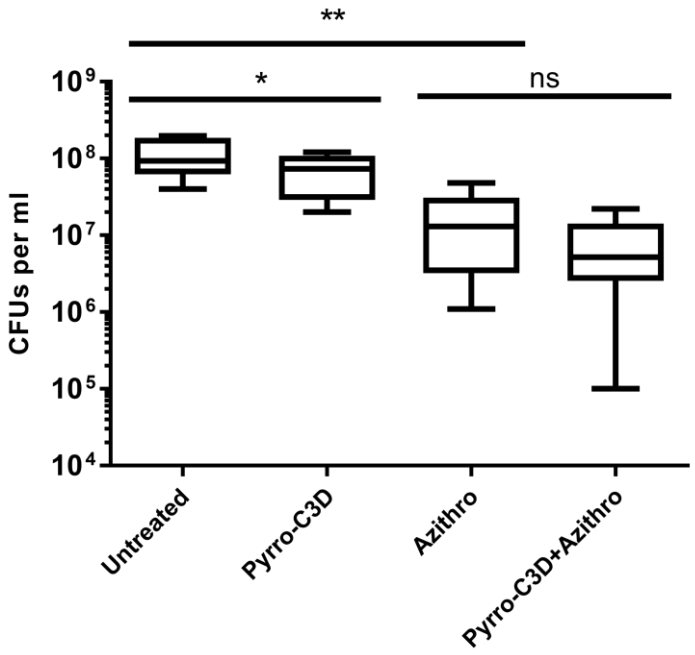

Figure 4-13. **PYRRO-C3D causes a decrease in viable bacteria in the supernatant of NTHi (HI4) biofilms but does not significantly increase the effect of azithromycin**. Effect of PYRRO-C3D (50µM) and azithromycin (4mg/ml) alone or in combination on number of viable bacteria in the supernatant above 2 hour treated 72h NTHi biofilms. CFU – colony forming unit. *$p<0.05$ **$p<0.001$ ns – not significant. (n=5)

4.4.6 Confirmation that the PYRRO-C3D enhancement of azithromycin treatment of NTHi biofilm is NO mediated

A number of controls were used to demonstrate that the enhancement of antibiotic susceptibility by PYRRO-C3D was due to the released NO, rather than a direct effect of the cephalosporin contained in PYRRO-C3D.

Clavulanic acid is a β-lactamase inhibitor that prevents cleavage of the β-lactam ring in the cephaloram portion of PYRRO-C3D and thus prevents release of PYRRO-NO, whereas 2-4-carboxyphenyl-4,4,5,5-tetramethylimidazoline-1-oxyl-3-oxide (cPTIO) is an NO scavenger that will scavenge the NO released by PYRRO-C3D. Both inhibition of NO release by clavulanic acid and scavenging of released NO by cPTIO effectively reversed the ability of PYRRO-C3D to enhance bacterial killing by azithromycin; there was no significant difference between azithromycin alone ($1.83x10^8$ CFU/cm^2) and PYRRO-C3D/azithromycin with PTIO ($1.08x10^8$ CFU/cm^2, p=0.32) or PYRRO-C3D/azithromycin with clavulanate ($1.79x10^8$ CFU/cm^2, p=0.9) (Figure 4-14a). The assays were repeated using cephaloram alone (the cephalosporin portion of PYRRO-C3D with no NO releasing capacity) and with "spent" PYRRO-C3D; this was obtained by placing 50μM PYRRO-C3D in BHI with 0.01u/μl of β-lactamase for an hour to pre-cleave the PYRRO-C3D and release the NO prior to assay. Neither "spent" PYRRO-C3D (p=0.44) or cephaloram (p=0.19) enhanced azithromycin treatment of NTHi biofilm. Cephaloram and "spent" PYRRO-C3D alone did not affect viability compared to untreated biofilms (Figure 4-14b).

The assays were repeated with Diethylamine NONOate (DEA/NO) to see whether the slower NO release profile of PYRRO-C3D is important. DEA/NO has a half-life of around 2 minutes at 37^oC [368] whilst PYRRO-NO has an NO release half-life of around 3 seconds [368], however the fact that PYRRO-C3D requires β-lactamase cleavage means the release is limited by this enzyme reaction (Figure 4-6) and data from 4.4.1 shows NO release is prolonged and sustained with a half-life of around 30 minutes. DEA/NO in combination with azithromycin did not significantly decrease viability compared to azithromycin alone (p=0.56), suggesting that the sustained release of NO from PYRRO-C3D is critical (Figure 4-14c).

Azithromycin is a macrolide antibiotic that does not contain a β-lactam ring [369] so in order to assess the effectiveness of antibiotics that may compete with PYRRO-C3D for β-lactamase and cause competitive inhibition, the assay was repeated with amoxicillin. PYRRO-C3D did not significantly improve the antimicrobial activity of amoxicillin (p=0.76, Figure 4-14d).

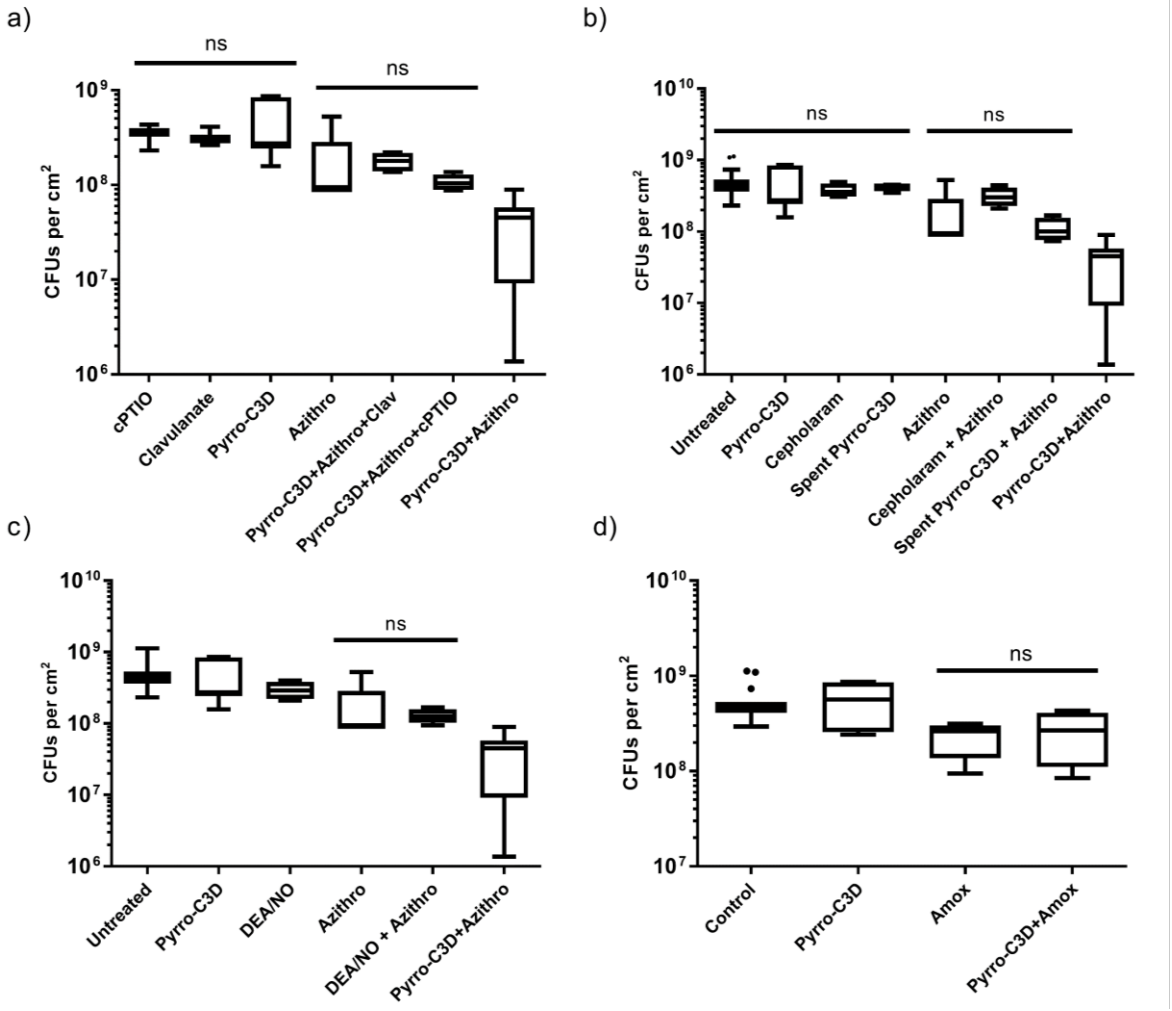

Figure 4-14. **PYRRO-C3D enhancement of azithromycin treatment is dependent on β-lactamase induced cleavage of PYRRO-C3D and subsequent NO release.** Effect of PYRRO-C3D (50µM) and azithromycin (4mg/ml) treatments on NTHi biofilm (strain HI4 unless otherwise specified). a) Addition of NO scavenger (50µM cPTIO) or β-lactamase inhibitor (50µM clavulanate) to prevent NO release reverses the effect of PYRRO-C3D on azithromycin treatment. b) Cephaloram alone or PYRRO-C3D that is pre-cleaved by β-lactamase (spent PYRRO-C3D) do not enhance azithromycin treatment. C) The effect of PYRRO-C3D is not replicated by using only the NONOate nitric oxide donor (DEA/NO 50µM) suggesting prolonged, sustained release by PYRRO-C3D is necessary. D) Use of amoxicillin (amox), a β-lactam antibiotic instead of azithromycin is not enhanced by PYRRO-C3D. (n=5 except PYRRO-C3D, azithro and PYRRO-C3D+azithro where n=8)

4.4.7 Other effects of PYRRO-C3D on NTHi biofilm

In order to gain further information about the effect of PYRRO-C3D treatment on biofilm, crystal violet assays were used to assess overall biomass (as per 2.2.4.1) alongside further

analysis of confocal imaging data. PYRRO-C3D alone had no effect on overall biomass as assessed by crystal violet (p=0.23) but azithromycin alone increased OD_{600} from 1.05 to 1.18 (p<0.05) whilst the combination of azithromycin and PYRRO-C3D increased OD_{600} to 1.17 (p<0.05). Compared to untreated biofilm, cephaloram alone also significantly increased OD_{600} to 1.17 (p<0.05). A combination of cephaloram and azithromycin increased biomass further to a mean of 1.40 which was significantly greater than azithromycin or cephaloram alone (both p<0.05) (Figure 4-15).

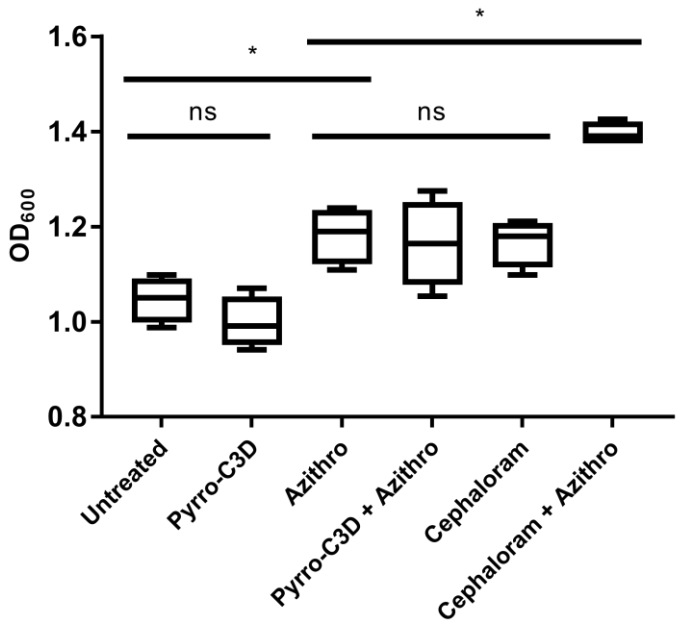

Figure 4-15. **Azithromycin and cephaloram increase biomass of NTHi biofilm but PYRRO-C3D does not.** Effect of PYRRO-C3D (50μM), azithromycin (4mg/ml) and cephaloram (50μM) 2 hour treatments, alone or in combination, on overall biomass of 72h NTHi (HI4 isolate) biofilms as assessed by crystal violet assay. OD_{600} – optical density at 600nm wavelength. ns-not significant, *p<0.05, n=5

Confocal imaging data using the live/dead stain (2.2.4.4) showed that cephaloram alone did not increase live staining (p=0.15) but did increase dead/eDNA staining from 8.9 to 26.0 $\mu m^3/\mu m^2$ (p<0.05), suggesting a stimulation of biofilm formation. Cephaloram did not change the effect of azithromycin on live (p=0.72)or dead/eDNA (p=0.89) staining, further supporting the evidence for NO release as the critical mechanism behind PYRRO-C3D's efficacy.

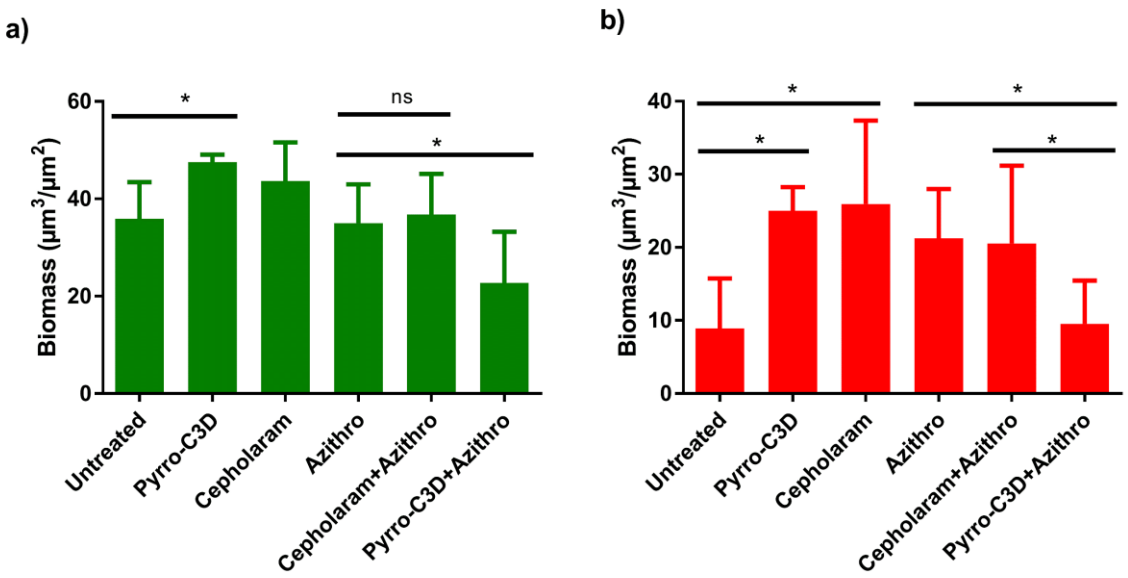

Figure 4-16. **PYRRO-C3D and cephaloram alone increase live and dead staining of NTHi biofilms whilst only a combination of PYRRO-C3D and azithromycin reduces both live and dead NTHI biofilm staining.** Biomass of live bacteria (green) and dead bacteria/extracellular DNA (red) in a 72h NTHi (HI4 isolate) *in vitro* biofilm following 2 hour treatment with PYRRO-C3D (50uM), Azithromycin (4mg/ml) or Cephaloram (50uM) alone or in combination. Fluorescent labelling with BacLight live/dead stain and confocal imaging followed by COMSTAT2 image analysis. ns-not significant, *p<0.05. (n=5, 4 fields of view in each)

Stimulation of biofilm formation by PYRRO-C3D and cephaloram is also shown by increased average diffusion distance to live bacteria (Figure 4-17a). This is calculated by the COMSTAT2 software and is a surrogate measure of how densely packed the biofilm is, for example, a decrease in spaces or channels will result in increased diffusion distance. Despite this, there is no significant change in the thickness of the biofilm with any of the treatments other than PYRRO-C3D/azithromycin, suggesting the changes in diffusion distance are representative of increasing biofilm density. The significant drop in maximum thickness caused by the PYRRO-C3D/azithromycin combination from 73.1µm to 56.4µm compared to untreated biofilm may represent a combination dispersal and killing response (Figure 4-17b).

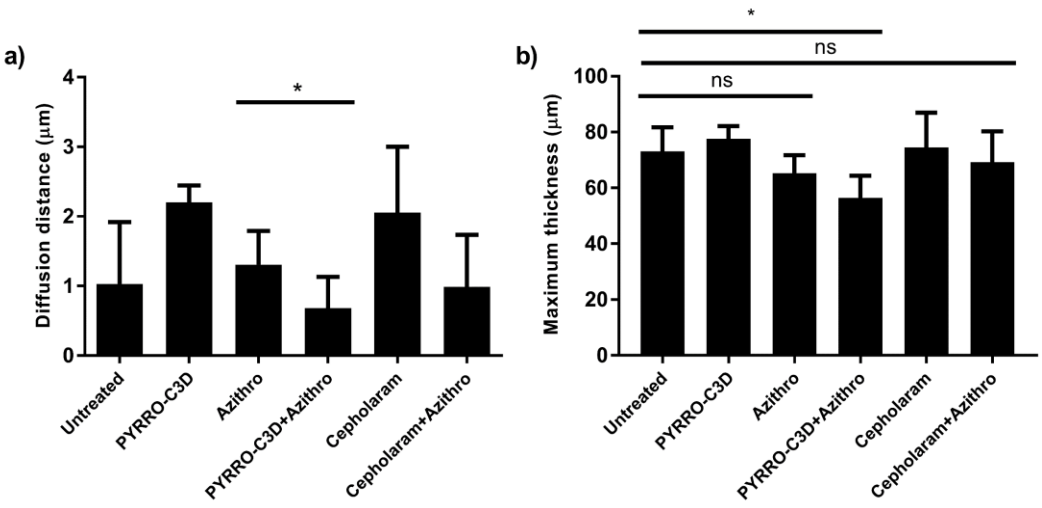

Figure 4-17. **PYRRO-C3D or cephaloram treatment alone results in increased diffusion distance in NTHi biofilms without decreased thickness of biofilm; this effect disappears when used in combination with azithromycin.** non-typeable *H.influenzae* (HI4 isolate) 72h *in vitro* biofilm following 2 hour treatment with PYRRO-C3D (50µM), Azithromycin (4mg/ml) or Cephaloram (50µM) alone or in combination. a) Average diffusion distance to live bacteria b) maximum thickness of biofilm. Fluorescent labelling with BacLight live/dead stain and confocal imaging followed by COMSTAT2 image analysis ns=not significant, *p<0.05. (n=5, 4 fields of view in each)

These data can be combined to give an impression of the overall biomass, biomass of bacteria, viability (CFU counts) and proportion of live/dead bacteria in the biofilm (Table 4-1). When looking at the combined data, PYRRO-C3D alone does not affect the viability of the biofilm (CFUs) but does appear to induce biofilm formation, as there is a small increase in live stain with a significant increase in dead bacteria/eDNA and average diffusion distance. This effect is likely due to the cephaloram within the PYRRO-C3D as cephaloram alone also causes increases in dead/eDNA stain, diffusion distance and crystal violet stain. Azithromycin alone induces biofilm formation (increased CV and dead/eDNA stain) but fails to reduce the number of live bacteria, even though fewer are culturable. This could represent a switch to dormant (non-culturable) but live bacteria within the biofilm. Only the combination of PYRRO-C3D and Azithromycin reduces viability (CFUs) and number of live bacteria with no concomitant increase in dead/eDNA or diffusion distance.

	Crystal Violet	CFU counts (viability)	Live stain	Dead/eDNA stain	Diffusion distance	Maximum thickness
Untreated	-	-	-	-	-	-
PYRRO-C3D	↔	↔	↑	↑	↑	↔
Azithro	↑	↓	↔	↑	↔	↔
PYRRO-C3D + Azithro	↑	↓↓	↓	↔	↔	↓
Cephaloram	↑	↔	↔	↑	↑	↔
Cephaloram + Azithro	↑↑	↔	↔	↑	↔	↔

Table 4-1. **Summary of biofilm changes in response to PYRRO-C3D (50µM), azithromycin (4mg/ml) and cephaloram (50µM) alone or in combination**. Crystal violet staining (overall biological material), biofilm viability (colony forming unit counts – CFUs), fluorescent staining of live bacteria (SYTO9) and dead bacteria/extracellular DNA (propidium iodide) followed by COMSTAT2 analysis of biomass of these stains as well as average diffusion distance to live bacteria and maximum thickness.

4.4.8 Co-culture with primary epithelial cells at air-liquid interface

Although the above demonstrates PYRRO-C3D enhancement of bacterial killing of *in vitro* biofilms by azithromycin, this does not necessarily translate to *in vivo* effectiveness since clinical NTHi biofilms occur on epithelial surfaces. In contrast to the *in vitro* model, biofilms on these cells are attempting to bind to a dynamic biological surface that possesses defense mechanisms against such colonisation. The epithelial cells actively secrete innate defense proteins and will attempt to counteract colonising bacteria. This interplay and the differential binding of NTHi to ciliated or unciliated regions of the cell will, potentially, alter the biofilm behaviour. Importantly, the epithelial cells are able to produce NO both constitutively and in response to bacterial infection thus the NTHi may have exposure to NO during the colonisation and not just during the treatment time with PYRRO-C3D, allowing potential adaptation by the NTHi to NO attack. Co-culture was performed as per 2.3.3. using primary epithelial cells obtained by nasal brushing from healthy and PCD subjects, then cultured at air-liquid interface. 72 hour co-culture with HI4 isolate of NTHi was followed by 2 hour treatment time. Biofilm

formation was confirmed using SEM (Figure 4-18). As seen *in vitro,* compared to azithromycin alone, 50µM PYRRO-C3D enhances azithromycin treatment of NTHi biofilms ($3.2x10^6$ vs $2.1x10^5$ CFU/cm^2, p<0.001), an effect which is more pronounced on PCD epithelium ($5.4x10^6$ vs $2.5x10^4$ CFU/cm^2, p<0.05) (Figure 4-19).

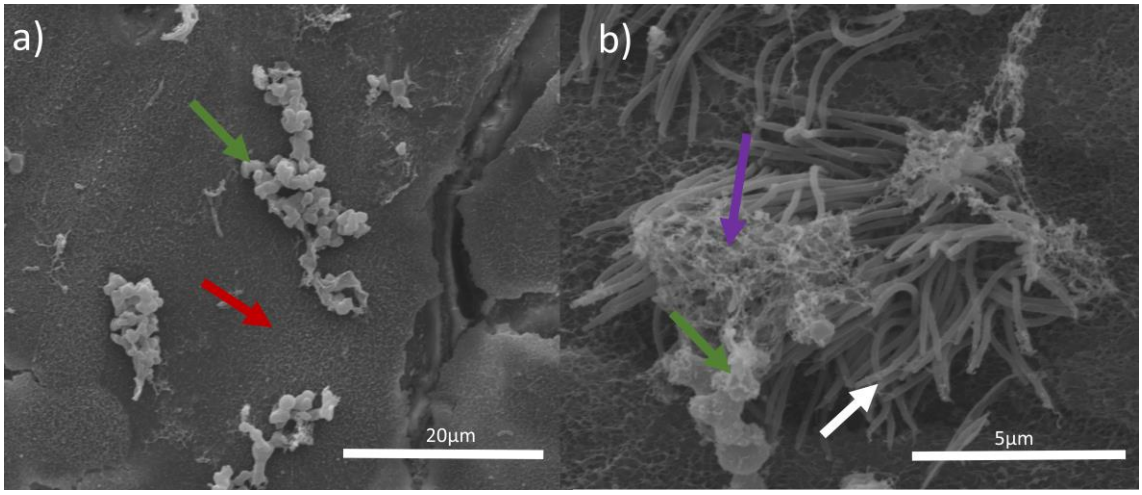

Figure 4-18. **Scanning electron microscope images confirming biofilm formation at 72 hours on primary respiratory epithelium cultured at air liquid interface**. a) Bacterial aggregates (green arrows) formed on the unciliated surface of the cultured epithelial cells (red arrow) at 2600x magnification. b) Aggregates of bacteria (green arrow) within secreted extracellular matrix (purple arrow) adherent to cilia (white arrow) at 11,000x magnification.

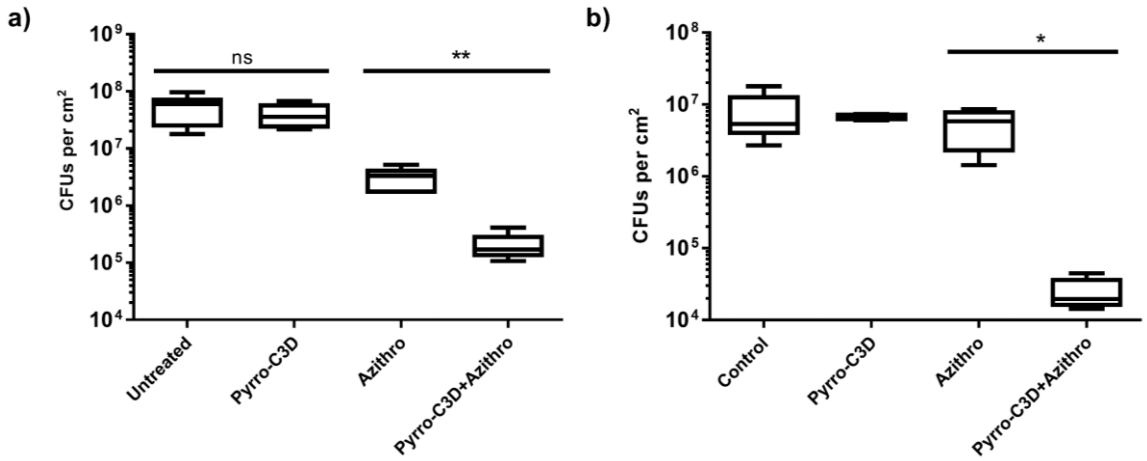

Figure 4-19. **PYRRO-C3D enhances azithromycin treatment of NTHi biofilm on a) healthy and b) PCD, cultured respiratory epithelium.** Effect of 2 hour treatment with 50µM PYRRO-C3D and azithromycin (4mg/ml) alone or in combination on the viability of NTHi (HI4 strain) biofilms on primary epithelial cells. Healthy (n=5 and PCD (n=4) cells cultured at air-liquid interface were co-cultured for 72 hours with HI4 strain of NTHi. CFU – colony forming units. *p<0.05, **p<0.001, ns-not significant

In order to confirm that the NO was not released at the epithelial surface in the absence of infection, an NO probe was used to measure NO release from PYRRO-C3D applied to cultured epithelial cells with or without NTHi biofilm. Figure 4-20 shows a steady baseline around 0 prior to addition of 50μM concentration of PYRRO-C3D, with no rise in NO concentration following this. Addition of 10u/ml β-lactamase confirms the ongoing potential of PYRRO-C3D to release NO.

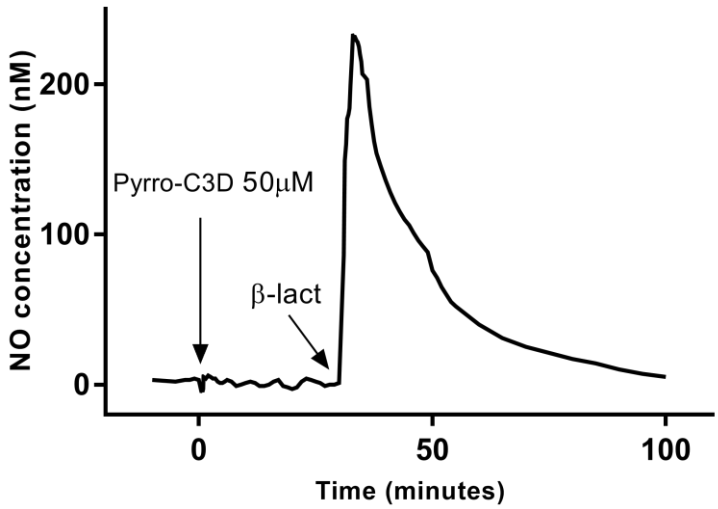

Figure 4-20. **Nitric oxide concentration in apical solution above primary epithelial cells from a healthy volunteer showing no detectable NO release from PYRRO-C3D without additional β-lactamase (β-lact).** 750μl PBS added to apical surface of primary respiratory epithelium cultured at air-liquid interface followed by insertion of NO probe to just above cell layer then addition of PYRRO-C3D (final concentration 50μM) with no detectable increase in NO. This was followed by 30u β-lactamase at 35 minutes with a rapid increase in released NO. n=2

A similar pattern is seen when using primary epithelial cells with a 72 hour NTHi biofilm on them, albeit with a baseline of around 50nM NO in solution. Although this suggests that the biofilm NTHi is not causing NO release, the assays in 4.4.6 show that NO release is required for the antibiotic-enhancing effect of NTHi. Addition of β-lactamase again shows the potential for rapid NO release is still present in the PYRRO-C3D, however it may be that the low levels of β-lactamase within the biofilm cause small amounts of local NO release that are subsequently scavenged by either bacterial or epithelial cells before the concentration in the solution is significantly altered. The induced release of NO by β-lactamase also seems to cause inhibition

of the baseline NO release as levels return to near zero once the PYRRO-C3D/β-lactamase reaction has finished (Figure 4-21).

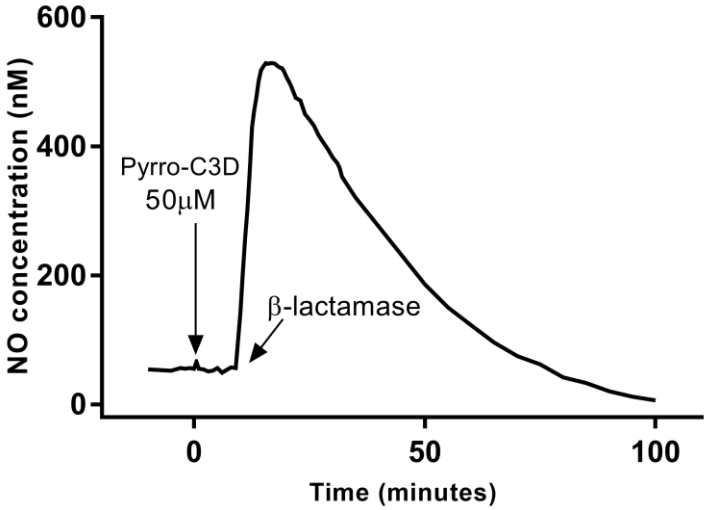

Figure 4-21. **Nitric oxide concentration in apical solution above primary epithelial cells from a healthy volunteer with a 72 hour NTHi biofilm.** 750μl PBS added to apical surface of primary respiratory epithelium previously cultured at air-liquid interface then co-cultured with NTHi (HI4 isolate) for 72 hours. NO probe inserted to just above cell layer and baseline NO level of around 50nM detected. Addition of PYRRO-C3D (final concentration 50μM) caused no detectable increase in NO. This was followed by 30u β-lactamase at 35 minutes with a rapid increase in released NO and eventual suppression of endogenous NO production. n=2

4.5 Discussion

CFU counts and confocal microscopy showed that NTHi biofilms are significantly more susceptible to azithromycin treatment when in the presence of PYRRO-C3D. This effect was dependent on NO release over a sustained period of time.

The effect was not seen in an NTHi strain that did not produce β-lactamase, demonstrating that β-lactamase is essential for PYRRO-C3D cleavage and subsequent NO release. This appears to be in contrast to other bacterial species such as *S.pneumoniae* where binding to penicillin-binding protein (PBP) without concomitant β-lactamase activity is sufficient for PYRRO-C3D efficacy [279]. The results were consistent across β-lactamase producing strains from both PCD lower airway and non-PCD upper airways. This is significant as the PCD airway (site of HI4 isolate) is a low NO environment where the bacteria are less likely to have been previously exposed to high NO concentrations. The non-PCD strains (HI5 and HI6) are from nasal carriage

studies; as the nasal cavity is the site of the highest NO levels in the respiratory tract [47] these bacteria have colonised a "higher" NO environment (estimated at 30µM concentration in healthy subjects using results from 3.4.1). This prior exposure to NO did not affect the susceptibility of HI6 (β-lactamase producer) to PYRRO-C3D. The effect of PYRRO-C3D was ablated by NO scavenging, inhibition of β-lactam cleavage (hence preventing PYRRO-NO release), use of cephalosporin portion of PYRRO-C3D alone and prior cleavage of NONOate group, showing that the mechanism of action was via NO release. However, proof of the pivotal role of β-lactamase would involve creation of a β-lactamase mutant of the HI4 isolate. Whereas the half-life of NO release for PYRRO-NO alone is around 2 seconds, NO release from PYRRO-C3D in solution with β-lactamase was sustained over at least 2 hours (Figure 4-5). The slow cleavage of PYRRO-C3D by β-lactamase seems to be an important part of its efficacy as use of DEA/NO alone in place of PYRRO-C3D is ineffective. The release of NO *in vivo* may be even more extended since the concentration of β-lactamase at the epithelial surface is likely to be much lower than that used in the solution experiments (10u/ml) or suspended planktonic NTHi. Interestingly, NO release was not detected from PYRRO-C3D treated NTHi biofilms on primary epithelium. This may be due to local scavenging/conversion of NO at the epithelial surface allied to much lower levels of β-lactamase than rapidly growing planktonic solutions of NTHi.

Treatment of planktonic NTHi showed that PYRRO-C3D completely inhibited growth at concentrations above 100µM, an effect that was likely due to the cephaloram component since cephaloram alone had the same effect but DEA/NO did not. Treatment of NTHi biofilms, however showed no effect on viability at concentrations of PYRRO-C3D up to 200µM showing the increased antibiotic tolerance of biofilm to cephaloram treatment. The planktonic data also showed a small spike in growth at the 50µM concentration that was replicated in the DEA/NO data and, potentially, with treatment of biofilms. This is consistent with previous work by Walker that showed stimulation of planktonic NTHi growth with low doses of SNP (below 100µM). At 50µM, PYRRO-C3D may be causing NO-induced stimulation of bacterial replication thus increasing susceptibility to azithromycin.

The lack of NO-triggered dispersal in NTHi was previously demonstrated by Walker using SNP [115]. This work supports this by showing a decrease in supernatant CFUs in response to PYRRO-C3D alone rather than dispersal and increase in CFUs. The drop is likely caused by killing of NTHi in the supernatant by cepholaram from within the PYRRO-C3D (50µM

cephaloram was sufficient to affect planktonic NTHi viability). There was a larger drop seen when using azithromycin alone, most likely due to the higher concentration of azithromycin compared to cephaloram.

The effect of PYRRO-C3D *in vitro* was replicated in the *ex vivo* model of cultured primary respiratory epithelium from healthy and PCD subjects. This is important as the *in vivo* interaction between host and NTHi is complex and may not be replicated by the *in vitro* environment, therefore, models of biofilm growth on primary epithelium are an important validation step and more representative of biofilms found in the human lung. The presence of epithelium and the many different bacteria in the airway may alter NO dynamics. There are also numerous interactions between bacterial species in the airway, for example, NTHi proliferates at a greater rate on nasal epithelium that is also colonised with *S.pneumoniae* and *S.aureus* [370]. Additionally, bacteria such as *P.aeruginosa* possess denitrification and scavenging pathways that prevent the released NO exerting its effect on NTHi [167].

The effect seen on PCD epithelium was slightly different from healthy epithelium. Azithromycin alone produced a significant drop in biofilm viability on healthy epithelium but not on PCD. However, the effect of PYRRO-C3D in combination with azithromycin was more pronounced for PCD; producing a 2 log fold drop in CFUs on PCD epithelium versus 1 log fold on healthy. The azithromycin tolerance of PCD biofilm may reflect a denser biofilm; although there was a log fold lower CFU count on untreated PCD epithelium, this may reflect an increase in dense, matrix-heavy, sessile biofilm growth mode that is, consequently, more resistant to antibiotic treatment. It is also consistent with some of the data from Walker's work on NTHi biofilm in PCD; during development of the co-culture model there was a log fold higher CFU count of NTHi biofilm on healthy epithelium versus biofilm on PCD epithelium [115] though this was not the case in later work as confocal imaging of NTHi biofilm showed a significantly higher number of bacteria in the PCD biofilm [115]. As the PCD epithelium is an inherently lower NO environment than healthy epithelium (1.6.3 and 3.4.2), the lower exposure to NO during establishment may render the biofilm more susceptible to exogenous NO.

The azithromycin dose used here may appear high, particularly given that the planktonic minimum inhibitory concentration of azithromycin on the HI4 strain from previous work (R.Allan, unpublished) was 1µg/mL (4000x lower than the dose used here). However, it is not uncommon for biofilms to be more tolerant of antibiotics to this degree [371]. Also, azithromycin is known to concentrate in lung tissue (particularly macrophages and lining fluid)

with concentrations peaking at around 464μg/mL in one study [372]. Although this is still 10x lower than the concentration used here, the NTHi biofilm in the lung is likely to be far sparser than *in vitro* biofilms and that seen on cultured respiratory epithelium.

Wu *et al* previously found that sub-inhibitory concentrations of β-lactam antibiotics enhance biofilm formation in NTHi biofilms by increasing extracellular matrix but decreasing the number of culturable bacteria [373]. An effect also triggered by azithromycin in other bacterial species [374,375] but not in NTHi biofilms [366]. This is consistent with this work as, although CFU counts reduced in response to azithromycin alone, live/dead staining showed no decrease in live bacteria with an increase in "dead" and crystal violet staining. The increased dead stain may reflect an increase in eDNA as part of extracellular matrix upregulation. Thus, azithromycin alone may be ineffective in reducing biofilm burden. However, treatment with PYRRO-C3D alongside azithromycin showed CFUs were reduced further and that there were fewer live bacteria by fluorescent staining with no increase in dead/eDNA stain or average diffusion distance.

As described by Wu *et al*, it is well recognised that sub-inhibitory concentrations of antibiotics can promote a more tightly packed biofilm. This work showed a reduction in diffusion distance in cephaloram treated versus untreated NTHi biofilms without reduction in number of live bacteria or maximum thickness but with an increase in eDNA/dead stain. It is likely that cephaloram at this dose is sub-therapeutic thus it may also promote the development of resistance to cephalosporins and other β-lactam antibiotics (penicillins). The dose of cephaloram is also tied to the NO dose by using PYRRO-C3D and it would be more versatile to have an NO donor at an optimal concentration with a choice of antibiotic at an appropriate dose. This raises the possibility that PYRRO-C3D would be more effective if it included a non-antibiotic portion containing a β-lactam ring rather than cephaloram. The feasibility of this would require further investigation, however diazeniumdiolates (such as PYRRO/NO) are relatively simple to modify in order to change their activation [376]. For example, V-PYRRO/NO was created as a liver-specific NO donor [377].

It appears that the sustained release of NO is required for PYRRO-C3D to have its effect. Use of DEA/NO alone was ineffective in enhancing antibiotic sensitivity. DEA/NO release of NO would cease within 2 minutes to 16 minutes (at 37^{o}C and 22-24^{o}C respectively [368]), whilst data here shows that the requirement for β-lactamase to cleave the PYRRO-C3D leads to prolonged release with a half-life of around 30 minutes (Figure 4-6). It may be possible to

prove the need for this release profile by using alternative NONOate controls, for example DPTA/NO has a half-life of 30 minutes [378,379]. This is another advantage of these compounds for administration to humans as the peak doses of NO will be much lower and, thus, potential side-effects minimised.

4.6 Conclusions

Targeted NO treatment of NTHi biofilms with PYRRO-C3D is a potentially novel way of enhancing antibiotic sensitivity. The effect is seen on both *in vitro* biofilms and those grown on *ex vivo* cultured respiratory epithelium. The effect of PYRRO-C3D is due to the slow release of NO at the biofilm surface and does not seem to be a simple triggering of dispersal from the biofilm as PYRRO-C3D alone does not result in increases in supernatant bacteria. This is in contrast to NO treatment of biofilms formed by other bacterial species [170]. Whilst azithromycin, cephaloram or PYRRO-C3D alone seems to stimulate biofilm formation, PYRRO-C3D and azithromycin in combination causes bacterial killing without an increase in biofilm. Also, the more pronounced effect seen in PCD raises the possibility that drugs of this class may be more effective in PCD patients.

As NTHi lack the NO sensing biofilm pathways of other bacterial species, there likely exist novel pathways that mediate the NO effect in NTHi.

Future work will need to focus on,

1. Effectiveness of PYRRO-C3D in animal models of lung infection
2. Investigation of PYRRO-C3D treatment on a wider range of bacterial biofilms
3. Development of additional compounds to overcome concerns about low antibiotic dosing with PYRRO-C3D administration

Chapter 5: Mechanisms of nitric oxide-induced biofilm changes in *non-typeable Haemophilus influenzae*

5.1 Introduction

The previous chapter has shown that sustained low dose nitric oxide can enhance NTHi biofilm susceptibility to antibiotic killing by azithromycin, however the mechanisms behind this are unknown. Extensive studies of *P.aeruginosa* have shown that NO triggers increased phosphodiesterase activity leading to breakdown of c-di-GMP and triggering of dispersal [150,151]. A similar mechanism seems to occur in other bacterial species [242]. As discussed in 1.6.2.1, genome sequencing of NTHi has failed to find any of the phosphodiesterase or cyclase domains that modulate c-di-GMP levels [243].

As very little is known about potential NO sensing mechanisms in NTHi, proteomic analysis is an attractive means to assess cellular changes in biofilm NTHi following exposure to nitric oxide. Several previous studies have used mass spectrometry (MS) based proteomics to look at NTHi biofilm, mainly aiming to characterise the adaptations from planktonic to biofilm growth mode (1.8.2). Post *et al* 's proteomic study of planktonic and biofilm NTHi identified that biofilm formation was associated with downregulation of metabolism and protein synthesis but not in those proteins required for growth factor acquisition and oxidative stress [309]. Other studies have identified proteins that are differentially expressed in biofilm compared to planktonic NTHi including outer membrane proteins (OMPs) 1, 2, 5 and 6, and several metabolic and transcriptional proteins [311–313].

It is possible that nitric oxide triggers a reversal of these changes, as seems to be the case in *P.aeruginosa* and *S.pneumoniae* [150,151], or that other signalling mechanisms cause an increase in susceptibility to antibiotics. Using a proteomic approach provides a global view of the cellular changes in NTHi and has the potential to provide insights into whether NO is triggering the bacteria within the biofilm to return to a planktonic state and/or altering other pathways.

Systems biology approaches (transcriptomics, proteomics, next generation genome sequencing) allow the study of the range of changes within a cell in an untargeted manner. This is particularly attractive as the range of pathways altered by a treatment can be flagged

and candidates for further investigation identified. Since biofilms are dynamic structures that will change their gene expression over the 72h time course used in these experiments (phase variation), proteomics is the best technique to capture the changes induced by NO treatment. By using advanced label-free proteomics, there is no need to attempt culture of the NTHi in heavy culture media or alter the bacteria themselves.

Proteomic analysis can also identify any changes in the target of azithromycin; the 50S ribosomal subunit of the 70S ribosome. Although there are 31 50S ribosomal proteins that can be detected by proteomics [380], the specific binding site of azithromycin is in the 23S RNA part of the ribosome, therefore any induced changes in this RNA domain will not be detected by proteomic approaches.

5.2 Aims

To quantify the changes in protein expression seen in 72 hour NTHi biofilms following treatment with nitric oxide, in order to reveal mechanisms underlying an increase in antibiotic susceptibility.

5.3 Methods

In vitro biofilms were grown for 72 hours in polystyrene 6 well plates as per 2.2.3. These were washed with HBSS then treated for 2 hours; this is in line with previous work in this laboratory looking at NO and NTHi biofilms [115]. Sodium nitroprusside (SNP) at a concentration of 100µM was used as the NO donor; this was as per previous work [115] and to ensure the resultant proteomic changes were purely due to NO and not due to the cephaloram backbone of PYRRO-C3D stimulating biofilm formation (Table 4-1). A concentration of 100µM SNP was used in these assays as this is equimolar to the 50µM of PYRRO-C3D used in the previous chapter. SNP releases 1 mol of NO per mol [381] whilst PYRRO/NO releases close to 2 mols per mol [379]. SNP has also been previously shown not to significantly alter planktonic growth of NTHi at a 100µM concentration [115]. D-methionine and L-methionine assays were performed at a range of concentrations with a 2 hour assay time and assessed as per 2.2.4.

Following the 2 hour exposure time, proteins were extracted and processed as per 2.4.1 for LC/MS label-free proteomic analysis. MS peaks were analysed using ProteinLynx Global Server 3.02 with ProteinLynx and MASCOT databases (Waters), then searched against the *non-typeable Haemophilus influenzae* (strain 3655) database on UniProtKB [324]. Unidentified

proteins were cross-checked against UniRef100 database for 100% sequence homology with proteins identified in other *H.influenzae* strains. Proteins were considered fully quantitative if present in ≥2 replicates of both biofilm and NO treated biofilm, and ≥2 MS runs in each replicate. ProteinLynx criteria for inclusion in quantitative analysis were ≥3 peptide matches and ≥7 peptides per protein with a false discovery rate of 4%.

5.3.1 Statistical analysis

Proteomic data was analysed as per 2.5. Identified proteins and quantities were normalised to total protein and then individual protein ratios of treated versus untreated were calculated using Microsoft Excel. Normalised quantities were also analysed in GraphPad Prism (version 7.01, 2016, GraphPad Software Inc.) for assessment of statistical significance by multiple t testing. In keeping with multiple comparisons used in high-throughput analyses such as proteomics, false discovery rate (FDR) was set at 5% or 1% [325].

5.4 Results

5.4.1 Proteomic analysis of NO treated biofilms

Protein samples were extracted in triplicate from NO treated and untreated NTHi biofilms as per 2.4.1 and then underwent LC/MS proteomic analysis. 277 proteins were identified in total, of which 250 met the inclusion criteria (5.3), with 127 present in both treated and untreated biofilm (full list in Appendix C). A greater than 1.5 fold upregulation or 0.7 fold downregulation was considered biologically relevant [382]; there were 111 upregulated and 1 downregulated proteins that fit these criteria. Figure 5-1 summarises the proteins identified at each stage of analysis. The 16 proteins that were statistically significant at the 5% false discovery rate are shown in Table 5-1.

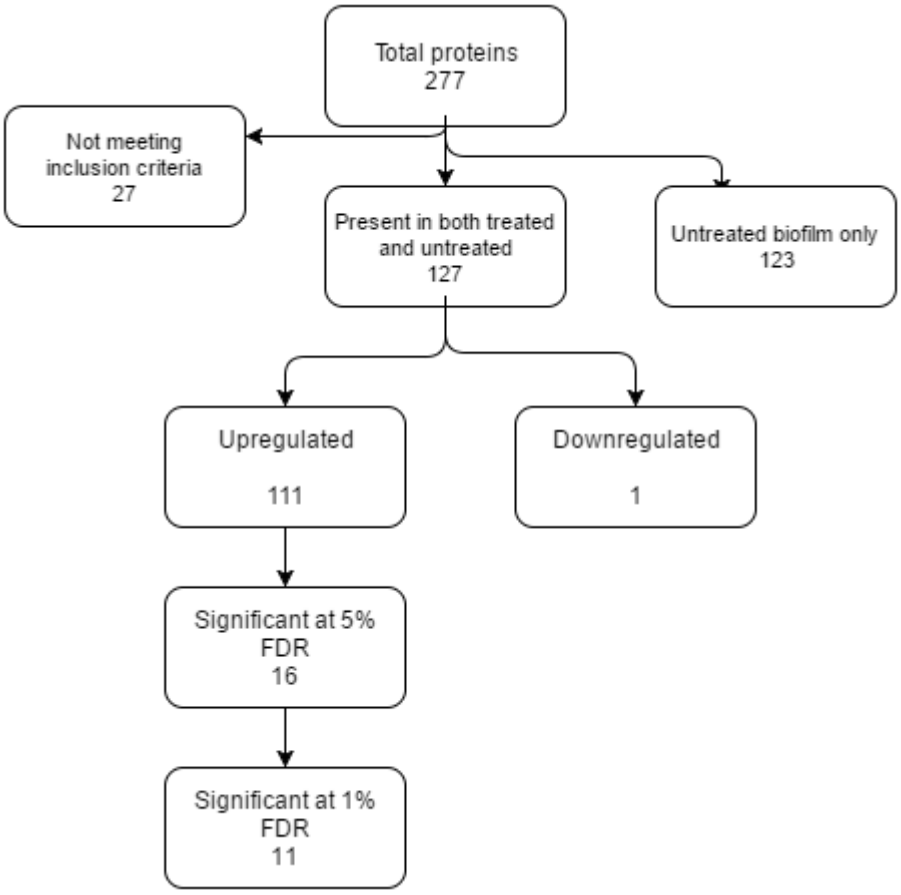

Figure 5-1. **Flow chart of proteins identified by proteomic analysis of NO-treated and untreated NTHi *in vitro* biofilms.** 72 hour biofilms were grown in polystyrene wells then treated for 2 hours with sodium nitroprusside 100µM or plain BHI culture media. Upregulated proteins were those with a greater than 1.5 fold increase in NO-treated biofilms whilst downregulated proteins were less than 0.7 fold downregulated.

Uniprot code	Protein name	gene	Ratio
A0A0H3PBJ4	Glucose-specific PTS system enzyme IIA component*	crr	24.1
A0A0H3PK54	Lipoprotein (D-methionine uptake)*	metQ	21.5
A0A0H3PBW8	Phosphoglycerate kinase*	pgk	21.0
A0A0H3PFB4	DNA-directed RNA polymerase subunit α*	rpoA	16.3
A0A0H3PJ51	2,3-bisphosphoglycerate-dependent phosphoglycerate mutase*	gpmA	13.4
A0A0H3PG63	Elongation factor G*	fusA	13.0
A0A0H3PMV3	Pyruvate kinase*	pykA	11.9
A0A0H3PI75	Inosine-5'-monophosphate dehydrogenase*	guaB	11.4
A0A0H3PCZ6	L-lactate dehydrogenase*	lldD	10.5
A0A0H3PF36	ATP synthase subunit β	atpD	10.0
A0A0H3PLN7	Pyridoxal 5'-phosphate synthase subunit*	pdxS	9.2
A0A0H3PLM6	Pyruvate dehydrogenase E1 component*	aceE	8.2
A0A0H3PG47	Chaperone protein ClpB	clpB	7.9
A0A0H3PC20	NAD nucleotidase	nucA	7.0
A0A0H3PFF9	Long-chain fatty acid transport protein	OMPp1	6.1
A0A0H3PF51	CTP synthetase	pyrG	5.8

Table 5-1. **Significantly upregulated proteins in NO-treated NTHi biofilms**. Ratio calculated as normalised quantity in NO treated biofilm/untreated biofilm. False discovery rate (FDR) 5%. *also significant at 1% FDR

5.4.2 Pathway analysis

KEGG analysis limited to the significant proteins in Table 5-1 showed that these proteins are involved mainly in glycolysis/gluconeogenesis (FDR 4.04×10^{-5}) and metabolic pathways (FDR 0.0177). However, as a whole, this group of proteins are not significantly more connected than random (string database PPI enrichment p-value 0.0616) suggesting that each significant protein is merely representative of its own network of proteins, with the others in their networks not reaching individual statistical significance.

The pathway analysis was then repeated using all proteins identified as up- or downregulated in NO treated NTHi biofilms (>1.5 fold or <0.7 fold) and not just those that were individually statistically significant. The string protein database (5.3.1) mapped 95 proteins (Figure 5-2) and found them to be highly connected with an enrichment p-value of 0 (803 observed connections versus 431 expected, Figure 5-2). The unmapped proteins are those that are classified as hypothetical or of unknown function within UniProt.

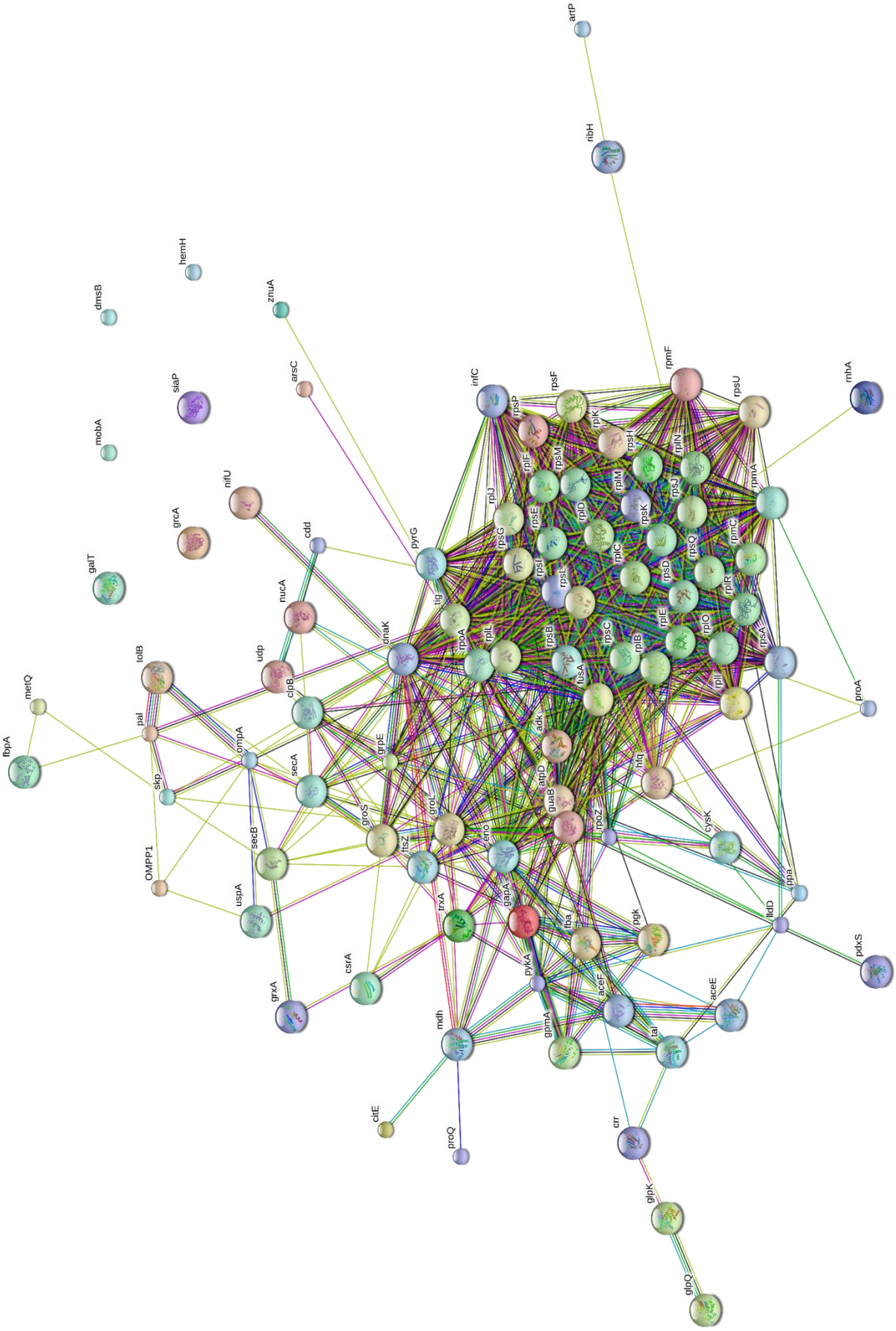
artP
ribH
hemH
dmsB
znuA
arsC
siaP
mobA
nifU
grcA
cdd
galT
pyrG
nucA
tig
dnaK
tolB
udp
clpB
metQ
pal
fbpA
ompA
skp
secA
grpE
OMPP1
secB
groS
groL
ftsZ
uspA
eno
guaB
rpoZ
hlq
cysK
ppa
lldD
pdxS
frxA
gapA
fba
pgk
csrA
pykA
aceF
aceE
grxA
mdh
gpmA
tal
citE
proQ
crr
glpK
glpQ
infC
rpsP
rpsF
rpsU
rpmF
rhlA
rplF
rpsM
rplM
rpsJ
rplJ
rpsE
rplD
rpsK
rpmA
rpsG
rplC
rpsQ
rpmC
rpsI
rpsL
rpsD
rplR
rplE
rplO
rpsC
rplB
rpsB
rplL
rpoA
tuf
rplI
rpsA
proA
adk
hlq
rpoZ
cysK
ppa
lldD
pdxS
pgk
fba
gapA
frxA
pykA
aceF
aceE
gpmA
tal
mdh
crr
glpK
glpQ
proQ
citE
csrA
grxA
uspA
OMPP1
secB
ftsZ
groL
groS
secA
grpE
ompA
skp
pal
tolB
udp
clpB
nucA
dnaK
tig
pyrG
cdd
nifU
grcA
galT
mobA
siaP
arsC
znuA
hemH
dmsB
metQ
fbpA
rplK
rplN
rpsH
rplM
rpsJ
rpmA
rplD
rpsK
rpsQ
rpmC
rplC
rpsD
rplR
rplE
rplO
rpsC
rplB
rpsB
rplL
rpoA
tuf
rplI
rpsA
proA
rpsL
rpsI
rpsG
rplJ
rpsE
rplF
rpsM
rpsP
infC
rpsF
rpsU
rpmF
rhlA
ribH
artP

Figure 5-2.(overleaf) **String database analysis showing protein interactions between proteins up- or downregulated in NO treated NTHi biofilms compared to untreated.** Connections derived by string online database (string-db.org) using proteins that were >1.5 fold upregulated (95 proteins) or <0.7 fold downregulated (1 protein). Network only shows protein connections and not changes in expression. Large circles indicate proteins with a known structure, small circles are proteins where this is unknown. Gene identifiers mapped to description in Appendix D, Table 8 1.

GO-PANTHER analysis mapped proteins across 3 primary processes (translation, glycolytic processes and protein folding) that were significantly over-represented in the up/downregulated proteins (significantly more members of that pathway than would be expected at random) (Table 5-2). KEGG analysis mapped 2 over-represented pathways within the differentially expressed proteins; translation was again identified (ribosome pathway) as well as glycolysis/gluconeogenesis (Table 5-3). These changes suggest that NO treatment triggers upregulation of translation machinery, energy metabolism (glucose) and protein metabolism.

GO-PANTHER biological process	Observed proteins	Expected proteins	Fold enrichment	p-value
Translation	19	4.82	3.94	3.95×10^{-15}
Glycolytic process	8	0.73	10.9	3.42×10^{-4}
Protein folding	7	1.07	6.54	4.38×10^{-2}

Table 5-2. **Significantly over-represented biological processes in NTHi biofilm in response to nitric oxide.** GO-enrichment pathway analysis of 95 mapped proteins that were upregulated in response to nitric oxide in NTHi biofilms. 0.05 significance level with Bonferroni correction for multiple testing.

KEGG pathway	No. proteins	FDR
Ribosome	34	6.83×10^{-26}
Glycolysis/gluconeogenesis	9	1.29×10^{-5}

Table 5-3. **KEGG pathway analysis of altered proteins in NTHi biofilms treated with NO**. KEGG analysis of 95 mapped proteins that were upregulated in response to nitric oxide in NTHi biofilms. Significant pathways at 1% FDR.

18 of the 31 50S ribosomal proteins were upregulated by NO treatment and 1 was downregulated (Table 5-4). Azithromycin acts by binding to the 50S ribosomal subunit of the 70S ribosome and preventing peptide translocation during the translation process, therefore upregulation of the 50S ribosome may improve azithromycin efficacy as seen in the previous chapter.

50S Ribosomal Protein	Ratio	50S Ribosomal Protein	Ratio
L14	4.5	L32	1.9
L2	4.3	L27	1.8
L4	3.5	L9	1.8
L15	3.2	L10	1.7
L13	2.6	L18	1.7
L3	2.5	L5	1.7
L6	2.3	L22	1.7
L7/L12	2.2	L1	1.5
L29	2.0	L28	0.6
L11	2.0		

Table 5-4. **Differentially expressed 50S ribosomal proteins in NO-treated NTHi biofilm**. 50S ribosome subunit is the target of azithromycin. Ratio is treated/untreated normalised protein quantities.

5.4.3 Effect of D-methionine on NTHi *in vitro* biofilms

The 21.5-fold upregulation of the D-methionine binding lipoprotein (MetQ) following NO treatment was notable (Table 5-1). The string database was, therefore, searched to identify the 10 strongest protein connections to MetQ. This showed a number of close links to iron transport proteins (Figure 5-3), including the iron-utilisation periplasmic protein identified in this work (2.3 fold upregulated in NO treated biofilm, Table 5-1).

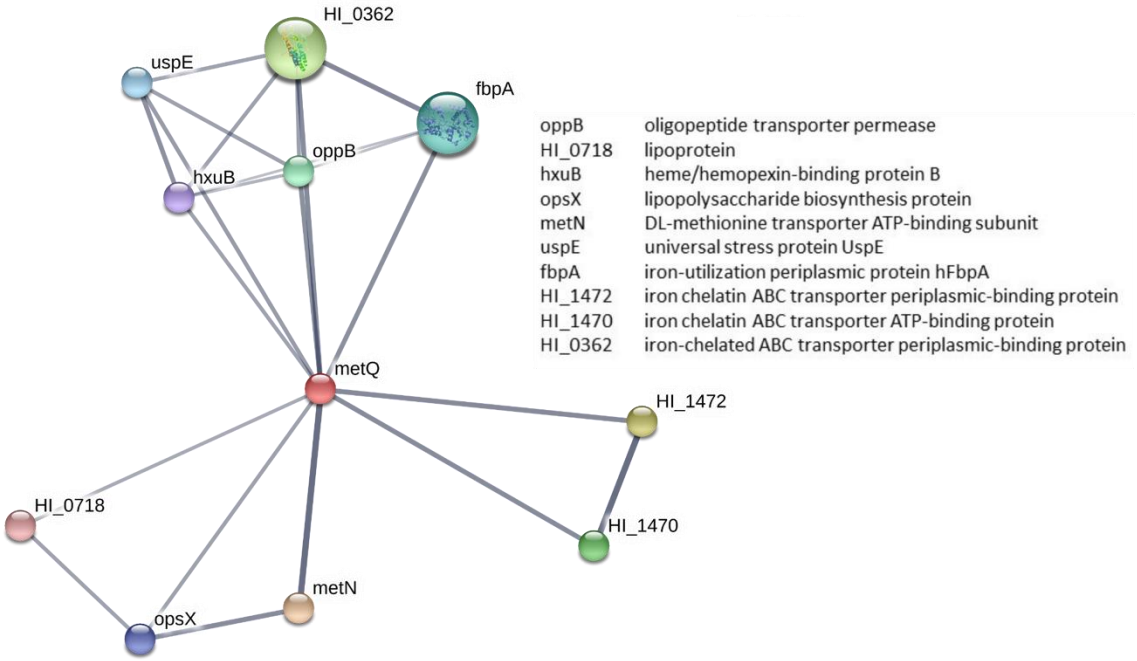

Figure 5-3. **String network view of D-methionine binding lipoprotein (MetQ).** Network shows 10 strongest connections to MetQ according to the string database. Likely interactions are seen with a variety of iron chelation and uptake processes.

This dramatic upregulation of the D-methionine uptake protein in response to NO-treatment suggests that D-methionine plays an important role in NTHi biofilm control and response to NO. Therefore, further studies were undertaken to assess the effect of exogenous methionine on NTHi biofilm. Initially, D-methionine alone was added to 72 hour NTHi biofilms at 20, 50 and 100mM concentrations for 2 hours. D-methionine was then used as a concomitant treatment with azithromycin (4mg/ml) and/or PYRRO-C3D (50µM) to assess the potential for synergy with the findings in 4.4 and ability to further improve azithromycin efficacy. Biofilms were assessed as per 5.3. Low dose D-methionine (20mM) had no effect on viability of NTHi biofilms ($p=0.41$), however 50mM dropped CFUs from $5.2x10^8/cm^2$ to $1.8x10^8/cm^2$ ($p<0.05$). 100mM D-methionine also reduced CFUs compared to untreated biofilm (down to $1.9x10^8/cm^2$, $p<0.05$). The same effect was not seen with L-methionine at 50mM ($p=0.25$) (Figure 5-4a). Neither enantiomer at 50mM enhanced the effect of azithromycin on biofilm viability (Figure 5-4b).

Addition of D-methionine to PYRRO-C3D did not alter the effect seen with D-methionine alone (p=0.24) and L-methionine plus PYRRO-C3D was not significantly different from PYRRO-C3D alone (p=0.40) (Figure 5-4c). L-methionine also had no effect on the combination of PYRRO-C3D and azithromycin (p=0.67). However, D-methionine 50mM effectively reversed the antibiotic enhancing effects of PYRRO-C3D (Figure 5-4d).

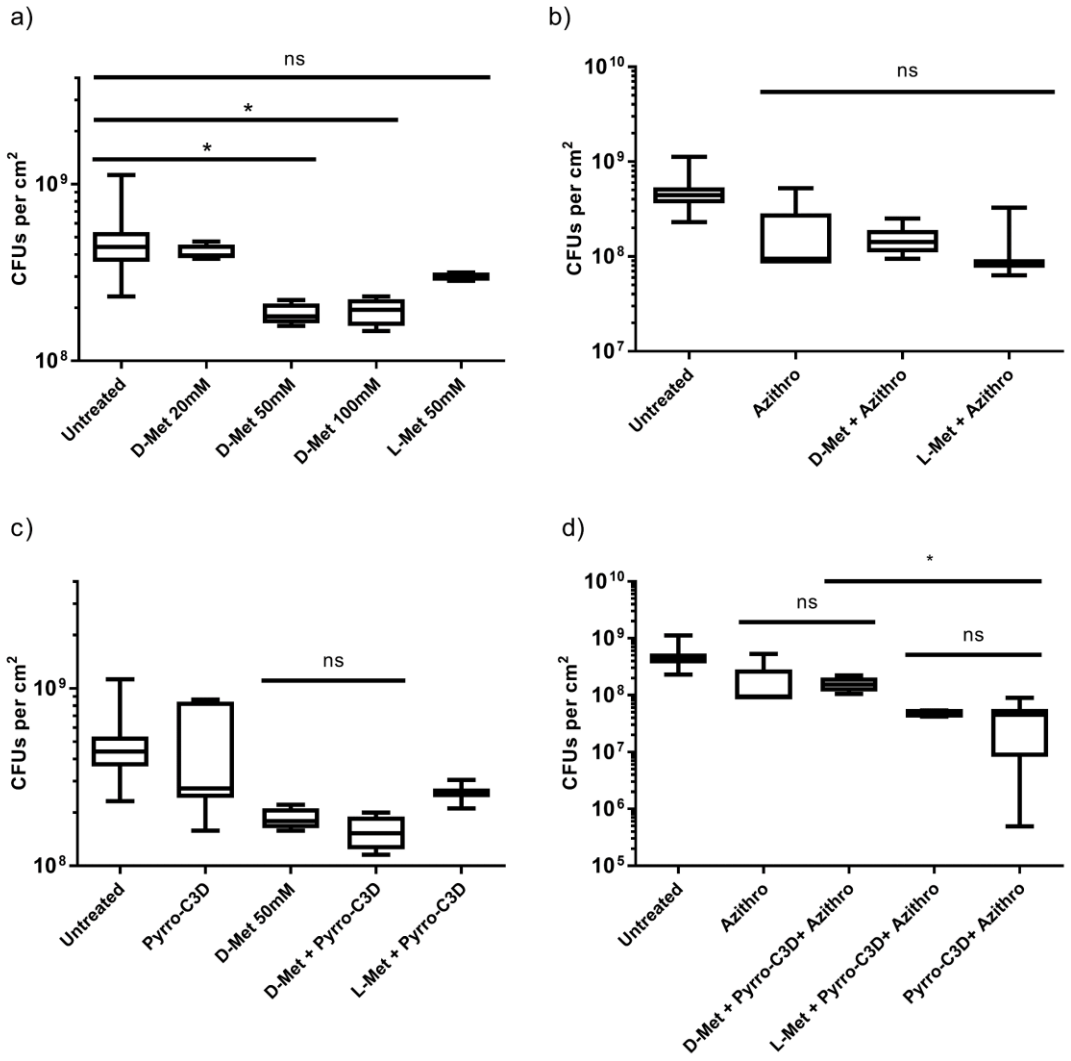

Figure 5-4. **D-methionine reduces biofilm viability and reverses the antibiotic-enhancing effect of PYRRO-C3D**. **a)** D-methionine reduces biofilm viability at concentrations above 50mM but L-methionine does not; 2 hour treatments of D- and L-methionine isomers were added to 72h NTHi (HI4 isolate) *in vitro* biofilms at varying concentrations **b)** Neither D- or L-methionine enhances azithromycin efficacy at 50mM concentrations; 50mM L- or D-methionine in combination with azithromycin (4mg/ml) **c)** Addition of 50µM PYRRO-C3D to the L- or D-methionine treatment does not further reduce viability **d)** D-methionine but not L-methionine reversed the antibiotic enhancing effect of PYRRO-C3D (50µM) on azithromycin (4mg/ml) treatment of 72h NTHi biofilm. All treatment times 2 hours. (n=5, except PYRRO-C3D+Azithro n=8)

5.4.3.1 Confocal imaging

Biofilms were stained with live/dead kit as per 2.2.4.4 and showed that both L-and D-methionine prevented the drop in live bacteria caused by PYRRO-C3D/azithromycin treatment; there was no significant difference between azithromycin alone and PYRRO-C3D/azithromycin with L-methionine (p=0.17) or D-methionine (p=0.10) (Figure 5-5a). Both isomers also caused an increase in dead/eDNA staining; increasing from 9.5µm^3/µm^2 in PYRRO-C3D/azithromycin alone to 30.5µm^3/µm^2 with the addition of L-methionine (p<0.001) and 35.6µm^3/µm^2 with the addition of D-methionine (p<0.001) (Figure 5-5b). Additionally, average diffusion distance to live bacteria increased from 0.68µm in PYRRO-C3D/azithro to 2.4µm with L-methionine and 2.8µm with D-methionine (both p<0.05, Figure 5-5c).

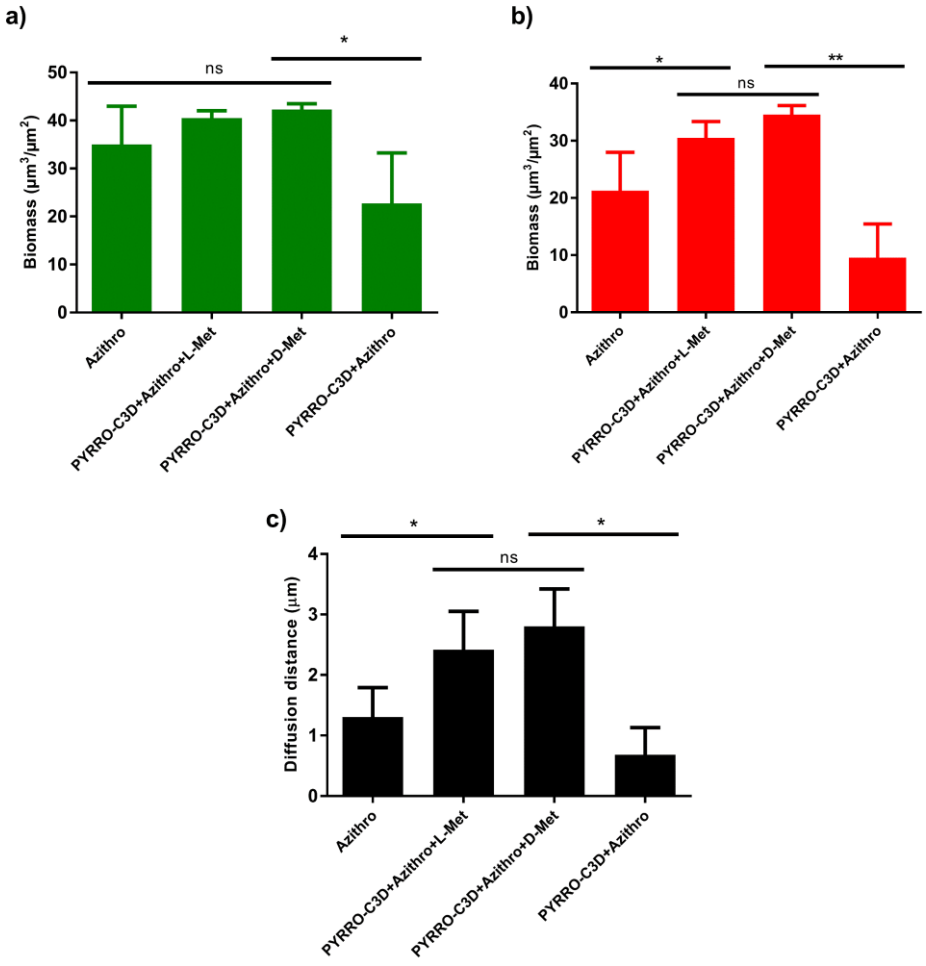

Figure 5-5. L- and D-methionine prevent PYRRO-C3D induced increase in susceptibility of NTHi biofilm to azithromycin and results in increased average diffusion distance to live bacteria. Graphs show staining of a) live bacteria and b) dead bacteria/extracellular DNA c) average diffusion distance to live bacteria following 2 hour treatment of 72h *in vitro* NTHi (HI4 isolate) biofilms. Addition of D-methionine or L-methionine (50mM) to the combination of PYRRO-C3D (50μM) and azithromycin (4mg/ml) resulted in reversal of the drop in live staining back to the level seen with azithromycin alone. Dead staining following addition of D- or L-methionine to PYRRO-C3D/azithro treatment resulted in reversion to the level of staining seen with PYRRO-C3D alone and significantly greater than with azithromycin alone. It also caused Biofilms were stained with live/dead kit and imaged at 1μm sections on a confocal microscope. Images processed using COMSTAT2 software, n=5 (4 fields of view per biofilm).

5.5 Discussion

Chapter 4: showed that targeted nitric oxide donors can enhance antibiotic killing of NTHi biofilm, however the mechanism behind this is unknown [243]. Label-free LC/MS proteomic analysis allowed the "hypothesis-free" interrogation of a large number of NTHi proteins to look for those that may be up- or downregulated after exposure to NO and revealed an upregulation in metabolic activity without a strict reversion to planktonic phenotype.

5.5.1 Proteomic changes in NTHi biofilm after NO exposure

Treatment of NTHi biofilm with the nitric oxide donor sodium nitroprusside resulted in 111 upregulated proteins (>1.5 fold increase) and 1 downregulated protein (<0.7 fold decrease) with 15 proteins unchanged. This shows that nitric oxide treatment results in wide ranging changes in NTHi protein expression, with the vast majority of changes resulting in upregulation of protein expression. Pathway analysis showed the enriched pathways within these proteins are involved in translation (including ribosomal pathways), protein metabolism and glycolysis/gluconeogenesis. Azithromycin targets the 50S ribosomal subunit and 19 of the 31 50S proteins were differentially regulated by NO (18 up and 1 down). This provides a potential mechanism for the increased sensitivity to azithromycin following NO treatment (Figure 4-9). It also, potentially, explains why PYRRO-C3D did not enhance amoxicillin treatment of NTHi biofilm since β-lactam antibiotics (penicillins, cephalosporins, carbapenems) act via inhibition of cell wall synthesis rather than protein synthesis. No peptidoglycan synthesis proteins were identified, therefore it is unclear whether NO is also stimulating this process. Other antibiotics that target the 50S ribosome and therefore may benefit from co-administration with an NO donor include other macrolides (e.g. erythromycin and clarithromycin), lincosamides (e.g. clindamycin) and oxazolidinones (e.g. linezolid) [383]. There were also 16 upregulated 30S

ribosomal proteins, which are the target of aminoglycosides (e.g. gentamicin, amikacin, tobramycin) and tetracycline [383]. In the future, PYRRO-C3D should be tested as a co-treatment with all of these antibiotic classes. Another potential antibiotic target is the 13 fold upregulation of elongation factor G; the target of fusidic acid.

Since the sessile, metabolically downregulated phenotype of a biofilm is a means to avoid antibiotic and immune killing, the NO-induced switch to a more metabolically active state would favour biofilm clearance. Upregulation of carbohydrate metabolism, however, is also linked to the biofilm lifecycle. NTHi mutants of several carbohydrate biosynthesis genes (*wecA, lsgB, siaA, pgm* and *siaB*) were unable to form biofilms but could still infect chinchilla middle ear, albeit with increased sensitivity to host immunity [384]. This suggests a critical role for carbohydrates in biofilm formation.

It is likely that these ribosomal/translation protein changes are not the only means of increasing antibiotic sensitivity as previous work by Walker showed NO treatment caused enhancement of NTHi biofilm killing by ceftazidime (a β-lactam antibiotic from the cephalosporin family) [115]. Nevertheless, antibiotics targeting ribosomes and translation seem the most appropriate choice for concomitant use with NO donors due to their mechanism of action and lack of competition for β-lactamase.

5.5.1.1 Comparison with previous NTHi biofilm work

Many of the proteins identified here have been seen in previous work on NTHi biofilm, however, the general pattern does not follow a simple reversal of planktonic-to-biofilm shifts in proteome.

Outer membrane protein P5 was upregulated (1.98 fold) following NO treatment and has been identified as biofilm specific in 2 studies [312,385], but downregulated in the switch from planktonic to biofilm growth in another study [309]. However, the methods differed between these studies, in particular, the study in which P5 was downregulated compared a 72 hour planktonic culture to a 72 hour biofilm [309], whilst the others analysed 24h [385] and 96 hour [386] biofilms rather than 72h. A 72h planktonic culture is likely to have progressed well past the exponential growth phase and be relatively quiescent, thus reducing the difference between biofilm and planktonic phenotype. This has been previously demonstrated in *P.aeruginosa* in relation to antibiotic tolerance [387]. P5 mutant strains of NTHi were still able to form biofilm but had impaired interaction with host epithelium in a mouse lung infection

model. Therefore, this protein may be more relevant to *in vivo* biofilms that are bound to epithelium rather than grown *in vitro* on a non-biological surface [213].

ClpB was upregulated 7.9 fold in NO-treated biofilm and belongs to the Clp family of chaperone proteins that could, potentially, render dormant and growing cells within the biofilm more susceptible to antibiotic treatment. Clp proteins have protease activity that degrades a wide range of proteins and leads to the death of both growing and dormant (persister) cells in *S.aureus* biofilm [388]. The Clp family of proteins are upregulated during biofilm formation in several NTHi biofilm studies [248,386] and following NTHi middle ear infection [314]. They have also been implicated in biofilm formation in other species, for example ClpP mutants of *S.epidermidis* have reduced biofilm formation and virulence [389].

The identification of a 2.3 fold upregulation in a periplasmic serine protease was notable as there is evidence from other bacterial species that these proteases are important in biofilm formation. Extracellular serine proteases have been shown to inhibit biofilm formation of *S.aureus* when secreted by *S.epidermidis* [390]. As free radical attack is employed by a number of bacterial species, including *P.aeruginosa*, upregulation of this protease by NTHi may be a protective strategy against other bacterial species when subjected to reactive nitrogen intermediates like NO. Serine proteases also inhibit extracellular matrix formation in *S.aureus* [391] and prevent biofilm formation in multi-species biofilms [392]. As well as attacking other bacterial species, the proteases may be important in extracellular matrix degradation and biofilm dispersal.

Comparison between proteins identified in this work and previous evidence linking them to biofilm formation shows that NO does not cause a consistent reversion to the planktonic phenotype (Table 5-5). However, an increase in proteins involved in glycolysis following NO-treatment is a reversal of the biofilm downregulation consistently seen in both NTHi [309] and other bacterial species [382].

Upregulated in biofilm or identified as biofilm specific	
Citrate lyase [309]	60 kDa chaperonin (GroEL protein) [248]
NAD nucleotidase [309]	DNA-directed RNA polymerase subunit α [309,312]
Outer membrane protein P5 [312] [385]	DNA-directed RNA polymerase subunit Ω [312]
Cytidine deaminase [373]	50S ribosomal protein L3 [309]
Purine nucleoside phosphorylase DeoD-type [312]	10 kDa chaperonin (GroES protein) [248]
Protein TolB (protein uptake) [386]	50S ribosomal protein L9 [309]
Glutaredoxin 1 [385]	30S ribosomal protein S7 [309]
Iron-utilization periplasmic protein hFbpA [309,312]	Chaperone protein DnaK [248,312]
Chaperone protein ClpB (related to heat shock) [248,386,389]	
Downregulated in biofilm	
*Pyruvate kinase [309]	Purine nucleoside phosphorylase DeoD-type [309]
*Phosphoglycerate kinase [309]	Thioredoxin reductase [309]
*Enolase [309]	Elongation factor G (EF-G) [309]
*Fructose-bisphosphate aldolase [309]	Cell division protein FtsZ [309]
*Glyceraldehyde-3-phosphate dehydrogenase [309,312]	50S ribosomal protein L14 [309]
Transaldolase [309]	30S ribosomal protein S5 [309]
Malate dehydrogenase [309]	30S ribosomal protein S21 [309]
CTP synthetase [309]	50S ribosomal protein L10 [309]
Putative sialic acid transporter [309]	50S ribosomal protein L17 [309]
Outer membrane protein P5 [309]	Elongation factor Tu (EF-Tu) [309]
Adenylate kinase [309]	

Table 5-5. **Proteins upregulated in response to NO treatment classified according to their previously identified role in NTHi biofilm formation**. Data split shows that NO-treatment is not solely a reversal of biofilm phenotype. *glycolytic enzymes

The most comprehensive study to date of proteomic changes in NTHi biofilm formation is by Post *et al*, who used "*Stable isotope labelling by amino acids in cell culture"* (SILAC) proteomics to analyse the differences between planktonic and biofilm populations of NTHi [309]. This method involved culturing the planktonic NTHi in a media containing normal isoleucine (C^{14}),

whilst the biofilm was grown on glass beads in a medium containing heavy isoleucine (C^{15}). An important consideration, however, is that the planktonic cultures were analysed after 72 hours, meaning the phenotype of the bacteria may be different from studies using 24h comparisons or bacteria in the exponential phase of growth. For example, data from *P.aeruginosa* shows that biofilm bacteria have much greater antibiotic tolerance than those in the exponential growth phase but not stationary phase planktonic cells [387]. After 72h, the bacteria are likely to be in this stationary phase. Also, their study used a continuous flow system rather than the static model used in this work. This may change the dynamics of biofilm growth and thus the proteomic changes. Table 5-6 shows how the proteins identified by Post *et al* compared to the changes seen in NO treated biofilm. Of the 127 proteins identified by Post *et al* as significantly altered during biofilm formation, 34 were also identified in this work in both NO-treated and untreated biofilms. Although the NO treatment does not cause a consistent reversal of the changes seen in biofilm formation, many of the changes in translation machinery (e.g. ribosomes) and carbohydrate metabolism do seem to be a reversion to planktonic phenotype.

Protein Name	NO treatment	Post et al
NAD nucleotidase	7.0↑	↑
outer membrane protein P5	2.0↑	↓
putative sialic acid transporter	2.3↑	↓
DNA-binding protein HU	2.2↑	↑
citrate lyase α chain	2.3↑	↑ (β chain)
transaldolase	4.0↑	↓
fructose-bisphosphate aldolase	1.8↑	↓
thioredoxin reductase	4.4↑	↓
malate dehydrogenase	2.8↑	↓
glyceraldehyde 3-phosphate dehydrogenase	2.8↑	↓
pyruvate kinase	11.9↑	↓
phosphoglycerate kinase	21.0↑	↓
enolase	2.3↑	↓
60 kDa chaperonin, GroEL	2.5↑	↑
chaperone protein DnaK	2.1↑	↑
protein-export protein SecB	3.1↑	↑
10 kDa chaperonin, GroES	1.8↑	↓
trigger factor	3.3↑	↓
30S ribosomal protein S7	1.6↑	↑
50S ribosomal protein L3	2.5↑	↑
50S ribosomal protein L9	1.8↑	↑
30S ribosomal protein S21	2.0↑	↓
elongation factor Ts	2.2↑	↓
elongation factor G	13.0↑	↓
ribosome recycling factor	1.4↔	↓
50S ribosomal protein L17	1.4↔	↓
50S ribosomal protein L10	1.7↑	↓
50S ribosomal protein L14	4.5↑	↓
50S ribosomal protein L5	1.7↑	↓

elongation factor Tu	1.1↔	↓
adenylate kinase	4.1↑	↓
CTP synthase	5.8↑	↓
DNA-directed RNA polymerase α chain	16.3↑	↑ (β chain)
high-affinity zinc uptake system protein	4.5↑	↓

Table 5-6. **Comparison between proteins identified as significantly up or downregulated in the Post *et al*** [309] **study of biofilm vs planktonic NTHi and fold-change in NO-treated biofilms.** Post *et al* compared 72h planktonic cultures of NTHi to 72h biofilms using SILAC proteomics. This work compared untreated 72h biofilms to those treated with an NO donor (SNP) for 2 hours.

Post *et al* performed KEGG pathway analysis on their data and found that biofilm growth was associated with changes in pyruvate metabolism, glycolysis and pentose phosphate pathways [309]. This is consistent with NO-induced reversal of biofilm phenotype since KEGG analysis of NO treated biofilm showed over-representation of glycolysis. Carbohydrate metabolism has also been previously identified as critical in NTHi biofilm formation in other studies [373].

Post *et al* also used selected reaction monitoring MS (SRM-MS) where peptides of particular interest are used in targeted quantitative proteomics. Whereas the proteomic approach used in this work, and the first part of Post *et al*'s work, involves tandem MS where peptides are ionised then fragmented, SRM-MS uses the first stage to select particular peptides of interest and then analyse only those. A predicted regulator of cell morphogenesis and NO signalling (Uniprot AAX88729.1) was found to be significantly downregulated in biofilm formation (0.7 fold) [309]. This protein was not identified in either NO-treated or untreated biofilms but does raise the possibility that there is an NO signalling pathway in NTHi. Further studies of the signalling networks of this protein, and how this may link to the proteins identified in this analysis, could elucidate the NO signalling mechanisms in NTHi. Of the other 9 proteins in the SRM-MS analysis, only NAD nucleotidase was seen in this work; Post *et al* noted it was 3.1 fold upregulated in biofilm formation and it was 7 fold upregulated in NO-treated biofilm in this work. This reinforces that not all NO-induced changes are a reversal of biofilm phenotype.

NAD nucleotidase (NucA) may have an important role in NTHi biofilm. It was identified as a highly-conserved surface antigen in NTHi and a target of the host immune response [393]. Cho *et al* examined the role of *nuc* in the chinchilla model of otitis media, finding that *nuc*

expression was much higher in planktonic than biofilm NTHi in contrast to the work of Post *et al*. However, *nuc* mutants formed excessively large biofilm aggregates that were unable to disperse and were mostly dead by 48h [244]. This was true of both *in vitro* and chinchilla biofilm. Nucleases are also important in biofilm formation of *Neisseria gonorrhoeae* and *S.aureus* biofilms; they appear to control extracellular DNA since *nuc* mutants form thicker, denser biofilms with more eDNA within them [394,395]. Although Post *et al* found NucA to be upregulated in biofilm formation, the data from Cho *et al* suggests NO-induced upregulation of NucA could be a triggering of a dispersal response.

Nitric oxide does not appear to act through reversal of the antibiotic-induced biofilm formation pathways. Wu *et al* found an increase in biomass (with decrease in viability) in response to β-lactam antibiotics and performed microarray transcriptomics on these ampicillin treated NTHi biofilms [373]. Although the 8 upregulated genes were primarily involved in carbohydrate metabolism, only 1 was seen in this proteomic analysis; cytidine deaminase (2.2 fold upregulated in NO treated biofilm). Of the 8 upregulated genes, 5 were involved in carbohydrate metabolism, similar to the significant enrichment of glycolysis/gluconeogenesis proteins in these NO experiments. Of the 51 downregulated genes in the Wu study, only 1 was altered by NO treatment; Ribonuclease H (upregulated 2 fold). It is likely, therefore, that the cephaloram within PYRRO-C3D causes increased ECM seen in the PYRRO-C3D/azithromycin experiments (Table 4-1) and not the NO itself as there is little overlap between this work and the mechanisms identified by Wu *et al*. This could be further investigated by specific fluorescent staining of the ECM, however the complexity of ECM components means there needs to be careful selection of which components to label (e.g. carbohydrates, nucleic acids, proteins) and then choice of imaging technique [396,397]. For example, the most commonly used stain for nucleic acids is SYTO9 that is also used as the "live" stain in most live/dead fluorescent staining kits.

5.5.2 D-methionine and NTHi biofilm

The 21.5-fold upregulation of a potential D-methionine binding lipoprotein (MetQ) in NO treated biofilm was an unexpected finding and was, therefore, further investigated. All amino acids except glycine can exist in two stereoisomeric forms termed levorotatory (L) and dextrorotatory (D) (Figure 5-6). D-amino acids are not found in human proteins but are essential to a number of bacterial processes [398].

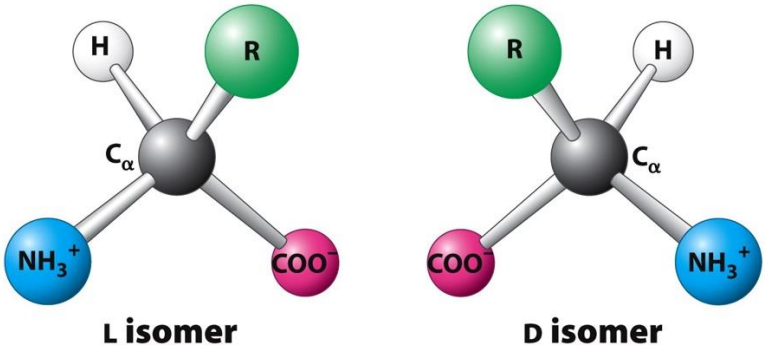

Figure 5-6. **Graphical representation of D- and L- stereoisomers of amino acids.** R is the variable portion of the amino acid structure. The isomers have identical chemical structure and bonding but are mirror images of each other and are, therefore, not super imposable and will interact differently with other molecules/binding sites. *From Biochemistry 8e, by Jeremy M. Berg, John L. Tymoczko, Gregory J. Gatto, Jr., Lubert Styer. Copyright 2015 by W.H. Freeman and Company/Macmillan Learning. Used with permission of publisher.*

There have been a number of studies showing D-amino acids are important for biofilm assembly and have the potential to disrupt established biofilm. Kolodkin-Gal *et al* used a *Bacillus subtilis in vitro* biofilm model to study biofilm disassembly by D-amino acids. They found that D-methionine, D-tyrosine, D-tryptophan and D-leucine in isolation and in combination triggered biofilm dispersal by causing release of amyloid fibres. This was reversed by D-alanine so these amino acids may act by replacing D-alanine in the amyloid fibres [399]. This group then showed the same effect in *S.aureus* [400]. Interestingly, D-amino acids did not prevent formation of biofilm in this model but separate work on D-tyrosine showed it can inhibit bacterial adhesion [401]. Supplementation with corresponding L-amino acids appears to reverse this effect and susceptibility was conferred by mutation in a specific gene (*dtd*) [402]. Sanchez *et al* used clinical isolates of *S.aureus* and *P.aeruginosa* to investigate dispersal of *in vitro* biofilms in response to D-amino-acids and antibiotics; a mix of D-Met, D-Phenylalanine and D-tryptophan was effective in enhancing antibiotic killing of biofilm but not planktonic bacteria [403]. However, attempts to replicate this work and show the effects of D-amino acid mixture on *B.subtilis, S.aureus and S.epidermidis* biofilms were unsuccessful [404]. Using bone biofilm models instead, and a slightly different D-proline, D-Met, D-Phe mix, biofilm formation was inhibited [405].

Using *in vitro P.aeruginosa* biofilms, D-tyrosine, D-Trp, D-Met and D-Leu each individually induced biofilm dispersal, with D-Tyr showing the greatest effect [406]. D-Tyr did not inhibit

planktonic growth but did enhance the activity of the antibiotic amikacin [406]. In contrast to this, Brandendburg *et al* found that D-Trp and D-Tyr were effective in inhibiting biofilm formation but D-Met and D-Leu were not. Also, L-Trp was as effective as D-Trp, with an L/D-Trp combination most effective [407]. In other studies, L-Met inhibited biofilm formation in *P.aeruginosa* and triggered dispersal by upregulating DNase genes with increased susceptibility to ciprofloxacin [408]. Between these studies on *P.aeruginosa*, D-Met has been shown to induce dispersal [406] or have no effect on biofilm [407] with L-M*et al*so effective in inhibiting formation [408]. Thus, the work to date remains equivocal on what role methionine may play in NTHi biofilm formation. However, insights from *E.coli* show that exposure to D-Met results in incorporation of this amino acid into peptidoglycans [409] and data from NTHi biofilms exposed to D-Met during biofilm formation showed upregulation of a number of proteins involved in peptidoglycan synthesis (R.Allan, unpublished).

In this work, D-methionine alone had no effect at 20mM but caused a decrease in CFU counts at concentrations of 50mM and over. The effect size was similar to that seen with 4mg/ml azithromycin and probably reflects a protective response by the biofilm rather than bacterial killing. It was notable that fluorescent labelling of bacteria in the biofilm did not show any difference in the effect of L- and D-methionine. Both isomers prevented the PYRRO-C3D-induced drop in live bacteria when used in combination with azithromycin and both isomers increased the dead/eDNA staining and average diffusion distance. The interference of methionine with the potentiating effect of PYRRO-C3D on azithromycin likely reflects that upregulation of the D-methionine binding lipoprotein seen in the proteomic analysis is a protective mechanism in response to exogenous NO or stress. Increased availability of the substrate for this lipoprotein (D-methionine) may help the bacteria to resist the effects of NO. The net effect may be to preserve viability at the expense of increased ECM. It is unclear whether L-methionine would also be bound by this lipoprotein, which is not well characterised in *H.influenzae,* but the downstream effects seem to be similar for both methionine isomers. Clarity on the role of the MetQ protein could be obtained by transcriptomic work or qPCR to validate changes in expression over the 72h biofilm time course. Further to this, characterising biofilm formation in a *metQ* mutant of NTHi would provide evidence for its importance in NTHi biofilms, and could be followed by studies on the response of such biofilms to NO.

Despite being an amino-acid, it is possible that methionine influences carbohydrate metabolism associated with biofilm extracellular matrix production. The network analysis also showed close links between the D-methionine lipoprotein and numerous iron binding

membrane components. Alongside the upregulated zinc uptake protein, which is associated with many iron binding proteins, this suggests a possible role for iron at the centre of biofilm control and the downstream effects of NO treatment.

5.5.3 Iron Metabolism

String analysis of the D-methionine uptake protein (MetQ) revealed close links to iron chelation and uptake proteins (Figure 5-3). Iron-utilization periplasmic protein (hFbpA) was upregulated 2.3 fold in NO-treated biofilm, whilst Post *et al* previously showed upregulation of 3 other heme-binding proteins (HbpA, HxuB, Hup) in biofilm formation. NO is known to alter heme containing complexes [174] and iron salts were shown to both interrupt biofilm formation and induce dispersal in *P.aeruginosa* biofilms [175]. Furthermore, work in *E.coli* has elucidated the role of Ferric uptake regulation protein (Fur), which uses iron as a co-factor and is a global regulator of metabolic function. Fur controls both iron homeostasis and NO-detoxifying enzymes (Hmp), however treatment with NO inhibits Fur activity thus, potentially, affecting iron homeostasis and other downstream metabolic processes as well as lowering the cell's resistance to the effect of NO [176].

Szelestey *et al's* work on heme-depleted NTHi and biofilm formation sheds further light on the potential role of iron in biofilm formation. They depleted NTHi of heme prior to biofilm formation and found that, compared to heme-replete NTHi, they formed larger biofilms without any change in viability [410]. This was true *in vitro* and in an experimental otitis media model where heme-depleted NTHi only made up 10% of the inoculum but constituted 99% of the biofilm bacterial load [410]. It was also found that heme-depleted NTHi may be more likely to invade epithelial cells, a finding backed up by increased intracellularisation of NTHi that are deficient in the SapA iron transport protein [411]. Szelestey *et al* also found that the heme-depleted NTHi caused a less severe infection in the otitis media model [410].

Iron-sulfur clusters also function in both detection of oxygen availability and defense against reactive nitrogen species. Although not identified in this analysis, NTHi possesses a formate-dependent nitrite reductase regulator (FNR) that has been shown to control a wide variety of genes involved in anaerobic respiration and nitrosative defense in other species [412–414]. Since NTHi only possesses a single nitrite reductase enzyme [186] under control of FNR (*nrfABCD* gene), iron proteins may be particularly important in resistance to NO treatment. A possible candidate for this is the NTHi gene *ytfE* which likely encodes a di-iron protein that is

similar to nitrosative defense iron-sulfur proteins seen in other species [415]. *ytfE* mutants of NTHi are more susceptible to both exogenous and macrophage derived NO [412].

Limiting the systemic availability of iron in response to infection or inflammation is a relatively newly described part of the innate immune system modulated largely by the cytokine hepcidin [416]. However, there are also hepcidin-independent pathways that operate at a local level to reduce iron availability in response to local inflammation [417]. NTHi has the ability to invade epithelium and become an intracellular pathogen [199,211]. Since heme-depleted NTHi are more likely to internalise into epithelial cells [410], this may be an attempt to access intracellularly sequestered host iron.

In addition to these NTHi factors, generation of nitric oxide in response to infection is via increased NOS2; an enzyme that requires insertion of a heme group after translation. This, therefore, provides a potential link between the presence of bacterial biofilm, resulting in both host sequestration and bacterial scavenging of available iron/heme, and reduced availability of iron for NOS2. NO signalling within mammals also affects post-transcriptional modifications via iron regulatory proteins [418].

Therefore, if MetQ upregulation is closely linked to iron uptake, this could explain the methionine induced reversal of the PYRRO-C3D treatment effect. Increased uptake of methionine could trigger a similar response to heme-depleted NTHi, resulting in increased biofilm formation and further resistance to azithromycin.

5.6 Conclusions

Nitric oxide treatment of NTHi biofilms is associated with changes in a wide range of proteins. Pathway analysis shows that this is primarily upregulation of translation and energy metabolism (particularly glucose), consistent with a reversal of the changes seen in the switch from planktonic to biofilm growth. Since it is known that planktonic bacteria are more susceptible to antibiotics than the sessile biofilm growth mode, these findings are consistent with increased antibiotic sensitivity. Not all changes, however, are consistent with a reversion to the planktonic phenotype. Previous work in NTHi biofilm has failed to show dispersal in response to NO [115]. However, data from this work, particularly upregulation of the NucA protein, suggests there may be some triggering of a dispersal response. Despite this, there was no significant increase in supernatant CFUs or reduction in biofilm thickness in PYRRO-C3D treated biofilms.

NO treatment of biofilm causes upregulation in a number 50S ribosomal subunit proteins. As this is the target of azithromycin, NO treatment may make NTHi more sensitive to macrolides than other classes of antibiotic. Other antibiotics that target the 50S ribosome include chloramphenicol and clindamycin.

Upregulated D-methionine uptake protein in the cell membrane is associated with multiple iron binding and transport proteins which, alongside an NO-induced upregulation of a heme-binding protein, suggests a potential role for iron/heme in the biofilm life-cycle of NTHi. This is consistent with a potential interaction between NO and iron homeostasis in other bacterial species [176] and the stimulation of biofilm growth in heme-depleted NTHi [410]. It is also likely that iron plays a central role in defense against NO [412,186,415] and in the host response to biofilm formation.

The D-methionine binding lipoprotein was upregulated following NO treatment but supplementation with D-methionine reversed the effect of the PYRRO-C3D on antibiotic sensitivity. This effect on viability was not seen with L-methionine, however fluorescent labelling of NTHi showed both isomers reversed the PYRRO-C3D enhancing effect on azithromycin. Methionine, therefore, potentially forms part of the protective mechanism against NO which is reflected by MetQ upregulation. The mechanism may be through the close links of MetQ to many iron uptake proteins or involvement in peptidoglycan synthesis and modification of penicillin-binding protein.

In summary, NO treatment reverses some of the biofilm phenotype of NTHi via upregulation of translation and energy metabolism pathways with ribosomal upregulation potentially resulting in increased azithromycin sensitivity. However, there are other proteomic changes that do not follow this trendl, including changes to D-methionine uptake and iron metabolism that suggest there are other pathways involved in biofilm control and enhanced antibiotic sensitivity in NTHi.

Chapter 6: The response of healthy and PCD epithelium to NTHi biofilm

6.1 Introduction

The immune response of respiratory epithelium to infection is dysfunctional in some chronic lung diseases such as cystic fibrosis, however it is not known whether this is the case in PCD. Although the primary defect in PCD is lack of mucociliary clearance, the early bacterial colonisation and lung damage show some similarities to CF and this raises the possibility that there are intrinsic defects in host response to infection or control of airway inflammation.

Non-typeable Haemophilus influenzae (NTHi) is the commonest colonising bacteria in the airways of young children with PCD [32,53,59,61], however NTHi is an extremely common nasal commensal found in up to 80% of healthy children without causing symptoms [232]. Once NTHi infects the lower airways it can cause inflammation through NF-κB activation (1.4.2) and directly inhibits ciliary motility [195–197]. This inflammation appears to contribute to the excessive inflammation in the airways of CF patients that leads to airway damage and *P.aeruginosa* colonisation, resulting in further damage and a drop in lung function [57]. This process may also take place in PCD patients [53]. NTHi is implicated in the pathogenesis of chronic rhinosinusitis, otitis media, sinusitis, COPD and persistent bacterial bronchitis [234].

NTHi colonisation of the respiratory tract occurs through biofilm formation, not only in PCD [116] but also in other chronic disease such as COPD [239], CF [131,209] and chronic rhinosinusitis [237]. These *in vivo* biofilms are adherent to the respiratory epithelium [237]; a pattern of biofilm growth on cultured primary epithelium that was confirmed in this model using scanning electron microscopy (Figure 4-3). The initial interaction between epithelium and NTHi has been well studied, but it is unclear how this alters once colonisation and chronic biofilm formation has occurred. It is possible that, at this stage, differences between healthy and diseased airway occur, with the latter setting up a pro-inflammatory micro-environment. Indeed, NTHi seems particularly adept at taking advantage of epithelial dysfunction in diseased airway (1.5).

Chapter 3: demonstrated that PCD and healthy airways differ in their nitric oxide levels, irrespective of the underlying PCD-causing mutation, whilst Chapter 4: showed that nitric oxide

disrupts NTHi biofilms *in vitro* and on cultured respiratory epithelium via significant alterations in the proteome of the NTHi (Chapter 5:). Since the healthy and PCD airways differ in their NO micro-environment, this may form the basis of differential response to NTHi.

The majority of proteomic studies on cultured respiratory epithelial cells have used transformed cell lines, which have been shown to be poorly representative of airway epithelium [291,292]. The use of primary cells, therefore, has the potential to more accurately model both altered cellular responses in PCD and the normal response of healthy cultured epithelium.

Since there is little known about the response of PCD epithelium to infection and current studies have failed to identify any differences when compared to healthy epithelium [115], a "hypothesis-free" approach like proteomics is an attractive prospect. There have been two studies using proteomics to examine healthy epithelium response to NTHi. Harrison *et al* used the chinchilla model of otitis media to study acute NTHi otitis media infection [314], whilst Val *et al* used an immortalised murine middle ear cell line exposed to NTHi lysate [315]. These are both modelling an acute infection in a related but different epithelial surface to the lung colonisation in this model, therefore findings may not be directly comparable. Baddal *et al* used a transcriptomic approach to classify host and NTHi response to infection. Although the authors used primary cultured respiratory epithelium, again, this was exposed to an acute otitis media isolate of NTHi [383]. Although they identified a large number of host and bacterial proteins over a 72 hour time course, cytotoxicity was seen in all epithelial cells by this time. This is in contrast to this model where a colonising biofilm is formed and cellular health is maintained to 72 hours.

6.2 Aims

To detect changes in proteome in response to colonisation with a 72 hour NTHi biofilm in healthy and PCD cultured respiratory epithelium by -

1. Characterising the response of healthy epithelium to NTHi colonisation through fold change in protein, within each subject, in exposed versus unexposed cultured respiratory epithelium
2. Performing the same comparison in PCD patients
3. Comparing baseline proteome of healthy and PCD cultured respiratory epithelium (unexposed to NTHi).

4. Comparing the response of healthy and PCD epithelium to NTHi colonisation to identify any potential differences in PCD airway response.
5. Comparing the above results to the changes seen in cystic fibrosis epithelium

6.3 Methods

Samples were obtained as per 2.1 via nasal brushing of healthy volunteers and PCD patients. Characteristics of these participants are shown in Table 6-1 with the eventual fate of the nasal brushing samples summarised in Appendix E.

Patient	Age	Sex	Genetic mutation	Ciliary abnormality	Cilia structure	Nasal nitric oxide (nl/min)
Healthy						
HV229	39y	M				
HV230	39y	M				
HV235	28y	M				
PCD						
PR853	26y	F	**DNAH11** [c.4348C>T; p.Arg1450*] [c.13192C>T; p.Gln4398*]	Immotile & dyskinetic	Normal	2.6
PR886	28y	M	**HYDIN** [c.1146delT; p.F382LfsX64] No 2nd mutation identified	Impaired amplitude and co-ordination	Normal	0.5
PR887	20y	M	**DNAH11** exon 39:c.6527C>A, g.21711640 C>A (heterozygous)	Immotile & dyskinetic	Normal	2.2
NB1807	6m	F	**DNAH11** exon 22:c4012-1G>C exon 78 c:G12899A:p.R4300H	Immotile & dyskinetic	Normal	Too young
NB1811	1y	M	**DNAH11** exon24:c.C4333T:p.R1445X (homozygous)	Immotile & dyskinetic	Normal	Too young
NB1813	31y	F	**DNAH11** exon40:c.C6664T:p.R2222X exon40:c.A6682T:p.K2228X	Immotile & dyskinetic	Normal	7.1

Table 6-1. **Characteristics of subjects providing nasal epithelial cells for culture and subsequent proteomic analysis.** Demographic details for healthy and PCD subjects in the proteomic studies as well as genetic, ciliary, nasal NO and ultrastructural abnormalities seen in the PCD patients. For comparison, healthy subjects have a mean nasal NO of approximately 265nl/min. EM- electron microscopy, DNAH11 – dynein heavy chain 11, nl/min – nanolitres/minute, CBF – ciliary beat frequency (normal 11-20Hz).

6.3.1 Cell culture, co-culture and protein extraction

Methods for culture of nasal brushings are described in detail in 2.3.1 with the procedure for co-culture with NTHi discussed in 2.3.3. Following a 72 hour co-culture time, integrity of the cell layer was assessed using trans-epithelial resistance (TEER) measures (2.3.2) and cells were discarded if there was a greater than 20% drop in TEER over the course of the co-culture. The co-cultures were also discarded if there was any colour change in the medium from red to brown, indicating an acidification of the culture and likely cell compromise.

Proteins were extracted via lysis of the cells using HBSS with 0.1% SDS, 100mM TEAB and Halt™ protease/phosphatase inhibitor (Life Technologies) at 3x concentration for 10 minutes as per 2.4.1.2. The final method used for proteomic analysis involved in-gel digestion of stained LDS-PAGE gels prior to MS analysis (2.4.2).

6.3.2 Statistical analysis

Proteomic data was analysed as per 2.5. Additionally, Linear Models for MicroArray Analyses (LIMMA) have become widespread in genetic high throughput analyses such as microarray, but have not become established in proteomics [419]. This approach was also used for the human proteins identified in order to identify a clustering when comparing PCD v healthy unexposed and NTHi-exposed cultures. Since traditional statistical techniques (e.g. student's t-test) discriminate against more abundant proteins (they tend to have higher variances), LIMMA calculates overall variances to be applied to all comparisons. Assumption of equal variances was also used when comparing proteins using multiple t-tests and the false discovery rate approach [325].

6.3.3 Modifications to analytical approach

Due to failure of epithelial cell culture at the primary cell culture and NTHi biofilm co-culture stages, as well as the loss of significant quantities of protein sample during the failed MS runs (2.4.2.2), the number of replicates was significantly reduced (Appendix E, Figure 8-3). As a result of this, the data from some experiments were pooled and fold change in protein in exposed/unexposed cultures from individual PCD patients could not be calculated. The response of the healthy epithelium was still characterised using fold change in exposed and unexposed cultures from the same subject. However, to maximise the potential of finding notable changes in PCD epithelium, proteins quantities were compared between pooled results for healthy and PCD NTHi-exposed co-cultures. The comparisons made were, therefore,

1. Characterising the response of healthy epithelium to NTHi colonisation by looking at fold change in proteins in exposed versus unexposed cultured respiratory epithelium from the same subjects (proteins must be in 2/3 paired samples to be included)
2. Comparing baseline proteome of healthy and PCD epithelium (unexposed to NTHi) (proteins must be in at least 2 healthy subject and 1 PCD sample)
3. Compare protein quantities in NTHi exposed healthy epithelium versus exposed PCD epithelium (presence in 2/3 healthy and 3/5 PCD required)
4. Apply a linear models approach to validate the clustering of samples

All CF sample cultures were unsuccessful with 14/14 failing during the cell culture process. This may reflect the range of colonising bacteria in the nose of adult CF patients, including *Burkholderia cenocepacia, Stenotrophomonas maltophilia, Acinetobacter baumanii, achromobacter xylosidans* and non-tubeculous mycobacteria, that would not be effectively killed by the streptomycin, penicillin and nystatin in culture media. There is a higher incidence of nasal polyps in CF patients, thus the nasal epithelium may be inflamed and proliferative at baseline. Also, abnormal airway-surface liquid in CF may manifest in culture as thickened, adherent mucus that may prevent binding of basal epithelial cells to the collagen-coated well; a step that is essential for successful culture.

6.4 Results

LDS-PAGE electrophoresis showed clear banding patterns in all samples but with no differences between exposed/unexposed or PCD/healthy obvious to the naked eye (Figure 6-1). After confirmation of the presence of banding pattern on the gel, the proteins were then processed for MS analysis. As described in 2.4.2.2, initial attempts at proteomic analysis via digestion and preparation of protein samples was unsuccessful and, eventually, the stained gels shown in Figure 6-1 were successfully processed for proteomic analysis.

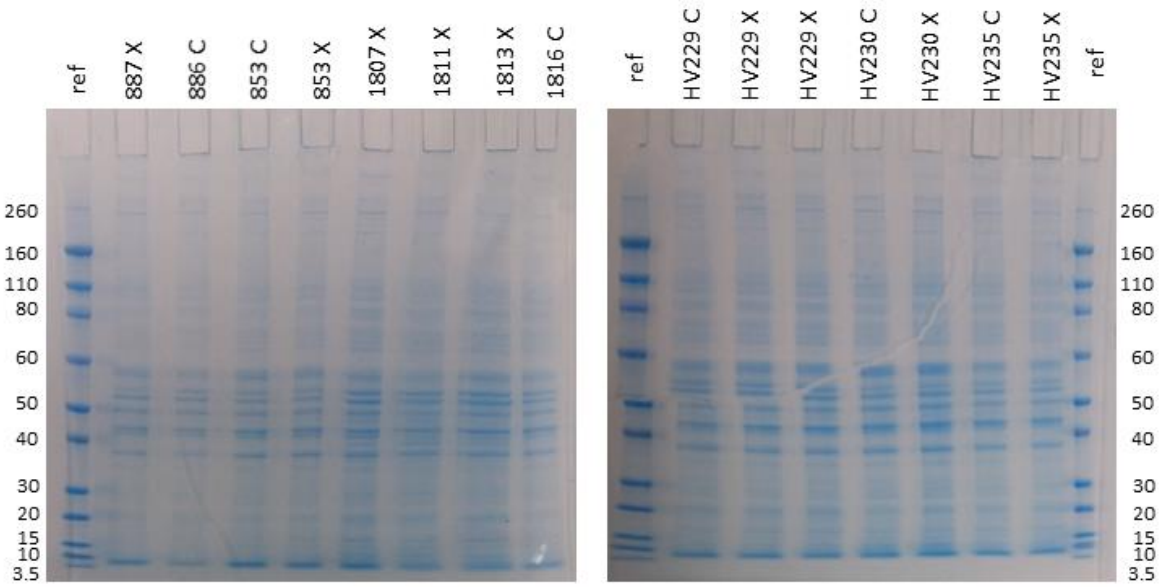

Figure 6-1. **LDS-PAGE electrophoresis stained gels of PCD (left) and healthy subject (right) co-culture samples demonstrating presence of a range of proteins**. 10µg of protein sample prepared according to manufacturer's instructions then run in a 4-12% Bis-Tris gel (Life Technologies) for 35 minutes then stained with colloidal blue kit (Life Technologies). C – unexposed, X – co-cultured with 72 hour NTHi (HI4 isolate) biofilm, ref – Novex sharp reference protein ladder with molecular weights in kilodaltons alongside.

A total of 1516 human and 83 NTHi proteins were detected across 14 samples; 3 healthy paired samples (3 patients with both exposed and unexposed samples) and 7 PCD samples from 6 different PCD patients (1 pair of exposed/unexposed from a PCD patient) (Table 6-1).

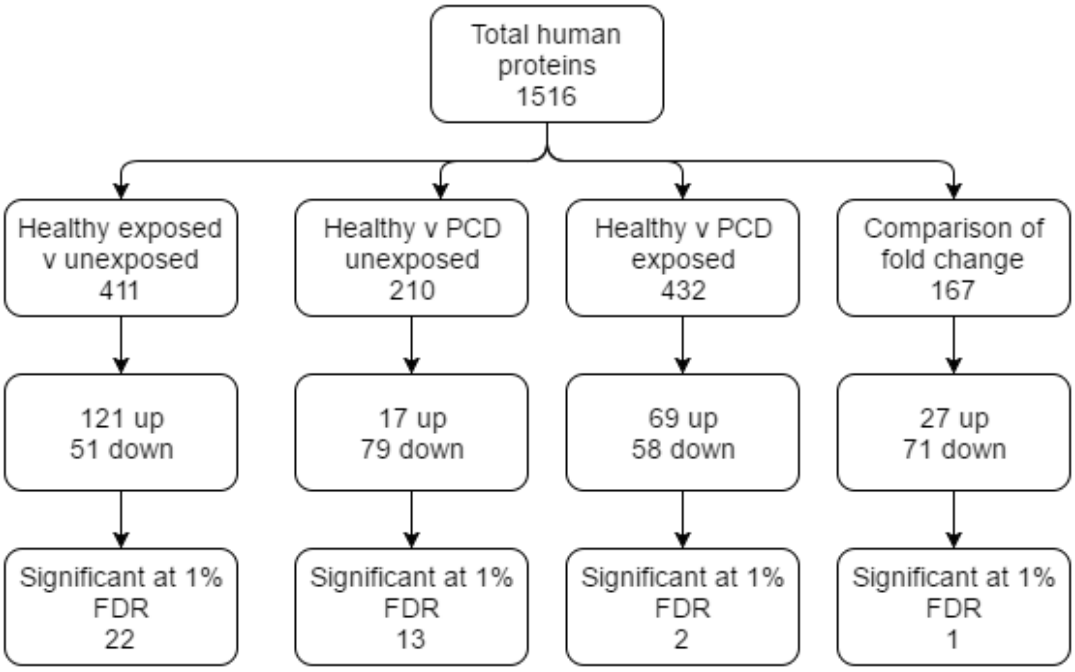

Figure 6-2. **Number of proteins identified in the 14 lysates from cultured respiratory epithelium +/- 72h NTHi biofilm.** Analysis included 6 healthy control samples (3 pairs of exposed and unexposed) and 7 samples from 6 different PCD patients. The 2nd row indicates the number of proteins included in that comparison (present in sufficient repeats in each compared group). 3rd row is the number of proteins that were upregulated (>1.5 fold change) or downregulated (<0.7 fold change) in that comparison. All proteins were then tested for statistical significance using multiple t tests at the 1% false discovery rate (FDR).

6.4.1 Response of healthy epithelium to NTHi biofilm

Proteomic results were available for 3 paired samples from healthy volunteers (an exposed and an unexposed sample from the same subject). This allowed calculation of the fold change in identified proteins following co-culture with NTHi biofilm for 72 hours. 411 proteins were present in both the exposed and unexposed samples of at least 2 out of 3 healthy volunteers, of which 121 were >1.5 fold upregulated and 51 were <0.7 fold downregulated (Full list in F.1, Table 8-3). 22 were significant at 1% FDR (Table 6-2), of which 8 had a fold change between 1.3 and 1.5 and, therefore, would not be included in the list of upregulated proteins using the predetermined cut-offs. Expansion of the definition of upregulation down to 1.3 fold, however, does not alter the pathways identified in the GO-PANTHER or KEGG analyses.

Uniprot	Protein name	Ratio
P30838	Aldehyde dehydrogenase_ dimeric NADP-preferring	2.05
P00558	Phosphoglycerate kinase 1	2.05
P06733	Alpha-enolase	1.94
P06576	ATP synthase subunit beta_ mitochondrial	1.78
P02538	Keratin_ type II cytoskeletal 6A	1.70
P04406	Glyceraldehyde-3-phosphate dehydrogenase	1.69
P08729	Keratin_ type II cytoskeletal 7	1.61
P07355	Annexin A2	1.60
P04075	Fructose-bisphosphate aldolase A	1.58
P13647	Keratin_ type II cytoskeletal 5	1.49
P68104	Elongation factor 1-alpha 1	1.45
Q04695	Keratin_ type I cytoskeletal 17	1.45
P08727	Keratin_ type I cytoskeletal 19	1.44
P29508	Serpin B3	1.42
P14618	Pyruvate kinase isozymes M1/M2	1.41
P05787	Keratin_ type II cytoskeletal 8	1.35
P60709	Actin_ cytoplasmic 1	1.31
P04264	Keratin_ type II cytoskeletal 1	0.67
Q71U36	Tubulin alpha-1A chain	0.46
Q01082	Spectrin beta chain_ non-erythrocytic 1	0.36
P35580	Myosin-10	0.30
P53621	Coatomer subunit alpha	0.19

Table 6-2. **Proteins that were individually statistically significantly different in healthy ALI cultures co-cultured with NTHi compared to unexposed cultures**. Ratio is normalised protein quantity in exposed/unexposed. Sequential t-tests with 1% false discovery rate.

GO-PANTHER analysis of these 22 proteins showed overrepresentation of canonical glycolysis, gluconeogenesis and cytoskeletal organisation. KEGG analysis identified glycolysis/gluconeogenesis, biosynthesis of amino acids and carbon metabolism as overrepresented pathways.

GO-PANTHER analysis of all up- or downregulated proteins revealed over-represented pathways in upregulation of metabolic processes, cytoskeletal organisation and catabolic processes as well as initiation of translation (Table 6-3). Downregulated pathways were involved in cell-cell adhesion and localisation, potentially to allow ingress of immune cells, and response to chemicals (potential control of the inflammatory response). The overall effect of these pathways is an increase in metabolic activity, catabolism and cytoskeletal modifications with a lessening of cell-cell adhesion to promote cellular ingress.

GO-PANTHER biological process	**Observed proteins**	**Expected proteins**	**Fold enrichment**	**p-value**
Upregulated				
Metabolic processes				
canonical glycolysis (GO:0061621)	5	0.15	32.52	4.84×10^{-3}
gluconeogenesis (GO:0006094)	6	0.27	22.06	3.31×10^{-3}
translational initiation (GO:0006413)	8	0.91	8.79	4.78×10^{-2}
cellular modified amino acid metabolic process (GO:0006575)	8	0.95	8.46	4.78×10^{-2}
cellular nitrogen compound catabolic process (GO:0044270)	12	2.31	5.19	3.38×10^{-2}
Infection/interaction				
phagocytosis (GO:0006909)	9	1.24	7.25	4.23×10^{-2}
actin cytoskeleton organization (GO:0030036)	13	2.44	5.32	9.95×10^{-3}
interspecies interaction between organisms (GO:0044419)	18	5.14	3.5	3.31×10^{-2}
Downregulated				
cell-cell adhesion (GO:0098609)	14	3.16	4.43	1.49×10^{-2}
response to chemical (GO:0042221)	25	9.63	2.6	9.25×10^{-3}
localization (GO:0051179)	28	12.09	2.32	1.34×10^{-2}

Table 6-3. **Significantly over-represented biological processes within those proteins up- or downregulated in healthy primary respiratory epithelial cultures exposed to 72 hour NTHi biofilm.** GO-PANTHER overrepresentation analysis of 79 upregulated (>1.5 fold) and 56 downregulated (<0.7 fold) mapped proteins. 0.05 significance level with Bonferroni correction for multiple comparisons.

KEGG analysis identified the upregulation of metabolic/energy pathways and amoebiasis (an actin protein and 3 serpin proteins (protease inhibitors)). Downregulation was seen in the pentose phosphate pathway (energy metabolism) and pathogenic *E.coli* infection (primarily tubulins stimulated by the invasive nature of *E.coli*) (Table 6-4).

KEGG pathway	**No. genes**	**FDR**
Upregulated		
Metabolic pathways	27	7.88×10^{-8}
Carbon metabolism	10	7.88×10^{-8}
Glycolysis / Gluconeogenesis	6	0.000133
Biosynthesis of amino acids	6	0.000249
Amoebiasis	6	0.00196
Phenylalanine metabolism	3	0.00603
Downregulated		
Pathogenic *Escherichia coli* infection	4	0.00175
Pentose phosphate pathway	3	0.00272

Table 6-4. **KEGG pathway analysis of up- and downregulated proteins in healthy cultured epithelium exposed to 72 hour NTHi biofilm.** KEGG analysis of 121 upregulated (>1.5 fold) and 51 downregulated (<0.7 fold) mapped proteins. FDR – false discovery rate. Pathways with FDR<1% shown.

Analysis of differentially regulated proteins using the InterPro protein families database showed significant downregulation of S100/calbindin-D9k domains (S100-A6, A8, A9 and P, FDR 7.69×10^{-5}).

6.4.2 Proteome of healthy and PCD cultures prior to biofilm exposure

Comparison was made between healthy subject ALI cultures and PCD ALI cultures without any exposure to NTHi. 210 proteins were present in at least 2 of 3 healthy subject and 2/2 PCD unexposed samples. Of these, 17 were >1.5 fold higher in PCD and 79 were <0.7 fold lower in PCD (F.2, Table 8-4). These were significantly more connected than expected (PPI enrichment p value 0.00082). The 14 differentially expressed proteins that were significant at the 1% FDR with sequential t-tests were primarily involved in the cytoskeleton and energy metabolism (Table 6-5).

Uniprot	Protein name	Ratio
P35580	Myosin-10	7.39
P02538	Keratin_ type II cytoskeletal 6A	0.62
P29508	Serpin B3	0.62
P68104	Elongation factor 1-α 1	0.51
P60709	Actin_ cytoplasmic 1	0.51
P07355	Annexin A2	0.49
P08727	Keratin_ type I cytoskeletal 19	0.46
P08729	Keratin_ type II cytoskeletal 7	0.45
Q71U36	Tubulin α-1A chain	0.44
P05787	Keratin_ type II cytoskeletal 8	0.43
P05023	Sodium/potassium- transporting ATPase subunit α-1	0.42
Q04695	Keratin_ type I cytoskeletal 17	0.41
P04406	Glyceraldehyde-3-phosphate dehydrogenase	0.38
P52272	Heterogeneous nuclear ribonucleoprotein M	0.28

Table 6-5. **Proteins that were individually statistically significantly different in PCD and healthy ALI cultures without exposure to NTHi biofilm.** Ratio is normalised protein quantity in PCD/healthy. Sequential t-tests with 1% false discovery rate.

GO-PANTHER overrepresentation analysis did not detect any upregulated pathways in PCD compared to healthy subject unexposed cultures but there were downregulated metabolic pathways and cytoskeletal/cell-cell adhesion proteins (Table 6-6). This was supported by the KEGG analysis (Table 6-7).

GO-PANTHER biological process	**Observed proteins**	**Expected proteins**	**Fold enrichment**	**p-value**
Upregulation				
Downregulation				
Metabolism				
monosaccharide biosynthetic process (GO:0046364)	9	0.2	43.97	7.59×10^{-9}
glucose metabolic process (GO:0006006)	7	0.47	14.86	4.39×10^{-3}
NAD metabolic process (GO:0019674)	5	0.22	23.12	2.39×10^{-2}
generation of precursor metabolites and energy (GO:0006091)	10	1.23	8.14	3.69×10^{-3}
Infection/response to microbes				
intermediate filament cytoskeleton organization (GO:0045104)	5	0.16	30.82	5.93×10^{-3}
interspecies interaction between organisms (GO:0044419)	16	3.33	4.8	1.44×10^{-3}
cell-cell adhesion (GO:0098609)	15	3.39	4.43	1.01×10^{-2}

Table 6-6. **Significantly over-represented biological processes within those proteins upregulated or downregulated in PCD cultures versus healthy cultures without exposure to NTHi**. GO-enrichment pathway analysis of 17 upregulated (>1.5 fold) and 80 downregulated (<0.7 fold) mapped proteins. 0.05 significance level with Bonferroni correction for multiple comparisons.

KEGG pathway	No. genes	FDR
Upregulated		
Downregulated		
Carbon metabolism	10	7.26×10^{-10}
Biosynthesis of amino acids	9	7.26×10^{-10}
Metabolic pathways	19	3.82×10^{-6}
Glycolysis / Gluconeogenesis	6	7.13×10^{-6}
2-Oxocarboxylic acid metabolism	4	2.44×10^{-5}
Pentose phosphate pathway	4	0.000125
Pathogenic Escherichia coli infection	4	0.0018
Citrate cycle (TCA cycle)	3	0.00563
Pentose and glucuronate interconversions	3	0.00822

Table 6-7. **KEGG pathway analysis of up- and downregulated proteins in PCD versus healthy epithelial cell cultures not exposed to NTHi.** 16 upregulated (>1.5 fold) and 77 downregulated (<0.7 fold) mapped proteins. FDR – false discovery rate. Pathways with FDR<1% shown.

Again, energy metabolism features in both analyses, including carbon metabolism, glucose metabolism and amino acid synthesis. It is possible that a lack of effective ciliary beating alters both cytoskeletal and energy usage pathways or that accumulation of improperly trafficked ciliary proteins interferes with these processes.

6.4.3 Healthy and PCD epithelium exposed to NTHi biofilm

This analysis compared pooled results from the NTHi-exposed healthy samples and the NTHi-exposed PCD samples. In total there were 432 proteins found in at least 2 out of 3 healthy and 3 out of 5 PCD samples. Of these, 69 were >1.5 fold upregulated and 58 were <0.7 fold downregulated (F.3, Table 8-5) in PCD compared to healthy epithelium. Only 1 reached statistical significance at the 1% FDR; keratin type 2 cytoskeletal protein (Uniprot P04264) which was 1.85 fold higher in the PCD samples.

Again, pathway analysis was performed on all up- or downregulated proteins. GO-PANTHER analysis showed an increase in sodium ion export and cell-cell adhesion in PCD but downregulation of cell spreading and cytoskeletal organisation (Table 6-8). KEGG analysis identified the response to *E.coli* as upregulated in PCD (3 tubulins and a cytoskeletal control protein) with downregulation in glycolysis/gluconeogenesis (Table 6-9)

GO-PANTHER biological process	Observed proteins	Expected proteins	Fold enrichment	p-value
Upregulation				
sodium ion export from cell (GO:1903278)	3	.03	91.18	4.52×10^{-2}
cell-cell adhesion (GO:0098609)	15	2.89	5.2	1.13×10^{-3}
Downregulation				
substrate adhesion-dependent cell spreading (GO:1900026)	4	0.09	43.69	2.01×10^{-2}
cytoskeleton organization (GO:0007010)	16	2.59	6.19	2.82×10^{-5}

Table 6-8. **Significantly over-represented biological processes within those proteins up- or downregulated in PCD cultures exposed to 72 hour NTHi biofilm compared to exposed healthy cultures**. GO-enrichment pathway analysis of 68 upregulated (>1.5 fold) and 56 downregulated (<0.7 fold) mapped proteins. 0.05 significance level with Bonferroni correction for multiple comparisons.

KEGG pathway	No. genes	FDR
Upregulation		
Pathogenic Escherichia coli infection	4	0.00769
Downregulation		
Glycolysis / Gluconeogenesis	4	0.00579

Table 6-9. **KEGG pathway analysis of up- or downregulated proteins in PCD cultures exposed to 72 hour NTHi biofilm compared to healthy cultures exposed to 72h NTHi biofilm compared to healthy cultures exposed to 72h NTHi biofilm.** Mapping of 68 upregulated (>1.5 fold) and 56 downregulated (<0.7 fold) proteins. FDR – false discovery rate. Pathways with FDR<1% shown.

Further analysis of these proteins using the InterPro protein families database [333] revealed significant enrichment of calcium binding domains associated with S100 proteins. These D9k-calbindin sites are related to the EF-hand calcium binding domains (Table 6-10) and mediate intracellular calcium diffusion [420].

InterPro domain description	No. genes	FDR
Upregulation		
S100/Calbindin-D9k, conserved site	5	2.18×10^{-6}
S100/CaBP-9k-type, calcium binding, subdomain	5	2.18×10^{-6}
EF-hand domain pair	7	0.0001
EF-hand domain	6	0.000644
EF-Hand 1, calcium-binding site	5	0.0043

Table 6-10. **InterPro protein family analysis of over-represented domains within proteins that were up- or downregulated in PCD epithelium exposed to NTHi biofilm compared to healthy exposed epithelium**. Mapping of 68 upregulated (>1.5 fold) and 56 downregulated (<0.7 fold) proteins. FDR – false discovery rate. Domains only shown in FDR<1%.

S100 proteins have diverse functions in immune response and cytoskeletal organisation [421]. A number of these were upregulated in PCD epithelium compared to healthy epithelium; Protein S100-P (P25815) 2.1 fold higher in PCD, S100-A10 (P60903) 1.7 fold, S100-A6 (P06703) 1.6 fold, S100-A8 (P05109) 1.6 fold, S100-A9 (P06702) 1.5 fold. S100-A2 (P29034) 1.2 fold, S100-A11 (P31949) 1.1 fold and S100-A4 (P26447) 0.9 fold were unchanged. GO-PANTHER pathway search for the S100 proteins that were >1.5 fold greater in PCD showed these proteins are involved in neutrophil aggregation, zinc sequestration, protein nitrosylation, chemokine production and leukocyte migration.

Other proteins that were up- or downregulated and contained the calcium binding EF-hand domains of the type found in the S100 proteins (Table 6-10) were Actin-4 (O43707) 3.3 fold difference in the PCD response compared to healthy response, calcyphosin (Q13938) 0.56 fold

difference, plastin-3 (P13797) 0.37 fold difference and Sorcin (P30626) 1.52 fold difference. However, string analysis shows that the 7 differentially expressed EF-hand proteins have no connections between them. By adding the 10 closest proteins to those identified, a common network can be established (Figure 6-3).

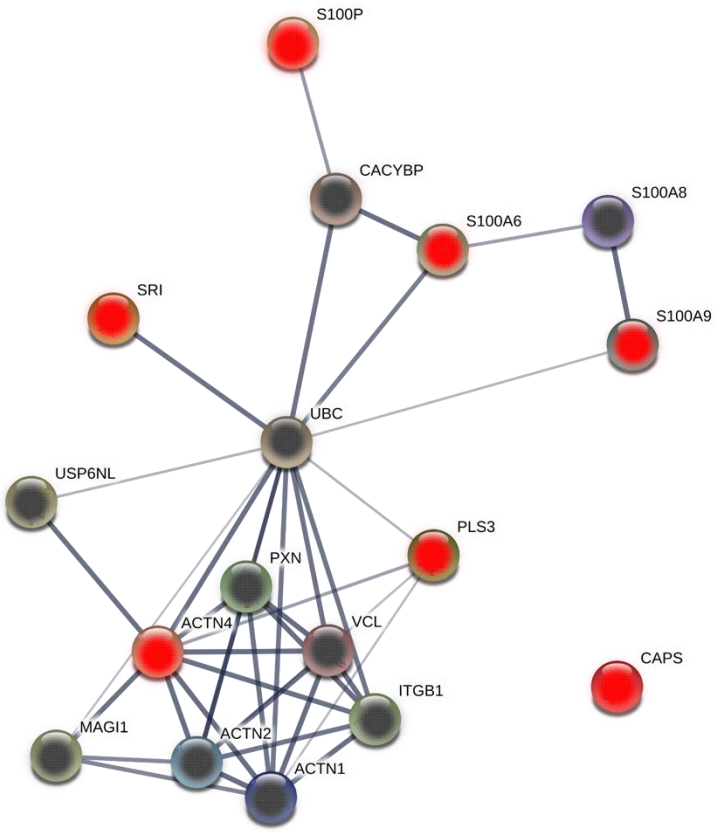

Figure 6-3. String network of potential connections between EF-hand calcium binding domain proteins identified in proteomic analysis of healthy and PCD epithelial responses to NTHi biofilm. String analysis added the 10 closest connections (grey) to the 7 identified proteins with EF-hand domains (red). Line thickness indicates strength of confidence in interaction. SRI – sorcin, PLS3 – plastin 3, CAPS – calyphosine, UBC – ubiquitin C, USP6NL – USP6 N-terminal like, ACTN1 – actinin alpha 1, ACTN2 – actinin alpha 2, ACTN4 – actinin alpha 4, VCL – vinculin, CACYBP – calcyclin binding protein, MAGI1 – membrane associated guanylate kinase, ITGB1 – integrin beta 1, PXN - paxillin

KEGG analysis of Figure 6-3 proteins shows this network links closely to leukocyte transendothelial migration (KEGG pathway 04670), adherens junctions (KEGG 04520) and actin cytoskeleton (KEGG 04810).

6.4.4 Linear mixed models approach to healthy and PCD epithelium

The linear mixed models analysis (LIMMA) approach is not well established in proteomic studies, however it may help to identify clustering in samples not otherwise identified by clinical, genetic or diagnostic criteria. Multidimensional scaling (MDS) plots were generated using the 50 biggest fold changes in protein between each possible pair of samples and representing this on a 2-dimensional plot. The closer samples are on the chart, the closer they are in protein expression. MDS plots show reasonable clustering of healthy unexposed samples, with a much wider spread of both healthy and PCD exposed samples. The 2 PCD unexposed samples plot well apart and, therefore, caution should be used when interpreting them as a "pooled" baseline (Figure 6-4).

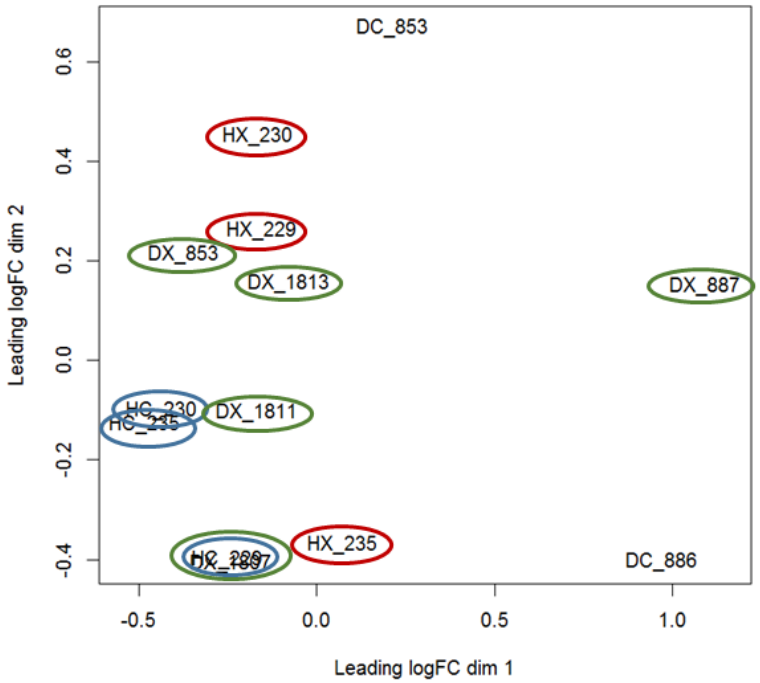

Figure 6-4. **Multi-dimensional scaling plot of proteomic samples using LIMMA approach**. Linear mixed models approach used the 50 most differentially expressed proteins to represent similarity in samples in 2 dimensions, the closer samples are on the plot, the closer their expression profile. HC – healthy unexposed (blue), HX – healthy exposed (red), DC – PCD unexposed(no colour), DX – PCD exposed(green).

LIMMA was then used to identify any clustering independent of known categories (e.g. PCD/healthy/exposed/unexposed) by using the 50 largest fold changes in protein in PCD versus healthy epithelium at baseline (Figure 6-5) then the 50 largest when comparing PCD versus healthy following NTHi exposure (Figure 6-6).

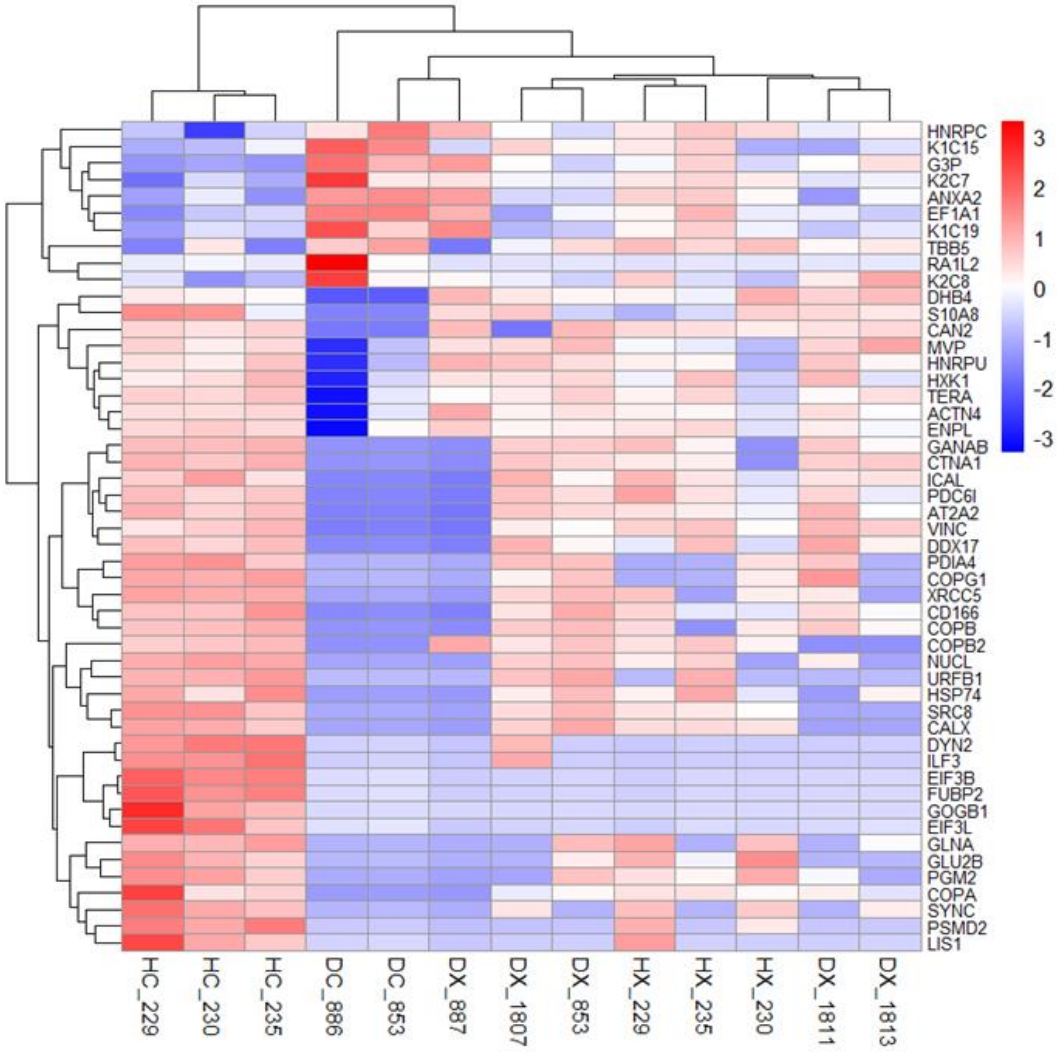

Figure 6-5. **Heat map generated using LIMMA approach to cluster proteomic samples**. 50 largest changes in protein between PCD and healthy cultures at baseline (unexposed) used to generate heat map for all samples using the linear mixed models approach. HC – healthy unexposed, HX – healthy exposed, DC – PCD unexposed, DX – PCD exposed.

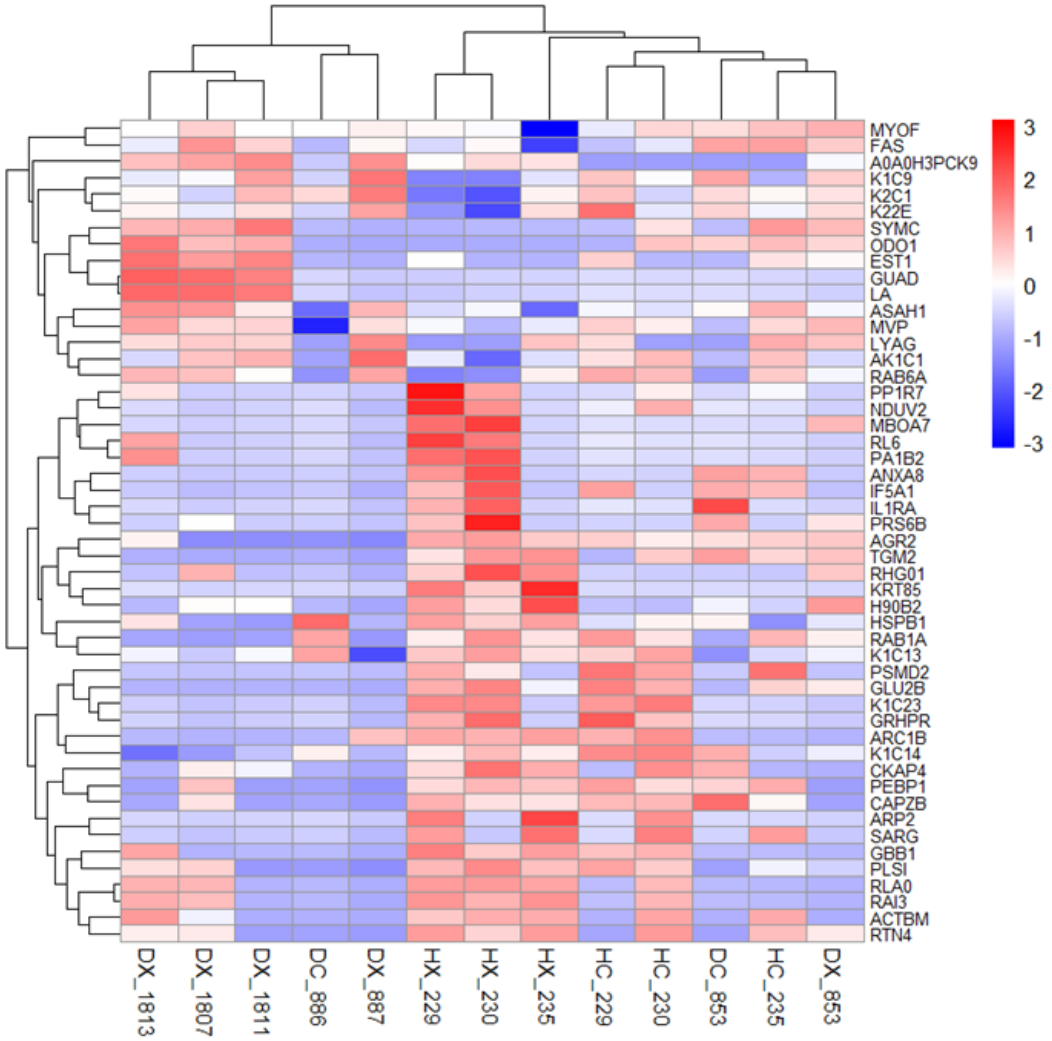

Figure 6-6. **Heat map generated using LIMMA approach to cluster proteomic samples.** 50 largest changes in protein between PCD and healthy cultures following 72 hour NTHi biofilm exposure used to generate heat map for all samples using the linear mixed models approach. HC – healthy unexposed, HX – healthy exposed, DC – PCD unexposed, DX – PCD exposed.

The heat map generated using differences in protein at baseline shows reasonable clustering of healthy unexposed (HC) samples compared to all others. Other clustering is not so clear but the PCD unexposed (DC) samples seem to cluster with the PR887 NTHi-exposed sample. Differences in PR886 unexposed heat mapping may reflect that this patient's PCD is likely to be caused by a HYDIN mutation rather than the DNAH11 mutations seen in all other patients. This clustering is also seen when using the differences following exposure; PR886 is an unexposed sample that clusters better with the PCD exposed samples than PCD or healthy unexposed.

The second heat map also reinforces the clustering of healthy epithelium with the exposed healthy samples clustering more closely than the other samples.

Overall, there is evidence to support common responses across healthy epithelium samples but there is a more disparate pattern of protein changes amongst other samples. In particular, the use of PCD samples 886 and 853 as unexposed controls should be interpreted with caution as their patterns of expression do not cluster well. This may represent the different underlying mutations causing their PCD or other modulating factors.

6.5 Discussion

Proteomic analysis of healthy and PCD epithelium exposed to NTHi biofilm identified a large number of differentially regulated proteins, several of which were statistically significant. Additionally, pathway analysis identified common pathways that are altered in response to NTHi and that are potentially differentially regulated in PCD epithelium compared to healthy.

6.5.1 Response of healthy epithelium to NTHi biofilm

The identification of proteomic changes in paired exposed/unexposed healthy epithelium provides novel insights into the normal epithelial responses to early NTHi biofilm formation. Pathway analysis of the 172 differentially expressed proteins suggest significant changes in cellular architecture (GO-PANTHER biological processes “phagocytosis”, “actin cytoskeleton organization” and “interspecies interaction between organisms”) and metabolic upregulation (glycolysis, gluconeogenesis, amino acid and nitrogen compound catabolism processes). “Interspecies interaction between organisms” reflects changes seen in the cytoskeleton known to be associated with invasion/internalisation. Upregulation in translational initiation is not unexpected given the need to respond to the infectious threat by producing innate defense and immune signalling proteins, however it is not clear which proteins are being upregulated. The identification of these defense proteins was likely hampered by the washing prior to lysis, with many of them being secreted and likely present in the removed supernatant. The 22 proteins that were individually statistically significant belonged to canonical glycolysis, gluconeogenesis and cytoskeleton organization according to GO-PANTHER. This supports the importance of these processes in response to NTHi biofilm. KEGG pathway analysis of the 172 differentially expressed proteins identified the same metabolic changes. The over-

representation of phagocytosis within the upregulated proteins shows the importance of intracellularisation of NTHi in the pathogenesis of colonisation. Whether this is induced by the NTHi is unclear, however, there is previous evidence that this may be the case [422].

InterPro analysis showed an over-representation of S100 proteins in the proteins downregulated in response to NTHi biofilm. S100 proteins have a number of functions including control of inflammation and cytoskeletal remodelling, thus downregulation could provide a brake on the inflammatory response to NTHi. These proteins are discussed further in 6.5.4 in the context of PCD and healthy epithelial responses.

6.5.1.1 Comparison with previous published data on NTHi and cultured epithelium

There have been two studies using proteomics to characterise the changes in epithelial cells following exposure to NTHi. Both used models of acute otitis media rather than lower respiratory epithelium; Harrison *et al* used a chinchilla model of acute otitis media and NTHi isolated from children with chronic otitis media [314] whilst Val *et al* used cultured, immortalised mouse middle ear epithelial cells exposed to the lysate of NTHi [423]. Another study used cultured human respiratory epithelium exposed to an otitis media isolate of NTHi and undertook transcriptomics (RNA sequencing) [235].

6.5.1.1.1 Murine cell line exposed to NTHi lysate and the role of keratins

Val *et al*'s use of cultured, immortalised mouse middle ear epithelial cells exposed to the lysate of NTHi provided insights into the role played by cytoskeletal rearrangement, particularly keratins, in the response to NTHi, even in the absence of intracellular invasion [423]. The identification of proteins involved in cell morphogenesis and structure was also common to many of the analyses in this work. These proteins, particularly cytoskeletal keratins, have been identified as important in epithelial response to NTHi [315], NTHi virulence and invasion [314] and in the control of epithelial proliferation and differentiation in response to a range of stimuli [424]. Val *et al* showed significant early (2 day) upregulation in keratins that had returned to normal by days 4 and 7 [423]. Type 1 cytoskeletal 16 and 17 and type 2 cytoskeletal 5 and 6A were also identified in this work, along with the controlling/interacting proteins involucrin and periplakin. Figure 6-7 shows that the degree of upregulation seen at 72 hours was entirely consistent with the changes seen in Val *et al's* work. This suggests a consistent response of epithelium to NTHi in terms of cytoskeletal remodelling and proliferation, and supports these proteomic results as consistent with known epithelial cell responses to NTHi in healthy cells.

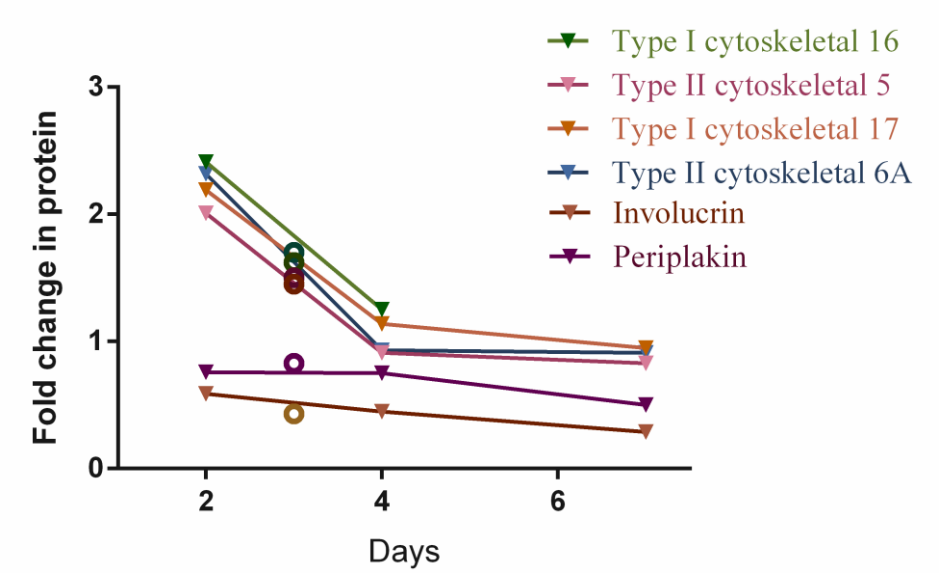

Figure 6-7. **Keratin upregulation in healthy epithelium in response to NTHi biofilm is consistent with previous changes seen on exposure to NTHi.** Fold change in keratin protein or keratin-regulating proteins (involucrin/periplakin) following 72 hour NTHi co-culture with healthy epithelium (open circles) is compared to the changes in these keratins from Val *et al* where murine middle ear epithelium is exposed to NTHi cell lysates (triangles and lines) [423].

Val *et al* saw an early increase, followed by later decrease in all keratins (6A, 17, 5, 75, 15, 16, 79) that are associated with epithelial differentiation and proliferation [423]. They also identified keratin 10 as being significantly upregulated at 1 week (16.5 fold, but not at 2 or 4 days); keratin 10 is found in differentiated cells where there is a downregulation of proliferation [423]. Keratin 10 was not identified in this proteomic analysis, however keratin 1 was downregulated after 72 hours in healthy cells (0.67 fold). Keratin 1 and 10 are known to both signify terminally differentiated epithelial cells [425]. Involucrin controls keratinocyte differentiation whilst periplakin (as part of the plakin family) crosslinks the keratin filaments and links them to membrane complexes thus maintaining epithelial layer integrity [426]. Changes in these proteins (involucrin 0.43 fold and periplakin 0.83 fold change on NTHi exposure) were consistent with that seen in the Val *et al* work. Related proteins plakophilin (0.49 fold change) and junctional plakoglobin (0.32 fold) were also downregulated in healthy epithelium exposed to NTHi in this work.

The work of Baddal *et al* using RNAseq to analyse primary human epithelium and NTHi supported these keratin findings. The early upregulation in K5 and K16 was seen, as well as

changes in keratins 6, 8,10, 14, 15 and 17 [235]. However, they identified upregulation in K10 (terminal differentiation keratin) at 72 hours, whereas the work here suggests hyper-proliferation at 72 hours.

Of the keratins that were upregulated by healthy epithelial cells in response to NTHi biofilm, 6A (1.7 fold), 5 (1.49 fold) and 16 (1.41 fold) are associated with hyper-proliferation and 17 (1.45 fold) with basal cells. Alongside the downregulation of the K1 terminal differentiation keratin mentioned above, K2 was also downregulated (0.58 fold). K2 is associated with highly differentiated epithelium. The greatest downregulation was seen in K24 (0.17 fold) which is of unknown function but most closely resembles the K10 terminal differentiation keratin [427]. This supports the idea that healthy epithelium remains in a proliferative state at 72 hours when exposed to NTHi biofilm.

K24 was also found in much higher quantities in both unexposed PCD epithelium (20.8x higher than healthy unexposed) and in NTHi-exposed (44.9x higher in PCD than NTHi-exposed healthy epithelium). Keratins 8, 7, 17, 1, 19 and 6a were all more than 1.5 fold higher in unexposed PCD epithelium than healthy whilst 6B was lower (0.6 fold). 8, 17, 7 and 19 are universal keratins found in all epithelium whilst 1 is the terminal differentiation keratin mentioned above. 6B, like 6A, is associated with hyper-proliferation [425]. This suggests that unexposed PCD epithelium is in a less proliferative state than unexposed healthy epithelium. When comparing the NTHi-exposed epithelia, the differences in keratins of terminal differentiation, K1 and K2, remained (1.85x and 1.70x respectively). However, the differences in a number of others keratins disappear once exposed to NTHi; including the proliferation keratins 6A, 6B, 17 and 5 and the universal keratins 19 and 7.

These changes in keratin expression show that -

- Healthy epithelium is in a proliferative state at 72 hours of NTHi biofilm exposure in line with the response seen to NTHi lysate
- PCD epithelium at ALI culture is more differentiated and less proliferative than healthy epithelium
- PCD epithelium fails to further upregulate proliferation in response to NTHi biofilm in the way healthy epithelium does

Two other proteins were found in healthy exposed/unexposed, PCD exposed/unexposed samples and the Val *et al* paper; NHE-RF1 and galectin-3. NHE-RF1 is a Na^+/H^+ exchange regulatory co-factor (Uniprot O14745). Val *et al* showed upregulation at 48 hour exposure to

NTHi lysate (2.12x) then slight downregulation at 96h (0.8) and 7 days (0.9) [423]. In this work, healthy epithelium showed no change in NHE-RF1 at 72h following NTHi biofilm exposure (0.94 fold change), which would be consistent with the trend seen by Val *et al*. However, levels were lower in PCD epithelium than healthy at baseline (0.55x) and higher in PCD epithelium following NTHi biofilm exposure (1.46x).

NHE-RF1 (gene SLC9A3R1) is implicated in a wide range of biological processes but, most notably, it is a negative regulator of SLC9A3, a sodium/hydrogen exchanger [428] that was identified as a significant modifier of lung disease in cystic fibrosis. Corvol *et al* performed a genome-wide analysis study (GWAS) on 6,365 CF patients and found a single nucleotide polymorphism (SNP, rs57221529) in SLC9A3 to be associated with a 190ml (4.64% of predicted) drop in FEV_1 for males and 130ml (3.98%) for females [82]. This finding was backed up by the work of Dorfman *et al* who found the rs4957061 SNP in the SLC9A3 gene was associated with earlier acquisition of *P.aeruginosa* and lower lung function at 10y of age (FEV_1 92.5% vs 87.4%) [429]. Since NHE-RF1 is a negative regulator, PCD epithelium may have higher levels of NHE (SLC9A3) sodium/hydrogen exchange at baseline that is downregulated following NTHi exposure (through upregulation of NHE-RF1). Pathway analysis, however suggests "sodium ion export from cell" is an upregulated pathway in PCD epithelium compared to healthy following NTHi exposure due to upregulation in proteins associated with potassium and sodium/potassium transporting ATPases.

NHE-RF1 is also necessary for recycling of β-adrenergic receptors (ADRB2) [430] and targeting of 5-hydroxytryptamine receptor 4 (HTR4) to microvilli [428], so may modulate changes in airway responsiveness in response to bacterial colonisation. Interaction between NHE-RF1 and platelet-derived growth factor (PDGF) has been identified and as a potential pathway for stimulation of cell growth by NHE-RF1 [431]. Upregulation of NHE-RF1 in PCD epithelium after NTHi biofilm exposure would stimulate growth and is in contrast to the keratin data that suggests lower levels of proliferation compared to healthy epithelium.

Galectin-3 (Uniprot P17931) is a galactose specific lectin that is involved in acute inflammation including triggering of neutrophil and macrophage migration and clearance of apoptotic neutrophils [432]. In Val *et al* 's work, there was no change at 48 hours (0.98 fold) but it then became downregulated at 96 hours (0.8) and 7 days (0.5) raising the possibility of suppression of immune response with longer exposure [423]. This work found no change in healthy epithelium following NTHi exposure (1.07 fold change), with no significant differences in

healthy/PCD epithelium at baseline (1.2x higher in PCD) or after exposure (1.06 higher in PCD). Thus, there does not appear to be intrinsic or extrinsic suppression of this immune pathway at the 72 hour NTHi biofilm exposure time point. In fact, the related galectin-7 (P47929) was upregulated 2.3 fold in healthy epithelium in response to NTHi.

The majority of proteins identified in this work as up- or downregulated in healthy epithelium following NTHi exposure were also identified in the Val *et al* work but, with the exception of those mentioned above, significant changes were not seen in their work. Thus, whilst there are some common pathways to the epithelial changes in the two studies, the many additional differentially regulated proteins this work suggest a wide range of additional processes occurring in human respiratory epithelium colonised by NTHi biofilm.

Of course, it is important to remember the limitations of the comparison between this work and that by Val *et al.* This work used whole bacteria as a colonising biofilm (supernatants were removed daily) rather than lysates and, perhaps most importantly, the cells in their work were immortalised and mouse-derived. This difference in cells could account for a number of different responses to NTHi including impaired immune response in immortalised cells (1.7) and altered immune response mechanisms in mouse versus human epithelium, particularly with regard to the role, and origin, of NO in the innate immune response (1.6.1.1.1).

6.5.1.1.2 Animal model of acute otitis media

Harrison *et al's* approach used an established chinchilla model of acute otitis media to look at the changes in proteome after 48 hours of infection. NTHi isolated from a child with chronic otitis media was instilled into chinchilla middle ear before excision of the ear tissue at 48 hours and label-free proteomic analysis was performed. A "sham" infection was used as comparison, where saline was instilled [314].

They acquired full quantitative data on 377 proteins, of which 105 were differentially regulated (44 up- and 61 downregulated). Pathway analysis was performed using the same GO tools used in this analysis and identified that 48 hours into acute otitis media infection epithelium was primarily undergoing actin morphogenesis and immune suppression. 61/377 proteins were also seen in this work when looking at fold change in exposed healthy epithelium. Of the 105 differentially regulated proteins identified by Harrison *et al,* 26 proteins were seen in the healthy baseline and exposed samples in this work. In total, of the 135 differentially regulated proteins in healthy epithelium identified in this work, 52 were seen in Harrison *et al's* analysis. As Table 6-11 shows, there was no clear correlation between the up- and downregulated

proteins in their model and this work, in fact, on 7/26 proteins changed in the same direction as in Harrison *et al's* work. These 7 proteins were not significantly connected in string analysis (PPI p value 0.34) and there were no significantly overrepresented pathways in GO-PANTHER or KEGG.

Uniprot	Protein name	Fold change in healthy respiratory epithelium	Acute otitis media model fold change (Harrison *et al*)
P48594	Serpin	2.97	0.45
P35613	Basigin	2.50	0.40
P23526	Adenosylhomocysteinase	2.12	0.45
P47755	F-actin-capping protein subunit α-2	1.65	0.48
P22626	Heterogeneous nuclear ribonucleoproteins A2/B1	1.58	0.48
P08865	40S ribosomal protein SA	1.54	0.15
P04083	Annexin A1	1.51	2.5
P18669	Phosphoglycerate mutase 1	1.50	2.5
Q13228	Selenium-binding protein 1	1.29	0.04
P00491	Purine nucleoside phosphorylase	1.26	0.43
P30626	Sorcin	1.15	0.43
P09382	Galectin-1	1.07	0.50
P02545	Prelamin-A/C	1.05	0.04
O15143	Actin-related protein 2/3 complex subunit 1B	1.03	2.5
Q9H8H3	Methyl transferase-like protein 7A	0.87	0.04
Q16836	Hydroxyacyl-coenzyme A dehydrogenase	0.85	0.45
P50995	Annexin A11	0.76	2.2
P07686	B-hexosaminidase subunit β	0.70	0.38
P06702	Protein S100-A9	0.67	3.5
P05109	Protein S100-A8	0.53	6.2
P20700	Lamin-B1	0.51	2.1
P16050	Arachidonate 15-lipoxygenase	0.51	0.04*
P13667	Protein disulfide-isomerase A4	0.42	0.40

P61626	Lysozyme C	0.41	4
P05062	Fructose-bisphosphate aldolase B	0.31	0.48
Q71U36	Tubulin α-1A chain	0.08	0.37

Table 6-11. **Comparison of proteins differentially regulated in a chinchilla acute otitis media model with those identified in this work**. Green indicates upregulated, grey no change and red downregulated. Chinchilla proteins were mapped to human orthologs by Harrison *et al* [314] *5 isoform

Comparison with the work of Harrison *et al* shows no clear similarities in response of healthy cultured primary respiratory epithelium to NTHi biofilm identified in this work and that seen in the chinchilla model of NTHi acute otitis media.

Based on the proteomic results, Harrison *et al*'s work particularly focused on actin morphogenesis and followed up with transcriptomic validation of the actin related protein 2/3 complex [314]. This protein was unchanged on exposure of healthy epithelium to NTHi in this work.

The lack of concordance between these studies is likely due to a number of reasons

- Human versus chinchilla epithelium
- Different epithelial tissue – middle ear *in vivo* versus respiratory culture
- Proteome of whole excised middle ear epithelium rather than primary culture
- Modelling of an acute infective process typical of middle ear infection rather than chronic colonisation/asymptomatic clearance seen in the respiratory tract

Overall, it is likely that chronic colonisation and biofilm formation requires downregulation of many of the NTHi virulence mechanisms and host inflammatory responses that characterise acute infective processes.

6.5.1.1.3 Cultured primary human epithelium exposed to NTHi

As briefly described above, Baddal *et al* used RNA sequencing to study the response of primary cultured epithelium to NTHi. Biofilm formation was not confirmed but imaging showed the NTHi preferentially bound to ciliated cells within the epithelium. 1068 NTHi genes and 1423 host genes were successfully sequenced. The top pathways identified in NTHi at 72 hours were protein synthesis, carbohydrate metabolism, amino acids, energy metabolism and

membrane transport. The top pathways in the host at 72 hours were cellular movement, cell death, cell-to-cell signalling, cellular growth and post-translational modification [235]. This is in broad agreement with the data from this work – NTHi downregulated their metabolism by 72 hours (7.4).

The epithelium responded to NTHi by remodelling cellular architecture and there were major changes in cellular keratins and associated genes. The authors postulate that this is due to intracellular NTHi rather than biofilm-induced changes in epithelium. Although intracellular invasion may play a part, the fact that extensive keratin remodelling was seen in Val *et al's* study, which used only NTHi lysates, suggests extracellular NTHi are responsible for this remodelling. NTHi also affected cell junction integrity and the NTHi themselves adapted to the host response by upregulating iron scavenging; supporting the discussion in 5.5.3 of a potentially important role for iron in biofilm control. They also identified upregulated innate immune components (CXCL5, CXCL10, CXCL11, CCL5, IL-1α, IL-8, and IL-23α) and confirmed the presence of these in basal supernatants [235].

The NTHi strain used by Baddal *et al* was from an outbreak of otitis media [235] and, therefore, may be more virulent/pathogenic than the strain used in this work which was a long-term coloniser in a PCD lung. The degree of intracellular invasion and host response may be more pronounced because of Baddal *et al's* use of this strain. There is also no evidence of biofilm formation and chronic infection in their model and this study may, therefore, be closer to Harrison *et al* 's acute otitis media infection model discussed above that did not correlate well with this work [314]. Also, the co-culture method used only a 1 hour exposure time for the initial inoculum before washing of the apical surface of the epithelial surface. This would favour bacteria that have attached and/or invaded the epithelial cells early and could lead to a more florid infection. There is some evidence that isolates from invasive disease such as otitis media and pneumonia bind earlier and more aggressively to epithelium than isolates from healthy carriers or lower airway colonisers (e.g. COPD) similar to the HI4 isolate used in this work [433]

6.5.2 Role of host cytoskeletal changes in NTHi biofilm formation

A consistent feature in previous studies [235,314,423] and in the proteomic changes in this work is the modulation of the host cell cytoskeleton, in particular actin filaments. The epithelial cell cytoskeleton is composed of 3 main elements;

1. Microfilaments – predominantly actin and involved in cell movement
2. Microtubules – α and β tubulin that acts as "tracks" for intracellular movement (e.g vesicles). Also the main components of motile cilia.
3. Intermediate filaments – mostly keratin and provide both tensile strength and perform regulatory function [434]

Constituents of each of these were significantly altered in response to NTHi including actin depolymerisation/repolymerisation upregulation, tubulin downregulation and changes to a number of keratins. This suggests extensive changes to all facets of the epithelial cell cytoskeleton.

Although Baddal *et al* postulated that the keratin changes were a result of NTHi invasion, the work by Val *et al* using NTHi lysates (and therefore no cellular invasion) suggests that other mechanisms also induce these changes. Notwithstanding that lysates may induce cytoskeletal changes that make the cells more receptive to intracellular invasion.

Manipulation of host cytoskeleton by bacteria is well described in other bacterial species [435]. Intracellular bacteria such as *Salmonella enterica* use host cytoskeletal changes to invade the cell and then exploit these changes for intracellular motility. For example, *S.enterica* injects an effector protein into cells that activates G proteins, causing actin filament changes that result in ruffling of the membrane and engulfment of the bacteria [435]. *Shigella spp.* polymerises actin once internalised in order to move through the cell [436]. *Enteropathogenic E.coli* is an extracellular pathogen but it also recruits actin by injecting an effector protein that causes actin changes below the surface and facilitates binding of the bacteria to the epithelial cell [437].

Significant changes in tubulins were also seen in this work, with tubulin α-1A chain 0.46 fold downregulated protein in healthy epithelium following NTHi exposure. Tubulins are constituents of microtubules and are targeted by a number of bacteria. For example, *Shigella spp.* destabilise microtubules in order to faciliate invasion [438]. "Pathogenic *E.coli* infection" was an over-represented pathway in KEGG analysis of healthy versus PCD epithelium; this was due to 3 tubulins and the cytoskeletal control protein, ezrin, being lower in the PCD exposed than healthy epithelium. GO-PANTHER analysis also identified a lower response in PCD in the "cytoskeletal organisation" pathway. It is, therefore, possible that PCD epithelium does not respond to NTHi with the same degree of cytoskeletal rearrangment. Since PCD is caused by dysfunctional microtubular proteins in many cases, including the DNAH11 mutations causing PCD in these NTHi-exposed samples, this is a potential source of altered response to infection.

There may even be differences in internalisation rates in PCD and healthy epithelium that could, potentially, account for the lower CFU counts in PCD biofilm versus healthy (Figure 4-19).

These other bacterial species all share an effector protein that is inserted into the host cell to begin the process of cytoskeletal rearrangement. However, sequencing of the NTHi genome reveals no genes encoding for such effector proteins [199], however NTHi are known to induce microvilli extension and facilitate internalisation; a process which is dependent on actin and tubulin rearrangements [422]. This leads to macropinocytosis, a receptor-independent uptake of bacteria [422], however receptor-dependent mechanisms such as β-glucan receptor and platelet activating factor receptor (PAFR) also lead to NTHi internalisation [439]. NTHi also shows a huge amount of inter-strain variability in its ability to invade host cells, as a result of highly variable lipooligosaccharide (LOS) structure and certain strains that do not express other adhesins (e.g. HMW1 and HMW2) [211,440]. Effective internalisation appears to also be dependent on NTHi secretion of human IgA1 protease [199], which was not identified in this *in vitro* or co-culture proteomic work. Genetic sequencing of the HI4 isolate used in this work would be required to determine whether it possesses this protease and other pro-invasive variants such as ChoP domains on LOS [422].

The changes in actin seen in this work (Table 6-3) suggests there is potential invasion of NTHi as well as biofilm formation. Although this was not seen on SEM, other imaging techniques such as transmission electron microscopy or fluorescent labelling and imaging of the NTHi would be needed to confirm. This would also need to be done over the 72 hour time course as it is likely that invasion is not taking place by 72 hours as this process occurs earlier in the infective process [235].

6.5.3 Differences between PCD and healthy epithelium

The primary baseline differences in PCD and healthy cultured respiratory epithelium, prior to any exposure to biofilm, were lower levels of metabolic activity and cytoskeletal/cell-cell adhesion proteins. As described in detail below (6.5.1.1.1) PCD cultures are, potentially, better differentiated at baseline but the NTHi-induced hyper-proliferation ablates this difference. Although this baseline difference could reflect differences in sample and culture characteristics such as age of culture and number of basal cells in original sample, strict criteria were applied to when the samples could be used for co-culture (2.3.3) to minimise any bias. Since there

were only 2 unexposed PCD samples, from patients with different underlying mutations, these differences must be interpreted with caution. This is especially true given the lack of clustering using the LIMMA approach.

Pathway analysis identified a higher level of sodium ion export and cell-cell adhesion proteins in the PCD response to NTHi biofilm with downregulation of adhesion-dependent cell spreading and cytoskeletal organisation. The identification of "pathogenic *Escherichia coli* infection" pathways in KEGG analysis reflects the changes in cytoskeleton and that some tubulins were higher in PCD. Cytoskeletal rearrangement involving actin and tubulin alterations is a central part of the pathogenicity of intracellular pathogens such as *E.coli, Shigella and salmonella typhi* [441]. Over-representation of these infection-associated tubulin pathways may reflect greater intracellular invasion in PCD epithelium or differences in cellular response to extracellular biofilm.

Further analysis of the significantly enriched protein domains (contained within the differential proteins) showed calcium binding domains were significantly over-represented in the proteins higher in the PCD response. The S100 proteins associated with these domains are involved in neutrophil aggregation, zinc sequestration, protein nitrosylation, chemokine production and leukocyte migration (GO pathway analysis). This raises the possibility that there are some differences in immune response regulators between healthy and PCD response to infection. Since it is calcium binding domains that are over-represented (D9k-calbindin and EF-hand), there exists a potential link with calcium control of ciliary beating and NO. A failure of appropriate calcium flux within and between adjacent epithelial cells as a result of failure of ciliary beating, may affect the availability/binding of calcium to S100 proteins resulting in impaired immune responses. String analysis of the 10 closest connections to these EF-hand containing proteins showed close connection to actins and thus cytoskeletal organisation.

Repeating the analysis using fold change within each healthy volunteer versus pooled fold change for PCD (to maximise number of identified proteins) did not significantly alter the conclusions above. Pathway analysis placed more emphasis on the cellular structure, but still identified differences in metabolism.

6.5.3.1 Potential implications of DNAH11 mutation on PCD proteome

DNAH11 is a heavy chain component of the outer dynein arms with its gene located on 7p15-21. It was first identified as a causative gene in PCD by Bartoloni *et al* in 2002 and is known to be associated with a normal ultrastructure of cilia on electron microscopy (TEM). As PCD

diagnosis previously relied on TEM analysis (and still does in many countries), it is likely that many PCD patients with DNAH11 mutations were dismissed as PCD negative due to normal ultrastructure.

The exact number of PCD patients with DNAH11 mutations is not accurately known for the reasons above, and because it is likely to be highly dependent on the population tested. Knowles *et al* sequenced 58 patients with PCD and normal ultrastructure and found 13 patients (22%) had biallelic mutations in DNAH11 [442]. None of the patients with ultrastructural abnormalities had DNAH11 mutations. Boon *et al* sequenced 68 PCD patients with normal ultrastructure and 21 patients (31%) had DNAH11 mutations [443]. Since 10-36% of PCD patients have normal ultrastructure [24,442,443], DNAH11 mutations are expected to cause 3-8% of PCD.

However, when examining local data in Southampton, the picture is quite different. To November 2016, 74 PCD patients had been tested via exome sequencing for disease causing mutations in 32 known genes. The commonest category was "no confirmed mutation" (n=19, 25.7%) followed by DNAH11 (n=15, 20.3%) then DNAH5 (n=11, 14.9%). This is in contrast to other published studies and is likely representative of the local population in Southampton.

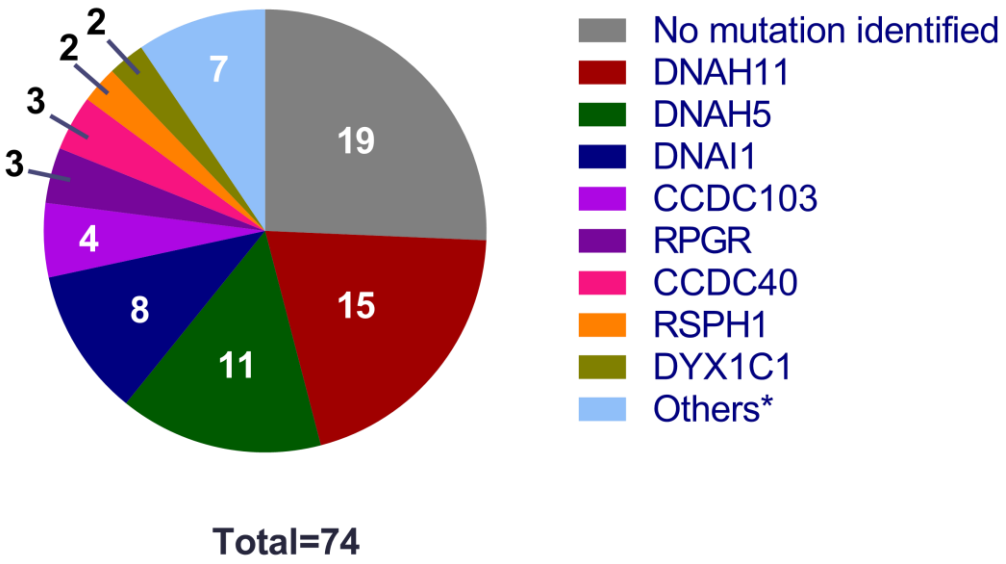

Figure 6-8. **Breakdown of mutated gene causing PCD amongst Southampton patients**. A total of 74 patients with PCD were exome sequenced in 32 known PCD causing genes. *genes where only 1 patient has disease caused by a mutation in that gene (CCNO, DNAH7, LRRC6, CCDC39, HYDIN, ZMYND10, RSPH4A).

As well as having normal ultrastructure, cilia with DNAH11 mutations do not exhibit the classical static (immotile) cilia of PCD [444]. This may be related to the site of localisation of DNAH11, which is largely proximal in the cilia [445] with the same function potentially undertaken by DNAH9 in the distal part of cilia [446]. It may be that the normal ultrastructure is a reflection of imaging cilia at both distal (normal) and proximal (ODA deficient) positions, resulting in an overall "normal" percentage of cilia with ODA present. This pattern of protein expression means DNAH11 patients are often described as having reduced amplitude of ciliary beat due to stiff proximal portion of the cilia and a hyper-kinetic distal segment [444]. However, DNAH11 patients seem to show a spectrum of ciliary abnormalities and all the patients in this work had a mixture of static and dyskinetic cilia (Table 6-1). This is supported by both human data and a mouse model of *situs inversus* (dnahc11(iv)) caused by DNAH11 ortholog mutations [269].

Despite these differences from the classic ODA deficiency and static cilia seen in the commonest PCD causing mutation DNAH5, there do not seem to be differences in clinical phenotype for DNAH11 patients and other PCD patients [443]. It is, therefore, unclear whether any differences in epithelial response to NTHi in DNAH11 deficient epithelium would be applicable to other PCD-causing mutations. However, since DNAH11 mutations are the commonest identified in the local population, the findings are particularly relevant to these patients.

6.5.4 S100 proteins and calcium-binding domains

Comparison of PCD and healthy epithelial responses to NTHi identified differences in S100 calcium binding domains, specifically the 9k sites of the EF-hand family that are involved in intracellular calcium diffusion (Table 6-10). S100 proteins were significantly downregulated in healthy epithelium in response to NTHi (0.13 to 0.87 fold). However, PCD epithelium did not seem to downregulate to the same degree thus this is a potential source of dysregulated response to NTHi.

S100 protein	Healthy epithelium response to NTHi	PCD versus healthy exposed	PCD versus healthy unexposed
P	0.33	2.1	2.2
A10	-	1.7	-
A9	0.67	1.6	3.9
A6	0.56	1.6	1.0
A8	0.53	1.6	-
A2	0.49	1.2	1.4
A11	0.72	1.1	1.2
A4	-	0.9	-

Table 6-12. **S100 proteins identified in proteomic analysis**. Healthy response is fold change in protein from unexposed to 72h NTHi-exposed epithelium. PCD versus healthy is ratio of protein in PCD/healthy epithelium. Dashes indicate that protein was not identified in this analysis or did not meet inclusion criteria. All ratios are those of normalised protein quantity.

The S100 family contains 25 proteins with a diverse range of functions including cell proliferation, calcium homeostasis, cytoskeletal organisation, response to reactive oxygen species and modulation of immune response [447]. They all share an EF-hand calcium binding domain. S100-P was 2.2 fold higher in PCD epithelium than healthy at baseline and 2.1 fold higher following exposure to NTHi biofilm. S100-P is involved in cytoskeletal changes and cell migration [447], as well as negatively regulating ubiquitin tagging and degradation of other proteins, including heat shock proteins (HSPs) 70/90 and SMAD1 [448]. These proteins are involved in a wide range of processes, including response to stressors and cell proliferation/death. Epithelial response to NTHi is primarily through NF- κB upregulation, a process which is controlled through deubiquitinases, such as CYLD, that remove ubiquitin from the cell [230,231]. S100-P is downregulated in the healthy response to NTHi (0.33 fold) and the ratio of PCD/healthy stays consistent (2.2 fold higher in PCD prior to exposure and 2.1 fold higher after) so there is also downregulation in PCD. This suggests that there are pre-existing and persistent raised S100-P levels in PCD epithelium that may promote more florid inflammation. This is supported by the fact that HSP70 is 2.2 fold higher in exposed PCD

epithelium than healthy with no change in healthy epithelium following exposure to NTHi (1.03 and 1.14 fold change). This is even more pronounced as HSP70 was 0.29 fold lower in PCD epithelium at baseline.

S100-A10 (1.7 fold higher in PCD) forms bonds between membrane proteins and annexin 2, assisting in trafficking to the membrane and providing stability once there [447]. This function includes actin binding protein AHNAK and an epithelial sodium channel [449]. This may complement the NHE-RF1 data (6.5.1.1.1) where this negative regulator of sodium/hydrogen exchange was lower in PCD epithelium at baseline but higher after exposure; resulting in lower sodium transport in PCD than healthy epithelium.

S100-A6 (1.6 fold higher) is involved in cell proliferation, cytoskeletal arrangement and immune responses [447]. Interestingly, A6 appears to have a role in HSP70, as mentioned above in relation to S100-P [450]. A2 was appropriately downregulated in response to NTHi (1.4 higher in unexposed PCD vs healthy, 1.2 fold higher in exposed PCD vs healthy) and has also been implicated in HSP control [450]

S100-A8 and A9 were 1.6 and 1.5 fold higher respectively in exposed PCD epithelium, and perform a wide range of tissue-specific functions, both individually and as a dimer. A8 deletion is lethal in mice, suggesting a non-redundant cellular function [451]. A8 is induced by oxidative stress and scavenges reactive oxygen species, whilst also stabilising nitric oxide [452]. A9 is important in the TLR-4 stimulated cytokine response and cytoskeletal rearrangements in response to infection and may mediate calcium signalling in some inflammatory pathways [453,454]. As a dimer, A8/9 is known as calprotectin and moderates ROS production in response to intracellular calcium [455] as well as migrating to the cell membrane to stabilise microtubules [453]. As a result, S100-A8/9 expressing epithelial cells seem more resistant to invasion by some bacteria [456]. S100-A9 was 3.9 fold higher in unexposed PCD epithelium so it is possible that PCD epithelium is more resistant to invasion and favours extracellular colonisation and inflammatory response. Calprotectin has also been found in neutrophil extracellular traps (NETs) so may have a role in the clearance of colonising bacteria [457] and higher expression in PCD may favour this inflammatory response. However, the failure of NETs to clear colonising bacteria and, subsequently, contribute to airway inflammation has been noted in CF [161]. Higher expression of calprotectin by PCD epithelium may, therefore, result in decreased intracellular invasion by NTHi but increased airway surface inflammation and more NETs. The increased baseline, with less pronounced difference following exposure, may

also represent a pre-existing pro-inflammatory state prior to infection and aberrant control of ROS production and/or intracellular calcium signalling.

Thus, increased baseline levels or failure of appropriate downregulation of these S100 proteins by PCD epithelium could result in increased neutrophil chemoattraction, a more pronounced TLR stimulation, ion transport defects and changes in intracellular calcium/ROS. There may also be alterations in the ubiquitin pathways that determine the cellular response to stressors (e.g. NTHi, ROS), and that regulate NTHi triggered inflammation via NF- κB. As a whole, the S100 proteins identified in this work are pro-inflammatory and, thus, their greater downregulation in the healthy epithelium compared to PCD suggests that PCD epithelium is more inflammatory in its response to NTHi.

6.5.5 Limitations

There are, of course, weaknesses in using this model to infer *in vivo* responses to bacterial infection. Despite the fact that nasal cells have been shown to model lower airways effectively [293,294], NTHi is an asymptomatic coloniser in the upper airway and is associated with disease in the lower airway, suggesting different mechanisms operating at these two sites. However, next generation sequencing techniques suggest this could be because lower airway commensal NTHi is not detected by conventional culture means [55,56]. Little sputum is expectorated from healthy lungs and healthy volunteers are unlikely to undergo lavage unless part of a research project addressing a specific question, so it is difficult to prove the presence of asymptomatic lower airway colonisation by NTHi.

The choice of a 72 hour time course reflects, in part, the previous work on this model and the validation work in *in vitro* NTHi biofilms. Whilst 72 hours is sufficient time to establish a biofilm (as evidenced by Figure 4-3 SEM images), evidence from the Val *et al* work on cell lines and NTHi lysates showed a switch from hyper-proliferative to quiescent cell state across 7 days of exposure. 72 hour exposure resulted in a keratin profile that is still relatively proliferative in this work and the Val *et al* study (Figure 6-7). *In vivo* biofilms are present over much longer time periods and, therefore, the proteome of the epithelium in the lung may be much more quiescent than seen in a 72 hour co-culture sample. However, when considering the difference between PCD and healthy lungs, these early responses to NTHi biofilm may be critical to determining whether long term colonisation is established.

The method of protein extraction may also affect the proteins detected. Secreted proteins are an essential part of a cellular response and the washes prior to cell lysis would remove most of these proteins. Of course, these proteins are trafficked intracellularly and are part of complex pathways that include intracellular proteins and membrane proteins which will be detected using this method but levels may be much lower/undetectable.

An important difference between the single organism co-culture employed here and the *in vivo* situation is the number of other microbial species present in the lung. The lung microbiome is a complex ecosystem that cannot be, currently, replicated in the laboratory so studies such as this that can elucidate the effect of individual species are still useful.

The nature of PCD as a disease is also an important consideration. Although 5/6 PCD patients had PCD caused by DNAH11, they all had different mutations of that gene and whilst previous evidence suggested DNAH11 only accounts for around 3-8% of PCD, local data puts this figure at around 20% (Figure 6-8). The huge number of causative genes, each with many different mutations, makes PCD studies very problematic and extrapolating results from studies such as this must be done with extreme caution. Whilst most PCD patients share the same clinical features, this may be the result on widely different pathogenesis leading to a similar clinical picture. Of course, as so little is known about the PCD epithelium and bacterial colonisation, this work still provides very useful insights into the disease.

A potential next step is to compare PCD responses in this model to those of CF. During this work, 14 brushings were taken but all failed during the culture process. This may reflect the organisms present in the nasal cavity of CF patients such as *Stenotrophomonas maltophilia*, *P.aeruginosa*, *Burkholderia cepacia* and non-tuberculous mycobacteria (NTM) that are potentially resistant to the antibiotics present in the culture medium (penicillin and streptomycin). Also, CF patients have a high incidence of nasal polyps and chronic rhinosinusitis which would result in inflamed nasal mucosa. As a result the nasal brushings may contain fewer suitable basal cells or be in a hyper-proliferative/exfoliative state that prevents culture [458]. Finally, the secretory abnormalities of CF epithelial cells (reduced airway surface liquid, acidification of periciliary fluid etc.) may result in cells that find it more difficult to adhere to the collagen coated culture well. Although previous studies have had success in culturing CF cells at ALI, many of these have used samples of lung from explanted tissue [459] or used CFTR-deficient cell lines [306–308]. Future studies could focus trying to obtain nasal brushings from young CF patients undergoing procedures under general

anaesthetic, where parents would find it acceptable for them to be brushed. This approach could potentially limit the existing infection and inflammation in the nasal cavity.

6.5.6 Conclusions

At baseline, cultured primary respiratory epithelium from PCD patients appears to be in a more differentiated, less proliferative state than identically cultured healthy epithelium. However, following exposure to NTHi biofilm, healthy epithelium becomes hyper-proliferative and shows cytoskeletal remodelling to a degree not seen in PCD epithelium. These changes in healthy epithelium are in keeping with that seen in previous work and validates this co-culture model. Comparison to models of otitis media models suggests that the epithelium responds in a markedly different way during lower airway colonisation with biofilm than when responding to a florid, acute infection in the middle ear.

Changes in cytoskeleton, particularly actin, are characteristic of NTHi infection and are not purely due to intracellular invasion. Differences in tubulins between PCD and healthy epithelium may lead to different cellular responses and alterations in intracellular invasion rates of NTHi.

PCD epithelium showed higher levels of S100 calcium-binding proteins that are involved in the immune response and calcium-mediated cytoskeletal re-arrangement. A number of these proteins were >1.5 fold higher in exposed PCD epithelium and may cause altered cellular responses to infection and control of inflammation. Dysregulation of calcium metabolism in PCD epithelium may also cause defects in ROS generation and NO generation/stability.

Chapter 7: Non-typeable *H.influenzae* proteins from biofilm on primary epithelial cells

7.1 Introduction

Alongside the changes in proteome of epithelial cells cultured with NTHi biofilm, proteomic analysis may also identify NTHi proteins in the co-culture; characterising both differential bacterial protein responses to the healthy and PCD epithelium, and validating *in vitro* biofilm proteins previously identified (Chapter 5:). To date, only one proteomic study has identified both host and NTHi proteins; Harrison *et al,* using the chinchilla model of acute otitis media, lysed the middle ear epithelium and identified both host proteomic changes and 27 NTHi proteins [314]. However, this model represents an acute infection with NTHi rather than the colonisation model here. Whilst Val *et al* did not perform proteomics on a co-culture model, they undertook separate proteomic studies to characterise the proteome of NTHi lysate [311] then the proteome of a cultured murine middle ear cell line exposed to this NTHi lysate [423]. A comparison between this work and theirs is made in 6.5.1.1.1, with their published lysate proteome allowing comparison with any NTHi proteins identified here to see if the same NTHi-derived proteins are likely to be triggering the cellular responses. Baddal *et al* applied transcriptomics to a co-culture model of acute otitis media and identified a total of 1068 NTHi genes (of which 412 were present at 72 hour analysis). Their study is potentially more relevant to this work as they used cultured primary respiratory epithelium, however the use of a virulent acute otitis media NTHi strain (as evidenced by 100% cytotoxicity at 72 hours) makes comparisons to this work difficult (where epithelial cells were still viable at 72 hours).

The biofilm proteins identified in Chapter 5: along with comparison to previous work on biofilm-associated proteins in NTHi [213,248,309,312,314,385,386] will allow validation of *in vitro* NTHi biofilm models and provide insights into *in vivo* biofilm formation.

7.2 Aim

To identify NTHi proteins associated with biofilm growth on primary epithelial cells and to identify any differences in biofilms grown on healthy and PCD epithelium.

7.3 Methods

7.3.1 Co-culture and protein extraction

Co-culture methods were used as per 2.3.3. Following a 72 hour co-culture time, proteins were extracted via lysis of the cells using 0.1% SDS, 100mM TEAB in HBSS with Halt™ protease/phosphatase inhibitor at 3x concentration (Life Technologies) for 10 minutes as per 2.4.1.2. As these were co-cultures, the NTHi proteins were identified from within the MS analysis performed in Chapter 6:. Proteins were included in the analysis if present in at least 1 healthy sample and 2 PCD samples. Protein quantities were normalised to total NTHi protein detected rather than the total protein in the sample (human and NTHi).

7.3.2 Statistical analysis

Proteomic data was analysed as per 2.5

7.4 Results

A total of 83 NTHi proteins were quantitatively identified in the co-culture proteomic analysis. 22 of these were found in both healthy and PCD samples (Figure 7-1).

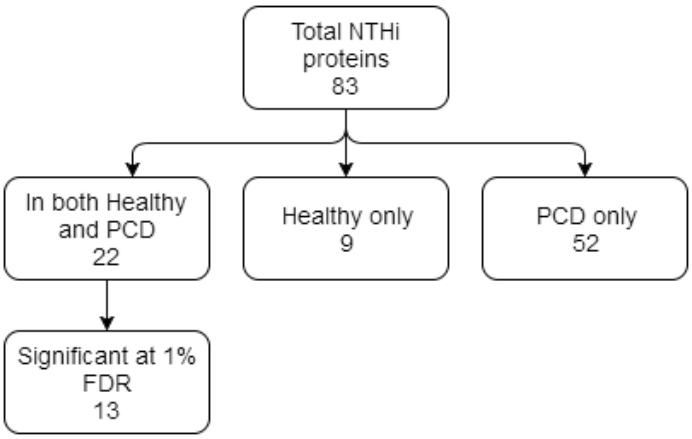

Figure 7-1. **Summary of NTHi proteins identified in the co-culture proteomic analysis**. Primary respiratory epithelium cultured at air-liquid interface (3 healthy, 5 PCD) with a 72 hour NTHi biofilm analysed using label-free proteomics.

There was a wide degree of variation between samples with only 14 proteins detected in at least 5/8 samples (Table 7-1); all 14 of these proteins were also present in the *in vitro* biofilms in 5.4. KEGG pathway analysis of these proteins identified only carbon metabolism as significantly enriched.

Uniprot	Protein name	Gene	Normalised quantity
A0A0H3PCK9	Elongation factor Tu	*tuf*	23.8
A0A0H3PCS3	Outer membrane protein P5	*ompA*	13.0
A0A0H3PDW2	Chaperone protein DnaK	*dnaK*	8.67
A0A0H3PFQ6	Lipoprotein E	*hel*	7.99
A0A0H3PCG3	Ribonuclease H	*rnhA*	7.96
A0A0H3PE68	Malate dehydrogenase	*mdh*	7.70
A0A0H3PG03	Phosphoenolpyruvate carboxykinase	*pckA*	6.80
A0A0H3PEV7	Enolase	*eno*	6.58
A0A0H3PGN2	Glyceraldehyde-3-phosphate dehydrogenase	*gapA*	6.43
A0A0H3PFC9	Galactose-1-phosphate uridylyl transferase	*galT*	5.89
A0A0H3PFR5	ATP synthase subunit α	*atpA*	4.49
A4N8V8	Putative metal ABC transporter substrate-binding protein Hpf	*hpf*	3.26
A0A0H3PCZ5	Cysteine synthase	*cysK*	3.10
A0A0H3PLN0	Uracil phosphoribosyl transferase	*upp*	2.00

Table 7-1. **NTHi proteins identified in at least 5 of 8 co-culture samples (healthy and PCD).** 14 of 14 proteins were also present in *in vitro* biofilm proteomic analysis. Quantities are raw nanogram weights normalised to total protein detected in the samples (eukaryotic and NTHi).

Pathway analysis of all proteins present in both healthy and PCD samples (n=22) identified carbon metabolism, metabolic and glycolysis/gluconeogenesis pathways. This correlates with pathways identified in Chapter 5: and in previous NTHi biofilm work [309,373]. Other metabolic pathways were also identified, such as amino acid synthesis (Table 7-2).

KEGG Pathway	No. genes	FDR
Carbon metabolism	15	5.48E-07
Microbial metabolism in diverse environments	18	1.26E-06
Pyruvate metabolism	10	2.32E-06
Glycolysis / Gluconeogenesis	8	8.83E-06
Metabolic pathways	33	2.01E-05
Biosynthesis of secondary metabolites	20	8.31E-05
Citrate cycle (TCA cycle)	5	0.00034
Alanine, aspartate and glutamate metabolism	5	0.00137
Biosynthesis of amino acids	11	0.00551

Table 7-2. **Significantly over-represented KEGG pathways in NTHi proteins identified in the proteome of the co-culture samples (PCD and healthy).** 71 mapped proteins. FDR-False discovery rate. Results shown where FDR<1%.

7.4.1 Comparison of NTHi proteins in PCD and healthy co-cultures

Of the 83 proteins detected, 52 were found only in the PCD co-cultures and 9 only in the healthy samples (Figure 7-1). This may represent a greater quantity of biofilm on PCD epithelium, as demonstrated by Walker using the same 72h NTHi biofilm on cultured epithelium as this work [115]. However, there was a wide range of identified protein quantities in the samples (Table 7-3).

Sample ID	Group	Quantity (ng)	Normalised to total protein in sample
229X	Healthy	46.6	77.6
230X	Healthy	75.8	84.3
235X	Healthy	10.2	21.0
853X	PCD	15.6	29.4
886X	PCD	16.6	79.5
1807X	PCD	176.0	185.8
1811X	PCD	193.9	222.5
1813X	PCD	144.8	131.6

Table 7-3. **Quantity of NTHi protein identified in co-culture samples**. Raw quantities detected in nanograms then quantities normalised to the total protein detected in that sample (human and NTHi).

Proteins were normalised to the total quantity of protein in the sample (human and NTHi). Of the 22 proteins seen in both PCD and healthy samples, 4 were upregulated in PCD samples (>1.5 fold), 11 were unchanged and 7 were downregulated (<0.7 fold) (Table 7-4). Only 7 of these proteins were identified in more than 1 healthy sample so the ratios need to be interpreted with extreme caution.

Uniprot	Protein name	Gene	Ratio PCD:Healthy
A0A0H3PFR5	*ATP synthase subunit α	*atpA*	6.33
A0A0H3PDW2	Chaperone protein DnaK	*dnaK*	1.91
A0A0H3PCZ5	Cysteine synthase	*cysK*	1.72
A0A0H3PCG3	*Ribonuclease H	*rnhA*	1.50
A0A0H3PHN6	Uncharacterized protein		1.47
A0A0H3PLN0	Uracil phosphoribosyl transferase	*upp*	1.31
A0A0H3PG63	Elongation factor G	*fusA*	1.30
A0A0H3PEV7	Enolase	*eno*	1.29
A0A0H3PFF9	Long-chain fatty acid transport protein	*ompp1*	1.18
A0A0H3PFC9	*Galactose-1-phosphate uridylyl transferase	*galT*	1.09
A0A0H3PGN2	Uncharacterized protein	*gapA*	0.98
A0A0H3PE68	*Malate dehydrogenase	*mdh*	0.90
A0A0H3PCK9	*Elongation factor Tu	*tuf*	0.87
A0A0H3PCS3	*Outer membrane protein P5	*ompA*	0.81
A0A0H3PEL2	Fumarate reductase flavoprotein subunit	*frdA*	0.71
A0A0H3PJK6	Outer membrane protein assembly factor	*bamA*	0.69
A0A0H3PFQ6	*Lipoprotein E	*hel*	0.64
A0A0H3PD53	Putative sialic acid transporter	*siaP*	0.51
A4N8V8	Putative metal ABC transporter substrate-binding protein	*hpf*	0.49
A0A0H3PG03	Phosphoenolpyruvate carboxykinase	*pckA*	0.41
A0A0H3PF23	Polyribonucleotide nucleotidyl transferase	*pnp*	0.21
A0A0H3PFY1	# 5-methylterahydropteroyltriglutamate--homocysteine methyltransferase	*metE*	0.03

Table 7-4. **NTHi proteins identified in both PCD and healthy co-culture samples expressed as normalised ratio of quantity found on PCD epithelium to that found on healthy epithelium.** #Likely outlier as single, extremely high level in 1 healthy sample. Green upregulated, red downregulated. *present in >1 healthy sample.

String analysis of the NTHi proteins that are higher/lower in PCD samples does not reveal significant connection (PPI enrichment p value 0.723) and there was no over-representation in either GO-PANTHER or KEGG analysis. Sequential t tests using 1% FDR showed only MetE was significant, however this may be a detection error as it was detected in only one healthy sample and at an extremely high level.

7.4.2 Comparison with *in vitro* biofilm proteins identified

Detection of NTHi proteins in the co-culture samples also allows validation of the *in vitro* biofilms as a model of biofilm growing on epithelial surfaces. Of the 83 NTHi proteins identified in all co-culture samples, 53 were also identified in the *in vitro* proteomics work in Chapter 5:, suggesting a high degree of overlap in the phenotype of *in vitro* and *ex vivo* NTHi biofilms. Pathway analysis showed continued consistency with identification of carbon metabolism and glycolysis/gluconeogenesis in KEGG analysis, as well as glycolytic pathways in GO-PANTHER (Table 7-5 and Table 7-6).

GO-PANTHER Pathway	Observed proteins	Expected proteins	Fold enrichment	p-value
Glycolytic process	6	0.35	16.9	$6.2x10^{-4}$
Pyruvate metabolic process	6	0.52	11.6	$5.4x10^{-3}$
Nicotinamide nucleotide process	8	0.65	12.2	$1.1x10^{-4}$

Table 7-5. **Significantly over-represented pathways within the NTHi proteins detected in 72h co-culture experiments that were also present in 72h *in vitro* NTHi biofilms**. GO-enrichment pathway analysis of 53 mapped proteins. 0.05 significance level with Bonferroni correction for multiple comparisons.

KEGG Pathway	No. genes	FDR
Carbon metabolism	14	3.4×10^{-8}
Glycolysis / Gluconeogenesis	8	1.01×10^{-6}
Pyruvate metabolism	9	1.31×10^{-6}
Microbial metabolism in diverse environments	14	6.95×10^{-6}
Citrate cycle (TCA cycle)	5	7.1×10^{-5}
Metabolic pathways	25	7.1×10^{-5}
Biosynthesis of secondary metabolites	16	0.0001
RNA degradation	4	0.0048

Table 7-6. **Significantly over-represented KEGG pathways within the NTHi proteins detected in 72h co-culture experiments that were also present in 72h *in vitro* NTHi biofilms**. 53 mapped proteins.

7.5 Discussion

This work is amongst the first to identify NTHi proteins in a co-culture model using primary human epithelium. Previous NTHi biofilm proteomics experiments were performed on *in vitro* biofilms [309,312], using chinchilla model of otitis media [313,314] or middle ear murine cell lines [315]. The proteins identified here, therefore, represent useful insights into NTHi biofilm on human respiratory epithelium. Although Baddal *et al* 's work used respiratory epithelium and transcriptomics to identify over 1000 NTHi genes at 1, 6, 24 and 72 hours (6.5.1.1.3), their work is not directly applicable because they modelled acute otitis media that resulted in 100% epithelial cell cytotoxicity by 72 hours. There was also no assessment of biofilm formation and co-culture was only 1 hour, potentially resulting in a high degree of intracellular invasion by NTHi [235]. It is also important to note that NTHi protein concentrations in this co-culture model are much lower than the host proteins present. This makes it much more difficult to properly quantify these NTHi proteins; as it is a particular weakness of proteomics that it can be difficult to detect low-abundance proteins. Compared to modern transcriptomic techniques, such as RNAseq, proteomics has a much lower dynamic range of concentrations which may reflect the lack of any amplification stage in proteomics [460]. Strategies to

overcome this could include the use of a heavy-labelled NTHi specific amino-acid or alternative physical mechanisms for shearing off the biofilm without releasing all host proteins.

It is particularly encouraging that all 14 proteins present in at least 5/8 co-cultures were found in the *in vitro* proteomic analysis in 5.4.1. This supports the idea that *in vitro* NTHi biofilms may be useful surrogates of *in vivo* biofilm. There is potential that some of these identified proteins could be used as biomarkers of biofilm formation within sputum and, therefore, more indicative of colonisation of the lower airways. 5 of the 14 proteins have been previously implicated in biofilm formation –

- **Elongation factor Tu** – downregulated in biofilm formation [309] and in P5 mutants [213]
- **Chaperone protein DnaK** – biofilm specific protein and found in extracellular matrix [248,312]
- **Malate dehydrogenase** – downregulated in biofilm formation [309]
- **Enolase** - downregulated in biofilm formation [309]
- **Outer membrane protein P5** – biofilm specific [312], expressed during biofilm formation [385], not essential for biofilm formation but required for epithelial cell interaction [213]. 1 study showed downregulation in biofilm formation [309]

DnaK and P5 show particular promise as biomarkers of NTHi biofilm formation. DnaK is an HSP70 protein, which binds TLR2 and triggers inflammation in the epithelium (Figure 1-10). Wu *et al* identified DnaK as biofilm specific [373], however it was also present in the NTHi lysates of Preciado *et al* [311]. This does not indicate how highly expressed the DnaK is in the lysate and whether it is being actively secreted by these NTHi. Wu *et al* also found that DnaK was present in biofilm extracellular matrix at 96 hours but not 24 [373], therefore DnaK may be a useful sputum marker of established colonisation. The pro-inflammatory nature of DnaK means it may reflect virulence/pathogenicity of NTHi biofilm within the airway; also making it a useful biomarker when deciding on the need for treatment. Whilst P5 is a membrane protein, its role in epithelial cell interaction means it may be more specific to *in vivo* biofilm formation; the contradictory study by Post *et al* suggesting downregulation in biofilm formation was in an *in vitro* model where the epithelial interaction is not required and there was prolonged quiescence of the planktonic comparison [309].

The proteomic data here showed a wide degree of variability in the proteins identified in each sample. This may partly reflect the differing quantities of protein detected in each sample (Table 7-3) but also the known inherent variability in NTHi expression. Preciado *et al* 's analysis of lysates of planktonic NTHi, which should be relatively homogenous in their phenotype, found only 113 of their 793 identified proteins were present in all 3 batches [311]. This effect will be exacerbated by the heterogeneous sub-populations of bacteria seen within biofilms and across the colonies of differing maturity co-existing on the same epithelial surface (phase variation in gene expression). It is also possible that biofilm attached to motile cilia, dyskinetic cilia and unciliated epithelium differ in their phenotype – further increasing the variability in proteome.

7.5.1 PCD versus healthy epithelium

Although there were obvious differences in the number of proteins identified and the quantities of the common proteins between PCD and healthy samples, the limitations mentioned above make it difficult to draw any clear conclusions. DnaK is discussed above as a potential marker of biofilm formation/NTHi colonisation and is present at 1.9 fold higher PCD co-cultures suggesting increased biofilm/virulence in PCD. However, the putative sialic acid transporter (SiaP) was 0.5 fold lower in PCD and has previously been identified in NTHi as important in the modification of LOS to evade host immunity and promote biofilm formation [461,462]. Lower levels of SiaP expression would, therefore, either favour clearance or result in a more florid inflammation at the epithelial surface.

The extreme variability in protein concentrations identified could reflect differences in quantity of biofilm between healthy and PCD epithelium but are more likely due to the limitations of NTHi protein detection including; low overall NTHi quantities compared to epithelium, use of only detergent-based protein extraction with a Gram-negative bacteria, nature of biofilm extracellular matrix and embedding of bacteria within this. In order to overcome this problem, trypsinisation of the co-culture followed by a combination of chemical and physical lysis (similar to that used in the *in vitro* NTHi work, 2.4.1) could increase the yield of bacterial proteins.

7.6 Conclusions

NTHi proteins can be successfully identified in co-cultures with primary respiratory epithelium. All 14 proteins that were universally present in the co-culture samples were also present in the

in vitro proteome, suggesting the *in vitro* system may be a good model of biofilm growth on epithelial surfaces. However, further investigation to correlate expression levels *in vitro* and in co-culture is required or to confirm that these are biofilm specific proteins found in both *in vitro* and *ex vivo* biofilms but not in planktonic cultures. Several of these identified proteins have been previously identified as associated with NTHi biofilm formation and are potential biomarkers of significant NTHi infection; DnaK is the most promising of these.

Chapter 8: Conclusions

- Systematic review and meta-analysis showed that almost all PCD patients have extremely low airway nitric oxide compared to airways of healthy subjects and other respiratory diseases
- PYRRO-C3D is able to target NO release to the site of β-lactamase producing *non-typeable Haemophilus influenzae* (NTHi) biofilms and successfully increases susceptibility to azithromycin
- Nitric oxide treatment of NTHi biofilms induces upregulation in metabolic pathways and 50S ribosomal proteins that are the target of azithromycin
- Healthy respiratory epithelium responds to NTHi biofilm by proliferating, modulating cytoskeleton and suppressing the immune response by downregulating S100 proteins.
- Several NTHi proteins are identified in the proteome of both *in vitro* NTHi biofilms and those grown on respiratory epithelium with DnaK and OMP5 of particular interest for further investigation.

PCD is characterised by a failure of ciliary beat resulting in ineffective mucociliary clearance. This manifests, clinically, as progressive lung function decline and airway damage with colonisation of the lower airways by a number of bacterial species, of which *non-typeable Haemophilus influenzae* (NTHi) is the commonest in early life. However, NTHi is common to a number of other chronic lung diseases with different underlying pathology and disease progression. This work suggests that the response of respiratory epithelium to NTHi in PCD is abnormal compared to healthy epithelium. There are three main possible reasons for this;

1. Failure of mucociliary motion causes dysregulation of proteins such as S100 that are associated with immune response and cytoskeletal reorganisation.
2. Intracellular changes such as calcium dysfunction that are common to both failure of ciliary action and immune regulation result in abnormal epithelial responses to NTHi.
3. Failure of ciliary co-ordination results in a failure of intracellular signalling/feedback, perhaps via calcium dysregulation, that also results in abnormal innate immunity.

Since this work uses a model where cilia are present and beating in their *in vivo* pattern but without mucociliary clearance, a combination of numbers 2 and 3 are the most likely. As an

example of this link, Chapter 3: showed that nitric oxide (NO) is extremely low in the airways of PCD patients compared to healthy individuals and disease controls. With only a few exceptions, this finding is independent of causative mutation and disease severity. Therefore, there is an, as yet, unknown mechanism linking ineffective ciliary beat to low NO levels. It is possible that there is a reciprocal relationship between cilia and NO since NOS inhibitors slow ciliary beat [269] and changes in calcium flux may mediate these changes [463] since primary (non-motile) cilia possess calcium channels that open in response to bending forces [464,465]. It is, therefore, possible that other processes may be affected by the cause of low NO or other downstream effects of lack of ciliary motility.

Chapter 6: used a proteomic approach to show that there may exist such inherent differences in the PCD epithelial response to NTHi. The main pathways that differed between PCD and healthy epithelium were cytoskeletal remodelling and the calcium-binding S100 proteins. Alterations in actin polymerisation may reflect differences in internalisation rates of NTHi or differences in protective cytoskeletal changes (those that prevent NTHi ingress but allow recruited immune cells to access bacteria on the epithelial surface). Healthy epithelium appeared to respond to NTHi with a more pronounced hyper-proliferation that may favour shedding and clearance. A failure to downregulate S100 proteins in PCD epithelium may favour a more vigorous inflammatory reaction in PCD airways. In particular, S100-P levels were 2.1 fold higher in exposed PCD epithelium and HSP70 was 2.2 fold higher; S100-P interacts closely with HSP70 and controls NF-κB mediated inflammation. Other S100 proteins that were higher in PCD are associated with changes in actin binding, epithelial sodium transport, intracellular calcium responses and cellular response to oxidative stress. S100 proteins all bind calcium, therefore there is another link to the calcium flux mentioned above. It is possible that failure of proper ciliary motion results in defective calcium influx through movement-triggered calcium channels. This lower intracellular calcium could result in changes to binding of calcium to S100 proteins and alterations in subsequent immune responses and appropriate cytoskeletal reorganisation. Future work could focus on studying the effect of calcium channel blockers on response to NTHi in healthy epithelium and S100 protein expression.

The link between S100-A10 (1.7 fold higher in PCD) and an epithelial sodium channel [449] links with the NHE-RF1 data. NHE-RF1, a negative regulator of sodium/hydrogen exchange, was unchanged in healthy epithelium following NTHi exposure but was 1.5x higher in exposed PCD epithelium than exposed healthy epithelium. The channel which NHE-RF1 regulates

(SLC9A3) has been identified as a significant modifier of lung disease severity in CF [82], therefore there is a link between these solute channels and lung function decline. It is possible that infection in PCD causes alterations in solute transport and periciliary fluid not seen in healthy epithelium and resulting in worsening of inflammation. Analysis of the periciliary fluid layer in healthy and PCD epithelium both before exposure to NTHi and after could clarify whether these differences in solute transport exist [466].

It is possible that low NO in PCD airways results in excessive inflammation since NO has been shown to inhibit the downstream effects of NF-κB by interfering with its DNA binding sites [467]. Constitutively low NO in PCD airways may cause a failure of this inhibitory mechanism and excessive NF-κB induced inflammation. The proteomic changes seen in this work may be downstream effects of this failure of NF-κB control. Approaches such as qPCR of NF-κB over the timecourse of NTHi colonisation in healthy and PCD airway would help elucidate these changes, particularly if they could be studied in epithelium from PCD patients with atypically high NO levels.

This model also allowed clarification of the response in healthy epithelium by using paired samples from the same patients. NTHi exposure was associated with cytoskeletal changes, particularly actin cytoskeleton and tight junctions, as well as upregulation of metabolism. These responses were in keeping with some previously published evidence, especially as it relates to keratin changes and the switch from hyper-proliferation to quiescence as the co-culture progresses [423]. Differences with 2 of the other published studies likely reflect their use of acute infective models that either rapidly induce epithelial death [235] or produce a far more inflammatory reaction than that seen in the colonised lower airways [314].

The knowledge that NO is low in PCD airways, and previous work on NO and biofilms, raises the possibility that NO donors are a therapeutic option that may be particularly effective in PCD. Chapter 4: demonstrated that a targeted NO donor (PYRRO-C3D) was able to enhance azithromycin treatment of NTHi biofilms both *in vitro* and on cultured respiratory epithelium. Interestingly, NTHi biofilms on PCD epithelium were more resistant to antibiotic treatment but this was significantly more enhanced by PYRRO-C3D than on healthy epithelium. This may reflect the low baseline NO environment of the PCD airway, thus rendering any biofilm more susceptible to NO. The only concern with PYRRO-C3D as a potential treatment strategy was the cephaloram component of the compound which, when administered at sub-inhibitory

concentrations, has the potential to stimulate biofilm formation and, potentially, favour the development of antibiotic resistance.

Proteomic analyses also provided mechanistic insights into the enhanced susceptibility of NTHi biofilms to azithromycin following sustained NO exposure. NO seems to upregulate metabolism and translational machinery (including many ribosome proteins). Whilst many of the changes seen on exposure to NO were a reversal of the biofilm formation phenotype, many changes were not; suggesting a more complex role for NO in antibiotic sensitivity than triggering dispersal alone. In addition to an upregulation in metabolic activity that may render the NTHi more susceptible to antibiotics, there was significant upregulation of 50S ribosomal proteins which are the target of azithromycin. Therefore, NO may act both to alter biofilm phenotype and specifically change the antibiotic target of the organism.

Upregulation of a D-methionine binding lipoprotein (MetQ) following NO exposure was an unexpected finding and thus further investigated. Both D- and L-methionine isomers prevented the PYRRO-C3D enhancement of azithromycin treatment suggesting the MetQ upregulation is a protective mechanism against NO. MetQ also links closely to iron uptake/metabolism and there were a number of iron-associated proteins that were altered following NO administration raising the possibility that iron has a central role in NTHi biofilm control. Since NTHi iron status is linked to virulence and biofilm formation [410], NO-induced changes in heme-associated proteins may trigger a switch from biofilm formation to virulence. Under normal conditions, host sequestration of iron may signal the need for NTHi to form biofilm and/or increase intracellularisation mediated by increases in iron transport or heme-binding proteins. NO may induce changes that trigger the reversal of this process and render NTHi more susceptible to antibiotic/immune clearance.

The proteomic data from this *in vitro* mechanistic work was also compared to the NTHi proteins identified in the co-culture work. Although the variability in identity and quantities of NTHi proteins in the co-culture samples made many comparisons difficult, there was a core of 14 proteins common to all samples and also present in the *in vitro* biofilm analysis. These proteins could form the basis for further mechanistic or biomarker work on *in vivo* NTHi biofilm, in particular the significance of the chaperone protein DnaK (HSP70) would warrant further investigation.

There are, of course, limitations in using this kind of co-culture model. A 72 hour co-culture of a single organism is not truly representative of the lower airways where myriad microbes co-exist for extended periods of time. Although studies suggest culturing primary respiratory

epithelium at ALI is representative of *in vivo* airway [292], the culture process may change cellular responses and there are many airway constituents that are missing, especially any immune cells (neutrophils, macrophages etc.) The number of samples that could be successfully analysed was also relatively low, in particular the inability to have a number of paired exposed and unexposed PCD samples hampered the work. As shown in Appendix E, a total of 80 brushings were taken to enable this work to take place. Although success rates for culture were consistent with the historical values within this laboratory, additional death at co-culture and need to spread non-PCD samples across a number of different analyses reduced the number of repeats further. Since parents did not usually want to subject their children to additional nasal brushings, availability of PCD samples was restricted to adult PCD patients seen in Southampton. There were only around 30 of these and many did not wish to undergo the uncomfortable brushing procedure more than once. There is, therefore, a need to identify models of epithelium that can be used to study PCD responses. This is particularly true when trying to identify any difference in response between genotypes. Since 6 of the 7 patients in this analysis had DNAH11 mutations, proteomic changes could be pooled more easily however DNAH11 only accounts for around 5-25% of PCD depending on the population studied.

8.1 Future work

8.1.1 Next steps in investigating the epithelial responses

The proteomic analysis has identified a number of possible avenues for future research, in particular

- The role of actin polymerisation in the epithelial response to NTHi and whether this is altered in PCD
- S100 proteins and PCD innate immunity
- Alterations in electrolyte transport in PCD epithelium as a modifier of inflammation
- Intracellular calcium flux linking ciliary beat to nitric oxide and innate immune responses
- Measures of NF-κB in early colonisation of PCD and healthy epithelium

Further proteomic work could help to clarify the role of the above, but addition of other approaches would also be useful. In particular, transcriptomics or q-PCR at several time points

of co-culture could identify changes in the proteins of interest. Measurement of electrolytes in apical supernatant may reveal changes related to co-culture, whilst measurement of proteins within both apical and baso-lateral supernatants would provide a better insight into secreted peptide responses (especially chemokines).

An obvious extension of this model would involve co-culture of primary epithelial cells with other bacterial species. Whilst *Staphylococcus aureus* is the other common colonising bacteria in children with PCD and CF, its invasive lifecycle and virulence can make it particularly difficult to co-culture with primary epithelium [235]. Also, *in vivo S.aureus* biofilms grow embedded in mucus/cell debris rather than attached to epithelium [214] and, only after an initial invasive/virulent phase, do they switch to a colonising small colony variant [371,372]. *Streptococcus pneumoniae* is an interesting possibility since this is able to form biofilms [382] and is a significant coloniser of PCD patients (Table 1-2).

Availability of cultured cells for this model is an issue, particularly when dealing with a rare disease like PCD. Although immortalised cell lines are an attractive prospect, they have been shown to poorly replicate *in vivo* responses [115,291] and do not usually ciliate. Thus, alternative approaches to model PCD using healthy epithelium are likely to represent the future. You *et al* successfully used short hairpin RNA (shRNA) to interfere with the DNAH6 protein, a constituent of inner dynein arms, in cultured inferior nasal turbinate tissue [468]. The shRNA was administered by a lentiviral vector and, by modulating dose of shRNA, they were able to create effective heterozygotes and homozygous knockouts. A major problem with this work was the restriction to, primarily, DNAH11 mutated PCD epithelium. The technique of You *et al* could allow investigation of a wide range of causative mutations by knocking down different cilia proteins. This approach would also allow clarification of cellular changes that are specific to the loss of a single protein and could be applied to other genes not implicated in PCD such as knockout of CFTR and direct comparison between ciliated PCD and CF cultures in their response to infection. It would also be useful to see if these specific knockout models still produce NO at healthy levels or if the mutations lead to the low NO typical of PCD. Culture from patients with PCD but normal NO could also be used to identify whether epithelial responses are a result of low NO rather than the particular causative mutation.

Once an effective model is established, genotype-specific response to infection can be studied. Specific characterisation of correlation between genotype and ciliary beat pattern could be

expanded, as well as stratification of cellular responses, ciliary beating, innate immunity etc. according to genotype, EM defect or ciliary beat pattern.

In terms of furthering mechanistic insights into NTHi biofilm, creation of isogenic mutants of the proteins of interest would be useful. For example, DnaK and OMPp5 were identified as candidates for future work and knock-outs of their genes encoding these proteins could reveal their role in biofilm formation, attachment to epithelium and response to nitric oxide. For example, NTHi P5 knockouts are able to form biofilm but not adhere to epithelium [213]. Although DnaK knockouts have not been performed in NTHi, this was done in *Streptococcus intermedius* with the mutants displaying slow growth, increased thermosensitivity and lower cytotoxicity to epithelial cells [469]. Therefore, DnaK in NTHi could be critical in responding to the environment by altering growth; this is a feature of biofilm/planktonic switching. Elongation factor Tu (EF-Tu) has been previously identified as downregulated in biofilm, with a similar change in expression observed in this biofilm work. There has been limited investigational studies performed on this protein, but work in *Francisella novicida,* a rare lung bacterial pathogen, showed EF-Tu was only present in virulent bacteria and triggered inflammation via TLR4.

Through the development of rapid testing (such as qPCR on sputum samples), DnaK (or potentially EF-Tu) could be used in a clinical setting to detect NTHi biofilm formation even when there is no culturable organism in the sputum. Additionally, further study of clinical outcomes in relation to DnaK/EF-Tu status in the sputum would allow stratification of the risk of chronic colonisation and thus more appropriate use of antimicrobials in PCD and CF patients.

Another area of interest in NTHi treatment is the development of vaccines, particularly given the success of vaccines against the capsule of *H.influenzae b*. Translating this work to NTHI, however, has been difficult given the huge genetic diversity seen between NTHi strains and the ability of NTHi to alter its major surface proteins. Whilst OMPp5 has shown limited success as a vaccine candidate [470], identification of such proteins that are important for biofilm formation, and therefore chronic colonisation, could represent attractive targets for the development of novel treatment strategies.

8.1.2 NO-donor compounds and biofilms

The results from the PYRRO-C3D work are very encouraging, particularly given the current global efforts to combat antibiotic resistance. NTHi now sits alongside a number of other bacteria that are potentially NO responsive and there is, therefore, a potential treatment niche for targeted NO donors. The next steps in investigation are likely to follow Figure 8-1.

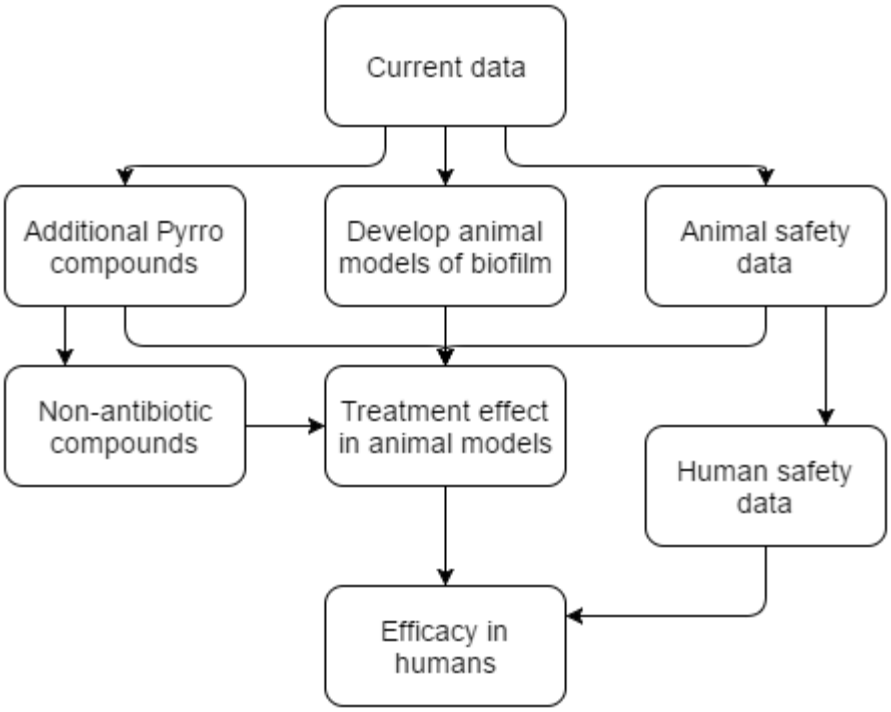

Figure 8-1. **Next steps in development of targeted NO donor compounds**. Current *in vitro*/*ex vivo* data can be used to develop animal models of biofilm infection then use PYRRO-C3D/other related compounds to establish *in vivo* effectiveness, before studies in humans. n.b extension to other ex-vivo models such as explant tissue could supplement the mechanistic understanding prior to/alongside animal work.

The most important next step in development will be effectiveness in animal models. As an adjunct to this, further work of *ex vivo* models such as explant adenoid tissue could help characterise the *in vivo* immune response; with these models including host tissue and adaptive immune responses lacking in the primary epithelial culture model. Initial safety data in animals and appropriate choice of an animal model of infection can be combined to show *in vivo* effectiveness of the compound. Work is already underway to develop an NTHi mouse colonisation model, whilst other mouse models of bacterial infection already exist, particularly for *P.aeruginosa* infection [471]. There also exists a mouse model of mutated DNAH11 that

was the cause of PCD in 6/7 patients in this work, which could be used to investigate the increased effectiveness of PYRRO-C3D on PCD epithelium [269,472]

Alongside this, additional related compounds with different NO release profiles and pharmacokinetics can be developed and then tested in the same animal models. PYRRO/NO compounds seem to be particularly suited to these modifications [376].This development could include the use of non-antibiotic NO-releasing compounds, or chemically altered cephaloram, to attempt to overcome the concerns over biofilm stimulation and antibiotic resistance that PYRRO-C3D may cause. Animal safety data can be used to inform Phase 1 trials in humans to identify pharmacokinetics, excretion and side-effect profiles. The model from this work using co-culture with primary epithelium may also be useful in establishing cellular responses to the drug and in dose identification. Once this data has been collected, Phase 2 trials in certain lung infections could begin; and if successful progress to larger Phase 3 randomised controlled trials and marketing authorisation. Choice of patient group would be important and the more severe, difficult to treat infections may be a better first target dependent on the side-effect profile in humans and thus the risk: benefit.

There are a number of other avenues currently being pursued to further harness NO-induced anti-biofilm properties. As well as the synthesis of compounds such as PYRRO-C3D [254], related compounds are being synthesised and combined with other agents to elicit anti-biofilm effects. For example, to overcome the issues with the short half-life of NO and many NO donors, nitroxides have been used to mimic the biological effects of NO [473,474] and they potentially have beneficial effects on biofilm formation and motility of *P.aeruginosa*. Another approach has been to combine NO donors with other anti-biofilm compounds such as those that inhibit quorum sensing (QS) [475] or those that aid with application of the NO donor to the biofilm [476].

8.2 Summary

In summary, PCD patients have low airway NO irrespective of the underlying disease causing mutation. This raises the prospect of epithelial dysfunction linked to lack of adequate ciliary motion rather than a particular disease-causing mutation. Targeted NO can enhance the treatment of NTHi biofilms with azithromycin and may be more effective in PCD patients. The mechanism behind this seems to involve both metabolic upregulation and upregulation of the

50S ribosomal target of azithromycin. Healthy epithelium responds to NTHi biofilm through proliferation, cytoskeletal modification and downregulation of S100 proteins, however PCD epithelium may fail to downregulate these S100 proteins to the same extent. This raises the possibility that ciliary dysfunction results in failure of this downregulation and a pro-inflammatory response; calcium is a potential mediator of this effect. Several proteins were identified as present in *in vitro* and co-culture biofilms, including DnaK, OMPp5 and EF-Tu which warrant further investigation.

Future work may focus on clarifying the role of the actin changes and S100 alterations in healthy and PCD epithelium, including measurement over the time course of infection by qPCR. Measurement of supernatant and periciliary solute changes with NTHi exposure could also be performed given the changes found in solute channel expression. Extension of the co-culture model could encompass other organisms common in PCD (such as *S.aureus* and *S.pneumoniae)* as well as PCD caused by other mutated genes with differing ciliary phenotypes. Further study of NTHi could encompass mutant strains of the proteins of interest, as well as extension of the co-culture model to a greater range of clinical NTHi strains. Identification of DnaK, OMPp5 or EF-Tu in sputum samples and correlation with clinical outcomes could yield potential as biomarkers to better target patient treatment.

To expand upon the potential of PYRRO-C3D as a novel treatment strategy future research will focus on the development alternative donor compounds, potentially without antibiotic backbones. Research will also be expanded to investigate its activity against other bacterial species and in animal models of infection, potentially leading to proof-of-concept studies in humans.

Appendices

Appendix A Systematic review protocol

Below is the systematic review protocol as specified prior to commencing the work.

A.1 Title:

Nasal nitric oxide in primary ciliary dyskinesia and disease/healthy controls

A.2 Background:

Decreased nasal nitric oxide (nNO) in primary ciliary dyskinesia (PCD) patients was first described in 1994 [46] and has subsequently been recommended as a screening test in the diagnosis of PCD [283]. A survey preceding the guidelines found that nNO was used in only 46% of European PCD centres [477]. A number of studies have investigated the accuracy of nNO in differentiating PCD patients from healthy controls.

The current European guidelines for diagnosis of PCD include high frequency video analysis of ciliary beat frequency and pattern and transmission electron microscopy (TEM) of cilia ultra-structure[283]. Supplementary diagnostic tests include immunofluorescence, radioaerosol mucociliary clearance, EM tomography and genotyping. All investigations are time consuming, technically demanding and only available in specialist centres. Accurate screening tests for PCD are therefore needed to rationalise referral for full diagnostic testing.

A.3 Aims:

Assess the level of nNO in the following situations:

1. nNO measured in PCD patients compared to healthy and disease control groups using stationary analysers during a velum closure technique (as recommended in the ATS/ ERS guidelines [283]) including a meta-analysis.
2. Nasal NO in patients with atypical PCD (normal electron microscopy).
3. Different respiratory manoeuvres during measurement of nNO that are in clinical use including breath holding, velum closure by forced expiration against resistance, tidal breathing and humming .

4. Measurement of nNO in young children (<5 years) including those unable to co-operate with respiratory manoeuvres.
5. Reliability of handheld NO analysers for screening for PCD in comparison to stationary chemiluminescence analysers.

A.4 PICO

Patient Population

Patients with a diagnosis of primary ciliary dyskinesia (with and without EM defects).

- All age groups
- Pre-school children and infants

Intervention

Measurement of nasal nitric oxide using

1. Stationary chemiluminescence analysers.
2. Hand-held analysers
3. Different respiratory manoeuvres (e.g. breath hold with velum closure, tidal breathing).

Comparator

1. PCD positive patients compared to healthy controls, patients with cystic fibrosis and other respiratory disease groups. Using stationary analyser during breath hold manoeuvre.
2. PCD patients with ultra-structural defect in comparison to PCD patients with normal ultrastructure by TEM.
3. Within-patient comparison of different respiratory manoeuvres during nNO measurement (e.g. breath hold plus velum closure, tidal breathing, humming).
4. Pre-school children/ infants with PCD in comparison to healthy control preschool children/ infants.
5. Within patient comparison of chemiluminescence stationary devices and handheld devices.

Outcome

Discriminatory value of nNO between PCD, CF and healthy/disease controls.

A.5 Search strategy

The following electronic databases will be searched: MEDLINE, EMBASE, PreMedline In-Process & Other Non-Indexed citation, Web of Knowledge Science Citation Index (SCI), Web of Knowledge ISI Proceedings and Cochrane Systematic Reviews Database. Additional references will be sought through citations listed in the identified studies. The OVID search strategy is given below;

1. exp ciliary dyskinesia, primary/

2. exp ciliary motility disorders/

3. exp kartageners syndrome/

4. "primary ciliary dyskinesia".ti,ab.

5. 1 or 2 or 3 or 4

6. nitric oxide/du

7. (nasal adj5 nitric oxide).ti,ab.

8. 6 or 7

9. 5 and 8

10. remove duplicates from 9

11. limit 10 to humans

12. (editorial or comment or letter).pt.

13. 11 not 12

A.6 Inclusion/Exclusion Criteria

A.6.1 Study selection

- Studies that evaluated nNO in adults or children with PCD will be included.
- All study designs will be included, but reviews, opinion papers, non-research articles and editorials will not.

- There is no gold standard diagnostic test for PCD, and studies where PCD had been confirmed by any of the methods recommended in the ERS Consensus guidelines [283] will be included.
- Details of measuring nNO will be required for inclusion (analyser, sampling flow rate, and breathing manoeuvre) with all methods of measuring nNO considered acceptable.
- Conference proceedings will be excluded if full data was later published in manuscript form.
- All selected studies will be included in a narrative synthesis of the literature, but only studies where suitable data were reported will be included in the meta-analysis.
- Two reviewers (SAC and JSL) will independently review titles and abstracts for eligibility.
- Full text versions will be reviewed independently for eligibility.
- Discrepancies will then be discussed and final choice of papers agreed.
- Data to be extracted and tabulated by SAC and quality assessments performed using QUADAS checklist points for studies of diagnostic tests [336] without applying a formal scoring system [478].
- Extracted data to include patient characteristics, details of comparator participants, details of nNO analyser, sampling rate, sampling manoeuvre and nNO data.

A.7 Summary -

Inclusion

- Original research reporting nasal nitric oxide (nNO) levels in primary ciliary dyskinesia patients
- Reliable diagnostic methods used to identify PCD patients
- Sampling technique and respiratory manoeuver described.
- Manufacturer of NO analyser and sampling flow rate reported
- Age range given
- Method of confirmation of PCD diagnosis reported

Exclusion

- Conference proceedings or other preliminary reports where data have subsequently appeared in a published research paper
- Lack of detail on nNO measurement (e.g. analyser, respiratory manoeuvre)

- Studies excluded from meta-analysis where mean and standard deviation not given
- No age range given
- Method of PCD diagnosis not given or inadequate testing performed

Additional criteria for each aim –

Aim 1: Inclusion – study reporting nNO values for PCD patients using stationary chemiluminescence analyser with a velum closure technique

Aim 2: Inclusion: study reporting nNO in PCD patients with and without ultrastructural defects on EM testing.

Aim 3: Inclusion – study reporting nNO levels by a manoeuvre other than solely velum closure

Aim 4: Inclusion– study reporting nNO levels in pre-school children (<5 years)

Aim 5: any study reporting nNO measurements in PCD patients via a handheld analyser

A.8 Assessment of quality

Modified QUADAS criteria will be used [336], however formal scoring will not be used in accordance with current recommendations [478].

1. Did the PCD group have their method of diagnosis clearly documented?
2. Did the authors state how these PCD patients and the comparator groups were selected (e.g. were these consecutive referrals)?
3. Was the method of nNO sampling stated including equipment used, sampling rate and manoeuvre (e.g. oral exhalation, breath hold)
4. Were nNO testers blinded to which group the patient was in (PCD, healthy etc.)?
5. Was the nNO measured via commercially available analyser using a procedure in line with the current recommendations at the time (e.g. ATS/ERS 1997 or 2005 guidelines)?
6. Did the study report subjects that were unable to perform nNO measurements?
7. Were the ages of PCD and comparator groups appropriately described?

A.9 Statistical analysis

Within aim 1 we will perform a meta-analysis of the mean difference in nNO between PCD patients and healthy controls, and between PCD patients and CF patients. The meta-analysis will use a generalised inverse variance as is customary for a continuous outcome [479]. Degree of heterogeneity will be assessed and if there is a moderate or high degree (I^2 greater than 25%) then a random effects model will be used (otherwise fixed effects will be used).

Manuscripts not suitable for meta-analysis will be included in the narrative synthesis where appropriate.

Appendix B Full list of studies assessed for inclusion in systematic review

Publication	Study population (n=)	Ages	Aim of study	Analyser & sampling method	Flow rate (l/min)	Comments/ Quality
Lundberg 1994 [46]	PCD 4 HC 24 Trach 4	PCD – 2.5-12y HC – 20 children (3-13y) HC – 4 adults Tracheostomy – 50-70 years	Determine origin on exhaled NO in children	CLD 700 (ECO Physics)	0.8	Excluded as nasal NO data for PCD not stated
Karadag *et al* 1999 [343]	PCD 21 HC 60	PCD – 7.6-14y HC – 7.3-14.3y	Compare upper and lower airway NO in PCD and healthy controls	LR 2000 – breath hold with CO_2 monitoring	0.25	
Grasemann *et al* 1999 [285]	PCD 7 CF 11 HC 11	11-39 years	Assess whether NO formation can be augmented by l-arginine and if this improves lung function in PCD/CF	Sievers 280A – breath hold	0.066	Excluded as contralateral nostril held closed

Narang *et al* 2002 [286]	PCD 31 HC 53 CF 17 Asthma 35 Bronchiectasis 21	PCD 11.0 (5.5-17.3) HC 10.7 (5.5-19.0) CF 13.2 (7.2-17.0) Asthma 11.9 (7.0-17.0) Bronchiectasis 11.6 (7.2-17.0) Mean (range)	Compare eNO and nNO levels in various inflammatory airway disease versus healthy to assess for diagnostic usefulness	LR 2000 Breath hold with CO_2 monitoring	0.25	
Horvath *et al* 2003 [344]	PCD 14 HC 37 Bronchiectasis 31 CF 20	PCD 35 CF 25.7 Non-PCD 45 Control 33 Mean	Compare eNO, nNO and carbon monoxide levels in bronchiectatic patients with PCD/CF/non-PCD	LR 2000 – breath hold	0.25	
Wodehouse *et al* 2003 [93]	PCD 42 HC 16 CF 15 Chronic sinusitis 18	PCD 34.2 (10.9) HC 36.2 (6.2) CF 22.4y (4.5y Sinusitis 45.3(15.4) Youngs 53.2 (9.9)	Comparison on nNO in PCD and comparator groups to assess for efficacy as a screening test.	LR 2000 – breath hold with CO_2 monitoring	0.25	Sampling rate from personal communication with manufacturer

	Youngs syndrome 12 Bronchiectasis 20	Bronchiectasis 46.8 (14.2) Mean (SD)				
Csoma & Bush 2003 [334]	PCD 15 HC 14	PCD 10.3 (0.7) HC 11.5 (0.4) Mean (SEM)	Investigate whether NO metabolites are reduced in PCD patients	LR 2000 Breath hold with CO2 monitoring	0.25	
Noone *et al* 2004 [32]	PCD 64 HC 27 CF 11	PCD 26.8 (range 0-73) HC 37 (2) CF 44 (2) Mean (SD)	Evaluation of biologic and phenotypic markers of disease in a cohort of PCD patients	Sievers 270B Breath hold	0.5	
Baraldi *et al* 2004 [354]	PCD 2 HC 5	PCD 4m and 6m HC 3m (range 1.3-7m)	Case report of nNO levels in 2 infants with PCD	CLD 77 (ECO Physics) tidal breathing	0.11	Case report of two PCD infants
Corbelli *et al* 2004 [339]	34 referrals for PCD (17 PCD) HC 24	11.4 (1.2) Mean (SEM)	Retrospective study of utility of eNO and nNO in those referred to a PCD service	Exhalyzer D, Ecomedics. Breath hold with velum closure	1.2	

Stehling *et al* 2006 [355]	PCD 1 HC 6 (newborns)	PCD 4d old HC 14d (2-24) Median (range)	Letter to the editor describing nNO in a single neonate with PCD	Tidal breathing. Analyser not reported.	Not described	One neonate case study, excluded as no details of analyser or sampling
Pifferi & Caramella 2007 [349]	64 recurrent pneumonia under investigation for PCD PCD (EM^+) 12 Secondary ciliary dyskinesia 50 Normal - 2	Children – ages not given	Assess the utility of nNO in atypical PCD (those with negative electron microscopy)	Not stated	0.11	Excluded as analyser not stated. Four patients labelled SCD were thought to have PCD (EM negative) had low nNO
Piacentini *et al* 2008 [340]	PCD 10 HC 77	PCD – mean 17y, 2 unco-operative children) HC – 50 under 12m, 27 school age able to perform test	Identify nNO levels in healthy young children (co-operative and unco-operative)	NIOX Flex Breath hold and tidal breathing	0.3	Healthy control data mainly in very young children

Bodini *et al* 2008 [480]	PCD 2 HC 20	PCD 5 days and 7y HC mean 30 days	Report nNO testing in young children	Not stated		Letter, excluded as no details given on sampling technique
Santamaria *et al* 2008 [345]	PCD 14 HC 14	PCD 15y (2-27y) HC 16 (7-27y) Mean (range)	Compare aspiration, exhalation and humming in the measurement of nNO	NIOX Flex Breath hold, oral exhalation, nasal exhalation and humming	3.0	
Shoemark et al 2009 [289]	PCD 20 Bronchiectasis 20 HC 20	PCD 40 (32-45) Bronchiectasis 41 (35-48) HC 37 (30-43) Mean (95% CI)	Compare bronchial and peripheral airway contributions to exhaled NO	LR 2000 Breath hold	0.25	
Moreno Galdo *et al* 2010 [341]	PCD 9 HC 37 Asthma 36 CF 31 Bronchiectasis 8	PCD 7-17y HC ages not stated Asthma 6-17y CF 6-14y	Compare nNO levels in PCD and relevant comparator groups	LR 2000 Breath hold	0.25	
Chawla *et al* 2010 [481]	PCD 53	PCD 10.2 (3.2) Probable 10.6 (3)	Assess year to year variability of nNO in PCD	Not stated	Not stated	Excluded as unclear if data subsequently reported in

	Probable PCD 23	Mean (SD)				Leigh *et al* , 2013 and no sampling details given
Shapiro *et al* 2011 [482]	336 referrals for PCD (?number positive)	Not stated	Study nNO levels in patients with heterotaxy	Not stated	Not stated	Excluded as unclear if data subsequently reported in Leigh *et al* , 2013 and no sampling details given
Beuchar *et al* 2011 [483]	PCD 4 PCD negative 12 Equivocal 2	Mean 6.8y (SD 3.9)	Retrospective review of 89 PCD referrals	Analyser not stated Breath hold	0.25	Excluded as analyser not stated and reason for subset having nNO analysis not clear
Degano *et al* 2011 [287]	PCD 5 HC 10 (referred for polypectomy) HC 10	PCD 42 (12-52y) Polypectomy 42 (11-55) Polyposis 37 (15-49) Median (range)	Assess the expression of nitric oxide synthases in upper airway tissue	EVA4000 Oral tidal breathing.	0.5	
Marthin & Nielsen 2011 [49]	117 referrals to a PCD centre	6.9 (0.0-62.4) Median (range)	Evaluate 3 different sampling methods for nNO in	NIOX Flex Breath hold, oral exhalation and tidal breathing	0.3	

			consecutive referrals to a PCD service			
Subset of patients that were PCD positive	PCD 59	PCD 17.4 (3.6-65.8) HC 29.5 (3.1-63.6) CF 16.4 (0.1-50.7) Median (range)		NIOX Flex Breath hold, oral exhalation and tidal breathing		
Mateos-Coral *et al* 2011 [342]	PCD 20 CF 32 Bronchiectasis 14 HC 19	PCD 11.4 (3.5) HC 11.0 (3.7) CF 11.0 (3.4) Bronchiectasis 10.9 (3.3) Means (SD)	Assess the ability of non-velum closure techniques can discriminate PCD from other groups	ECO PHYSICS CLD 88SP Exhalation against resistance (VC) breath hold (no VC), tidal breathing(mouth open), tidal breathing (mouth closed) and humming	0.33 3.0 (humming)	
Montella *et al* 2011 [352]	PCD 14 CF 11 HC 13	PCD 11.5y (7-27) CF 12.5 (9-24) HC 14.0 (7-27) Median (range)	Assess nNO levels in nasal exhalation and humming in PCD, CF and healthy subjects	NIOX FLEX + NIOX MINO Nasal exhalation and humming	0.3	No breath hold

Pifferi *et al* 2011 [484]	86 referrals to PCD service PCD 41 SCD 45	46 children mean 10.7 (range 8-17) 40 adults mean 32.0 (range 18-58)	To assess the relationship between sinus agenesis and nNO levels/upper airway disease	Not stated	Not stated	Excluded as no sampling details and unclear if PCD patients included in ref [348]
Pifferi *et al* 2011 [348]	Referrals PCD 48 SCD 161 HC 3	6.2 (1m to 17.5y) Median (range)	Assess nasal nNO synthase expression in PCD and SCD patients	Listed as ATS/ERS protocol	ATS/ERS protocol	Excluded as poor details of sampling and unclear if PCD patients included in ref [484]
Baker *et al* 2011 [485]	336 referrals (7 sites) PCD 150 Non-PCD 186	Not stated	Assess effectiveness of nNO screening for PCD in a multi-centre cross sectional study	No details	No details	Excluded as abstract publication. Excluded as data subsequently published in another paper (Leigh *et al* , 2013)
Montella *et al* 2012 [486]	PCD 23 HC 23	PCD 15.8 (4.6-32.8) HC 15.7 (4.3-32.1) Median (range)	Assess whether handheld measurement of nNO discriminates between PCD and healthy controls	NIOX MINO Oral breathing through mouthpiece	Not given	Excluded as sampling rate not given and no details of PCD diagnosis.
Harrison *et al* 2012 [338]	PCD 4	Not stated	Assess utility of hand held NO analysers in differentiating PCD	NIOX-MINO	0.3	Abstract publication.

	HC 5 CF 6 Bronchiect 7 COPD 4		patients from comparator groups	Tidal breathing	
Leigh *et al* 2013 [48]	PCD 149 HC 78 CF 77 Asthma 37 COPD 32 155 referrals	PCD 19.1 (5.1-73.0) HC 20.9 (5-73.6) Asthma 14.8 (5.4-53.5) CF 16.0 (5.5-56.0) COPD 61.1 (43.2-77.8) Referrals - PCD 23.3 (5.1-69.0) Indeterminate 31.8 (5.5-79.6) Mean (range)	Use a standard protocol for nNO measurement to establish disease specific cut-offs then validate at 6 other sites.	Sievers, CLD 88SP (ECO PHYSICS), NIOX Flex Oral exhalation velum closure	Sievers 0.5 CLD 0.33 NIOX 0.3

Marthin & Nielsen 2013 [50]	PCD 16 HC 20 CF 21	PCD 25.9 (8.4-60.9) HC 31.0 (15.6-58.4) CF 11.0 (3.9-23.2) Median (range)	Assess discriminative power of hand-held tidal breathing measurements of nNO and compare to stationary tidal breathing and velum closure nNO.	NIOX FLEX NIOX-MINO CLD 88SP (ECO PHYSICS) Breath hold and tidal breathing	NIOX 0.3 CLD 0.33
Walker *et al* 2013 [266]	PCD 14 CF 12 Asthma 18 HC 18	Mean (SD) PCD 12.8 (3.9) HC 14.1 (2.3) CF 11.7 (3.1) Asthma 13.5 (3.5)	Compare bronchial and alveolar NO levels in PCD patients and comparator groups.	NIOX FLEX Breath hold	
Harris *et al* [347]	PCD 13 HC 15 Chronic suppurative lung disease (CSLD) 22	Mean (range) PCD 23y (5-71) HC 31y (8-65) CF 15y (6-29) CSLD 36y (8-79)	Evaluate discriminatory ability of hand-held nNO measurement in PCD/CF/healthy subjects and compare to stationary nNO.	NIOX FLEX – breath hold NIOX-MINO – tidal breathing	0.3

Knowles *et al* 2014 [30]	PCD with RSPH1 mutation 16	Not stated	Identification of novel disease causing mutations in PCD patients	Not stated		Excluded as data likely reported elsewhere and sampling details not given
Boon *et al* 2014 [346]	PCD 38 HC 49 CF 46 Asthma 45 Humoral immunodef 48	Median (IQR) PCD 14.3 (8.8-18.1) HC 14.9 (10.8-20.4) CF 14.0 (9.2-17.9) Asthma 12.1 (9.8-16.5) HID 10.7 (8.2-15.6)	Investigate the diagnostic accuracy of eNO and nNO in PCD and comparator groups.	CLD 88(EcoMedics) Tidal breathing and oral exhalation against resistance for velum closure	0.3	Insufficient data for meta-analysis

Appendix C Growth kinetics of NTHi strains

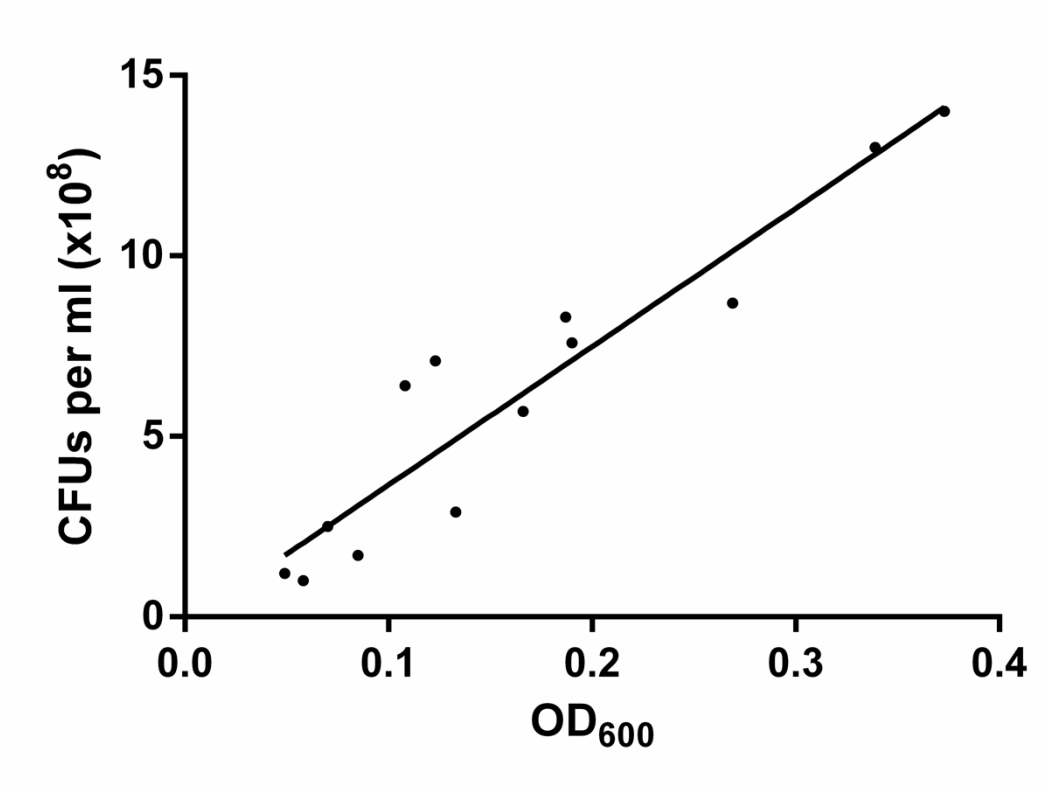

Figure 8-2. **Growth kinetics of HI4 isolate of non-typeable *H.influenzae***. Samples taken over 6 hours with optical density (OD_{600}) measured and colony forming units assessed by serial dilution.

Appendix D Full list of proteins identified in NTHi *in vitro* biofilm proteomic analysis

D.1 Proteins identified in both NO treated and untreated NTHi biofilms

UniProt code	Protein name	*Gene*	Ratio
A0A0H3PBJ4	Glucose-specific PTS system enzyme IIA component	*crr*	24.15
A0A0H3PK54	Lipoprotein (D-methionine uptake)	*metQ*	21.52
A0A0H3PBW8	Phosphoglycerate kinase	*pgk*	21.00
A0A0H3PFB4	DNA-directed RNA polymerase subunit α	*rpoA*	16.33
A0A0H3PJ51	2,3-bisphosphoglycerate-dependent phosphoglycerate mutase	*gpmA*	13.37
A0A0H3PG63	Elongation factor G	*fusA*	12.96
A0A0H3PMV3	Pyruvate kinase	*pykA*	11.85
A0A0H3PI75	Inosine-5'-monophosphate dehydrogenase	*guaB*	11.41
A0A0H3PCZ6	L-lactate dehydrogenase	*lldD*	10.50
A0A0H3PF36	ATP synthase subunit β	*atpD*	9.97
A0A0H3PDY1	Iron-sulfur cluster assembly scaffold protein	*IscU*	9.84
A0A0H3PDS9	Cell division protein FtsZ	*ftsZ*	9.80
A0A0H3PLN7	Pyridoxal 5'-phosphate synthase subunit	*pdxS*	9.15
A0A0H3PLM6	Pyruvate dehydrogenase E1 component	*aceE*	8.25
A0A0H3PG47	Chaperone protein ClpB	*clpB*	7.89
A0A0H3PC20	NAD nucleotidase	*nucA*	6.99
A0A0H3PMY6	Arsenate reductase	*arsC*	6.68
A0A0H3PP08	Carbon storage regulator homolog	*csrA*	6.44
A0A0H3PFF9	Long-chain fatty acid transport protein	*OMPp1*	6.09
A0A0H3PF51	CTP synthetase	*pyrG*	5.75
A0A0H3PFZ5	30S ribosomal protein S13	*rpsM*	5.47
A0A0H3PJ92	30S ribosomal protein S4	*rpsD*	5.41

A0A0H3PCF5	Inorganic pyrophosphatase	*ppa*	5.28
A0A0H3PH30	RNA chaperone ProQ	*proQ*	4.79
A0A0H3PF33	Alkyl hydroperoxide reductase AhpD	*ahpD*	4.79
A0A0H3PHN6	Uncharacterized protein	*CGSHi3655_08691*	4.78
A0A0H3PCF1	High-affinity zinc uptake system protein ZnuA	*znuA*	4.54
A0A0H3PFA1	50S ribosomal protein L14	*rplN*	4.48
A0A0H3PDR3	Thioredoxin reductase	*hemH*	4.43
A0A0H3PH06	30S ribosomal protein S1	*rpsA*	4.30
A0A0H3PFX6	50S ribosomal protein L2	*rplB*	4.27
A0A0H3PNX3	30S ribosomal protein S3	*rpsC*	4.21
A0A0H3PL18	30S ribosomal protein S6	*rpsF*	4.18
A0A0H3PII1	Adenylate kinase	*adk*	4.17
A0A0H3PFG8	RNA-binding protein Hfq	*hfq*	4.02
A0A0H3PEE1	Transaldolase	*tal*	3.99
A0A0H3PDC6	Glutaredoxin 1	*grxA*	3.77
A0A0H3PC43	Glycerol kinase	*glpK*	3.61
A0A0H3PKC7	Peptidyl-prolyl cis-trans isomerase	*glpQ*	3.47
A0A0H3PF89	50S ribosomal protein L4	*rplD*	3.46
A0A0H3PK29	Trigger factor	*tig*	3.25
A0A0H3PJ88	50S ribosomal protein L15	*rplO*	3.23
A0A0H3PEJ8	Universal stress protein	*uspA*	3.16
A0A0H3PDW6	Acetyltransferase component of pyruvate dehydrogenase complex	*aceF*	3.10
A0A0H3PCE0	Dihydrolipoyl dehydrogenase	*proA*	3.09
A0A0H3PNU6	Protein-export protein SecB	*secB*	3.05
A0A0H3PGG3	Protein GrpE	*grpE*	2.97
A0A0H3PGN2	Glyceraldehyde-3-phosphate dehydrogenase	*gapA*	2.83
A0A0H3PE68	Malate dehydrogenase	*mdh*	2.75
A0A0H3PEG7	Ribosome-associated factor Y	*yfiA*	2.69
A0A0H3PEK8	50S ribosomal protein L13	*rplM*	2.63

A0A0H3PD92	30S ribosomal protein S12	*rpsL*	2.62
A0A0H3PCQ7	60 kDa chaperonin (GroEL protein)	*groEL*	2.51
A0A0H3PDY4	Protein TolB	*tolB*	2.49
A0A0H3PJ67	50S ribosomal protein L3	*rplC*	2.47
A0A0H3PGL8	Autonomous glycyl radical cofactor	*grcA*	2.45
A0A0H3PJ84	30S ribosomal protein S8	*rpsH*	2.40
A0A0H3PEI6	30S ribosomal protein S11	*rpsK*	2.36
A0A0H3PFZ1	30S ribosomal protein S5	*rpsE*	2.35
A0A0H3PDV0	Probable periplasmic serine protease do/HhoA-like	*degQ*	2.34
A0A0H3PFA5	50S ribosomal protein L6	*rplF*	2.32
A0A0H3PC17	Citrate lyase β chain	*citE*	2.28
A0A0H3PFT6	Iron-utilization periplasmic protein hFbpA	*hFbpA*	2.27
A0A0H3PCP4	30S ribosomal protein S16	*rpsP*	2.27
A0A0H3PD53	Putative sialic acid transporter	*siaP*	2.26
A0A0H3PEV7	Enolase	*eno*	2.25
A0A0H3PPC1	Elongation factor Ts (EF-Ts)	*rpsB*	2.25
A0A0H3PKI7	UPF0319 protein CGSHi3655_00871	*CGSHi3655_00871*	2.25
A0A0H3PIQ3	DNA-binding protein HU	*hupA*	2.24
A0A0H3PBY1	Putative translation initiation inhibitor, YjgF family protein	*rutC*	2.24
A0A0H3PEM2	Thiol:disulfide interchange protein	*mobA*	2.23
A0A0H3PB62	50S ribosomal protein L7/L12	*rplL*	2.19
A0A0H3PDB6	Cytidine deaminase	*cdd*	2.18
A0A0H3PCZ5	Cysteine synthase	*cysK*	2.16
A0A0H3PDW2	Chaperone protein DnaK	*dnaK*	2.14
A0A0H3PDR1	6,7-dimethyl-8-ribityllumazine synthase (Lumazine synthase)	*ribH*	2.11
A0A0H3PFE4	Outer membrane protein P6	*pal*	2.07

A0A0H3PEH1	50S ribosomal protein L29	*rpmC*	2.05
A0A0H3PDF1	30S ribosomal protein S21	*rpsU*	2.04
A0A0H3PPL0	Anaerobic dimethyl sulfoxide reductase chain B	*dmsB*	2.03
A0A0H3PJC6	Uncharacterized protein	*CGSHi3655_07119*	2.01
A0A0H3PL46	50S ribosomal protein L11	*rplK*	2.00
A0A0H3PEG5	30S ribosomal protein S10	*rpsJ*	1.98
A0A0H3PCS3	Outer membrane protein P5	*ompA*	1.98
A0A0H3PCG3	Ribonuclease H (EC 3.1.26.4)	*rnhA*	1.89
A0A0H3PCH9	50S ribosomal protein L32	*rpmF*	1.88
A0A0H3PHD5	Arginine transporter ATP-binding subunit	*artP*	1.84
A0A0H3PET8	Outer membrane protein 26	*skp*	1.82
A4N8V8	Putative metal ABC transporter substrate-binding protein Hpf	*hpf*	1.80
A0A0H3PGD5	Fructose-bisphosphate aldolase	*fba*	1.79
A0A0H3PL23	10 kDa chaperonin (GroES protein)	*groS*	1.79
A0A0H3PP90	50S ribosomal protein L27	*rpmA*	1.78
A0A0H3PGC1	50S ribosomal protein L9	*rplI*	1.78
A0A0H3PLC6	DNA-directed RNA polymerase subunit omega	*rpoZ*	1.77
A0A0H3PDN8	Uridine phosphorylase	*udp*	1.76
A0A0H3PD21	30S ribosomal protein S9	*rpsI*	1.75
A0A0H3PFV0	Thioredoxin	*trxA*	1.75
A0A0H3PCI1	50S ribosomal protein L10	*rplJ*	1.74
A0A0H3PNY9	50S ribosomal protein L18	*rplR*	1.72
A0A0H3PFY8	50S ribosomal protein L5	*rplE*	1.70
A0A0H3PJ76	30S ribosomal protein S17	*rpsQ*	1.66
A0A0H3PF94	50S ribosomal protein L22	*rplB*	1.65
A0A0H3PDA0	Uncharacterized protein (?glutathione peroxidase)	*CGSHi3655_05114*	1.62
A0A0H3PJK1	30S ribosomal protein S2	*secA*	1.62
A0A0H3PCL4	Peptidyl-prolyl cis-trans isomerase	*fkbY*	1.61

A0A0H3PHE6	UPF0265 protein CGSHi3655_06049	*CGSHi3655_06049*	1.58
A0A0H3PBR3	30S ribosomal protein S7	*rpsG*	1.56
A0A0H3PFC9	Galactose-1-phosphate uridylyltransferase	*galT*	1.56
A0A0H3PLF1	Integration host factor subunit α (IHF-α)	*infC*	1.54
A0A0H3PDG1	50S ribosomal protein L1	*rplK*	1.52
A0A0H3PFQ6	Lipoprotein E	*hel*	1.47
A0A0H3PLN0	Uracil phosphoribosyltransferase	*upp*	1.46
A0A0H3PFR7	Tryptophanase	*tnaA*	1.45
A0A0H3PC92	Cell division protein ZapB	*zapB*	1.45
A0A0H3PNZ8	50S ribosomal protein L17	*rplQ*	1.44
A0A0H3PP03	Ribosome-recycling factor	*frr*	1.42
A0A0H3PFA7	Elongation factor P	*efp*	1.38
A0A0H3PCJ8	Transcription termination/antitermination protein NusG	*nusG*	1.37
A0A0H3PF11	DNA-binding protein	*stpA*	1.30
A0A0H3PNY4	50S ribosomal protein L24	*rplN*	1.26
A0A0H3PCK9	Elongation factor Tu	*tuf*	1.14
A0A0H3PG61	50S ribosomal protein L21	*rplU*	1.14
A0A0H3PG32	N-acetylneuraminate epimerase	*nanM*	0.92
A0A0H3PD00	30S ribosomal protein S15	*rpsO*	0.90
A0A0H3PKT0	Acyl carrier protein (ACP)	*acpP*	0.84
A0A0H3PPF4	50S ribosomal protein L28	*rpmG*	0.60

Table 8-1. **Full list of proteins identified in both NO treated and untreated NTHi (HI4 isolate) *in vitro* biofilms analysed using label-free LC/MS proteomic analysis.**

D.2 Proteins identified in untreated NTHi biofilms but not NO-treated

Uniprot code	Protein name	*Gene*	Normalised quantity
A0A0H3PFJ7	Protein translocase subunit	*secA*	0.355089
A0A0H3PCV6	Signal recognition particle protein (Fifty-four homolog)	*ffh*	0.159269
A0A0H3PNW0	3,4-dihydroxy-2-butanone 4-phosphate synthase	*ribB*	0.108032
A0A0H3PEN4	Molybdenum cofactor biosynthesis protein	*CGSHi3655_02184*	0.107856
A0A0H3PL07	6-phosphogluconolactonase	*CGSHi3655_05209*	0.106576
A0A0H3PGL4	Citrate lyase α chain	*CGSHi3655_04295*	0.087504
A0A0H3PLY5	Lysine--tRNA ligase	*lysS*	0.084885
A0A0H3PE76	Spermidine/putrescine import ATP-binding protein	*potA*	0.083648
A0A0H3PIL6	Ribosome-binding ATPase	*ychF*	0.076536
A0A0H3PIN7	Ribonuclease E	*rne*	0.072178
A0A0H3PE49	Phosphate-binding periplasmic protein	*CGSHi3655_09196*	0.062714
A0A0H3PEA0	Peptidylprolyl isomerase	*tdk*	0.062185
A0A0H3PJ22	Nitrate/nitrite response regulator protein	*CGSHi3655_06469*	0.056566
A0A0H3PF25	D-3-phosphoglycerate dehydrogenase	*CGSHi3655_02914*	0.054882
A0A0H3PIK0	Cysteine desulfurase	*iscS*	0.054281
A0A0H3PDK4	Queuine tRNA-ribosyltransferase	*tgt*	0.052958
A0A0H3PFG4	Acetyl-coenzyme A carboxylase carboxyl transferase subunit α	*accA*	0.051089
A0A0H3PH25	Uncharacterized protein	*CGSHi3655_03886*	0.051014
A0A0H3PDB0	Orotidine 5'-phosphate decarboxylase	*pyrF*	0.048357
A0A0H3PKA4	Uncharacterized protein	*CGSHi3655_04464*	0.048037
A0A0H3PFF4	Uncharacterized protein	*CGSHi3655_02474*	0.04792
A0A0H3PKS2	Putative N-acetylmannosamine-6-phosphate 2-epimerase	*nanE*	0.047837
A0A0H3PE40	Fumarate hydratase class II	*fumC*	0.04749
A0A0H3PGJ8	Rod shape-determining protein	*CGSHi3655_04220*	0.046851
A0A0H3PJ25	Proline--tRNA ligase	*cyaY*	0.045555
A0A0H3PJM1	Glycine--tRNA ligase β subunit	*glyS*	0.045074
A0A0H3PBZ6	Aspartate-semialdehyde dehydrogenase	*asd*	0.044161

A0A0H3PEW1	Extragenic suppressor	*CGSHi3655_07714*	0.044089
A0A0H3PLJ1	Iron-sulfur cluster carrier protein	*CGSHi3655_03521*	0.043364
A0A0H3PCM9	Glucose-6-phosphate 1-dehydrogenase	*zwf*	0.043198
A0A0H3PCV9	GTP cyclohydrolase 1 type 2 homolog	*CGSHi3655_01377*	0.042026
A0A0H3PE44	Adenylosuccinate synthetase	*purA*	0.041798
A0A0H3PEY6	1,4-dihydroxy-2-naphthoyl-CoA synthase	*menB*	0.04099
A0A0H3PHK3	Deoxyribose-phosphate aldolase	*deoC*	0.038667
A0A0H3PD08	Probable cytosol aminopeptidase	*pepA*	0.038323
A0A0H3PGE4	DNA-directed RNA polymerase subunit β	*rpoC*	0.038277
A0A0H3PJU7	UPF0234 protein	*serB*	0.037525
A0A0H3PNB6	Co-chaperone protein HscB homolog	*hscB*	0.037349
A0A0H3PE21	Ribose-phosphate pyrophosphokinase	*prs*	0.036824
A0A0H3PCS2	Ketol-acid reductoisomerase	*ilvC*	0.036779
A0A0H3PCR4	RNA polymerase sigma factor RpoD (Sigma-70)	*aspA*	0.036735
A0A0H3PJ01	ATP synthase epsilon chain	*atpC*	0.036079
A0A0H3PNR0	ATP synthase gamma chain	*atpG*	0.035969
A0A0H3PBZ9	Mannonate dehydratase	*uxuA*	0.035578
A0A0H3PEI2	50S ribosomal protein L30	*rpmD*	0.035545
A0A0H3PEW4	Bifunctional protein	*hldE*	0.035492
A0A0H3PEL2	Fumarate reductase flavoprotein subunit	*CGSHi3655_07064*	0.035481
A0A0H3PD84	Na(+)-translocating NADH-quinone reductase subunit A	*nqrA*	0.035325
A0A0H3PGB5	6-phosphogluconate dehydrogenase, decarboxylating	*CGSHi3655_05224*	0.035295
A0A0H3PDL4	4-hydroxy-tetrahydrodipicolinate synthase (HTPA synthase)	*dapA*	0.033661
A0A0H3PDT0	Aspartyl-tRNA synthetase	*CGSHi3655_02099*	0.033246
A0A0H3PDS8	Transcription termination/antitermination protein	*nusA*	0.033085
A0A0H3PDZ3	ATP-dependent zinc metalloprotease FtsH	*ftsH*	0.033058
A0A0H3PBS5	Ribulose-phosphate 3-epimerase	*CGSHi3655_05144*	0.032827
A0A0H3PNE6	Pyridoxal kinase PdxY (PL kinase)	*pdxY*	0.032723
A0A0H3PDT8	UDP-N-acetylmuramoyl-L-alanyl-D-glutamate--2,6-diaminopimelate ligase	*murE*	0.032242

A0A0H3PIU9	Fused fructose-specific PTS enzymes: IIA component/HPr component	*CGSHi3655_02859*	0.031685
A0A0H3PFM3	Shikimate kinase (SK)	*aroK*	0.031115
A0A0H3PFF2	Tryptophan--tRNA ligase	*trpS*	0.031053
A0A0H3PEP4	GTP-binding protein	*CGSHi3655_07264*	0.031034
A0A0H3PBR4	Protein RecA (Recombinase A)	*recA*	0.030772
A0A0H3PGY8	Phosphate acetyltransferase	*CGSHi3655_03661*	0.029993
A0A0H3PGC8	Aspartate ammonia-lyase (Aspartase)	*CGSHi3655_05324*	0.029471
A0A0H3PB52	Peptide deformylase	*def*	0.028963
A0A0H3PJK6	Outer membrane protein assembly factor	*bamA*	0.028799
A0A0H3PKN2	Argininosuccinate synthase	*argG*	0.028568
A0A0H3PNV0	LexA repressor	*lexA*	0.028282
A0A0H3PG03	Phosphoenolpyruvate carboxykinase	*pckA*	0.027881
A0A0H3PN17	Orotate phosphoribosyltransferase	*pyrE*	0.027538
A0A0H3PPH8	ATP-dependent 6-phosphofructokinase	*pfkA*	0.026478
A0A0H3PCK3	Tyrosine--tRNA ligase	*tyrS*	0.025747
A0A0H3PDS2	Ribosome-binding factor A	*rbfA*	0.02568
A0A0H3PFI9	Fe/S biogenesis protein	*nfuA*	0.025286
A0A0H3PDM7	Branched-chain-amino-acid aminotransferase	*CGSHi3655_05929*	0.024815
A0A0H3PCX0	Exodeoxyribonuclease III	*CGSHi3655_04200*	0.024696
A0A0H3PBX4	DNA-directed RNA polymerase subunit β	*rpoB*	0.024599
A0A0H3PJ71	30S ribosomal protein S19	*CGSHi3655_06769*	0.02457
A0A0H3PGR6	Phenylalanine--tRNA ligase α subunit	*CGSHi3655_03261*	0.02436
A0A0H3PG46	Phosphatidylserine decarboxylase	*CGSHi3655_04926*	0.023828
A0A0H3PCU0	Regulator of ribonuclease activity B	*rraB*	0.023731
A0A0H3PCC2	Predicted plasmid maintenance system antidote protein	*CGSHi3655_03631*	0.023616
A0A0H3PFL9	GTP cyclohydrolase-2	*ribA*	0.023471
A0A0H3PGK9	4-hydroxy-3-methylbut-2-enyl diphosphate reductase	*ispH*	0.023107
A0A0H3PF23	Polyribonucleotide nucleotidyltransferase	*pnp*	0.022808
A0A0H3PI53	Glucose-6-phosphate isomerase	*pgi*	0.022807
A0A0H3PC26	Flavodoxin	*CGSHi3655_00645*	0.022771

A0A0H3PI20	3-oxoacyl-(Acyl carrier protein) synthase I	*CGSHi3655_09466*	0.022674
A0A0H3PCK8	HicB	*HicB*	0.021878
A0A0H3PEM4	Phosphoribosylglycinamide formyltransferase	*purN*	0.021458
A0A0H3PG22	Succinate dehydrogenase iron-sulfur subunit	*CGSHi3655_07059*	0.021259
A0A0H3PNS4	ATP-dependent protease ATPase subunit	*hslU*	0.021084
A0A0H3PD35	Universal stress protein	*UspE*	0.021001
A0A0H3PCE1	Enoyl-[acyl-carrier-protein] reductase	*CGSHi3655_01141*	0.020799
A0A0H3PG59	Peptidase B	*pepB*	0.020648
A0A0H3PHX3	Ferritin	*CGSHi3655_09191*	0.02049
A0A0H3PC22	50S ribosomal protein L19	*rplS*	0.020263
A0A0H3PBC3	Glycerophosphoryl diester phosphodiesterase	*CGSHi3655_04549*	0.020085
A0A0H3PF59	Ribonuclease PH	*rph*	0.020077
A0A0H3PG65	Serine hydroxymethyltransferase	*glyA*	0.019976
A0A0H3PGF1	Acetyl-CoA carboxylase	*CGSHi3655_07884*	0.019002
A0A0H3PCM3	2,3,4,5-tetrahydropyridine-2,6-dicarboxylate N-succinyltransferase	*dapD*	0.018985
A0A0H3PC34	Triosephosphate isomerase	*tpiA*	0.018729
A0A0H3PEX5	Predicted nitroreductase	*CGSHi3655_09506*	0.01757
A0A0H3PK97	Flavodoxin FldA	*CGSHi3655_00650*	0.017549
A0A0H3PCP3	Acetate kinase	*ackA*	0.017412
A0A0H3PPG2	HIT-related protein	*CGSHi3655_07829*	0.016854
A0A0H3PPK0	Transketolase	*CGSHi3655_08079*	0.016728
A0A0H3PD26	Cold shock-like protein	*CspD*	0.016723
A0A0H3PIY6	Ribose-5-phosphate isomerase A	*rpiA*	0.016512
A0A0H3PEY9	Glycerate dehydrogenase	*CGSHi3655_09581*	0.015835
A0A0H3PCZ2	Guanylate kinase	*gmk*	0.015668
A0A0H3PM87	ADP-L-glycero-D-manno-heptose-6-epimerase	*hldD*	0.015592
A0A0H3PN61	Probable transcriptional regulatory protein	*CGSHi3655_02089*	0.015557
A0A0H3PE57	Fructose-1,6-bisphosphatase class 1	*fbp*	0.015006

A0A0H3PFY1	5-methyltetrahydropteroyltriglutamate--homocysteine methyltransferase	*metE*	0.014424
A0A0H3PDQ5	Phenylalanine--tRNA ligase β subunit	*pheT*	0.014297
A0A0H3PP50	Heme-binding lipoprotein	*CGSHi3655_07154*	0.014183
A0A0H3PN35	Periplasmic mercury transport-like protein	*CGSHi3655_01939*	0.014092
A0A0H3PBV8	30S ribosomal protein S18	*rpsR*	0.014024
A0A0H3PLZ5	50S ribosomal protein L3 glutamine methyltransferase	*prmB*	0.013937
A0A0H3PCV1	Glutathione S-transferase	*CGSHi3655_01327*	0.013866
A0A0H3PFV6	Probable Fe(2+)-trafficking protein	*CGSHi3655_06659*	0.012696
A0A0H3PGR3	Superoxide dismutase	*CGSHi3655_08359*	0.009998

Table 8-2. **Full list of proteins identified only in untreated NTHi (HI4 isolate) *in vitro* biofilms and not in NO-treated biofilms**. Quantities shown are absolute mass of protein in nanograms normalised to total protein in each replicate, therefore do not have units attached.

Appendix E Summary of outcome of all nasal brushings taken

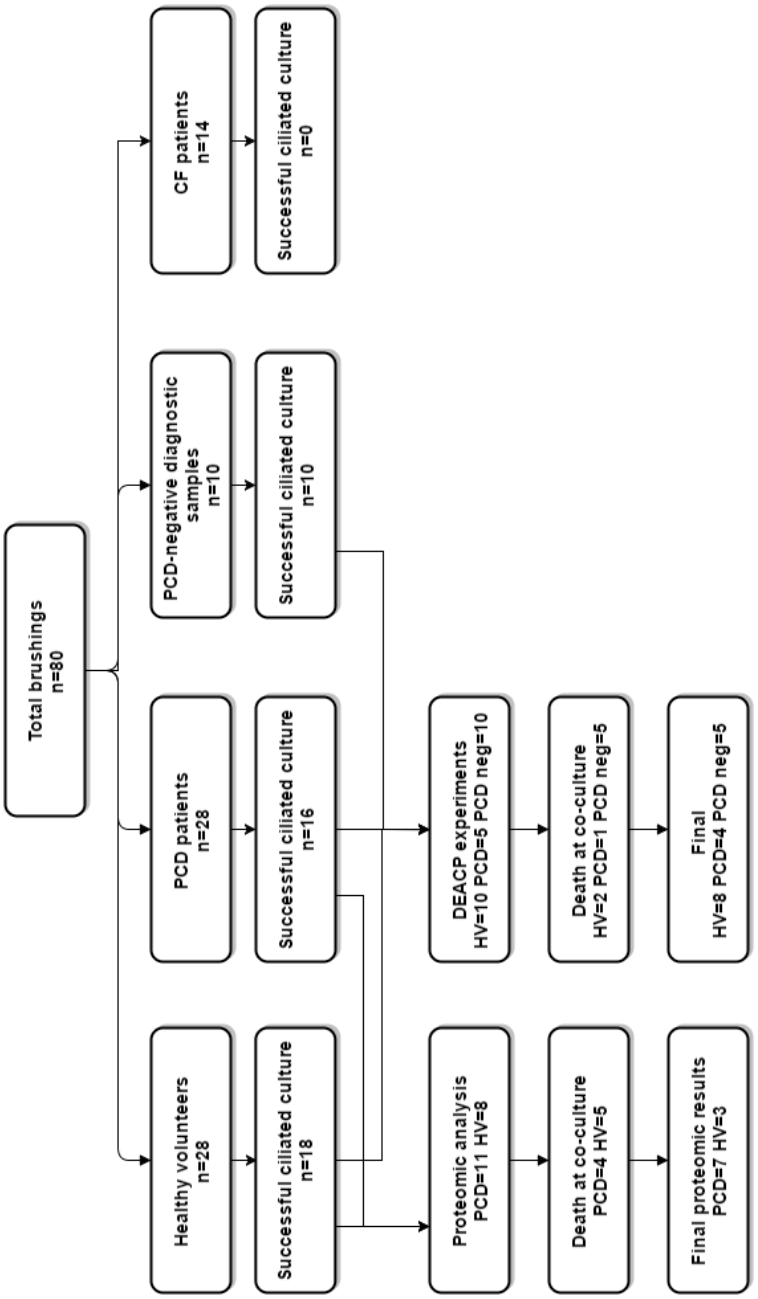

Figure 8-3. **Flow of nasal brushing samples taken for experiments in this thesis.** 85 brushings were taken in total. Rate of successful culture to ciliation is similar to that seen in this laboratory over the last 5 years (approx. 50% success) – the exception to this is CF culture which were all unsuccessful. Number of transwells available from each brushing varied from 1 to 8, therefore total number of experiments exceeds number of brushings taken. Numbers reflect total number of brushings which may have been repeated on the same patient.

Appendix F Full list of up/downregulated proteins identified in co-culture experiments

F.1 Healthy response to NTHi biofilm

Uniprot	Protein	Ratio
Upregulated		
Q13509	Tubulin β-3 chain	17.65
P35749	Myosin-11	6.86
O00764	Pyridoxal kinase	4.49
P17858	6-phosphofructokinase_ liver type	3.42
P48594	Serpin B4	2.97
P11055	Myosin-3	2.89
Q13813	Spec in alpha chain_ non-erythrocytic 1	2.83
P52907	F-actin-capping protein subunit alpha-1	2.81
P36578	60S ribosomal protein L4	2.81
P50991	T-complex protein 1 subunit delta	2.79
P36871	Phosphoglucomutase-1	2.58
P00387	NADH-cytochrome b5 reductase 3	2.58
O75665	Oral-facial-digital syndrome 1 protein	2.54
P35613	Basigin	2.50
Q13423	NAD(P) transhydrogenase_ mitochondrial	2.36
P31939	Bifunctional purine biosynthesis protein PURH	2.34
P47929	Galectin-7	2.33
Q15084	Protein disulfide-isomerase A6	2.32
P09758	Tumor-associated calcium signal transducer 2	2.27
P62158	Calmodulin	2.27
P25789	Proteasome subunit alpha type-4	2.26

P31153	S-adenosylmethionine synthase isoform type-2	2.26
Q86UP2	Kinectin	2.24
P30050	60S ribosomal protein L12	2.20
Q13938	Calcyphosin	2.15
P23526	Adenosylhomocysteinas	2.12
P38919	Eukaryotic initiation factor 4A-III	2.08
P28070	Proteasome subunit β type-4	2.08
P30048	Thioredoxin-dependent peroxide reductase_ mitochondrial	2.07
P00558	Phosphoglycerate kinase 1	2.04
Q14103	Heterogeneous nuclear ribonucleoprotein D0	2.03
P09651	Heterogeneous nuclear ribonucleoprotein A1	1.97
P12277	Creatine kinase B-type	1.94
P07437	Tubulin β chain	1.93
P26641	Elongation factor 1-gamma	1.92
P21980	Protein-glutamine gamma-glutamyl transferase 2	1.90
P26038	Moesin	1.87
Q15717	ELAV-like protein 1	1.84
Q9Y315	Putative deoxyribose-phosphate aldolase	1.84
Q16658	Fascin	1.82
P36542	ATP synthase subunit gamma_ mitochondrial	1.79
P23284	Peptidyl-prolyl cis-trans isomerase B	1.78
P38606	V-type proton ATPase catalytic subunit A	1.74
P06748	Nucleophosmin	1.74
Q12905	Interleukin enhancer-binding factor 2	1.73
P52597	Heterogeneous nuclear ribonucleoprotein F	1.72
Q14894	Thiomorpholine-carboxylate dehydrogenase	1.70
P02538	Keratin_ type II cytoskeletal 6A	1.70
P15531	Nucleoside diphosphate kinase A	1.69
Q15366	Poly(rC)-binding protein 2	1.69
P36957	Dihydrolipoyllysine-residue succinyl transferase component	1.68
P35579	Myosin-9	1.67

P08729	Keratin_ type II cytoskeletal 7	1.66
P47755	F-actin-capping protein subunit alpha-2	1.65
P61106	Ras-related protein Rab-14	1.64
P37837	transaldolase	1.64
P35237	Serpin B6	1.62
Q04695	Keratin_ type I cytoskeletal 17	1.62
P22695	Cytochrome b-c1 complex subunit 2_ mitochondrial	1.61
Q9HC35	Echinoderm microtubule-associated protein-like 4	1.60
P13489	Ribonuclease inhibitor	1.59
P05388	60S acidic ribosomal protein P0	1.58
P12532	Creatine kinase U-type_ mitochondrial	1.58
P22626	Heterogeneous nuclear ribonucleoproteins A2/B1	1.58
P36952	Serpin B5	1.57
P37802	transgelin-2	1.57
P15313	V-type proton ATPase subunit B_ kidney isoform	1.56
P62913	60S ribosomal protein L11	1.56
P23528	Cofilin-1	1.54
P21796	Voltage-dependent anion-selective channel protein 1	1.54
P00441	Superoxide dismutase [Cu-Zn]	1.54
P13797	Plastin-3	1.54
P08865	40S ribosomal protein SA	1.54
P29508	Serpin B3	1.54
P19404	NADH dehydrogenase [ubiquinone] flavoprotein 2_ mitochondrial	1.54
Q6NUK1	Calcium-binding mitochondrial carrier protein SCaMC-1	1.51
P04083	Annexin A1	1.51
P18669	Phosphoglycerate mutase 1	1.50
P13647	Keratin_ type II cytoskeletal 5	1.50

Downregulated

P07686	B-hexosaminidase subunit β	0.70
P08238	Heat shock protein H 90-β	0.70
O43707	Alpha-actinin-4	0.69
P28838	Cytosol aminopeptidase	0.69
P35908	Keratin_ type II cytoskeletal 2 epidermal	0.68
P04264	Keratin_ type II cytoskeletal 1	0.68
O95716	Ras-related protein Rab-3D	0.68
O15195	Villin-like protein	0.68
P06702	Protein S100-A9	0.67
P12236	ADP/ATP translocase 3	0.67
O60763	General vesicular transport factor p115	0.67
Q13765	Nascent polypeptide-associated complex subunit alpha	0.63
P13010	X-ray repair cross-complementing protein 5	0.62
P33121	Long-chain-fatty-acid--CoA ligase 1	0.62
P07737	Profilin-1	0.62
P33176	Kinesin-1 heavy chain	0.61
P11940	Polyadenylate-binding protein 1	0.60
O43776	Asparagine-- NA ligase_ cytoplasmic	0.60
Q08378	Golgin subfamily A member 3	0.57
P06703	Protein S100-A6	0.56
Q9BRP8	Partner of Y14 and mago	0.56
P28331	NADH-ubiquinone oxidoreductase 75 kDa subunit	0.56
P19338	Nucleolin	0.55
P10599	Thioredoxin	0.55
O43653	Prostate stem cell antigen	0.54
Q16181	Septin-7	0.54
P05109	Protein S100-A8	0.53
P62942	Peptidyl-prolyl cis-trans isomerase FKBP1A	0.53
P11279	Lysosome-associated membrane glycoprotein 1	0.52
P20700	Lamin-B1	0.51
Q14764	Major vault protein	0.51

P16050	Arachidonate 15-lipoxygenase	0.51
Q9Y678	Coatomer subunit gamma-1	0.51
P29034	Protein S100-A2	0.49
Q6S8J3	POTE ankyrin domain family member E	0.49
Q13835	Plakophilin-1	0.49
Q14247	Src substrate cortactin	0.46
P62424	60S ribosomal protein L7a	0.45
P07476	Involucrin	0.43
Q9BSJ8	Extended synaptotagmin-1	0.43
P13667	Protein disulfide-isomerase A4	0.42
P61626	Lysozyme C	0.41
P35580	Myosin-10	0.39
Q01082	Spec in β chain_ non-erythrocytic 1	0.34
P25815	Protein S100-P	0.33
P14923	Junction plakoglobin	0.32
Q9UHL4	Dipeptidyl peptidase 2	0.32
P26640	Valine-- NA ligase	0.31
P05062	Fructose-bisphosphate aldolase B	0.31
P35080	Profilin-2	0.19
P35241	Radixin	0.19
Q2M2I5	Keratin_ type I cytoskeletal 24	0.18
P60903	Protein S100-A10	0.13
P11217	Glycogen phosphorylase_ muscle form	0.12
Q71U36	Tubulin alpha-1A chain	0.08
P50502	Hsc70-interacting protein	0.02

Table 8-3. **List of up- and downregulated proteins identified following exposure of healthy epithelium to 72h NTHi biofilm.** Culture primary epithelium from healthy subjects co-cultured with NTHi (HI4 isolate) for 72h then analysed using LC/MS proteomics. Upregulated proteins (>1.5 fold higher in exposed epithelium) and downregulated proteins (<0.7 fold lower in exposed epithelium). Ratio is normalised quantities in exposed/unexposed.

F.2 Healthy versus PCD epithelium not exposed to NTHi

Uniprot	Protein	Ratio
Upregulated		
P35580	Myosin-10	7.39
Q8TDL5	BPI fold-containing family B member 1	4.89
Q04828	Aldo-keto reductase family 1 member C1	4.68
P06702	Protein S100-A9	3.92
P11413	Glucose-6-phosphate 1-dehydrogenase	3.85
P04080	Cystatin-B	2.57
P25815	Protein S100-P	2.24
P35232	Prohibitin	1.95
P17987	T-complex protein 1 subunit alpha	1.93
P00390	Glutathione reductase_ mitochondrial	1.86
P04259	Keratin_ type II cytoskeletal 6B	1.66
P00367	Glutamate dehydrogenase 1_ mitochondrial	1.66
P07737	Profilin-1	1.64
Q9NP55	BPI fold-containing family A member 1	1.58
Q01469	Fatty acid-binding protein_ epidermal	1.55
Q96KP4	Cytosolic non-specific dipeptidase	1.54
Q00610	Clathrin heavy chain 1	1.51
Downregulated		
O75390	Citrate synthase_ mitochondrial	0.70
Q99798	Aconitate hydratase_ mitochondrial	0.70
Q9Y265	RuvB-like 1	0.69
Q16698	2_4-dienoyl-CoA reductase_ mitochondrial	0.68
P14550	Alcohol dehydrogenase [NADP(+)]	0.68
P37837	Transaldolase	0.67

P12429	Annexin A3	0.66
O60218	Aldo-keto reductase family 1 member B10	0.66
P29401	Transketolase	0.66
P08779	Keratin_ type I cytoskeletal 16	0.65
P48735	Isocitrate dehydrogenase [NADP]_ mitochondrial	0.65
P11166	HUMAN Solute carrier family facilitated glucose transporter member 1	0.64
P04843	Dolichyl-diphosphooligosaccharide--protein glycosyl transferase subunit 1	0.64
P04792	Heat shock protein β-1	0.64
P21796	Voltage-dependent anion-selective channel protein 1	0.64
Q06830	Peroxiredoxin-1	0.64
P30838	Aldehyde dehydrogenase_ dimeric NADP-preferring	0.63
P50993	Sodium/potassium- transporting ATPase subunit alpha-2	0.63
P02538	Keratin_ type II cytoskeletal 6A	0.62
P36952	Serpin B5	0.62
P29508	Serpin B3	0.62
P12532	Creatine kinase U-type_ mitochondrial	0.61
Q9UHQ9	NADH-cytochrome b5 reductase 1	0.61
P52895	Aldo-keto reductase family 1 member C2	0.60
P26641	Elongation factor 1-gamma	0.60
P68366	Tubulin alpha-4A chain	0.59
P31943	Heterogeneous nuclear ribonucleoprotein H	0.59
Q96A08	Histone H2B type 1-A	0.58
P33121	Long-chain-fatty-acid--CoA ligase 1	0.57
Q15084	Protein disulfide-isomerase A6	0.56
Q96KK5	Histone H2A type 1-H	0.56
P00558	Phosphoglycerate kinase 1	0.55
P04075	Fructose-bisphosphate aldolase A	0.55
P40926	Malate dehydrogenase_ mitochondrial	0.55
O14745	Na(+)/H(+) exchange regulatory cofactor NHE-RF1	0.55

P04066	Tissue alpha-L-fucosidase	0.55
P06733	Alpha-enolase	0.55
P52209	6-phosphogluconate dehydrogenase_ decarboxylating	0.54
P00505	Aspartate amino transferase_ mitochondrial	0.54
O15144	Actin-related protein 2/3 complex subunit 2	0.53
P06576	ATP synthase subunit β_ mitochondrial	0.52
P52907	F-actin-capping protein subunit alpha-1	0.52
Q9Y230	RuvB-like 2	0.52
P62263	40S ribosomal protein S14	0.51
P68104	Elongation factor 1-alpha 1	0.51
P60709	Actin_ cytoplasmic 1	0.51
Q13938	Calcyphosin	0.50
P35579	Myosin-9	0.49
P62826	GTP-binding nuclear protein Ran	0.49
Q15365	Poly(rC)-binding protein 1	0.49
P07355	Annexin A2	0.49
P40394	Alcohol dehydrogenase class 4 mu/sigma chain	0.47
P08758	Annexin A5	0.47
Q15366	Poly(rC)-binding protein 2	0.47
Q16851	UTP--glucose-1-phosphate uridylyl transferase	0.47
P15924	Desmoplakin	0.46
Q99623	Prohibitin-2	0.46
P07437	Tubulin β chain	0.46
P08727	Keratin_ type I cytoskeletal 19	0.46
P08729	Keratin_ type II cytoskeletal 7	0.45
Q71U36	Tubulin alpha-1A chain	0.44
P05787	Keratin_ type II cytoskeletal 8	0.43
P05023	Sodium/potassium- transporting ATPase subunit alpha-1	0.42
Q04695	Keratin_ type I cytoskeletal 17	0.41
P12277	Creatine kinase B-type	0.40
P35749	Myosin-11	0.39

P00924	Enolase 1	0.39
P04406	Glyceraldehyde-3-phosphate dehydrogenase	0.38
P08865	40S ribosomal protein SA	0.37
Q96TA1	Niban-like protein 1	0.37
Q13509	Tubulin β-3 chain	0.34
Q14568	Putative heat shock protein H 90-alpha A2	0.32
P13489	Ribonuclease inhibitor	0.32
P14136	Glial fibrillary acidic protein	0.32
P17066	Heat shock 70 kDa protein 6	0.30
P07910	Heterogeneous nuclear ribonucleoproteins C1/C2	0.29
P08670	Vimentin	0.29
P52272	Heterogeneous nuclear ribonucleoprotein M	0.28
P23396	40S ribosomal protein S3	0.27
P60842	Eukaryotic initiation factor 4A-I	0.25
Q99456	Keratin_ type I cytoskeletal 12	0.10

Table 8-4. **List of up- and downregulated in epithelial cells from healthy and PCD subjects unexposed to biofilm.** Culture primary epithelium from healthy and PCD subjects analysed using LC/MS proteomics. Upregulated proteins (>1.5 fold higher in exposed epithelium) and downregulated proteins (<0.7 fold lower in exposed epithelium). Ratio is normalised quantities in PCD/healthy.

F.3 Healthy versus PCD epithelium exposed to NTHi biofilm

Uniprot	Protein	Ratio
Upregulated		
P35749	Myosin-11	5.33
Q9Y3Z3	SAM domain and HD domain-containing protein 1	5.26
P23141	Liver carboxylesterase 1	4.74
P17844	Probable ATP-dependent RNA helicase DDX5	4.44
Q86UP2	Kinectin	4.34
P26038	Moesin	4.20

Q8TDL5	BPI fold-containing family B member 1	3.86
P20648	Potassium- transporting ATPase alpha chain 1	3.83
Q04828	Aldo-keto reductase family 1 member C1	3.70
P61163	Alpha-centractin	3.28
Q13510	Acid ceramidase	3.12
O00571	ATP-dependent RNA helicase DDX3X	2.93
Q7KZF4	Staphylococcal nuclease domain-containing protein 1	2.92
P62942	Peptidyl-prolyl cis- trans isomerase FKBP1A	2.89
P33121	Long-chain-fatty-acid--CoA ligase 1	2.59
Q14764	Major vault protein	2.56
P48594	Serpin B4	2.48
P04350	Tubulin β-4A chain	2.45
P80723	Brain acid soluble protein 1	2.45
P38606	V-type proton ATPase catalytic subunit A	2.44
Q9H8H3	Methyltransferase-like protein 7A	2.31
P54707	Potassium- transporting ATPase alpha chain 2	2.30
P40394	Alcohol dehydrogenase class 4 mu/sigma chain	2.28
P00367	Glutamate dehydrogenase 1_ mitochondrial	2.20
P54652	Heat shock-related 70 kDa protein 2	2.18
P15924	Desmoplakin	2.14
Q13885	Tubulin β-2A chain	2.07
P25815	Protein S100-P	2.05
Q15233	Non-POU domain-containing octamer-binding protein	2.01
P02792	Ferritin light chain	1.93
P49327	Fatty acid synthase	1.92
P51572	B-cell receptor-associated protein 31	1.91
P52272	Heterogeneous nuclear ribonucleoprotein M	1.90
Q00839	Heterogeneous nuclear ribonucleoprotein U	1.87
O60701	UDP-glucose 6-dehydrogenase	1.86
P04264	Keratin_ type II cytoskeletal 1	1.85
P10599	Thioredoxin	1.85

Q9Y678	Coatomer subunit gamma-1	1.78
P07858	Cathepsin B	1.75
P15559	NAD(P)H dehydrogenase [quinone] 1	1.74
P62424	60S ribosomal protein L7a	1.73
P35908	Keratin_ type II cytoskeletal 2 epidermal	1.70
P60903	Protein S100-A10	1.68
Q01082	Spectrin β chain_ non-erythrocytic	1.66
P08865	40S ribosomal protein SA	1.66
P62913	60S ribosomal protein L11	1.66
Q9BQE3	Tubulin alpha-1C chain	1.64
P06703	Protein S100-A6	1.63
P16050	Arachidonate 15-lipoxygenase	1.62
Q9UHL4	Dipeptidyl peptidase 2	1.62
O43707	Alpha-actinin-4	1.60
Q16881	Thioredoxin reductase 1_ cytoplasmic	1.60
P12235	ADP/ATP translocase 1	1.57
Q92841	Probable ATP-dependent RNA helicase DDX17	1.57
Q96A08	Histone H2B type 1-A	1.57
Q13740	CD166 antigen	1.56
P40939	trifunctional enzyme subunit alpha_ mitochondrial	1.56
Q99623	Prohibitin-2	1.55
Q14240	Eukaryotic initiation factor 4A-II	1.55
P05109	Protein S100-A8	1.55
P15311	Ezrin	1.54
P78371	T-complex protein 1 subunit β	1.54
P31943	Heterogeneous nuclear ribonucleoprotein H	1.53
P43304	Glycerol-3-phosphate dehydrogenase_ mitochondrial	1.53
Q9NP58	ATP-binding cassette sub-family B member 6_ mitochondrial	1.53
P06702	Protein S100-A9	1.52

P38646	Stress-70 protein_ mitochondrial	1.51
P22570	NADPH:adrenodoxin oxidoreductase_ mitochondrial	1.51
P05026	Sodium/potassium- transporting ATPase subunit β-1	1.50

Downregulated		
P37837	Transaldolase	0.70
P06753	Tropomyosin alpha-3 chain	0.69
P13804	Elec on transfer flavoprotein subunit alpha_ mitochondrial	0.69
P13797	Plastin-3	0.69
P09651	Heterogeneous nuclear ribonucleoprotein A1	0.69
P31947	14-3-3 protein sigma	0.69
P08779	Keratin_ type I cytoskeletal 16	0.68
P27797	Calreticulin	0.68
O00151	PDZ and LIM domain protein 1	0.67
P21333	Filamin-A	0.66
P19013	Keratin_ type II cytoskeletal 4	0.65
P04792	Heat shock protein β-1	0.65
P05091	Aldehyde dehydrogenase_ mitochondrial	0.65
Q00796	Sorbitol dehydrogenase	0.64
O75665	Oral-facial-digital syndrome 1 protein	0.63
P61981	14-3-3 protein gamma	0.63
P61158	Actin-related protein 3	0.63
P53621	Coatomer subunit alpha	0.63
P48668	Keratin_ type II cytoskeletal 6C	0.62
P52907	F-actin-capping protein subunit alpha-1	0.61
P31153	S-adenosylmethionine synthase isoform type-2	0.60
P00387	NADH-cytochrome b5 reductase 3	0.60
Q9NR45	Sialic acid synthase	0.60
P62249	40S ribosomal protein S16	0.59
P14866	Heterogeneous nuclear ribonucleoprotein L	0.59
Q9NP55	BPI fold-containing family A member 1	0.59

P34931	Heat shock 70 kDa protein 1-like	0.58
O15144	Actin-related protein 2/3 complex subunit 2	0.57
Q01469	Fatty acid-binding protein_ epidermal	0.57
P35580	Myosin-10	0.57
P61019	Ras-related protein Rab-2A	0.56
P62158	Calmodulin	0.56
P16152	Carbonyl reductase [NADPH] 1	0.56
P52565	Rho GDP-dissociation inhibitor 1	0.56
Q53FA7	Quinone oxidoreductase PIG3	0.55
Q9H4B7	Tubulin β-1 chain	0.55
P18669	Phosphoglycerate mutase 1	0.55
P22392	Nucleoside diphosphate kinase B	0.55
P17661	Desmin	0.54
P07437	Tubulin β chain	0.53
Q58FF8	Putative heat shock protein H 90-β 2	0.53
O43390	Heterogeneous nuclear ribonucleoprotein R	0.52
P09758	Tumor-associated calcium signal transducer 2	0.51
P09972	Fructose-bisphosphate aldolase C	0.51
O60506	Heterogeneous nuclear ribonucleoprotein Q	0.51
Q15084	Protein disulfide-isomerase A6	0.50
Q14651	Plastin-1	0.49
Q07021	Complement component 1 Q	0.49
P20700	Lamin-B1	0.48
Q6ZMR3	L-lactate dehydrogenase A-like 6A	0.46
P12236	ADP/ATP translocase 3	0.42
Q9NQC3	Reticulon-4	0.41
P02533	Keratin_ type I cytoskeletal 14	0.33
P46459	Vesicle-fusing ATPase	0.31
P52789	Hexokinase-2	0.25

Q14533	Keratin_ type II cuticular Hb1	0.10
Q15323	Keratin_ type I cuticular Ha1	0.08
P68363	Tubulin alpha-1B chain	0.06

Table 8-5. **List of up- and downregulated proteins identified following exposure of healthy and PCD epithelium to 72h NTHi biofilm.** Cultured primary epithelium from healthy and PCD subjects co-cultured with NTHi (HI4 isolate) for 72h then analysed using LC/MS proteomics. Upregulated proteins (>1.5 fold higher in exposed epithelium) and downregulated proteins (<0.7 fold lower in exposed epithelium). Ratio is normalised quantities in PCD/healthy.

References

1. Bush A, Chodhari R, Collins N, Copeland F, Hall P, Harcourt J, Hariri M, Hogg C, Lucas J, Mitchison HM, O'Callaghan C, Phillips G. Primary ciliary dyskinesia: current state of the art. Arch Dis Child. 2007 Dec;92(12):1136–40.

2. Kuehni CE, Frischer T, Strippoli M-PF, Maurer E, Bush A, Nielsen KG, Escribano A, Lucas JSA, Yiallouros P, Omran H, Eber E, O'Callaghan C, Snijders D, Barbato A. Factors influencing age at diagnosis of primary ciliary dyskinesia in European children. Eur Respir J. 2010 Dec;36(6):1248–58.

3. O'Callaghan C, Chetcuti P, Moya E. High prevalence of primary ciliary dyskinesia in a British Asian population. Arch Dis Child. 2010 Jan;95(1):51–2.

4. Siewart A. Uber einem Fall von Bronchiectasie bei einem Patienten mit Situs inversus viscerum. Berliner Klin Wochenschrift. 1904;41:139–41.

5. Kartagener M. Zur Pathogenese der Bronchiektasien. Situs viscerum inversus und polyposis nasi in einem Falle familiärer Bronchiektasien. Beiträge zur Klin und Erforsch der Tuberkulose und der Lungenkrankenheiten. 1935;87:489.

6. Afzelius BA. A human syndrome caused by immotile cilia. Science. 1976 Jul 23;193(4250):317–9.

7. Sleigh MA. Primary Ciliary Dyskinesia. Lancet. 1981 Aug;318(8244):476.

8. Stannard W, O'Callaghan C. Ciliary function and the role of cilia in clearance. J Aerosol Med. 2006 Jan;19(1):110–5.

9. Lodish H, Berk A, Zipursky SL, Matsudaira P, Baltimore D, Darnell J. Cilia and Flagella: Structure and Movement. W. H. Freeman; 2000.

10. Munro NC, Currie DC, Lindsay KS, Ryder TA, Rutman A, Dewar A, Greenstone MA, Hendry WF, Cole PJ. Fertility in men with primary ciliary dyskinesia presenting with respiratory infection. Thorax. 1994 Jul;49(7):684–7.

11. Halbert SA, Patton DL, Zarutskie PW, Soules MR. Function and structure of cilia in the fallopian tube of an infertile woman with Kartagener's syndrome. Hum Reprod. 1997 Jan;12(1):55–8.

12. Zhu L, Belmont JW, Ware SM. Genetics of human heterotaxias. Eur J Hum Genet. 2006 Jan;14(1):17–25.

13. Ferkol TW, Leigh MW. Ciliopathies: the central role of cilia in a spectrum of pediatric disorders. J Pediatr. 2012 Mar;160(3):366–71.

14. Wanner A, Salathé M, O'Riordan TG. Mucociliary clearance in the airways. Am J Respir Crit Care Med. 1996 Dec;154(6 Pt 1):1868–902.

15. Serafini SM, Michaelson ED. Length and distribution of cilia in human and canine airways. Bull Eur Physiopathol Respir. 1977;13(4):551–9.

16. Raidt J, Wallmeier J, Hjeij R, Onnebrink JG, Pennekamp P, Loges NT, Olbrich H, Häffner K, Dougherty GW, Omran H, Werner C. Ciliary beat pattern and frequency in genetic variants of primary ciliary dyskinesia. Eur Respir J. 2014 Sep 3;44(6):1579–88.

17. Stannard WA, Chilvers MA, Rutman AR, Williams CD, O'Callaghan C. Diagnostic Testing of Patients Suspected of Primary Ciliary Dyskinesia. Am J Respir Crit Care Med. 2010 Feb 15;181(4):307–14.

18. King PT. The pathophysiology of bronchiectasis. Int J Chron Obstruct Pulmon Dis. 2009 Jan;4:411–9.

19. Cole PJ. Inflammation: a two-edged sword--the model of bronchiectasis. Eur J Respir Dis Suppl. 1986 Jan;147:6–15.

20. Gherman A, Davis EE, Katsanis N. The ciliary proteome database: an integrated community resource for the genetic and functional dissection of cilia. Nat Genet. 2006 Sep;38(9):961–2.

21. Pennarun G, Escudier E, Chapelin C, Bridoux AM, Cacheux V, Roger G, Clément A, Goossens M, Amselem S, Duriez B. Loss-of-function mutations in a human gene related to Chlamydomonas reinhardtii dynein IC78 result in primary ciliary dyskinesia. Am J Hum Genet. 1999 Dec;65(6):1508–19.

22. Collins S, Walker W, Lucas J. Genetic Testing in the Diagnosis of Primary Ciliary Dyskinesia: State-of-the-Art and Future Perspectives. J Clin Med. 2014 May 9;3(2):491–503.

23. Lucas JS, Barbato A, Collins SA, Goutaki M, Behan L, Caudri D, Dell S, Eber E, Escudier E, Hirst RA, Hogg C, Jorissen M, Latzin P, Legendre M, Leigh MW, Midulla F, Nielsen KG,

Omran H, Papon J-F, Pohunek P, Redfern B, Rigau D, Rindlisbacher B, Santamaria F, Shoemark A, Snijders D, Tonia T, Titieni A, Walker WT, Werner C, Bush A, Kuehni CE. European Respiratory Society guidelines for the diagnosis of primary ciliary dyskinesia. Eur Respir J. 2016;

24. Shoemark A, Dixon M, Corrin B, Dewar A. Twenty-year review of quantitative transmission electron microscopy for the diagnosis of primary ciliary dyskinesia. J Clin Pathol. 2012 Mar;65(3):267–71.

25. Chilvers MA, Rutman A, O'Callaghan C. Ciliary beat pattern is associated with specific ultrastructural defects in primary ciliary dyskinesia. J Allergy Clin Immunol. 2003 Sep;112(3):518–24.

26. Schwabe GC, Hoffmann K, Loges NT, Birker D, Rossier C, de Santi MM, Olbrich H, Fliegauf M, Failly M, Liebers U, Collura M, Gaedicke G, Mundlos S, Wahn U, Blouin J-L, Niggemann B, Omran H, Antonarakis SE, Bartoloni L. Primary ciliary dyskinesia associated with normal axoneme ultrastructure is caused by DNAH11 mutations. Hum Mutat. 2008 Feb;29(2):289–98.

27. Shah A, Shoemark A, MacNeill SJ, Bhaludin B, Rogers A, Bilton D, Hansell DM, Wilson R, Loebinger MR. A longitudinal study characterising a large adult primary ciliary dyskinesia population. Eur Respir J. 2016 Aug 10;48(2):441–50.

28. Davis SD, Ferkol TW, Rosenfeld M, Lee H-S, Dell SD, Sagel SD, Milla C, Zariwala MA, Pittman JE, Shapiro AJ, Carson JL, Krischer JP, Hazucha MJ, Cooper ML, Knowles MR, Leigh MW. Clinical features of childhood primary ciliary dyskinesia by genotype and ultrastructural phenotype. Am J Respir Crit Care Med. 2015 Feb 1;191(3):316–24.

29. Onoufriadis A, Shoemark A, Schmidts M, Patel M, Jimenez G, Liu H, Thomas B, Dixon M, Hirst RA, Rutman A, Burgoyne T, Williams C, Scully J, Bolard F, Lafitte J-J, Beales PL, Hogg C, Yang P, Chung EMK, Emes RD, O'Callaghan C, Bouvagnet P, Mitchison HM. Targeted NGS gene panel identifies mutations in RSPH1 causing primary ciliary dyskinesia and a common mechanism for ciliary central pair agenesis due to radial spoke defects. Hum Mol Genet. 2014 Jul 1;23(13):3362–74.

30. Knowles MR, Ostrowski LE, Leigh MW, Sears PR, Davis SD, Wolf WE, Hazucha MJ, Carson JL, Olivier KN, Sagel SD, Rosenfeld M, Ferkol TW, Dell SD, Milla CE, Randell SH, Yin W, Sannuti A, Metjian HM, Noone PJPG, Noone PJPG, Olson CA, Patrone M V, Dang

H, Lee H-S, Hurd TW, Gee HY, Otto EA, Halbritter J, Kohl S, Kircher M, Krischer J, Bamshad MJ, Nickerson DA, Hildebrandt F, Shendure J, Zariwala MA. Mutations in RSPH1 cause primary ciliary dyskinesia with a unique clinical and ciliary phenotype. Am J Respir Crit Care Med. 2014 Mar 15;189(6):707–17.

31. Coren ME, Meeks M, Morrison I, Buchdahl RM, Bush A. Primary ciliary dyskinesia: age at diagnosis and symptom history. Acta Paediatr. 2002 Jan;91(6):667–9.

32. Noone PG, Leigh MW, Sannuti A, Minnix SL, Carson JL, Hazucha M, Zariwala MA, Knowles MR. Primary ciliary dyskinesia: diagnostic and phenotypic features. Am J Respir Crit Care Med. 2004 Mar 15;169(4):459–67.

33. Kennedy MP, Omran H, Leigh MW, Dell S, Morgan L, Molina PL, Robinson B V, Minnix SL, Olbrich H, Severin T, Ahrens P, Lange L, Morillas HN, Noone PG, Zariwala MA, Knowles MR. Congenital heart disease and other heterotaxic defects in a large cohort of patients with primary ciliary dyskinesia. Circulation. 2007 Jun 5;115(22):2814–21.

34. Wessels MW, den Hollander NS, Willems PJ. Mild fetal cerebral ventriculomegaly as a prenatal sonographic marker for Kartagener syndrome. Prenat Diagn. 2003 Mar;23(3):239–42.

35. Ferkol T, Leigh M. Primary ciliary dyskinesia and newborn respiratory distress. Semin Perinatol. 2006 Dec;30(6):335–40.

36. Brown DE, Pittman JE, Leigh MW, Fordham L, Davis SD. Early lung disease in young children with primary ciliary dyskinesia. Pediatr Pulmonol. 2008 May;43(5):514–6.

37. Marthin JK, Petersen N, Skovgaard LT, Nielsen KG. Lung function in patients with primary ciliary dyskinesia: a cross-sectional and 3-decade longitudinal study. Am J Respir Crit Care Med. 2010 Jun 1;181(11):1262–8.

38. Ellerman A, Bisgaard H. Longitudinal study of lung function in a cohort of primary ciliary dyskinesia. Eur Respir J. 1997 Oct 1;10(10):2376–9.

39. Aurora P, Bush A, Gustafsson P, Oliver C, Wallis C, Price J, Stroobant J, Carr S, Stocks J. Multiple-breath washout as a marker of lung disease in preschool children with cystic fibrosis. Am J Respir Crit Care Med. 2005 Feb 1;171(3):249–56.

40. Gustafsson PM, De Jong PA, Tiddens HAWM, Lindblad A. Multiple-breath inert gas washout and spirometry versus structural lung disease in cystic fibrosis. Thorax. 2008 Feb;63(2):129–34.

41. Green K, Buchvald FF, Marthin JK, Hanel B, Gustafsson PM, Nielsen KG. Ventilation inhomogeneity in children with primary ciliary dyskinesia. Thorax. 2012 Jan;67(1):49–53.

42. Date H, Yamashita M, Nagahiro I, Aoe M, Andou A, Shimizu N. Living-donor lobar lung transplantation for primary ciliary dyskinesia. Ann Thorac Surg. 2001 Jun;71(6):2008–9.

43. Kott E, Legendre M, Copin B, Papon J-F, Dastot-Le Moal F, Montantin G, Duquesnoy P, Piterboth W, Amram D, Bassinet L, Beucher J, Beydon N, Deneuville E, Houdouin V, Journel H, Just J, Nathan N, Tamalet A, Collot N, Jeanson L, Le Gouez M, Vallette B, Vojtek A-M, Epaud R, Coste A, Clement A, Housset B, Louis B, Escudier E, Amselem S. Loss-of-function mutations in RSPH1 cause primary ciliary dyskinesia with central-complex and radial-spoke defects. Am J Hum Genet. 2013 Sep 5;93(3):561–70.

44. Boon M, Wallmeier J, Ma L, Loges NT, Jaspers M, Olbrich H, Dougherty GW, Raidt J, Werner C, Amirav I, Hevroni A, Abitbul R, Avital A, Soferman R, Wessels M, O'Callaghan C, Chung EMK, Rutman A, Hirst R a, Moya E, Mitchison HM, Van Daele S, De Boeck K, Jorissen M, Kintner C, Cuppens H, Omran H. MCIDAS mutations result in a mucociliary clearance disorder with reduced generation of multiple motile cilia. Nat Commun. 2014 Jan;5:4418.

45. Wallmeier J, Al-Mutairi DA, Chen C-T, Loges NT, Pennekamp P, Menchen T, Ma L, Shamseldin HE, Olbrich H, Dougherty GW, Werner C, Alsabah BH, Köhler G, Jaspers M, Boon M, Griese M, Schmitt-Grohé S, Zimmermann T, Koerner-Rettberg C, Horak E, Kintner C, Alkuraya FS, Omran H. Mutations in CCNO result in congenital mucociliary clearance disorder with reduced generation of multiple motile cilia. Nat Genet. 2014 Jun 20;46(6):646–51.

46. Lundberg J, Weitzberg E. Primarily nasal origin of exhaled nitric oxide and absence in Kartagener's syndrome. Eur Respir J. 1994 Aug;7(8):1501–4.

47. Collins SA, Gove K, Walker W, Lucas JSA. Nasal nitric oxide screening for primary ciliary dyskinesia: systematic review and meta-analysis. Eur Respir J. 2014 Dec 16;44(6):1589–99.

48. Leigh MW, Hazucha MJ, Chawla KK, Baker BR, Shapiro AJ, Brown DE, Lavange LM, Horton BJ, Qaqish B, Carson JL, Davis SD, Dell SD, Ferkol TW, Atkinson JJ, Olivier KN, Sagel SD, Rosenfeld M, Milla C, Lee H-S, Krischer J, Zariwala MA, Knowles MR.

Standardizing nasal nitric oxide measurement as a test for primary ciliary dyskinesia. Ann Am Thorac Soc. 2013 Dec;10(6):574–81.

49. Marthin JK, Nielsen KG. Choice of nasal nitric oxide technique as first-line test for primary ciliary dyskinesia. Eur Respir J. 2011 Mar;37(3):559–65.

50. Marthin JK, Nielsen KG. Hand-held tidal breathing nasal nitric oxide measurement--a promising targeted case-finding tool for the diagnosis of primary ciliary dyskinesia. PLoS One. 2013 Jan;8(2):e57262.

51. Marthin JK, Mortensen J, Pressler T, Nielsen KG. Pulmonary radioaerosol mucociliary clearance in diagnosis of primary ciliary dyskinesia. Chest. 2007 Sep;132(3):966–76.

52. Omran H, Loges NT. Immunofluorescence staining of ciliated respiratory epithelial cells. Methods Cell Biol. 2009 Jan;91:123–33.

53. Lefeuvre S, Deneuville E, Deblic J, Vigier C, Tamalet A, Beucher J. Primary ciliary dyskinesia: Respiratory tract infections and impact of *Pseudomonas aeruginosa*. Eur Respir J. 2014 Dec 23;44(Suppl 58).

54. Mahenthiralingam E. Emerging cystic fibrosis pathogens and the microbiome. Paediatr Respir Rev. 2014 Jun;15 Suppl 1:13–5.

55. Stressmann FA, Rogers GB, Klem ER, Lilley AK, Donaldson SH, Daniels TW, Carroll MP, Patel N, Forbes B, Boucher RC, Wolfgang MC, Bruce KD. Analysis of the bacterial communities present in lungs of patients with cystic fibrosis from American and British centers. J Clin Microbiol. 2011 Jan;49(1):281–91.

56. Rogers GB, Carroll MP, Zain NMM, Bruce KD, Lock K, Walker W, Jones G, Daniels TW V, Lucas JS. Complexity, temporal stability, and clinical correlates of airway bacterial community composition in primary ciliary dyskinesia. J Clin Microbiol. 2013 Dec;51(12):4029–35.

57. Pillarisetti N, Williamson E, Linnane B, Skoric B, Robertson CF, Robinson P, Massie J, Hall GL, Sly P, Stick S, Ranganathan S. Infection, inflammation, and lung function decline in infants with cystic fibrosis. Am J Respir Crit Care Med. 2011 Jul 1;184(1):75–81.

58. Das RR, Kabra SK, Singh M. Treatment of *Pseudomonas* and *Staphylococcus* bronchopulmonary infection in patients with cystic fibrosis. Sci World J. 2013 Jan;2013:645653.

59. Santamaria F, Montella S, Tiddens HAWM, Guidi G, Casotti V, Maglione M, de Jong PA. Structural and functional lung disease in primary ciliary dyskinesia. Chest. 2008 Aug;134(2):351–7.

60. Cohen-Cymberknoh M, Simanovsky N, Hiller N, Hillel AG, Shoseyov D, Kerem E. Differences in disease expression between primary ciliary dyskinesia and cystic fibrosis with and without pancreatic insufficiency. Chest. 2013 Oct 3;145(4):738–44.

61. Alanin MC, Nielsen KG, von Buchwald C, Skov M, Aanaes K, Høiby N, Johansen HK. A longitudinal study of lung bacterial pathogens in patients with primary ciliary dyskinesia. Clin Microbiol Infect. 2015 Dec 1;21(12):1093.e1-1093.e7.

62. Stressmann FA, Rogers GB, van der Gast CJ, Marsh P, Vermeer LS, Carroll MP, Hoffman L, Daniels TW V, Patel N, Forbes B, Bruce KD. Long-term cultivation-independent microbial diversity analysis demonstrates that bacterial communities infecting the adult cystic fibrosis lung show stability and resilience. Thorax. 2012 Oct 1;67(10):867–73.

63. Trust CF. UK Cystic Fibrosis Registry Annual data report 2015. 2016.

64. Amirav I, Cohen-Cymberknoh M, Shoseyov D, Kerem E. Primary ciliary dyskinesia: prospects for new therapies, building on the experience in cystic fibrosis. Paediatr Respir Rev. 2009 Jun;10(2):58–62.

65. Sosnay PR, Siklosi KR, Van Goor F, Kaniecki K, Yu H, Sharma N, Ramalho AS, Amaral MD, Dorfman R, Zielenski J, Masica DL, Karchin R, Millen L, Thomas PJ, Patrinos GP, Corey M, Lewis MH, Rommens JM, Castellani C, Penland CM, Cutting GR. Defining the disease liability of variants in the cystic fibrosis transmembrane conductance regulator gene. Nat Genet. 2013 Oct;45(10):1160–7.

66. Cystic Fibrosis Mutation Database [Internet]. [cited 2016 Oct 28]. Available from: http://www.genet.sickkids.on.ca/cftr/app

67. Anderson M, Gregory R, Thompson S, Souza D, Paul S, Mulligan R, Smith A, Welsh M. Demonstration that CFTR is a chloride channel by alteration of its anion selectivity. Science (80-). 1991 Jul 12;253(5016):202–5.

68. Stutts M, Canessa C, Olsen J, Hamrick M, Cohn J, Rossier B, Boucher R. CFTR as a cAMP-dependent regulator of sodium channels. Science (80-). 1995 Aug 11;269(5225):847–50.

69. Smith JJ, Welsh MJ. cAMP stimulates bicarbonate secretion across normal, but not cystic fibrosis airway epithelia. J Clin Invest. 1992 Apr 1;89(4):1148–53.

70. Longo DL, Stoltz DA, Meyerholz DK, Welsh MJ. Origins of Cystic Fibrosis Lung Disease. N Engl J Med. 2015 Jan 22;372(4):351–62.

71. Livraghi-Butrico A, Kelly EJ, Klem ER, Dang H, Wolfgang MC, Boucher RC, Randell SH, O'Neal WK. Mucus clearance, MyD88-dependent and MyD88-independent immunity modulate lung susceptibility to spontaneous bacterial infection and inflammation. Mucosal Immunol. 2012 Jul;5(4):397–408.

72. Dawson M, Wirtz D, Hanes J. Enhanced viscoelasticity of human cystic fibrotic sputum correlates with increasing microheterogeneity in particle transport. J Biol Chem. 2003 Dec 12;278(50):50393–401.

73. Sriramulu DD, Lünsdorf H, Lam JS, Römling U. Microcolony formation: a novel biofilm model of *Pseudomonas aeruginosa* for the cystic fibrosis lung. J Med Microbiol. 2005 Jul 1;54(Pt 7):667–76.

74. Matsui H, Verghese MW, Kesimer M, Schwab UE, Randell SH, Sheehan JK, Grubb BR, Boucher RC. Reduced three-dimensional motility in dehydrated airway mucus prevents neutrophil capture and killing bacteria on airway epithelial surfaces. J Immunol. 2005 Jul 15;175(2):1090–9.

75. Hoegger MJ, Awadalla M, Namati E, Itani OA, Fischer AJ, Tucker AJ, Adam RJ, McLennan G, Hoffman EA, Stoltz DA, Welsh MJ. Assessing mucociliary transport of single particles in vivo shows variable speed and preference for the ventral trachea in newborn pigs. Proc Natl Acad Sci. 2014 Jan 28;111(6):2355–60.

76. Hoegger MJ, Fischer AJ, McMenimen JD, Ostedgaard LS, Tucker AJ, Awadalla MA, Moninger TO, Michalski AS, Hoffman EA, Zabner J, Stoltz DA, Welsh MJ. Impaired mucus detachment disrupts mucociliary transport in a piglet model of cystic fibrosis. Science (80-). 2014 Aug 15;345(6198):818–22.

77. Trevani AS, Andonegui G, Giordano M, López DH, Gamberale R, Minucci F, Geffner JR. Extracellular acidification induces human neutrophil activation. J Immunol. 1999 Apr 15;162(8):4849–57.

78. Allen DB. Wound Hypoxia and Acidosis Limit Neutrophil Bacterial Killing Mechanisms. Arch Surg. 1997 Sep 1;132(9):991.

79. Khan TZ, Wagener JS, Bost T, Martinez J, Accurso FJ, Riches DW. Early pulmonary inflammation in infants with cystic fibrosis. Am J Respir Crit Care Med. 1995 Apr;151(4):1075–82.

80. Cohen TS, Prince A. Cystic fibrosis: a mucosal immunodeficiency syndrome. Nat Med. 2012 Apr 5;18(4):509–19.

81. Hartl D, Gaggar A, Bruscia E, Hector A, Marcos V, Jung A, Greene C, McElvaney G, Mall M, Döring G. Innate immunity in cystic fibrosis lung disease. J Cyst Fibros. 2012 Sep;11(5):363–82.

82. Corvol H, Blackman SM, Boëlle P-Y, Gallins PJ, Pace RG, Stonebraker JR, Accurso FJ, Clement A, Collaco JM, Dang H, Dang AT, Franca A, Gong J, Guillot L, Keenan K, Li W, Lin F, Patrone M V., Raraigh KS, Sun L, Zhou Y-H, O'Neal WK, Sontag MK, Levy H, Durie PR, Rommens JM, Drumm ML, Wright FA, Strug LJ, Cutting GR, Knowles MR. Genome-wide association meta-analysis identifies five modifier loci of lung disease severity in cystic fibrosis. Nat Commun. 2015 Sep 29;6:8382.

83. Lim M, Wallis C, Price JF, Carr SB, Chavasse RJ, Shankar A, Seddon P, Balfour-Lynn IM. Diagnosis of cystic fibrosis in London and South East England before and after the introduction of newborn screening. Arch Dis Child. 2013 Nov 15;

84. Behan L, Dimitrov BD, Kuehni CE, Hogg C, Carroll M, Evans HJ, Goutaki M, Harris A, Packham S, Walker WT, Lucas JS. PICADAR: a diagnostic predictive tool for primary ciliary dyskinesia. Eur Respir J. 2016 Apr;47(4):1103–12.

85. van der Gast CJ, Cuthbertson L, Rogers GB, Pope C, Marsh RL, Redding GJ, Bruce KD, Chang AB, Hoffman LR. Three Clinically Distinct Chronic Pediatric Airway Infections Share a Common Core Microbiota. Ann Am Thorac Soc. 2014 Mar 5;

86. Daniels TW V, Rogers GB, Stressmann FA, van der Gast CJ, Bruce KD, Jones GR, Connett GJ, Legg JP, Carroll MP. Impact of antibiotic treatment for pulmonary exacerbations on bacterial diversity in cystic fibrosis. J Cyst Fibros. 2013 Jan;12(1):22–8.

87. Cystic Fibrosis Trust. Antibiotic Treatment for cystic fibrosis Antibiotic treatment for cystic fibrosis – 3rd edition. 2009.

88. Robinson M, Bye PTB. Mucociliary clearance in cystic fibrosis. Pediatr Pulmonol. 2002 Apr;33(4):293–306.

89. Locke LW, Myerburg MM, Weiner DJ, Markovetz MR, Parker RS, Muthukrishnan A, Weber L, Czachowski MR, Lacy RT, Pilewski JM, Corcoran TE. *Pseudomonas* infection and mucociliary and absorptive clearance in the cystic fibrosis lung. Eur Respir J. 2016 May 1;47(5):1392–401.

90. Cowley EA, Wang CG, Gosselin D, Radzioch D, Eidelman DH. Mucociliary clearance in cystic fibrosis knockout mice infected with *Pseudomonas aeruginosa*. Eur Respir J. 1997 Oct;10(10):2312–8.

91. Bush A, Payne D, Pike S, Jenkins G, Henke MO, Rubin BK. Mucus properties in children with primary ciliary dyskinesia: comparison with cystic fibrosis. Chest. 2006 Jan 1;129(1):118–23.

92. Ratjen F, Waters V, Klingel M, McDonald N, Dell S, Leahy TR, Yau Y, Grasemann H. Changes in airway inflammation during pulmonary exacerbations in patients with cystic fibrosis and primary ciliary dyskinesia. Eur Respir J. 2016 Mar 19;47(3):829–36.

93. Wodehouse T, Kharitonov S a., Mackay IS, Barnes PJ, Wilson R, Cole PJ. Nasal nitric oxide measurements for the screening of primary ciliary dyskinesia. Eur Respir J. 2003 Jan 1;21(1):43–7.

94. Sansonetti PJ. To be or not to be a pathogen: that is the mucosally relevant question. Mucosal Immunol. 2011 Jan;4(1):8–14.

95. Harbitz O, Jenssen AO, Smidsrød O. Lysozyme and lactoferrin in sputum from patients with chronic obstructive lung disease. Eur J Respir Dis. 1984 Oct;65(7):512–20.

96. Diamond G, Bevins CL. beta-Defensins: endogenous antibiotics of the innate host defense response. Clin Immunol Immunopathol. 1998 Sep;88(3):221–5.

97. Travis SM, Conway BAD, Zabner J, Smith JJ, Anderson NN, Singh PK, Greenberg EP, Welsh MJ. Activity of abundant antimicrobials of the human airway. Am J Respir Cell Mol Biol. 1999;20(5):872–9.

98. Tecle T, Tripathi S, Hartshorn KL. Review: Defensins and cathelicidins in lung immunity. Innate Immun. 2010 Jun 1;16(3):151–9.

99. Voynow JA, Rubin BK. Mucins, mucus, and sputum. Chest. 2009 Feb;135(2):505–12.

100. Bhattacharya J, Matthay MA. Regulation and repair of the alveolar-capillary barrier in acute lung injury. Annu Rev Physiol. 2013 Jan;75:593–615.

101. Sanderson MJ, Chow I, Dirksen ER. Intercellular communication between ciliated cells in culture. Am J Physiol. 1988 Jan;254(1 Pt 1):C63-74.

102. Boitano S, Dirksen ER, Sanderson MJ. Intercellular propagation of calcium waves mediated by inositol trisphosphate. Science. 1992 Oct 9;258(5080):292–5.

103. Davis CW, Lazarowski E. Coupling of airway ciliary activity and mucin secretion to mechanical stresses by purinergic signaling. Respir Physiol Neurobiol. 2008 Nov 30;163(1–3):208–13.

104. Martin FJ, Prince AS. TLR2 regulates gap junction intercellular communication in airway cells. J Immunol. 2008 Apr 1;180(7):4986–93.

105. Sarieddine MZR, Scheckenbach KEL, Foglia B, Maass K, Garcia I, Kwak BR, Chanson M. Connexin43 modulates neutrophil recruitment to the lung. J Cell Mol Med. Jan;13(11–12):4560–70.

106. Chanson M, Berclaz PY, Scerri I, Dudez T, Wernke-Dollries K, Pizurki L, Pavirani A, Fiedler MA, Suter S. Regulation of gap junctional communication by a pro-inflammatory cytokine in cystic fibrosis transmembrane conductance regulator-expressing but not cystic fibrosis airway cells. Am J Pathol. 2001 May;158(5):1775–84.

107. Cannon CL, Kowalski MP, Stopak KS, Pier GB. *Pseudomonas aeruginosa*-induced apoptosis is defective in respiratory epithelial cells expressing mutant cystic fibrosis transmembrane conductance regulator. Am J Respir Cell Mol Biol. 2003 Aug;29(2):188–97.

108. Shuto T, Xu H, Wang B, Han J, Kai H, Gu XX, Murphy TF, Lim DJ, Li JD. Activation of NF-kappa B by nontypeable *Hemophilus influenzae* is mediated by toll-like receptor 2-TAK1-dependent NIK-IKK alpha /beta-I kappa B alpha and MKK3/6-p38 MAP kinase signaling pathways in epithelial cells. Proc Natl Acad Sci U S A. 2001 Jul 17;98(15):8774–9.

109. Lugade AA, Bogner PN, Murphy TF, Thanavala Y. The role of TLR2 and bacterial lipoprotein in enhancing airway inflammation and immunity. Front Immunol. 2011 Jan;2:10.

110. Takeuchi O, Hoshino K, Akira S. Cutting Edge: TLR2-Deficient and MyD88-Deficient Mice Are Highly Susceptible to *Staphylococcus aureus* Infection. J Immunol. 2000 Nov

15;165(10):5392–6.

111. Echchannaoui H, Frei K, Schnell C, Leib SL, Zimmerli W, Landmann R. Toll-like receptor 2-deficient mice are highly susceptible to *Streptococcus pneumoniae* meningitis because of reduced bacterial clearing and enhanced inflammation. J Infect Dis. 2002 Sep 15;186(6):798–806.

112. Akira S, Uematsu S, Takeuchi O. Pathogen recognition and innate immunity. Cell. 2006 Feb 24;124(4):783–801.

113. Medzhitov R. Recognition of microorganisms and activation of the immune response. Nature. 2007 Oct 18;449(7164):819–26.

114. Fujisawa T, Chang MM-J, Velichko S, Thai P, Hung L-Y, Huang F, Phuong N, Chen Y, Wu R. NF-κB mediates IL-1β- and IL-17A-induced MUC5B expression in airway epithelial cells. Am J Respir Cell Mol Biol. 2011 Aug;45(2):246–52.

115. Walker WT. Cilia, nitric oxide and *non-typeable Haemophilus influenzae* biofilm infection. University of Southampton; 2015.

116. Walker WT, Jackson CL, Coles J, Lackie PM, Faust SN, Hall-Stoodley L, Lucas JS. Ciliated cultures from patients with primary ciliary dyskinesia produce nitric oxide in response to *Haemophilus influenzae* infection and proinflammatory cytokines. Chest. 2014 Mar 1;145(3):668–9.

117. Smith CM, Fadaee-Shohada MJ, Sawhney R, Baker N, Williams G, Hirst RA, Andrew PW, O'Callaghan C. Ciliated cultures from patients with primary ciliary dyskinesia do not produce nitric oxide or inducible nitric oxide synthase during early infection. Chest. 2013 Nov 1;144(5):1671–6.

118. Census Department U. US Census 1900 [Internet]. 2000. Available from: http://www2.census.gov/prod2/decennial/documents/13982433v3ch02.pdf

119. Costerton JW. Bacterial Biofilms: A Common Cause of Persistent Infections. Science (80-). 1999 May 21;284(5418):1318–22.

120. Hall-Stoodley L, Stoodley P. Evolving concepts in biofilm infections. Cell Microbiol. 2009 Jul;11(7):1034–43.

121. Costerton JW, Geesey GG, Cheng KJ. How bacteria stick. Sci Am. 1978;238(1):86–95.

122. Donlan RM, Costerton JW. Biofilms: survival mechanisms of clinically relevant

microorganisms. Clin Microbiol Rev. 2002 Apr;15(2):167–93.

123. Ciofu O, Mandsberg LF, Wang H, Høiby N. Phenotypes selected during chronic lung infection in cystic fibrosis patients: implications for the treatment of *Pseudomonas aeruginosa* biofilm infections. FEMS Immunol Med Microbiol. 2012 Jul;65(2):215–25.

124. Høiby N, Bjarnsholt T, Givskov M, Molin S, Ciofu O. Antibiotic resistance of bacterial biofilms. Int J Antimicrob Agents. 2010 Apr;35(4):322–32.

125. Krishnamurthy A, Kyd J. The roles of epithelial cell contact, respiratory bacterial interactions and phosphorylcholine in promoting biofilm formation by *Streptococcus pneumoniae* and nontypeable *Haemophilus influenzae*. Microbes Infect. 2014 Aug;16(8):640–7.

126. Fux CA, Costerton JW, Stewart PS, Stoodley P. Survival strategies of infectious biofilms. Trends Microbiol. 2005 Jan;13(1):34–40.

127. Johnson GM, Lee DA, Regelmann WE, Gray ED, Peters G, Quie PG. Interference with granulocyte function by *Staphylococcus epidermidis* slime. Infect Immun. 1986;54(1):13–20.

128. Rani SA, Pitts B, Beyenal H, Veluchamy RA, Lewandowski Z, Davison WM, Buckingham-Meyer K, Stewart PS. Spatial patterns of DNA replication, protein synthesis, and oxygen concentration within bacterial biofilms reveal diverse physiological states. J Bacteriol. 2007 Jun;189(11):4223–33.

129. Høiby N, Ciofu O, Johansen HK, Song Z, Moser C, Jensen PØ, Molin S, Givskov M, Tolker-Nielsen T, Bjarnsholt T. The clinical impact of bacterial biofilms. Int J Oral Sci. 2011 Apr;3(2):55–65.

130. Baldan R, Cigana C, Testa F, Bianconi I, De Simone M, Pellin D, Di Serio C, Bragonzi A, Cirillo DM. Adaptation of *Pseudomonas aeruginosa* in Cystic Fibrosis airways influences virulence of *Staphylococcus aureus* in vitro and murine models of co-infection. Palaniyar N, editor. PLoS One. 2014 Jan;9(3):e89614.

131. Starner TD, Zhang N, Kim G, Apicella MA, McCray PB. *Haemophilus influenzae* forms biofilms on airway epithelia: implications in cystic fibrosis. Am J Respir Crit Care Med. 2006 Jul 15;174(2):213–20.

132. Hudson VL, Wielinski CL, Regelmann WE. Prognostic implications of initial oropharyngeal bacterial flora in patients with cystic fibrosis diagnosed before the age of two years. J Pediatr. 1993 Jun;122(6):854–60.

133. Bjarnsholt T, Jensen PØ, Fiandaca MJ, Pedersen J, Hansen CR, Andersen CB, Pressler T, Givskov M, Høiby N. *Pseudomonas aeruginosa* biofilms in the respiratory tract of cystic fibrosis patients. Pediatr Pulmonol. 2009 Jun;44(6):547–58.

134. Lam J, Chan R, Lam K, Costerton JW. Production of mucoid microcolonies by *Pseudomonas aeruginosa* within infected lungs in cystic fibrosis. Infect Immun. 1980;28(2):546–56.

135. Baltimore RS, Christie CDC, Walker Smith GJ. Immunohistopathologic localization of *Pseudomonas aeruginosa* in lungs from patients with cystic fibrosis. Implications for the pathogenesis of progressive lung deterioration. Am Rev Respir Dis. 1989;140(6):1650–61.

136. Kragh KN, Alhede M, Jensen PØ, Moser C, Scheike T, Jacobsen CS, Seier Poulsen S, Eickhardt-Sørensen SR, Trøstrup H, Christoffersen L, Hougen H-P, Rickelt LF, Kühl M, Høiby N, Bjarnsholt T. Polymorphonuclear leukocytes restrict growth of *Pseudomonas aeruginosa* in the lungs of cystic fibrosis patients. Infect Immun. 2014 Nov 1;82(11):4477–86.

137. Jensen PØ, Bjarnsholt T, Phipps R, Rasmussen TB, Calum H, Christoffersen L, Moser C, Williams P, Pressler T, Givskov M, Høiby N. Rapid necrotic killing of polymorphonuclear leukocytes is caused by quorum-sensing-controlled production of rhamnolipid by *Pseudomonas aeruginosa*. Microbiology. 2007 May;153(Pt 5):1329–38.

138. Harmsen M, Yang L, Pamp SJ, Tolker-Nielsen T. An update on *Pseudomonas aeruginosa* biofilm formation, tolerance, and dispersal. FEMS Immunol Med Microbiol. 2010 Aug;59(3):253–68.

139. Govan JRW, Deretic V. Microbial pathogenesis in cystic fibrosis: Mucoid *Pseudomonas aeruginosa* and *Burkholderia cepacia*. Vol. 60, Microbiological Reviews. 1996. p. 539–74.

140. Purevdorj-Gage B, Costerton WJ, Stoodley P. Phenotypic differentiation and seeding dispersal in non-mucoid and mucoid *Pseudomonas aeruginosa* biofilms. Microbiology. 2005 May;151(Pt 5):1569–76.

141. Ma L, Jackson KD, Landry RM, Parsek MR, Wozniak DJ. Analysis of *Pseudomonas aeruginosa* Conditional Psl Variants Reveals Roles for the Psl Polysaccharide in Adhesion and Maintaining Biofilm Structure Postattachment. J Bacteriol. 2006 Sep 15;188(23):8213–21.

142. Friedman L, Kolter R. Two Genetic Loci Produce Distinct Carbohydrate-Rich Structural Components of the *Pseudomonas aeruginosa* Biofilm Matrix. J Bacteriol. 2004 Jul 1;186(14):4457–65.

143. Whitchurch CB, Tolker-Nielsen T, Ragas PC, Mattick JS. Extracellular DNA required for bacterial biofilm formation. Science. 2002 Feb 22;295(5559):1487.

144. Parks QM, Young RL, Poch KR, Malcolm KC, Vasil ML, Nick JA. Neutrophil enhancement of *Pseudomonas aeruginosa* biofilm development: human F-actin and DNA as targets for therapy. J Med Microbiol. 2009 Apr;58(Pt 4):492–502.

145. Hickman JW, Tifrea DF, Harwood CS. A chemosensory system that regulates biofilm formation through modulation of cyclic diguanylate levels. Proc Natl Acad Sci U S A. 2005 Oct 4;102(40):14422–7.

146. Römling U. Microbiology: bacterial communities as capitalist economies. Nature. 2013 May 16;497(7449):321–2.

147. Lee VT, Matewish JM, Kessler JL, Hyodo M, Hayakawa Y, Lory S. A cyclic-di-GMP receptor required for bacterial exopolysaccharide production. Mol Microbiol. 2007 Sep;65(6):1474–84.

148. Rao F, Yang Y, Qi Y, Liang Z-X. Catalytic mechanism of cyclic di-GMP-specific phosphodiesterase: a study of the EAL domain-containing RocR from *Pseudomonas aeruginosa*. J Bacteriol. 2008 May;190(10):3622–31.

149. An S, Wu J, Zhang L-H. Modulation of *Pseudomonas aeruginosa* biofilm dispersal by a cyclic-Di-GMP phosphodiesterase with a putative hypoxia-sensing domain. Appl Environ Microbiol. 2010 Dec 15;76(24):8160–73.

150. Barraud N, Hassett DJ, Hwang S-H, Rice SA, Kjelleberg S, Webb JS. Involvement of nitric oxide in biofilm dispersal of *Pseudomonas aeruginosa*. J Bacteriol. 2006 Nov 1;188(21):7344–53.

151. Li Y, Heine S, Entian M, Sauer K, Frankenberg-Dinkel N. NO-induced biofilm dispersion in *Pseudomonas aeruginosa* is mediated by an MHYT domain-coupled phosphodiesterase. J Bacteriol. 2013 Aug 15;195(16):3531–42.

152. Juhas M, Eberl L, Tümmler B. Quorum sensing: the power of cooperation in the world of Pseudomonas. Environ Microbiol. 2005 Apr;7(4):459–71.

153. Yang L, Hu Y, Liu Y, Zhang J, Ulstrup J, Molin S. Distinct roles of extracellular polymeric substances in *Pseudomonas aeruginosa* biofilm development. Environ Microbiol. 2011 Jul;13(7):1705–17.

154. Walters MC, Roe F, Bugnicourt A, Franklin MJ, Stewart PS. Contributions of Antibiotic Penetration, Oxygen Limitation, and Low Metabolic Activity to Tolerance of *Pseudomonas aeruginosa* Biofilms to Ciprofloxacin and Tobramycin. Antimicrob Agents Chemother. 2003 Jan 1;47(1):317–23.

155. Castillo-Juárez I, Maeda T, Mandujano-Tinoco EA, Tomás M, Pérez-Eretza B, García-Contreras SJ, Wood TK, García-Contreras R. Role of quorum sensing in bacterial infections. World J Clin cases. 2015 Jul 16;3(7):575–98.

156. Ochsner UA, Koch AK, Fiechter A, Reiser J. Isolation and characterization of a regulatory gene affecting rhamnolipid biosurfactant synthesis in *Pseudomonas aeruginosa*. J Bacteriol. 1994 Apr;176(7):2044–54.

157. Xiao G, He J, Rahme LG. Mutation analysis of the *Pseudomonas aeruginosa* mvfR and pqsABCDE gene promoters demonstrates complex quorum-sensing circuitry. Microbiology. 2006 Jun;152(Pt 6):1679–86.

158. Cornforth DM, Popat R, McNally L, Gurney J, Scott-Phillips TC, Ivens A, Diggle SP, Brown SP. Combinatorial quorum sensing allows bacteria to resolve their social and physical environment. Proc Natl Acad Sci U S A. 2014 Mar 18;111(11):4280–4.

159. Bjarnsholt T, Jensen PØ, Burmølle M, Hentzer M, Haagensen JAJ, Hougen HP, Calum H, Madsen KG, Moser C, Molin S, Høiby N, Givskov M. *Pseudomonas aeruginosa* tolerance to tobramycin, hydrogen peroxide and polymorphonuclear leukocytes is quorum-sensing dependent. Microbiology. 2005 Feb;151(Pt 2):373–83.

160. Schaber JA, Carty NL, McDonald NA, Graham ED, Cheluvappa R, Griswold JA, Hamood AN. Analysis of quorum sensing-deficient clinical isolates of *Pseudomonas aeruginosa*. J Med Microbiol. 2004 Sep;53(Pt 9):841–53.

161. Rybtke M, Hultqvist LD, Givskov M, Tolker-Nielsen T. *Pseudomonas aeruginosa* biofilm infections: community structure, antimicrobial tolerance and immune response. J Mol Biol. 2015 Aug 25;427(23):3628–45.

162. Mahenthiralingam E, Speert DP. Nonopsonic phagocytosis of *Pseudomonas aeruginosa* by macrophages and polymorphonuclear leukocytes requires the presence of the bacterial flagellum. Infect Immun. 1995 Nov;63(11):4519–23.

163. Managò A, Becker KA, Carpinteiro A, Wilker B, Soddemann M, Seitz AP, Edwards MJ, Grassmé H, Szabò I, Gulbins E. *Pseudomonas aeruginosa* pyocyanin induces neutrophil death via mitochondrial reactive oxygen species and mitochondrial acid sphingomyelinase. Antioxid Redox Signal. 2015 May 1;22(13):1097–110.

164. Pamp SJ, Gjermansen M, Johansen HK, Tolker-Nielsen T. Tolerance to the antimicrobial peptide colistin in *Pseudomonas aeruginosa* biofilms is linked to metabolically active cells, and depends on the pmr and mexAB-oprM genes. Mol Microbiol. 2008 Apr;68(1):223–40.

165. Tseng BS, Zhang W, Harrison JJ, Quach TP, Song JL, Penterman J, Singh PK, Chopp DL, Packman AI, Parsek MR. The extracellular matrix protects *Pseudomonas aeruginosa* biofilms by limiting the penetration of tobramycin. Environ Microbiol. 2013 Jul;15(10).

166. Hentzer M, Teitzel GM, Balzer GJ, Heydorn A, Molin S, Givskov M, Parsek MR. Alginate Overproduction Affects *Pseudomonas aeruginosa* Biofilm Structure and Function. J Bacteriol. 2001 Sep 15;183(18):5395–401.

167. Sauer K, Cullen MC, Rickard AH, Zeef LAH, Davies DG, Gilbert P. Characterization of nutrient-induced dispersion in *Pseudomonas aeruginosa* PAO1 biofilm. J Bacteriol. 2004 Nov;186(21):7312–26.

168. Sternberg C, Christensen BB, Johansen T, Nielsen AT, Andersen JB, Givskov M, Molin S. Distribution of bacterial growth activity in flow-chamber biofilms. Appl Environ Microbiol. 1999;65(9):4108–17.

169. Webb JS, Thompson LS, James S, Charlton T, Tolker-Nielsen T, Koch B, Givskov M, Kjelleberg S. Cell death in *Pseudomonas aeruginosa* biofilm development. J Bacteriol. 2003 Aug;185(15):4585–92.

170. Barraud N, Schleheck D, Klebensberger J, Webb JS, Hassett DJ, Rice SA, Kjelleberg S.

Nitric oxide signaling in *Pseudomonas aeruginosa* biofilms mediates phosphodiesterase activity, decreased cyclic di-GMP levels, and enhanced dispersal. J Bacteriol. 2009 Dec 1;191(23):7333–42.

171. Barraud N, Storey M V, Moore ZP, Webb JS, Rice SA, Kjelleberg S. Nitric oxide-mediated dispersal in single- and multi-species biofilms of clinically and industrially relevant microorganisms. Microb Biotechnol. 2009 May;2(3):370–8.

172. Schlag S, Nerz C, Birkenstock TA, Altenberend F, Götz F. Inhibition of staphylococcal biofilm formation by nitrite. J Bacteriol. 2007 Nov;189(21):7911–9.

173. Boon EM, Marletta MA. Ligand specificity of H-NOX domains: from sGC to bacterial NO sensors. J Inorg Biochem. 2005 Apr;99(4):892–902.

174. Stamler J, Singel D, Loscalzo J. Biochemistry of nitric oxide and its redox-activated forms. Science (80-). 1992 Dec 18;258(5090):1898–902.

175. Musk DJ, Banko DA, Hergenrother PJ. Iron salts perturb biofilm formation and disrupt existing biofilms of *Pseudomonas aeruginosa*. Chem Biol. 2005 Jul;12(7):789–96.

176. D'Autreaux B, Touati D, Bersch B, Latour J-M, Michaud-Soret I. Direct inhibition by nitric oxide of the transcriptional ferric uptake regulation protein via nitrosylation of the iron. Proc Natl Acad Sci. 2002 Dec 10;99(26):16619–24.

177. Morgan R, Kohn S, Hwang S-H, Hassett DJ, Sauer K. BdlA, a chemotaxis regulator essential for biofilm dispersion in *Pseudomonas aeruginosa*. J Bacteriol. 2006 Nov 1;188(21):7335–43.

178. Armbruster CE, Hong W, Pang B, Dew KE, Juneau RA, Byrd MS, Love CF, Kock ND, Swords WE. LuxS Promotes Biofilm Maturation and Persistence of Nontypeable *Haemophilus influenzae* In Vivo via Modulation of Lipooligosaccharides on the Bacterial Surface. Infect Immun. 2009 Jun 29;77(9):4081–91.

179. Klausen M, Aaes-Jørgensen A, Molin S, Tolker-Nielsen T. Involvement of bacterial migration in the development of complex multicellular structures in *Pseudomonas aeruginosa* biofilms. Mol Microbiol. 2003 Aug 14;50(1):61–8.

180. Alhede M, Kragh KN, Qvortrup K, Allesen-Holm M, van Gennip M, Christensen LD, Jensen PØ, Nielsen AK, Parsek M, Wozniak D, Molin S, Tolker-Nielsen T, Høiby N, Givskov M, Bjarnsholt T. Phenotypes of non-attached *Pseudomonas aeruginosa* aggregates resemble surface attached biofilm. PLoS One. 2011 Jan 21;6(11):e27943.

181. Folsom JP, Richards L, Pitts B, Roe F, Ehrlich GD, Parker A, Mazurie A, Stewart PS. Physiology of *Pseudomonas aeruginosa* in biofilms as revealed by transcriptome analysis. BMC Microbiol. 2010 Jan 17;10(1):294.

182. Bakaletz LO. Chinchilla as a robust, reproducible and polymicrobial model of otitis media and its prevention. Expert Rev Vaccines. 2009 Aug;8(8):1063–82.

183. Cash HA, Woods DE, McCullough B, Johanson WG, Bass JA. A rat model of chronic respiratory infection with *Pseudomonas aeruginosa*. Am Rev Respir Dis. 1979;119(3):453–9.

184. Pezzulo AA, Tang XX, Hoegger MJ, Alaiwa MHA, Ramachandran S, Moninger TO, Karp PH, Wohlford-Lenane CL, Haagsman HP, van Eijk M, Bánfi B, Horswill AR, Stoltz DA, McCray PB, Welsh MJ, Zabner J. Reduced airway surface pH impairs bacterial killing in the porcine cystic fibrosis lung. Nature. 2012 Jul 5;487(7405):109–13.

185. Kuhnert P, Christensen H. Pasteurellaceae: Biology, Genomics and Molecular Aspects. 2008.

186. Fleischmann RD, Adams MD, White O, Clayton RA, Kirkness EF, Kerlavage AR, Bult CJ, Tomb JF, Dougherty BA, Merrick JM, Al. E. Whole-genome random sequencing and assembly of *Haemophilus influenzae* Rd. Science (80-). 1995 Jul 28;269(5223):496–512.

187. Kilian M. Haemophilus. In: Bergey's Manual of Systematics of Archaea and Bacteria. John Wiley & Sons, Ltd; 2015. p. 885–901.

188. Ishak N, Tikhomirova A, Bent SJ, Ehrlich GD, Hu FZ, Kidd SP. There is a specific response to pH by isolates of *Haemophilus influenzae* and this has a direct influence on biofilm formation. BMC Microbiol. 2014 Feb 21;14:47.

189. Tristram S, Jacobs MR, Appelbaum PC. Antimicrobial resistance in *Haemophilus influenzae*. Clin Microbiol Rev. 2007 Apr;20(2):368–89.

190. St Geme JW, Takala A, Esko E, Falkow S. Evidence for capsule gene sequences among pharyngeal isolates of nontypeable *Haemophilus influenzae*. J Infect Dis. 1994 Feb;169(2):337–42.

191. Erwin AL, Sandstedt SA, Bonthuis PJ, Geelhood JL, Nelson KL, Unrath WCT, Diggle MA, Theodore MJ, Pleatman CR, Mothershed EA, Sacchi CT, Mayer LW, Gilsdorf JR, Smith AL.

Analysis of genetic relatedness of *Haemophilus influenzae* isolates by multilocus sequence typing. J Bacteriol. 2008 Feb;190(4):1473–83.

192. Collins S, Vickers A, Ladhani SN, Flynn S, Platt S, Ramsay ME, Litt DJ, Slack MPE. Clinical and Molecular Epidemiology of Childhood Invasive *Nontypeable Haemophilus influenzae* Disease in England and Wales. Pediatr Infect Dis J. 2016 Mar;35(3):e76–84.

193. Skaare D, Anthonisen IL, Caugant DA, Jenkins A, Steinbakk M, Strand L, Sundsfjord A, Tveten Y, Kristiansen B-E. Multilocus sequence typing and ftsI sequencing: a powerful tool for surveillance of penicillin-binding protein 3-mediated beta-lactam resistance in *nontypeable Haemophilus influenzae*. BMC Microbiol. 2014 May 20;14:131.

194. Novotny LA, Jurcisek JA, Pichichero ME, Bakaletz LO. Epitope mapping of the outer membrane protein P5-homologous fimbrin adhesin of *nontypeable Haemophilus influenzae*. Infect Immun. 2000 Apr;68(4):2119–28.

195. Denny FW. Effect of a toxin produced by *Haemophilus influenzae* on ciliated respiratory epithelium. J Infect Dis. 1974 Feb;129(2):93–100.

196. Janson H, Carl n B, Cervin A, Forsgren A, Magnusdottir AB, Lindberg S, Runer T. Effects on the ciliated epithelium of protein D-producing and -nonproducing *nontypeable Haemophilus influenzae* in nasopharyngeal tissue cultures. J Infect Dis. 1999 Sep;180(3):737–46.

197. Bailey KL, LeVan TD, Yanov DA, Pavlik JA, DeVasure JM, Sisson JH, Wyatt TA. *Non-typeable Haemophilus influenzae* decreases cilia beating via protein kinase Cε. Respir Res. 2012 Jan;13(1):49.

198. Mulks MH, Kornfeld SJ, Plaut AG. Specific proteolysis of human IgA by *Streptococcus pneumoniae* and *Haemophilus influenzae*. J Infect Dis. 1980 Apr;141(4):450–6.

199. Clementi CF, Håkansson AP, Murphy TF. Internalization and trafficking of nontypeable *Haemophilus influenzae* in human respiratory epithelial cells and roles of IgA1 proteases for optimal invasion and persistence. Infect Immun. 2014 Jan;82(1):433–44.

200. Gilsdorf JR, Chang HY, McCrea KW, Bakaletz LO. Comparison of hemagglutinating pili of *Haemophilus influenzae* type b with similar structures of nontypeable H. influenzae. Infect Immun. 1992 Feb;60(2):374–9.

201. Jackson AD, Rayner CF, Dewar A, Cole PJ, Wilson R. A human respiratory-tissue organ culture incorporating an air interface. Am J Respir Crit Care Med. 1996

Mar;153(3):1130–5.

202. Read RC, Wilson R, Rutman A, Lund V, Todd HC, Brain AP, Jeffery PK, Cole PJ. Interaction of nontypable *Haemophilus influenzae* with human respiratory mucosa in vitro. J Infect Dis. 1991 Mar;163(3):549–58.

203. Barenkamp SJ, Leininger E. Cloning, expression, and DNA sequence analysis of genes encoding nontypeable *Haemophilus influenzae* high-molecular-weight surface-exposed proteins related to filamentous hemagglutinin of Bordetella pertussis. Infect Immun. 1992 Apr;60(4):1302–13.

204. Winter LE, Barenkamp SJ. Antibodies to the HMW1/HMW2 and Hia Adhesins of *Nontypeable Haemophilus influenzae* Mediate Broad-Based Opsonophagocytic Killing of Homologous and Heterologous Strains. Clin Vaccine Immunol. 2014;21(5):613–21.

205. St Geme JW, Kumar V V, Cutter D, Barenkamp SJ. Prevalence and distribution of the hmw and hia genes and the HMW and Hia adhesins among genetically diverse strains of nontypeable *Haemophilus influenzae*. Infect Immun. 1998 Jan;66(1):364–8.

206. St Geme JW, de la Morena ML, Falkow S. A *Haemophilus influenzae* IgA protease-like protein promotes intimate interaction with human epithelial cells. Mol Microbiol. 1994 Oct;14(2):217–33.

207. Fakih MG, Murphy TF, Pattoli MA, Berenson CS. Specific binding of *Haemophilus influenzae* to minor gangliosides of human respiratory epithelial cells. Infect Immun. 1997 May;65(5):1695–700.

208. Winter LE, Barenkamp SJ. Antibodies to the HMW1/HMW2 and Hia Adhesins of *Nontypeable Haemophilus influenzae* Mediate Broad-Based Opsonophagocytic Killing of Homologous and Heterologous Strains. Clin Vaccine Immunol. 2014 May 1;21(5):613–21.

209. Cardines R, Giufrè M, Pompilio A, Fiscarelli E, Ricciotti G, Bonaventura G Di, Cerquetti M, Di Bonaventura G, Cerquetti M. *Haemophilus influenzae* in children with cystic fibrosis: antimicrobial susceptibility, molecular epidemiology, distribution of adhesins and biofilm formation. Int J Med Microbiol. 2012 Jan;302(1):45–52.

210. Barenkamp SJ. Immunization with high-molecular-weight adhesion proteins of *nontypeable Haemophilus influenzae* modifies experimental otitis media in chinchillas.

Infect Immun. 1996 Apr;64(4):1246–51.

211. Clementi CF, Murphy TF. *Non-typeable Haemophilus influenzae* invasion and persistence in the human respiratory tract. Front Cell Infect Microbiol. 2011 Jan;1(November):1.

212. Kaur R, Sharma A, Majumdar S, Ganguly NK, Chakraborti A. Outer-membrane-protein subtypes of *Haemophilus influenzae* isolates from North India. J Med Microbiol. 2003 Aug 1;52(8):693–6.

213. Euba B, Moleres J, Viadas C, Ruiz de los Mozos I, Valle J, Bengoechea JA, Garmendia J. Relative Contribution of P5 and Hap Surface Proteins to *Nontypable Haemophilus influenzae* Interplay with the Host Upper and Lower Airways. PLoS One. 2015 Jan;10(4):e0123154.

214. Rosadini C V, Ram S, Akerley BJ. Outer membrane protein P5 is required for resistance of *nontypeable Haemophilus influenzae* to both the classical and alternative complement pathways. Infect Immun. 2014 Feb;82(2):640–9.

215. Murphy TF, Bartos LC. Human bactericidal antibody response to outer membrane protein P2 of *nontypeable Haemophilus influenzae*. Infect Immun. 1988 Oct;56(10):2673–9.

216. Sharpe SW, Kuehn MJ, Mason KM. Elicitation of epithelial cell-derived immune effectors by outer membrane vesicles of *nontypeable Haemophilus influenzae*. Infect Immun. 2011 Nov 1;79(11):4361–9.

217. Hotomi M, Ikeda Y, Suzumoto M, Yamauchi K, Green BA, Zlotnick G, Billal DS, Shimada J, Fujihara K, Yamanaka N. A recombinant P4 protein of *Haemophilus influenzae* induces specific immune responses biologically active against nasopharyngeal colonization in mice after intranasal immunization. Vaccine. 2005;23(10):1294–300.

218. Pichichero ME, Kaur R, Casey JR, Sabirov A, Khan MN, Almudevar A. Antibody response to *Haemophilus influenzae* outer membrane protein D, P6, and OMP26 after nasopharyngeal colonization and acute otitis media in children. Vaccine. 2010 Oct 18;28(44):7184–92.

219. Vogel L, Duim B, Geluk F, Eijk P, Jansen H, Dankert J, vanAlphen L. Immune selection for antigenic drift of major outer membrane protein P2 of *Haemophilus influenzae* during persistence in subcutaneous tissue cages in rabbits. Infect Immun. 1996 Mar;64(3):980–

6.

220. Weiser JN. Relationship between colony morphology and the life cycle of *Haemophilus influenzae*: the contribution of lipopolysaccharide phase variation to pathogenesis. J Infect Dis. 1993 Sep;168(3):672–80.

221. Halbert RJ, Natoli JL, Gano A, Badamgarav E, Buist AS, Mannino DM. Global burden of COPD: systematic review and meta-analysis. Eur Respir J. 2006 Sep;28(3):523–32.

222. Papi A, Bellettato CM, Braccioni F, Romagnoli M, Casolari P, Caramori G, Fabbri LM, Johnston SL. Infections and airway inflammation in chronic obstructive pulmonary disease severe exacerbations. Am J Respir Crit Care Med. 2006 May 15;173(10):1114–21.

223. Groenewegen KH, Wouters EFM. Bacterial infections in patients requiring admission for an acute exacerbation of COPD; a 1-year prospective study. Respir Med. 2003 Jul;97(7):770–7.

224. Otczyk DC, Clancy RL, Cripps AW. *Haemophilus influenzae* and smoking-related obstructive airways disease. 2011;6(1):345–51.

225. Berenson CS, Kruzel RL, Eberhardt E, Sethi S. Phagocytic dysfunction of human alveolar macrophages and severity of chronic obstructive pulmonary disease. J Infect Dis. 2013 Dec 15;208(12):2036–45.

226. Donnelly D, Critchlow A, Everard ML. Outcomes in children treated for persistent bacterial bronchitis. Thorax. 2007 Jan;62(1):80–4.

227. King P, Holdsworth S, Freezer N, Holmes P. Bronchiectasis. Intern Med J. 2006 Nov;36(11):729–37.

228. Watanabe T, Jono H, Han J, Lim DJ, Li J-D. Synergistic activation of NF-kappaB by *nontypeable Haemophilus influenzae* and tumor necrosis factor alpha. Proc Natl Acad Sci U S A. 2004 Mar 9;101(10):3563–8.

229. Xu X, Steere RR, Fedorchuk CA, Pang J, Lee J-Y, Lim JH, Xu H, Pan ZK, Maggirwar SB, Li J-D. Activation of epidermal growth factor receptor is required for NTHi-induced NF-κB-dependent inflammation. PLoS One. 2011;6(11):e28216.

230. Lim JH, Jono H, Koga T, Woo C-H, Ishinaga H, Bourne P, Xu H, Ha U-H, Xu H, Li J-D.

Tumor suppressor CYLD acts as a negative regulator for non-typeable Haemophilus influenza-induced inflammation in the middle ear and lung of mice. PLoS One. 2007;2(10):e1032.

231. Wertz IE, O'Rourke KM, Zhou H, Eby M, Aravind L, Seshagiri S, Wu P, Wiesmann C, Baker R, Boone DL, Ma A, Koonin E V, Dixit VM. De-ubiquitination and ubiquitin ligase domains of A20 downregulate NF-kappaB signalling. Nature. 2004 Aug 5;430(7000):694–9.

232. Mukundan D, Ecevit Z, Patel M, Marrs CF, Gilsdorf JR. Pharyngeal colonization dynamics of *Haemophilus influenzae* and *Haemophilus haemolyticus* in healthy adult carriers. J Clin Microbiol. 2007;45(10):3207–17.

233. Erwin AL, Smith AL. *Nontypeable Haemophilus influenzae*: understanding virulence and commensal behavior. Trends Microbiol. 2007 Aug;15(8):355–62.

234. Van Eldere J, Slack MPE, Ladhani S, Cripps AW. Non-typeable *Haemophilus influenzae*, an under-recognised pathogen. Lancet Infect Dis. 2014;14(12):1281–92.

235. Baddal B, Muzzi A, Censini S, Calogero RA, Torricelli G, Guidotti S, Taddei AR, Covacci A, Pizza M, Rappuoli R, Soriani M, Pezzicoli A. Dual RNA-seq of *Nontypeable Haemophilus influenzae* and Host Cell Transcriptomes Reveals Novel Insights into Host-Pathogen Cross Talk. MBio. 2015;6(6):e01765-15.

236. Hasegawa K, Mansbach JM, Ajami NJ, Espinola JA, Henke DM, Petrosino JF, Piedra PA, Shaw CA, Sullivan AF, Camargo CA. Association of nasopharyngeal microbiota profiles with bronchiolitis severity in infants hospitalised for bronchiolitis. Eur Respir J. 2016;48(5).

237. Swords WE. *Nontypeable Haemophilus influenzae* biofilms: role in chronic airway infections. Front Cell Infect Microbiol. 2012;2(July):97.

238. Hall-Stoodley L, Hu FZ, Gieseke A, Nistico L, Nguyen D, Hayes J, Forbes M, Greenberg DP, Dice B, Burrows A, Wackym PA, Stoodley P, Post JC, Ehrlich GD, Kerschner JE. Direct detection of bacterial biofilms on the middle-ear mucosa of children with chronic otitis media. JAMA. 2006 Jul 12;296(2):202–11.

239. Murphy TF, Kirkham C, Sethi S, Lesse AJ. Expression of a peroxiredoxin-glutaredoxin by *Haemophilus influenzae* in biofilms and during human respiratory tract infection. FEMS Immunol Med Microbiol. 2005 Apr 1;44(1):81–9.

240. Obaid NA, Jacobson GA, Tristram S. Relationship between clinical site of isolation and ability to form biofilms in vitro in *nontypeable Haemophilus influenzae*. Can J Microbiol. 2015 Mar;61(3):243–5.

241. Unal CM, Singh B, Fleury C, Singh K, Chávez de Paz L, Svensäter G, Riesbeck K, Ünal CM, Singh B, Fleury C, Singh K, Chávez de Paz L, Svensäter G, Riesbeck K. QseC controls biofilm formation of non-typeable *Haemophilus influenzae* in addition to an AI-2-dependent mechanism. Int J Med Microbiol. 2012 Nov;302(6):261–9.

242. Caly D, Bellini D. Targeting Cyclic di-GMP Signalling: A Strategy to Control Biofilm Formation? Curr Pharm Des. 2015;21(1):12–24.

243. Chou S-H, Galperin MY. Diversity of c-di-GMP-binding proteins and mechanisms. J Bacteriol. 2015 Jun 8;

244. Cho C, Chande A, Gakhar L, Bakaletz LO, Jurcisek JA, Ketterer M, Shao J, Gotoh K, Foster E, Hunt J, O'Brien E, Apicella MA. Role of the nuclease of *nontypeable Haemophilus influenzae* in dispersal of organisms from biofilms. Infect Immun. 2015 Mar;83(3):950–7.

245. Zhang B, Xu C, Zhou S, Feng S, Zhang L, He Y, Liao M. Comparative proteomic analysis of a *Haemophilus parasuis* SC096 mutant deficient in the outer membrane protein P5. Microb Pathog. 2012 Feb;52(2):117–24.

246. Vogel AR, Szelestey BR, Raffel FK, Sharpe SW, Gearinger RL, Justice SS, Mason KM. SapF-mediated heme-iron utilization enhances persistence and coordinates biofilm architecture of *Haemophilus*. Front Cell Infect Microbiol. 2012 Jan;2(April):42.

247. Harrison A, Santana EA, Szelestey BR, Newsom DE, White P, Mason KM. Ferric uptake regulator and its role in the pathogenesis of *nontypeable haemophilus influenzae*. Infect Immun. 2013 Apr;81(4):1221–33.

248. Pang B, Hong W, Kock ND, Swords WE. Dps promotes survival of *nontypeable Haemophilus influenzae* in biofilm communities in vitro and resistance to clearance in vivo. Front Cell Infect Microbiol. 2012 Jan;2:58.

249. Bogdan C. Nitric oxide synthase in innate and adaptive immunity: an update. Trends Immunol. 2015 Feb;36(3):161–78.

250. Hussain R, Oliynyk I, Roomans GM, Björkqvist M. Modulation of ENaC, CFTR, and iNOS expression in bronchial epithelial cells after stimulation with *Staphylococcus epidermidis* (94B080) and *Staphylococcus aureus* (90B083). APMIS. 2013 Sep;121(9):814–26.

251. Bogdan C. Regulation of Lymphocytes by Nitric Oxide. In: Cuturi MC, Anegon I, editors. Suppression and Regulation of Immune Responses SE - 24. Humana Press; 2011. p. 375–93. (Methods in Molecular Biology; vol. 677).

252. Jyoti A, Singh AK, Dubey M, Kumar S, Saluja R, Keshari RS, Verma A, Chandra T, Kumar A, Bajpai VK, Barthwal MK, Dikshit M. Interaction of inducible nitric oxide synthase with rac2 regulates reactive oxygen and nitrogen species generation in the human neutrophil phagosomes: implication in microbial killing. Antioxid Redox Signal. 2014 Jan 20;20(3):417–31.

253. Serbina N V, Salazar-Mather TP, Biron C a, Kuziel W a, Pamer EG. TNF/iNOS-producing dendritic cells mediate innate immune defense against bacterial infection. Immunity. 2003 Jul;19(1):59–70.

254. Barraud N, Kelso M, Rice S, Kjelleberg S. Nitric Oxide: A Key Mediator of Biofilm Dispersal with Applications in Infectious Diseases. Curr Pharm Des. 2014;21(1):31–42.

255. Bove PF, van der Vliet A. Nitric oxide and reactive nitrogen species in airway epithelial signaling and inflammation. Free Radic Biol Med. 2006 Aug 15;41(4):515–27.

256. Furchgott RF, Zawadzki J V. The obligatory role of endothelial cells in the relaxation of arterial smooth muscle by acetylcholine. Nature. 1980 Nov 27;288(5789):373–6.

257. Palmer RM, Ferrige AG, Moncada S. Nitric oxide release accounts for the biological activity of endothelium-derived relaxing factor. Nature. Jan;327(6122):524–6.

258. Pepke-Zaba J, Higenbottam TW, Dinh-Xuan AT, Stone D, Wallwork J. Inhaled nitric oxide as a cause of selective pulmonary vasodilatation in pulmonary hypertension. Lancet. 1991 Nov 9;338(8776):1173–4.

259. Belvisi MG, Stretton CD, Yacoub M, Barnes PJ. Nitric oxide is the endogenous neurotransmitter of bronchodilator nerves in humans. Eur J Pharmacol. 1992 Jan 14;210(2):221–2.

260. Ricciardolo FLM, Sterk PJ, Gaston B, Folkerts G. Nitric oxide in health and disease of the respiratory system. Physiol Rev. 2004 Jul 1;84(3):731–65.

261. Jiang J, Malavia N, Suresh V, George SC. Nitric oxide gas phase release in human small airway epithelial cells. Respir Res. 2009 Jan;10:3.

262. Lane C, Knight D, Burgess S, Franklin P, Horak F, Legg J, Moeller A, Stick S. Epithelial inducible nitric oxide synthase activity is the major determinant of nitric oxide concentration in exhaled breath. Thorax. 2004 Sep 1;59(9):757–60.

263. Gross TJ, Kremens K, Powers LS, Brink B, Knutson T, Domann FE, Philibert RA, Milhem MM, Monick MM. Epigenetic silencing of the human NOS2 gene: rethinking the role of nitric oxide in human macrophage inflammatory responses. J Immunol. 2014 Mar 1;192(5):2326–38.

264. Thoma-Uszynski S, Stenger S, Takeuchi O, Ochoa MT, Engele M, Sieling PA, Barnes PF, Rollinghoff M, Bolcskei PL, Wagner M, Akira S, Norgard M V, Belisle JT, Godowski PJ, Bloom BR, Modlin RL. Induction of direct antimicrobial activity through mammalian toll-like receptors. Science. 2001 Feb 23;291(5508):1544–7.

265. Thomassen MJ, Buhrow LT, Connors MJ, Kaneko FT, Erzurum SC, Kavuru MS. Nitric oxide inhibits inflammatory cytokine production by human alveolar macrophages. Am J Respir Cell Mol Biol. 1997 Sep;17(3):279–83.

266. Walker WT, Liew A, Harris A, Cole J, Lucas JS. Upper and lower airway nitric oxide levels in primary ciliary dyskinesia, cystic fibrosis and asthma. Respir Med. 2013 Mar;107(3):380–6.

267. Darling KEA, Evans TJ. Effects of Nitric Oxide on *Pseudomonas aeruginosa* Infection of Epithelial Cells from a Human Respiratory Cell Line Derived from a Patient with Cystic Fibrosis. Infect Immun. 2003 May 1;71(5):2341–9.

268. Jain B, Rubinstein I, Robbins RA, Leise KL, Sisson JH. Modulation of airway epithelial cell ciliary beat frequency by nitric oxide. Biochem Biophys Res Commun. 1993 Feb 26;191(1):83–8.

269. Lucas JS, Adam EC, Goggin PM, Jackson CL, Powles-Glover N, Patel SH, Humphreys J, Fray MD, Falconnet E, Blouin J-L, Cheeseman MT, Bartoloni L, Norris DP, Lackie PM. Static respiratory cilia associated with mutations in Dnahc11/DNAH11: a mouse model of PCD. Hum Mutat. 2012 Mar;33(3):495–503.

270. Adler KB, Fischer BM, Li H, Choe NH, Wright DT. Hypersecretion of mucin in response to

inflammatory mediators by guinea pig tracheal epithelial cells in vitro is blocked by inhibition of nitric oxide synthase. Am J Respir Cell Mol Biol. 1995 Nov;13(5):526–30.

271. Duszyk M, Radomski MW. The role of nitric oxide in the regulation of ion channels in airway epithelium: implications for diseases of the lung. Free Radic Res. 2000 Nov;33(5):449–59.

272. Grasemann H, Al-Saleh S, Scott JA, Shehnaz D, Mehl A, Amin R, Rafii M, Pencharz P, Belik J, Ratjen F. Asymmetric dimethylarginine contributes to airway nitric oxide deficiency in patients with cystic fibrosis. Am J Respir Crit Care Med. 2011 May 15;183(10):1363–8.

273. Marozkina N V, Yemen S, Borowitz M, Liu L, Plapp M, Sun F, Islam R, Erdmann-Gilmore P, Townsend RR, Lichti CF, Mantri S, Clapp PW, Randell SH, Gaston B, Zaman K. Hsp 70/Hsp 90 organizing protein as a nitrosylation target in cystic fibrosis therapy. Proc Natl Acad Sci U S A. 2010 Jun 22;107(25):11393–8.

274. Wells SM, Holian A. Asymmetric dimethylarginine induces oxidative and nitrosative stress in murine lung epithelial cells. Am J Respir Cell Mol Biol. 2007 May;36(5):520–8.

275. Fang FC. Antimicrobial reactive oxygen and nitrogen species: concepts and controversies. Nat Rev Microbiol. 2004 Oct;2(10):820–32.

276. Cusumano ZT, Watson ME, Caparon MG. *Streptococcus pyogenes* arginine and citrulline catabolism promotes infection and modulates innate immunity. Infect Immun. 2014 Jan 1;82(1):233–42.

277. Grasemann H, Schwiertz R, Grasemann C, Vester U, Racké K, Ratjen F. Decreased systemic bioavailability of L-arginine in patients with cystic fibrosis. Respir Res. 2006 Jan;7:87.

278. Grasemann H, Waters V, McDonald N, Yay Y, Dell S, Ratjen F. Differences in airway inflammation between children with primary ciliary dyskinesia (PCD) and cystic fibrosis (CF). Eur Respir J. 2014;44: Suppl.(58):1207.

279. Allan RN, Morgan S, Brito-Mutunayagam S, Skipp P, Feelisch M, Hayes SM, Hellier W, Clarke SC, Stoodley P, Burgess A, Ismail-Koch H, Salib RJ, Webb JS, Faust SN, Hall-Stoodley L. Low concentrations of nitric oxide modulate *Streptococcus pneumoniae* biofilm metabolism and antibiotic tolerance. Antimicrob Agents Chemother. 2016 Feb 8;AAC.02432-15-.

280. Lindberg S, And AC, Runer T. Nitric Oxide (NO) Production in the Upper Airways is Decreased in Chronic Sinusitis. Acta Otolaryngol. 2009 Jul 8;117(1):113–7.

281. Jardeleza C, Thierry B, Rao S, Rajiv S, Drilling A, Miljkovic D, Paramasivan S, James C, Dong D, Thomas N, Vreugde S, Prestidge CA, Wormald P-J. An in vivo safety and efficacy demonstration of a topical liposomal nitric oxide donor treatment for *Staphylococcus aureus* biofilm-associated rhinosinusitis. Transl Res. 2015 Dec;166(6):683–92.

282. Cathie K, Howlin R, Carroll M, Clarke S, Connett G, Cornelius V, Daniels T, Duignan C, Hall-Stoodley L, Jefferies J, Kelso M, Kjelleberg S, Legg J, Pink S, Rogers G, Salib R, Stoodley P, Sukhtankar P, Webb J, Faust S. G385 RATNO - Reducing Antibiotic Tolerance using Nitric Oxide in Cystic Fibrosis: report of a proof of concept clinical trial. Arch Dis Child. 2014 Apr 1;99(Suppl 1):A159–A159.

283. Barbato a, Frischer T, Kuehni CE, Snijders D, Azevedo I, Baktai G, Bartoloni L, Eber E, Escribano A, Haarman E, Hesselmar B, Hogg C, Jorissen M, Lucas J, Nielsen KG, O'Callaghan C, Omran H, Pohunek P, Strippoli M-PF, Bush A. Primary ciliary dyskinesia: a consensus statement on diagnostic and treatment approaches in children. Eur Respir J. 2009 Dec;34(6):1264–76.

284. Gaston B, Ratjen F, Vaughan JW, Malhotra NR, Canady RG, Snyder AH, Hunt JF, Gaertig S, Goldberg JB. Nitrogen redox balance in the cystic fibrosis airway: effects of antipseudomonal therapy. Am J Respir Crit Care Med. 2002 Feb 1;165(3):387–90.

285. Grasemann H, Gärtig SS, Wiesemann HG, Teschler H, Konietzko N, Ratjen F. Effect of L-arginine infusion on airway NO in cystic fibrosis and primary ciliary dyskinesia syndrome. Eur Respir J. 1999 Jan;13(1):114–8.

286. Narang I, Ersu R, Wilson N, Bush A. Nitric oxide in chronic airway inflammation in children: diagnostic use and pathophysiological significance. Thorax. 2002 Jul;57(7):586–9.

287. Degano B, Valmary S, Serrano E, Brousset P, Arnal J-F. Expression of nitric oxide synthases in primary ciliary dyskinesia. Hum Pathol. 2011 Dec;42(12):1855–61.

288. Paraskakis E, Zihlif N, Bush A. Nitric oxide production in PCD: possible evidence for differential nitric oxide synthase function. Pediatr Pulmonol. 2007 Oct;42(10):876–80.

289. Shoemark A, Wilson R. Bronchial and peripheral airway nitric oxide in primary ciliary

dyskinesia and bronchiectasis. Respir Med. 2009 May;103(5):700–6.

290. Mahut B, Escudier E, de Blic J, Zerah-Lancner F, Coste A, Harf A, Delclaux C. Impairment of nitric oxide output of conducting airways in primary ciliary dyskinesia. Pediatr Pulmonol. 2006 Feb;41(2):158–63.

291. Pezzulo AA, Starner TD, Scheetz TE, Traver GL, Tilley AE, Harvey B-G, Crystal RG, McCray PB, Zabner J. The air-liquid interface and use of primary cell cultures are important to recapitulate the transcriptional profile of in vivo airway epithelia. AJP Lung Cell Mol Physiol. 2010 Oct 22;300(1):L25–31.

292. Dvorak A, Tilley AE, Shaykhiev R, Wang R, Crystal RG. Do Airway Epithelium Air–Liquid Cultures Represent the In Vivo Airway Epithelium Transcriptome? 2012 Dec 20;

293. Thavagnanam S, Parker JC, McBrien ME, Skibinski G, Shields MD, Heaney LG. Nasal epithelial cells can act as a physiological surrogate for paediatric asthma studies. PLoS One. 2014 Jan;9(1):e85802.

294. Lopez-Guisa JM, Powers C, File D, Cochrane E, Jimenez N, Debley JS. Airway epithelial cells from asthmatic children differentially express proremodeling factors. J Allergy Clin Immunol. 2012 Apr;129(4):990–7.e6.

295. Klose J. Protein mapping by combined isoelectric focusing and electrophoresis of mouse tissues. A novel approach to testing for induced point mutations in mammals. Humangenetik. 1975 Jan;26(3):231–43.

296. Cravatt BF, Simon GM, Yates JR. The biological impact of mass-spectrometry-based proteomics. Nature. 2007 Dec 13;450(7172):991–1000.

297. Otto A, Becher D, Schmidt F. Quantitative proteomics in the field of microbiology. Proteomics. 2014 Mar;14(4–5):547–65.

298. Qu B-H, Strickland EH, Thomas PJ. Localization and Suppression of a Kinetic Defect in Cystic Fibrosis Transmembrane Conductance Regulator Folding. J Biol Chem. 1997 Jun 20;272(25):15739–44.

299. Wang X, Venable J, LaPointe P, Hutt DM, Koulov A V, Coppinger J, Gurkan C, Kellner W, Matteson J, Plutner H, Riordan JR, Kelly JW, Yates JR, Balch WE. Hsp90 cochaperone Aha1 downregulation rescues misfolding of CFTR in cystic fibrosis. Cell. 2006 Nov 17;127(4):803–15.

300. Wiese S, Reidegeld KA, Meyer HE, Warscheid B. Protein labeling by iTRAQ: a new tool for quantitative mass spectrometry in proteome research. Proteomics. 2007 Feb;7(3):340–50.

301. Megger DA, Bracht T, Meyer HE, Sitek B. Label-free quantification in clinical proteomics. Biochim Biophys Acta. 2013 Aug;1834(8):1581–90.

302. McShane AJ, Bajrami B, Ramos AA, Diego-Limpin PA, Farrokhi V, Coutermarsh BA, Stanton BA, Jensen T, Riordan JR, Wetmore D, Joseloff E, Yao X. Targeted proteomic quantitation of the absolute expression and turnover of cystic fibrosis transmembrane conductance regulator in the apical plasma membrane. J Proteome Res. 2014 Nov 7;13(11):4676–85.

303. Hare NJ, Solis N, Harmer C, Marzook NB, Rose B, Harbour C, Crossett B, Manos J, Cordwell SJ. Proteomic profiling of *Pseudomonas aeruginosa* AES-1R, PAO1 and PA14 reveals potential virulence determinants associated with a transmissible cystic fibrosis-associated strain. BMC Microbiol. 2012 Jan;12:16.

304. Rath T, Hage L, Kügler M, Menendez Menendez K, Zachoval R, Naehrlich L, Schulz R, Roderfeld M, Roeb E. Serum proteome profiling identifies novel and powerful markers of cystic fibrosis liver disease. PLoS One. 2013 Jan;8(3):e58955.

305. Ciavardelli D, D'Orazio M, Pieroni L, Consalvo A, Rossi C, Sacchetta P, Di Ilio C, Battistoni A, Urbani A. Proteomic and ionomic profiling reveals significant alterations of protein expression and calcium homeostasis in cystic fibrosis cells. Mol Biosyst. 2013 Jun;9(6):1117–26.

306. Pankow S, Bamberger C, Calzolari D, Martínez-Bartolomé S, Lavallée-Adam M, Balch WE, Yates JR. ΔF508 CFTR interactome remodelling promotes rescue of cystic fibrosis. Nature. 2015 Nov 30;528(7583):510–6.

307. Peters-Hall JR, Brown KJ, Pillai DK, Tomney A, Garvin LM, Wu X, Rose MC. Quantitative Proteomics Reveals an Altered Cystic Fibrosis In Vitro Bronchial Epithelial Secretome. Am J Respir Cell Mol Biol. 2015 Feb 18;

308. Balch WE, Yates JR. Application of mass spectrometry to study proteomics and interactomics in cystic fibrosis. Methods Mol Biol. 2011 Jan;742:227–47.

309. Post D, Held JM, Ketterer MR, Phillips NJ, Sahu A, Apicella MA, Gibson BW. Comparative

analyses of proteins from *Haemophilus influenzae* biofilm and planktonic populations using metabolic labeling and mass spectrometry. BMC Microbiol. 2014;14(1):329.

310. Qu J, Lesse AJ, Brauer AL, Cao J, Gill SR, Murphy TF. Proteomic expression profiling of *Haemophilus influenzae* grown in pooled human sputum from adults with chronic obstructive pulmonary disease reveal antioxidant and stress responses. BMC Microbiol. 2010 Jan;10:162.

311. Preciado D, Poley M, Tsai S, Tomney A, Brown K, Val S. A proteomic characterization of NTHi lysates. Int J Pediatr Otorhinolaryngol. 2016 Jan;80:8–16.

312. Wu S, Baum MM, Kerwin J, Guerrero D, Webster S, Schaudinn C, VanderVelde D, Webster P. Biofilm-specific extracellular matrix proteins of *nontypeable Haemophilus influenzae*. Pathog Dis. 2014 Dec 1;72(3):143–60.

313. Das S, Rosas LE, Jurcisek JA, Novotny LA, Green KB, Bakaletz LO. Improving patient care via development of a protein-based diagnostic test for microbe-specific detection of chronic rhinosinusitis. Laryngoscope. 2014 Mar;124(3):608–15.

314. Harrison A, Dubois LG, St. John-Williams L, Moseley MA, Hardison RL, Heimlich DR, Stoddard A, Kerschner JE, Justice SS, Thompson JW, Mason KM. Comprehensive Proteomic and Metabolomic Signatures of *Nontypeable Haemophilus influenzae*-Induced Acute Otitis Media Reveal Bacterial Aerobic Respiration in an Immunosuppressed Environment. Mol Cell Proteomics. 2016;15(3):1117–38.

315. Val S, Burgett K, Brown KJ, Preciado D. SuperSILAC Quantitative Proteome Profiling of Murine Middle Ear Epithelial Cell Remodeling with NTHi. PLoS One. 2016;11(2):e0148612.

316. Preciado D, Burgett K, Ghimbovschi S, Rose M. NTHi induction of Cxcl2 and middle ear mucosal metaplasia in mice. Laryngoscope. 2013 Nov;123(11):E66-71.

317. Obaid NA, Tristram S, Narkowicz CK, Jacobson GA. Reliability of *Haemophilus influenzae* biofilm measurement via static method, and determinants of in vitro biofilm production. Can J Microbiol. 2016 Jul 20;1–8.

318. Givskov M, Hentzer M, Ersbøll BK, Heydorn A, Sternberg C, Nielsen AT, Molin S. Quantification of biofilm structures by the novel computer program comstat. Microbiology. 2000 Oct 1;146(10):2395–407.

319. COMSTAT 2.1 [Internet]. Technical University of Denmark; 2016 [cited 2016 Oct 31].

Available from: www.comstat.dk

320. Denker BM, Nigam SK. Molecular structure and assembly of the tight junction. Am J Physiol. 1998 Jan;274(1 Pt 2):F1-9.

321. Jackson CL, Behan L, Collins SA, Goggin PM, Adam EC, Coles JL, Evans HJ, Harris A, Lackie P, Packham S, Page A, Thompson J, Walker WT, Kuehni C, Lucas JS. Accuracy of diagnostic testing in primary ciliary dyskinesia. Eur Respir J. 2016 Dec 2;47(3):837–48.

322. Hirst RA, Jackson CL, Coles JL, Williams G, Rutman A, Goggin PM, Adam EC, Page A, Evans HJ, Lackie PM, O'Callaghan C, Lucas JS. Culture of Primary Ciliary Dyskinesia Epithelial Cells at Air-Liquid Interface Can Alter Ciliary Phenotype but Remains a Robust and Informative Diagnostic Aid. PLoS One. 2014 Feb;9(2):e89675.

323. Shevchenko A, Tomas H, Havlis J, Olsen J V, Mann M. In-gel digestion for mass spectrometric characterization of proteins and proteomes. Nat Protoc. 2006;1(6):2856–60.

324. UniProt Consortium TU. UniProt: a hub for protein information. Nucleic Acids Res. 2015 Jan;43(Database issue):D204-12.

325. Benjamini Y, Hochberg Y. Controlling the False Discovery Rate: A Practical and Powerful Approach to Multiple Testing. J R Stat Soc Ser B. 1995;57(1):289–300.

326. Szklarczyk D, Franceschini A, Wyder S, Forslund K, Heller D, Huerta-Cepas J, Simonovic M, Roth A, Santos A, Tsafou KP, Kuhn M, Bork P, Jensen LJ, von Mering C. STRING v10: protein-protein interaction networks, integrated over the tree of life. Nucleic Acids Res. 2015 Jan;43(Database issue):D447-52.

327. Ashburner M, Ball CA, Blake JA, Botstein D, Butler H, Cherry JM, Davis AP, Dolinski K, Dwight SS, Eppig JT, Harris MA, Hill DP, Issel-Tarver L, Kasarskis A, Lewis S, Matese JC, Richardson JE, Ringwald M, Rubin GM, Sherlock G. Gene Ontology: tool for the unification of biology. Nat Genet. 2000 May;25(1):25–9.

328. Gene Ontology Consortium TGO. Gene Ontology Consortium: going forward. Nucleic Acids Res. 2015 Jan;43(Database issue):D1049-56.

329. Mi H, Poudel S, Muruganujan A, Casagrande JT, Thomas PD. PANTHER version 10: expanded protein families and functions, and analysis tools. Nucleic Acids Res. 2016 Jan

4;44(D1):D336-42.

330. Mi H, Muruganujan A, Casagrande JT, Thomas PD. Large-scale gene function analysis with the PANTHER classification system. Nat Protoc. 2013 Aug;8(8):1551–66.

331. Kanehisa M, Goto S. KEGG: kyoto encyclopedia of genes and genomes. Nucleic Acids Res. 2000 Jan 1;28(1):27–30.

332. Kanehisa M, Sato Y, Kawashima M, Furumichi M, Tanabe M. KEGG as a reference resource for gene and protein annotation. Nucleic Acids Res. 2016 Jan 4;44(D1):D457-62.

333. Mitchell A, Chang H-Y, Daugherty L, Fraser M, Hunter S, Lopez R, McAnulla C, McMenamin C, Nuka G, Pesseat S, Sangrador-Vegas A, Scheremetjew M, Rato C, Yong S-Y, Bateman A, Punta M, Attwood TK, Sigrist CJA, Redaschi N, Rivoire C, Xenarios I, Kahn D, Guyot D, Bork P, Letunic I, Gough J, Oates M, Haft D, Huang H, Natale DA, Wu CH, Orengo C, Sillitoe I, Mi H, Thomas PD, Finn RD. The InterPro protein families database: the classification resource after 15 years. Nucleic Acids Res. 2015 Jan;43(Database issue):D213-21.

334. Csoma Z, Bush A. Nitric oxide metabolites are not reduced in exhaled breath condensate of patients with primary ciliary dyskinesia. Chest. 2003 Aug;124(2):633–8.

335. ATS/ERS recommendations for standardized procedures for the online and offline measurement of exhaled lower respiratory nitric oxide and nasal nitric oxide, 2005. Am J Respir Crit Care Med. 2005 Apr 15;171(8):912–30.

336. Whiting P, Rutjes AWS, Reitsma JB, Bossuyt PMM, Kleijnen J. The development of QUADAS: a tool for the quality assessment of studies of diagnostic accuracy included in systematic reviews. BMC Med Res Methodol. 2003 Nov 10;3(1):25.

337. Moher D, Liberati A, Tetzlaff J, Altman DG. Preferred reporting items for systematic reviews and meta-analyses: the PRISMA statement. PLoS Med. 2009 Jul 21;6(7):b2535.

338. Harrison M, Barry J, Burke L, Dinneen S, Murphy D, Henry M, Plant B, Kennedy MP. The clinical utility of a hand-held nasal nitric oxide (NNO) electrochemical analyser to screen patients with bronchiectasis for primary ciliary dyskinesia (PCD) and cystic fibrosis (CF). Ir J Med Sci. 2012 Nov 4;181(S10):S403–4.

339. Corbelli R, Bringolf-Isler B, Amacher A, Sasse B, Spycher M, Hammer J. Nasal nitric oxide measurements to screen children for primary ciliary dyskinesia. Chest. 2004

Oct;126(4):1054–9.

340. Piacentini GL, Bodini A, Peroni D, Rigotti E, Pigozzi R, Pradal U, Boner AL. Nasal nitric oxide for early diagnosis of primary ciliary dyskinesia: practical issues in children. Respir Med. 2008 Apr;102(4):541–7.

341. Moreno Galdó A, Vizmanos Lamotte G, Reverte Bover C, Gartner S, Cobos Barroso N, Rovira Amigo S, Liñán Cortés S, Lloreta Trull J, Busquets Monge R, Moreno Galdo A, Vizmanos Lamotte G, Reverte Bover C, Gartner S, Cobos Barroso N, Rovira Amigo S, Linan Cortes S, Lloreta Trull J, Busquets Monge R, Moreno Galdó A, Vizmanos Lamotte G, Reverte Bover C, Gartner S, Cobos Barroso N, Rovira Amigo S, Liñán Cortés S, Lloreta Trull J, Busquets Monge R. [Value of nasal nitric oxide in the diagnosis of primary ciliary dyskinesia]. An Pediatr (Barc). 2010 Aug;73(2):88–93.

342. Mateos-Corral D, Coombs R, Grasemann H, Ratjen F, Dell SD. Diagnostic value of nasal nitric oxide measured with non-velum closure techniques for children with primary ciliary dyskinesia. J Pediatr. 2011 Sep;159(3):420–4.

343. Karadag B, James a J, Gültekin E, Wilson NM, Bush a. Nasal and lower airway level of nitric oxide in children with primary ciliary dyskinesia. Eur Respir J. 1999 Jun;13(6):1402–5.

344. Horváth I, Loukides S, Wodehouse T, Csiszér E, Cole PJ, Kharitonov S a, Barnes PJ. Comparison of exhaled and nasal nitric oxide and exhaled carbon monoxide levels in bronchiectatic patients with and without primary ciliary dyskinesia. Thorax. 2003 Jan;58(1):68–72.

345. Santamaria F, De Stefano S, Montella S, Barbarano F, Iacotucci P, Ciccarelli R, Sofia M, Maniscalco M. Nasal nitric oxide assessment in primary ciliary dyskinesia using aspiration, exhalation, and humming. Med Sci Monit. 2008 Feb;14(2):CR80-85.

346. Boon M, Meyts I, Proesmans M, Vermeulen FL, Jorissen M, De Boeck K. Diagnostic accuracy of nitric oxide measurements to detect Primary Ciliary Dyskinesia. Eur J Clin Invest. 2014 Mar 5;

347. Harris A, Bhullar E, Gove K, Joslin R, Pelling J, Evans HJ, Walker WT, Lucas JS. Validation of a portable nitric oxide analyzer for screening in primary ciliary dyskinesias. BMC Pulm Med. 2014;14(1):18.

348. Pifferi M, Bush A, Maggi F, Michelucci A, Ricci V, Conidi ME, Cangiotti AM, Bodini A, Simi P, Macchia P, Boner AL. Nasal nitric oxide and nitric oxide synthase expression in primary ciliary dyskinesia. Eur Respir J. 2011 Mar;37(3):572–7.

349. Pifferi M, Caramella D, Cangiotti AM, Ragazzo V, Macchia P, Boner AL. Nasal Nitric Oxide in Atypical Primary Ciliary Dyskinesia. Chest. 2007 Mar;131(3):870–3.

350. Piacentini GL, Bodini A, Peroni DG, Sandri M, Brunelli M, Pigozzi R, Boner AL. Nasal nitric oxide levels in healthy pre-school children. Pediatr Allergy Immunol. 2010 Dec;21(8):1139–45.

351. Maniscalco M, Weitzberg E, Sundberg J, Sofia M, Lundberg JO. Assessment of nasal and sinus nitric oxide output using single-breath humming exhalations. Eur Respir J. 2003 Aug 1;22(2):323–9.

352. Montella S, Alving K, Maniscalco M, Sofia M, De Stefano S, Raia V, Santamaria F. Measurement of nasal nitric oxide by hand-held and stationary devices. Eur J Clin Invest. 2011 Oct;41(10):1063–70.

353. Struben VMD, Wieringa MH, Mantingh CJ, Bommeljé C, Don M, Feenstra L, de Jongste JC. Nasal NO: normal values in children age 6 through to 17 years. Eur Respir J. 2005 Sep;26(3):453–7.

354. Baraldi E, Pasquale MF, Cangiotti AM, Zanconato S, Zacchello F. Nasal nitric oxide is low early in life: case study of two infants with primary ciliary dyskinesia. Eur Respir J. 2004 Nov;24(5):881–3.

355. Stehling F, Roll C, Ratjen F, Grasemann H. Nasal nitric oxide to diagnose primary ciliary dyskinesia in newborns. Arch Dis Child Fetal Neonatal Ed. 2006 May;91(3):F233.

356. Alsaadi MM, Habib SS, Al Muqhem BA, Aldrees A, Al Zamil JF, Alsadoon HA. Significance of fractional exhaled nitric oxide measurements in detecting primary ciliary dyskinesia in Saudi children. Saudi Med J. 2013 Jan;34(1):24–8.

357. Lundberg J, Nordvall S. Exhaled nitric oxide in paediatric asthma and cystic fibrosis. … Dis Child. 1996 Oct;75(4):323–6.

358. Franklin PJ, Hall GL, Moeller A, Horak F, Brennan S, Stick SM. Exhaled nitric oxide is not reduced in infants with cystic fibrosis. Eur Respir J. 2006 Feb;27(2):350–3.

359. Moeller A, Horak F, Lane C, Knight D, Kicic A, Brennan S, Franklin P, Terpolilli J,

Wildhaber JH, Stick SM. Inducible NO synthase expression is low in airway epithelium from young children with cystic fibrosis. Thorax. 2006 Jun;61(6):514–20.

360. Grasemann H, Ratjen F. Cystic fibrosis lung disease: The role of nitric oxide. Pediatr Pulmonol. 1999 Dec;28(6):442–8.

361. Zuckerbraun BS, George P, Gladwin MT. Nitrite in pulmonary arterial hypertension: therapeutic avenues in the setting of dysregulated arginine/nitric oxide synthase signalling. Cardiovasc Res. 2011 Feb 15;89(3):542–52.

362. Hunter CJ, Dejam A, Blood AB, Shields H, Kim-Shapiro DB, Machado RF, Tarekegn S, Mulla N, Hopper AO, Schechter AN, Power GG, Gladwin MT. Inhaled nebulized nitrite is a hypoxia-sensitive NO-dependent selective pulmonary vasodilator. Nat Med. 2004 Oct 12;10(10):1122–7.

363. Clutton-Brock J. Two cases of poisoning by contamination of nitrous oxide with higher oxides of nitrogen during anaesthesia. Br J Anaesth. 1967 May;39(5):388–92.

364. Yepuri NR, Barraud N, Mohammadi NS, Kardak BG, Kjelleberg S, Rice SA, Kelso MJ. Synthesis of cephalosporin-3'-diazeniumdiolates: biofilm dispersing NO-donor prodrugs activated by β-lactamase. Chem Commun (Camb). 2013 May 25;49(42):4791–3.

365. Roberts MC, Soge OO, No DB. Characterization of macrolide resistance genes in *Haemophilus influenzae* isolated from children with cystic fibrosis. J Antimicrob Chemother. 2011;66(1):100–4.

366. Starner TD, Shrout JD, Parsek MR, Appelbaum PC, Kim G. Subinhibitory Concentrations of Azithromycin Decrease *Nontypeable Haemophilus influenzae* Biofilm Formation and Diminish Established Biofilms. Antimicrob Agents Chemother. 2008 Jan 1;52(1):137–45.

367. García-Cobos S, Moscoso M, Pumarola F, Arroyo M, Lara N, Pérez-Vázquez M, Aracil B, Oteo J, García E, Campos J. Frequent carriage of resistance mechanisms to β-lactams and biofilm formation in *Haemophilus influenzae* causing treatment failure and recurrent otitis media in young children. J Antimicrob Chemother. 2014 Sep;69(9):2394–9.

368. Keefer LK, Nims RW, Davies KM, Wink DA. "NONOates" (1-substituted diazen-1-ium-1,2-diolates) as nitric oxide donors: convenient nitric oxide dosage forms. Methods Enzymol. 1996;268:281–93.

369. Parnham MJ, Erakovic Haber V, Giamarellos-Bourboulis EJ, Perletti G, Verleden GM, Vos R. Azithromycin: mechanisms of action and their relevance for clinical applications. Pharmacol Ther. 2014 Aug;143(2):225–45.

370. Margolis E, Yates A, Levin BR. The ecology of nasal colonization of *Streptococcus pneumoniae*, *Haemophilus influenzae* and *Staphylococcus aureus*: the role of competition and interactions with host's immune response. BMC Microbiol. 2010 Jan;10:59.

371. Hoyle BD, Costerton JW. Bacterial resistance to antibiotics: the role of biofilms. Prog drug Res Fortschritte der Arzneimittelforschung Progrès des Rech Pharm. 1991;37:91–105.

372. Olsen KM, San Pedro G, Gann LP, Gubbins PO, Halinski DM, Campbell GD. Intrapulmonary pharmacokinetics of azithromycin in healthy volunteers given five oral doses. Antimicrob Agents Chemother. 1996 Nov;40(11):2582–5.

373. Wu S, Li X, Gunawardana M, Maguire K, Guerrero-Given D, Schaudinn C, Wang C, Baum MM, Webster P. Beta- Lactam Antibiotics Stimulate Biofilm Formation in Non-Typeable *Haemophilus influenzae* by Up-Regulating Carbohydrate Metabolism. PLoS One. 2014 Jan;9(7):e99204.

374. Mart'ianov S V, Zhurina M V, Él'-Registan GI, Plakunov VK. [Activation of formation of bacterial biofilms by azithromycin and prevention of this effect]. Mikrobiologiia. 84(1):27–36.

375. Aka ST, Haji SH. Sub-MIC of antibiotics induced biofilm formation of *Pseudomonas aeruginosa* in the presence of chlorhexidine. Braz J Microbiol. 2015 Mar;46(1):149–54.

376. Keefer L. Nitric Oxide (NO)- and Nitroxyl (HNO)-Generating Diazeniumdiolates (NONOates): Emerging Commercial Opportunities. Curr Top Med Chem. 2005 Jul 1;5(7):625–36.

377. Hong F, Wang Y, Liu H, Yang M, Yang S. V-PYRRO/NO downregulates mRNA expression levels of leukotriene C4 synthase during hepatic ischemia reperfusion injury in rats via inhibition of the nuclear factor-κB activation pathway. Biomed Reports. 2015 Oct 16;112–6.

378. Hrabie JA, Klose JR, Wink DA, Keefer LK. New nitric oxide-releasing zwitterions derived from polyamines. J Org Chem. 1993 Mar 1;58(6):1472–6.

379. Keefer LK. Fifty years of diazeniumdiolate research. From laboratory curiosity to broad-spectrum biomedical advances. ACS Chem Biol. 2011 Nov 18;6(11):1147–55.

380. Ban N, Nissen P, Hansen J, Moore PB, Steitz TA. The complete atomic structure of the large ribosomal subunit at 2.4 A resolution. Science. 2000 Aug 11;289(5481):905–20.

381. Grossi L, D'Angelo S. Sodium Nitroprusside: Mechanism of NO Release Mediated by Sulfhydryl-Containing Molecules. J Med Chem. 2005 Apr;48(7):2622–6.

382. Allan RN, Skipp P, Jefferies J, Clarke SC, Faust SN, Hall-Stoodley L, Webb J. Pronounced metabolic changes in adaptation to biofilm growth by *Streptococcus pneumoniae*. PLoS One. 2014 Jan;9(9):e107015.

383. Wilson DN. Ribosome-targeting antibiotics and mechanisms of bacterial resistance. Nat Rev Micro. 2014 Jan;12(1):35–48.

384. Jurcisek J, Greiner L, Watanabe H, Zaleski A, Apicella MA, Bakaletz LO. Role of sialic acid and complex carbohydrate biosynthesis in biofilm formation by *nontypeable Haemophilus influenzae* in the chinchilla middle ear. Infect Immun. 2005 Jun;73(6):3210–8.

385. Murphy TF, Kirkham C. Biofilm formation by *nontypeable Haemophilus influenzae*: strain variability, outer membrane antigen expression and role of pili. BMC Microbiol. 2002 Apr 15;2:7.

386. Gallaher TK, Wu S, Webster P, Aguilera R. Identification of biofilm proteins in non-typeable *Haemophilus influenzae*. BMC Microbiol. 2006 Jan 19;6(1):65.

387. Spoering AL, Lewis K. Biofilms and planktonic cells of *Pseudomonas aeruginosa* have similar resistance to killing by antimicrobials. J Bacteriol. 2001 Dec;183(23):6746–51.

388. Conlon BP, Nakayasu ES, Fleck LE, LaFleur MD, Isabella VM, Coleman K, Leonard SN, Smith RD, Adkins JN, Lewis K. Activated ClpP kills persisters and eradicates a chronic biofilm infection. Nature. 2013 Nov 21;503(7476):365–70.

389. Wang C, Li M, Dong D, Wang J, Ren J, Otto M, Gao Q. Role of ClpP in biofilm formation and virulence of *Staphylococcus epidermidis*. Microbes Infect. 2007 Sep;9(11):1376–83.

390. Vandecandelaere I, Depuydt P, Nelis HJ, Coenye T. Protease production by Staphylococcus epidermidis and its effect on *Staphylococcus aureus* biofilms. Pathog

Dis. 2014 Apr 1;70(3):321–31.

391. Chen C, Krishnan V, Macon K, Manne K, Narayana SVL, Schneewind O. Secreted proteases control autolysin-mediated biofilm growth of *Staphylococcus aureus*. J Biol Chem. 2013 Oct 11;288(41):29440–52.

392. Hangler M, Burmølle M, Schneider I, Allermann K, Jensen B. The serine protease Esperase HPF inhibits the formation of multispecies biofilm. Biofouling. 2009 Oct;25(7):667–74.

393. Zagursky RJ, Ooi P, Jones KF, Fiske MJ, Smith RP, Green BA. Identification of a *Haemophilus influenzae* 5'-nucleotidase protein: Cloning of the nucA gene and immunogenicity and characterization of the NucA protein. Infect Immun. 2000 May;68(5):2525–34.

394. Olson ME, Nygaard TK, Ackermann L, Watkins RL, Zurek OW, Pallister KB, Griffith S, Kiedrowski MR, Flack CE, Kavanaugh JS, Kreiswirth BN, Horswill AR, Voyich JM. *Staphylococcus aureus* nuclease is an SaeRS-dependent virulence factor. Infect Immun. 2013 Apr;81(4):1316–24.

395. Steichen CT, Cho C, Shao JQ, Apicella MA. The *Neisseria gonorrhoeae* biofilm matrix contains DNA, and an endogenous nuclease controls its incorporation. Infect Immun. 2011 Apr;79(4):1504–11.

396. Flemming H-C, Wingender J. The biofilm matrix. Nat Rev Microbiol. 2010 Aug 2;8(9):623.

397. Khajotia SS, Smart KH, Pilula M, Thompson DM. Concurrent Quantification of Cellular and Extracellular Components of Biofilms. J Vis Exp. 2013 Dec 10;(82):e50639–e50639.

398. Hernández SB, Cava F. Environmental roles of microbial amino acid racemases. Environ Microbiol. 2015 Sep 30;

399. Kolodkin-Gal I, Romero D, Cao S, Clardy J, Kolter R, Losick R. D-Amino Acids Trigger Biofilm Disassembly. Science (80-). 2010 Apr 29;328(5978):627–9.

400. Hochbaum AI, Kolodkin-Gal I, Foulston L, Kolter R, Aizenberg J, Losick R. Inhibitory effects of D-amino acids on *Staphylococcus aureus* biofilm development. J Bacteriol. 2011 Oct;193(20):5616–22.

401. Xing S-F, Sun X-F, Taylor AA, Walker SL, Wang Y-F, Wang S-G. D-amino acids inhibit

initial bacterial adhesion: thermodynamic evidence. Biotechnol Bioeng. 2015 Apr;112(4):696–704.

402. Leiman SA, May JM, Lebar MD, Kahne D, Kolter R, Losick R. D-amino acids indirectly inhibit biofilm formation in *Bacillus subtilis* by interfering with protein synthesis. J Bacteriol. 2013 Dec;195(23):5391–5.

403. Sanchez CJ, Akers KS, Romano DR, Woodbury RL, Hardy SK, Murray CK, Wenke JC. D-amino acids enhance the activity of antimicrobials against biofilms of clinical wound isolates of *Staphylococcus aureus* and *Pseudomonas aeruginosa*. Antimicrob Agents Chemother. 2014 Aug;58(8):4353–61.

404. Sarkar S, Pires MM. d-Amino acids do not inhibit biofilm formation in *Staphylococcus aureus*. PLoS One. 2015 Jan;10(2):e0117613.

405. Harmata AJ, Ma Y, Sanchez CJ, Zienkiewicz KJ, Elefteriou F, Wenke JC, Guelcher SA. D-amino acid inhibits biofilm but not new bone formation in an ovine model. Clin Orthop Relat Res. 2015 Dec;473(12):3951–61.

406. She P, Chen L, Liu H, Zou Y, Luo Z, Koronfel A, Wu Y. The effects of D-Tyrosine combined with amikacin on the biofilms of *Pseudomonas aeruginosa*. Microb Pathog. 2015 Sep;86:38–44.

407. Brandenburg KS, Rodriguez KJ, McAnulty JF, Murphy CJ, Abbott NL, Schurr MJ, Czuprynski CJ. Tryptophan inhibits biofilm formation by *Pseudomonas aeruginosa*. Antimicrob Agents Chemother. 2013 Apr;57(4):1921–5.

408. Gnanadhas DP, Elango M, Datey A, Chakravortty D. Chronic lung infection by *Pseudomonas aeruginosa* biofilm is cured by L-Methionine in combination with antibiotic therapy. Sci Rep. 2015 Jan;5:16043.

409. Caparrós M, Pisabarro AG, de Pedro MA. Effect of D-Amino Acids on Structure and Synthesis of Peptidoglycan in *Escherichia coli*. J Bacteriol. 1992;174(17):5549–59.

410. Szelestey BR, Heimlich DR, Raffel FK, Justice SS, Mason KM. *Haemophilus* responses to nutritional immunity: epigenetic and morphological contribution to biofilm architecture, invasion, persistence and disease severity. PLoS Pathog. 2013;9(10):e1003709.

411. Raffel FK, Szelestey BR, Beatty WL, Mason KM. The *Haemophilus influenzae* Sap transporter mediates bacterium-epithelial cell homeostasis. Infect Immun. 2013 Jan;81(1):43–54.

412. Harrington JC, Wong SMS, Rosadini C V, Garifulin O, Boyartchuk V, Akerley BJ. Resistance of *Haemophilus influenzae* to reactive nitrogen donors and gamma interferon-stimulated macrophages requires the formate-dependent nitrite reductase regulator-activated ytfE gene. Infect Immun. 2009 May;77(5):1945–58.

413. Lazazzera BA, Beinert H, Khoroshilova N, Kennedy MC, Kiley PJ. DNA binding and dimerization of the Fe-S-containing FNR protein from *Escherichia coli* are regulated by oxygen. J Biol Chem. 1996 Feb 2;271(5):2762–8.

414. Poole RK, Anjum MF, Membrillo-Hernández J, Kim SO, Hughes MN, Stewart V. Nitric oxide, nitrite, and Fnr regulation of hmp (flavohemoglobin) gene expression in Escherichia coli K-12. J Bacteriol. 1996 Sep;178(18):5487–92.

415. Overton TW, Justino MC, Li Y, Baptista JM, Melo AMP, Cole JA, Saraiva LM. Widespread distribution in pathogenic bacteria of di-iron proteins that repair oxidative and nitrosative damage to iron-sulfur centers. J Bacteriol. 2008 Mar;190(6):2004–13.

416. Ganz T. Hepcidin and iron regulation, 10 years later. Blood. 2011 Apr 28;117(17):4425–33.

417. Guida C, Altamura S, Klein FA, Galy B, Boutros M, Ulmer AJ, Hentze MW, Muckenthaler MU. A novel inflammatory pathway mediating rapid hepcidin-independent hypoferremia. Blood. 2015 Apr 2;125(14):2265–75.

418. Bouton C, Drapier J-C. Iron regulatory proteins as NO signal transducers. Sci STKE. 2003 May 13;2003(182):pe17.

419. Kammers K, Cole RN, Tiengwe C, Ruczinski I. Detecting Significant Changes in Protein Abundance. EuPA open proteomics. 2015 Jun;7:11–9.

420. Bronner F. Mechanisms of intestinal calcium absorption. J Cell Biochem. 2003 Feb 1;88(2):387–93.

421. Emberley ED, Murphy LC, Watson PH. S100 proteins and their influence on pro-survival pathways in cancer. Biochem Cell Biol. 2004 Aug;82(4):508–15.

422. Ketterer MR, Shao JQ, Hornick DB, Buscher B, Bandi VK, Apicella MA. Infection of

primary human bronchial epithelial cells by *Haemophilus influenzae*: macropinocytosis as a mechanism of airway epithelial cell entry. Infect Immun. 1999 Aug;67(8):4161–70.

423. Moll R, Divo M, Langbein L. The human keratins: biology and pathology. Histochem Cell Biol. 2008 Jun;129(6):705–33.

424. Chu PG, Weiss LM. Keratin expression in human tissues and neoplasms. Histopathology. 2002 May;40(5):403–39.

425. Roop DR. Regulation of keratin gene expression during differentiation of epidermal and vaginal epithelial cells. Curr Top Dev Biol. 1987;22:195–207.

426. Ruhrberg C, Watt FM. The plakin family: versatile organizers of cytoskeletal architecture. Curr Opin Genet Dev. 1997;7(3):392–7.

427. Sprecher E, Uitto J, Richard G, Itin P, Whittock N V., McGrath JA, Meyer R, DiGiovanna JJ, Bale SJ. Refined Mapping of Naegeli–Franceschetti– Jadassohn Syndrome to a 6 cM Interval on Chromosome 17q11.2-q21 and Investigation of Candidate Genes. J Invest Dermatol. 2002;119(3):692–8.

428. Yun CH, Oh S, Zizak M, Steplock D, Tsao S, Tse CM, Weinman EJ, Donowitz M. cAMP-mediated inhibition of the epithelial brush border Na+/H+ exchanger, NHE3, requires an associated regulatory protein. Proc Natl Acad Sci U S A. 1997 Apr 1;94(7):3010–5.

429. Dorfman R, Taylor C, Lin F, Sun L, Sandford A, Paré P, Berthiaume Y, Corey M, Durie P, Zielenski J, Members of Canadian Consortium for CF Genetic Studies. Modulatory effect of the SLC9A3 gene on susceptibility to infections and pulmonary function in children with cystic fibrosis. Pediatr Pulmonol. 2011 Apr;46(4):385–92.

430. Cao TT, Deacon HW, Reczek D, Bretscher A, von Zastrow M. A kinase-regulated PDZ-domain interaction controls endocytic sorting of the beta2-adrenergic receptor. Nature. 1999 Sep 16;401(6750):286–90.

431. Maudsley S, Zamah AM, Rahman N, Blitzer JT, Luttrell LM, Lefkowitz RJ, Hall RA. Platelet-Derived Growth Factor Receptor Association with Na+/H+ Exchanger Regulatory Factor Potentiates Receptor Activity. Mol Cell Biol. 2000 Nov 15;20(22):8352–63.

432. Henderson NC, Sethi T. The regulation of inflammation by galectin-3. Immunol Rev.

2009 Jul;230(1):160–71.

433. Puig C, Domenech A, Garmendia J, Langereis JD, Mayer P, Calatayud L, Liñares J, Ardanuy C, Marti S. Increased biofilm formation by *nontypeable Haemophilus influenzae* isolates from patients with invasive disease or otitis media versus strains recovered from cases of respiratory infections. Appl Environ Microbiol. 2014 Nov;80(22):7088–95.

434. Windoffer R, Beil M, Magin TM, Leube RE. Cytoskeleton in motion: the dynamics of keratin intermediate filaments in epithelia. J Cell Biol. 2011;194(5).

435. Hardt WD, Chen LM, Schuebel KE, Bustelo XR, Galán JE. S. typhimurium encodes an activator of Rho GTPases that induces membrane ruffling and nuclear responses in host cells. Cell. 1998 May 29;93(5):815–26.

436. Egile C, Loisel TP, Laurent V, Li R, Pantaloni D, Sansonetti PJ, Carlier MF. Activation of the CDC42 effector N-WASP by the *Shigella flexneri* IcsA protein promotes actin nucleation by Arp2/3 complex and bacterial actin-based motility. J Cell Biol. 1999 Sep 20;146(6):1319–32.

437. Gruenheid S, DeVinney R, Bladt F, Goosney D, Gelkop S, Gish GD, Pawson T, Finlay BB. *Enteropathogenic E. coli* Tir binds Nck to initiate actin pedestal formation in host cells. Nat Cell Biol. 2001 Sep;3(9):856–9.

438. Yoshida S, Katayama E, Kuwae A, Mimuro H, Suzuki T, Sasakawa C. *Shigella* deliver an effector protein to trigger host microtubule destabilization, which promotes Rac1 activity and efficient bacterial internalization. EMBO J. 2002 Jun 17;21(12):2923–35.

439. Ahrén IL, Janson H, Forsgren A, Riesbeck K. Protein D expression promotes the adherence and internalization of non-typeable *Haemophilus influenzae* into human monocytic cells. Microb Pathog. 2001 Sep;31(3):151–8.

440. van Schilfgaarde M, van Ulsen P, van Der Steeg W, Winter V, Eijk P, Everts V, Dankert J, van Alphen L. Cloning of genes of *nontypeable Haemophilus influenzae* involved in penetration between human lung epithelial cells. Infect Immun. 2000 Aug;68(8):4616–23.

441. Finlay BB, Ruschkowski S, Kenny B, Stein M, Reinscheid DJ, Stein MA, Rosenshine I. *Enteropathogenic E. coli* exploitation of host epithelial cells. Ann N Y Acad Sci. 1996 Oct 25;797:26–31.

442. Knowles MR, Leigh MW, Carson JL, Davis SD, Dell SD, Ferkol TW, Olivier KN, Sagel SD, Rosenfeld M, Burns KA, Minnix SL, Armstrong MC, Lori A, Hazucha MJ, Loges NT, Olbrich H, Becker-Heck A, Schmidts M, Werner C, Omran H, Zariwala MA. Mutations of DNAH11 in patients with primary ciliary dyskinesia with normal ciliary ultrastructure. Thorax. 2012 May;67(5):433–41.

443. Boon M, Smits A, Cuppens H, Jaspers M, Proesmans M, Dupont LJ, Vermeulen FL, Van Daele S, Malfroot A, Godding V, Jorissen M, De Boeck K. Primary ciliary dyskinesia: critical evaluation of clinical symptoms and diagnosis in patients with normal and abnormal ultrastructure. Orphanet J Rare Dis. 2014 Jan;9(1):11.

444. Raidt J, Wallmeier J, Grose Onnebrink J, Pennekamp P, Loges NT, Olbrich H, Dougherty G, Omran H, Werner C. Identification of distinct ciliary beat pattern abnormalities by high-speed video microscopy in primary ciliary dyskinesia. Pediatr Pulmonol. 2014;49:S48.

445. Dougherty GW, Loges NT, Klinkenbusch JA, Olbrich H, Pennekamp P, Menchen T, Raidt J, Wallmeier J, Werner C, Westermann C, Ruckert C, Mirra V, Hjeij R, Memari Y, Durbin R, Kolb-Kokocinski A, Praveen K, Kashef MA, Kashef S, Eghtedari F, Häffner K, Valmari P, Baktai G, Aviram M, Bentur L, Amirav I, Davis EE, Katsanis N, Brueckner M, Shaposhnykov A, Pigino G, Dworniczak B, Omran H. DNAH11 Localization in the Proximal Region of Respiratory Cilia Defines Distinct Outer Dynein Arm Complexes. Am J Respir Cell Mol Biol. 2016 Feb 24;

446. Fliegauf M, Olbrich H, Horvath J, Wildhaber JH, Zariwala MA, Kennedy M, Knowles MR, Omran H. Mislocalization of DNAH5 and DNAH9 in respiratory cells from patients with primary ciliary dyskinesia. Am J Respir Crit Care Med. 2005 Jun 15;171(12):1343–9.

447. Donato R, Cannon BR, Sorci G, Riuzzi F, Hsu K, Weber DJ, Geczy CL. Functions of S100 proteins. Curr Mol Med. 2013 Jan;13(1):24–57.

448. Shimamoto S, Kubota Y, Yamaguchi F, Tokumitsu H, Kobayashi R. Ca2+/S100 proteins act as upstream regulators of the chaperone-associated ubiquitin ligase CHIP (C terminus of Hsc70-interacting protein). J Biol Chem. 2013 Mar 8;288(10):7158–68.

449. Rescher U, Gerke V. S100A10/p11: family, friends and functions. Pflügers Arch Eur J Physiol. 2008 Jan;455(4):575–82.

450. Shimamoto S, Takata M, Tokuda M, Oohira F, Tokumitsu H, Kobayashi R. Interactions of S100A2 and S100A6 with the tetratricopeptide repeat proteins, Hsp90/Hsp70-organizing protein and kinesin light chain. J Biol Chem. 2008 Oct 17;283(42):28246–58.

451. Passey RJ, Williams E, Lichanska AM, Wells C, Hu S, Geczy CL, Little MH, Hume DA. A null mutation in the inflammation-associated S100 protein S100A8 causes early resorption of the mouse embryo. J Immunol. 1999 Aug 15;163(4):2209–16.

452. Lim SY, Raftery M, Cai H, Hsu K, Yan WX, Hseih H-L, Watts RN, Richardson D, Thomas S, Perry M, Geczy CL. S-nitrosylated S100A8: novel anti-inflammatory properties. J Immunol. 2008 Oct 15;181(8):5627–36.

453. Vogl T, Ludwig S, Goebeler M, Strey A, Thorey IS, Reichelt R, Foell D, Gerke V, Manitz MP, Nacken W, Werner S, Sorg C, Roth J. MRP8 and MRP14 control microtubule reorganization during transendothelial migration of phagocytes. Blood. 2004 Dec 15;104(13):4260–8.

454. Vogl T, Tenbrock K, Ludwig S, Leukert N, Ehrhardt C, van Zoelen MAD, Nacken W, Foell D, van der Poll T, Sorg C, Roth J. Mrp8 and Mrp14 are endogenous activators of Toll-like receptor 4, promoting lethal, endotoxin-induced shock. Nat Med. 2007 Sep;13(9):1042–9.

455. Steinckwich N, Schenten V, Melchior C, Bréchard S, Tschirhart EJ. An essential role of STIM1, Orai1, and S100A8-A9 proteins for Ca2+ signaling and FcγR-mediated phagosomal oxidative activity. J Immunol. 2011 Feb 15;186(4):2182–91.

456. Zaia AA, Sappington KJ, Nisapakultorn K, Chazin WJ, Dietrich EA, Ross KF, Herzberg MC. Subversion of antimicrobial calprotectin (S100A8/S100A9 complex) in the cytoplasm of TR146 epithelial cells after invasion by Listeria monocytogenes. Mucosal Immunol. 2009 Jan;2(1):43–53.

457. Urban CF, Ermert D, Schmid M, Abu-Abed U, Goosmann C, Nacken W, Brinkmann V, Jungblut PR, Zychlinsky A. Neutrophil extracellular traps contain calprotectin, a cytosolic protein complex involved in host defense against Candida albicans. PLoS Pathog. 2009 Oct;5(10):e1000639.

458. Kang SH, Dalcin P de TR, Piltcher OB, Migliavacca R de O. Chronic rhinosinusitis and nasal polyposis in cystic fibrosis: update on diagnosis and treatment. J Bras Pneumol. 2015;41(1):65–76.

459. Brodlie M, McKean MC, Johnson GE, Perry JD, Nicholson A, Verdon B, Gray MA, Dark JH, Pearson JP, Fisher AJ, Corris PA, Lordan J, Ward C. Primary bronchial epithelial cell culture from explanted cystic fibrosis lungs. Exp Lung Res. 2010 Mar;36(2):101–10.

460. Wang Z, Gerstein M, Snyder M. RNA-Seq: a revolutionary tool for transcriptomics. Nat Rev Genet. 2009 Jan;10(1):57–63.

461. Severi E, Randle G, Kivlin P, Whitfield K, Young R, Moxon R, Kelly D, Hood D, Thomas GH. Sialic acid transport in *Haemophilus influenzae* is essential for lipopolysaccharide sialylation and serum resistance and is dependent on a novel tripartite ATP-independent periplasmic transporter. Mol Microbiol. 2005 Nov;58(4):1173–85.

462. Swords WE, Moore ML, Godzicki L, Bukofzer G, Mitten MJ, VonCannon J. Sialylation of lipooligosaccharides promotes biofilm formation by *nontypeable Haemophilus influenzae*. Infect Immun. 2004 Jan;72(1):106–13.

463. Schmid A, Salathe M. Ciliary beat co-ordination by calcium. Biol Cell. 2011 Apr;103(4):159–69.

464. Yuan S, Zhao L, Brueckner M, Sun Z. Intraciliary calcium oscillations initiate vertebrate left-right asymmetry. Curr Biol. 2015 Mar 2;25(5):556–67.

465. Yoshiba S, Shiratori H, Kuo IY, Kawasumi A, Shinohara K, Nonaka S, Asai Y, Sasaki G, Belo JA, Sasaki H, Nakai J, Dworniczak B, Ehrlich BE, Pennekamp P, Hamada H. Cilia at the node of mouse embryos sense fluid flow for left-right determination via Pkd2. Science. 2012 Oct 12;338(6104):226–31.

466. Tarran R, Button B, Picher M, Paradiso AM, Ribeiro CM, Lazarowski ER, Zhang L, Collins PL, Pickles RJ, Fredberg JJ, Boucher RC. Normal and cystic fibrosis airway surface liquid homeostasis. The effects of phasic shear stress and viral infections. J Biol Chem. 2005 Oct 21;280(42):35751–9.

467. Matthews JR, Botting CH, Panico M, Morris HR, Hay RT. Inhibition of NF-kappaB DNA binding by nitric oxide. Nucleic Acids Res. 1996 Jun 15;24(12):2236–42.

468. Li Y, Yagi H, Onuoha EO, Damerla RR, Francis R, Furutani Y, Tariq M, King SM, Hendricks G, Cui C, Saydmohammed M, Lee DM, Zahid M, Sami I, Leatherbury L, Pazour GJ, Ware SM, Nakanishi T, Goldmuntz E, Tsang M, Lo CW. DNAH6 and Its Interactions with PCD Genes in Heterotaxy and Primary Ciliary Dyskinesia. PLoS Genet. 2016;12(2):1–20.

469. Tomoyasu T, Tabata A, Imaki H, Tsuruno K, Miyazaki A, Sonomoto K, Whiley RA, Nagamune H. Role of *Streptococcus intermedius* DnaK chaperone system in stress tolerance and pathogenicity. Cell Stress Chaperones. 2012 Jan;17(1):41–55.

470. Kyd JM, Cripps AW, Novotny LA, Bakaletz LO. Efficacy of the 26-kilodalton outer membrane protein and two P5 fimbrin-derived immunogens to induce clearance of *nontypeable Haemophilus influenzae* from the rat middle ear and lungs as well as from the chinchilla middle ear and nasopharynx. Infect Immun. 2003 Aug;71(8):4691–9.

471. Hoffmann N, Rasmussen TB, Jensen PØ, Stub C, Hentzer M, Molin S, Ciofu O, Givskov M, Johansen HK, Høiby N. Novel mouse model of chronic *Pseudomonas aeruginosa* lung infection mimicking cystic fibrosis. Infect Immun. 2005 Apr;73(4):2504–14.

472. Lucas JS, Adam EC, Goggin P, Jackson CL, Powles-Glover N, Humphreys J, Fray M, Cheeseman M, Norris DP, Lackie PM. Static respiratory cilia with normal ultrastructure in inversus viscerum (IV) mouse- A potential model of primary ciliary dyskinesia? Am J Respir Crit Care Med. 2010 May;181(1 MeetingAbstracts):A6724–A6724.

473. Alexander S-A, Kyi C, Schiesser CH. Nitroxides as anti-biofilm compounds for the treatment of *Pseudomonas aeruginosa* and mixed-culture biofilms. Org Biomol Chem. 2015 Apr 28;13(16):4751–9.

474. de la Fuente-Núñez C, Reffuveille F, Fairfull-Smith KE, Hancock REW. Effect of nitroxides on swarming motility and biofilm formation, multicellular behaviors in *Pseudomonas aeruginosa*. Antimicrob Agents Chemother. 2013 Oct;57(10):4877–81.

475. Kutty SK, Barraud N, Pham A, Iskander G, Rice SA, Black DS, Kumar N. Design, synthesis, and evaluation of fimbrolide-nitric oxide donor hybrids as antimicrobial agents. J Med Chem. 2013 Dec 12;56(23):9517–29.

476. Marvasi M, Durie IA, McLamore ES, Vanegas DC, Chaturvedi P. Salmonella enterica biofilm-mediated dispersal by nitric oxide donors in association with cellulose nanocrystal hydrogels. AMB Express. 2015;5:28.

477. Strippoli M-PF, Frischer T, Barbato A, Snijders D, Maurer E, Lucas JSA, Eber E, Karadag B, Pohunek P, Zivkovic Z, Escribano A, O'Callaghan C, Bush A, Kuehni CE. Management of primary ciliary dyskinesia in European children: recommendations and clinical practice. Eur Respir J. 2012 Jun 1;39(6):1482–91.

478. Whiting P, Harbord R, Kleijnen J. No role for quality scores in systematic reviews of

diagnostic accuracy studies. BMC Med Res Methodol. 2005 Jan;5:19.

479. Deeks J, Altman D, Bradburn M. Statistical methods for examining heterogeneity and combining results from several studies in meta-analysis. In: Eggar M, Davey-SMith G, Altman D, editors. Systematic Review in Health Care: Meta-Analysis in Context. London: BMJ Books; 2001. p. 285–312.

480. Bodini A, Rugolotto S, Pradal U, Zanotto G, Peroni D. Nasal nitric oxide for early diagnosis of familial primary ciliary dyskinesia. Arch Dis Child. 2008 May 1;93(5):452–3.

481. Chawla KK, Hazucha MJ, Dell SD, Ferkol TW, Sagel SD, Rosenfeld M, Baker B, Davis SD, Knowles MR, Leigh MW. A multi-center, longitudinal study of nasal nitric oxide in children with primary ciliary dyskinesia. Vol. 181, American Journal of Respiratory and Critical Care Medicine. American Thoracic Society; 2010.

482. Shapiro AJ, Chawla KK, Baker BR, Minnix S, Davis SD, Knowles MR, Leigh MW. Nasal nitric oxide and clinical characteristics of patients with heterotaxy: Comparison to primary ciliary dyskinesia. Vol. 183, American Journal of Respiratory and Critical Care Medicine. American Thoracic Society; 2011.

483. Beucher J, Chambellan A, Segalen J, Deneuville E. [Primary ciliary dyskinesia: a retrospective review of clinical and paraclinical data]. Rev Mal Respir. 2011 Sep;28(7):856–63.

484. Pifferi M, Bush A, Caramella D, Di Cicco M, Zangani M, Chinellato I, Macchia P, Boner AL. Agenesis of paranasal sinuses and nasal nitric oxide in primary ciliary dyskinesia. Eur Respir J. 2011 Mar;37(3):566–71.

485. Baker B, Chawla K, Hazucha M, Knowles M, Leigh MW. Toward standardization of nasal nitric oxide testing for primary ciliary dyskinesia. Am J Respir Crit Care Med. 2011;183:A1210.

486. Montella S, Alving K, De Stefano S, Di Micco L, Di Giorgio A, Santamaria F. Nasal nitric oxide measurement using continuous aspiration by hand-held device discriminates patients with primary ciliary dyskinesia from healthy subjects. Eur Respir J. 2012;40:598s.

487. Cutruzzola F, Frankenberg-Dinkel N. Origin and impact of nitric oxide in *Pseudomonas aeruginosa* biofilms. J Bacteriol. 2015 Aug 10;